North American bats and their viruses: The effect of stressors on persistent infections and viral shedding

A thesis submitted to the

College of Graduate and Postdoctoral studies

in Partial fulfillment of the requirements for the

Degree of Doctor of Philosophy

in the department of Veterinary Microbiology

University of Saskatchewan

By

SONU SUBUDHI

© Copyright Sonu Subudhi, May 2019. All rights reserved.

Permission to use

In presenting this thesis or dissertation in partial fulfillment of the requirements for a Postgraduate degree from the University of Saskatchewan, I agree that the Libraries of this University may make it freely available for inspection. I further agree that permission for copying of this thesis or dissertation in any manner, in whole or in part, for scholarly purposes may be granted by the professor or professors who supervised my thesis work or, in their absence, by the Head of the Department or the Dean of the College in which my thesis work was done. It is understood that any copying or publication or use of this thesis or parts of thereof for financial gain shall not be allowed without my written permission. It is also understood that due recognition shall be given to me and to the University of Saskatchewan in any scholarly use which may be made of any material in my thesis or dissertation.

Requests for permission to copy or to make other uses of materials in this thesis or dissertation in whole or in part should be addressed to:

Head of the Department of Veterinary Microbiology,
2601-52 Campus Drive,
University of Saskatchewan,
Saskatoon, SK – S7N 5B4
Canada

OR

Dean,
College of Graduate and Postdoctoral studies,
University of Saskatchewan,
116 Thorvaldson Building, 110 Science place,
Saskatoon, SK – S7N 5C9
Canada

Abstract

There is direct or circumstantial evidence that several viruses that cause no obvious disease in bats have spilled over into humans and other species causing serious and often fatal disease. The reasons for the lack of disease in bats or for the spillover of these viruses from bats are poorly understood. While there is considerable literature on the interactions of these viruses with their secondary hosts or their surrogates, little is known about the interactions of bat viruses in their natural hosts. We used a coronavirus detected in little brown bat (*Myotis lucifugus*) and a herpesvirus, detected in the big brown bat (*Eptesicus* fuscus), as models to understand the factors that might alter bat-virus relationships. We demonstrated that a coronavirus (*Myotis lucifugus* coronavirus – *Myl*-CoV) detected in the intestines of little brown bats, could persist in them during the 4 months of hibernation. Using this coronavirus-bat model, we showed that the stress of fungal infection by *Pseudogymnoascus destructans* (*Pd*), which causes bat white-nose syndrome (WNS), led to a 60-fold increase in viral replication in intestines than bats with virus alone. Increased viral replication correlated with the severity of *Pd*-related pathology and the intestine of fungus-infected bats showed changes in gene expression suggesting suppressed innate antiviral response and increased apoptotic responses. Our results suggest that the systemic effects of WNS leads to a resurgence of virus replication and increases the potential of virus shedding. Using a bat cell culture model, we showed that viral persistence could be disrupted by artificially suppressing the host cell's antiviral response and was mediated through similar pathways that were observed during *in-vivo* experiments. To ascertain whether the effect of stressor could disrupt viral persistence in other bat-virus relationships, I studied the big brown bat herpesvirus. As herpesviruses inherently establish life-long latent infections in their hosts and reactivate periodically in response to stress, we used this model to study the effects of natural stressors on

the bat-virus relationship. We characterized the herpesvirus and developed techniques for detecting the virus as well as for monitoring the adaptive antibody response against the virus. We showed that the bat gammaherpesvirus reactivates at the end of hibernation and was accompanied by a lower antibody level, which subsequently increased upon arousal. Our studies on coronavirus and herpesvirus show that bats have a long-term balanced and benign relationships with viruses and a variety of stressors could disrupt this balance allowing an increase in viral replication.

Acknowledgements

First of all, I am extremely grateful to my supervisor Dr. Vikram Misra for providing me with this wonderful opportunity to pursue a PhD under his supervision. His expertise in the field of virology and his friendly demeanor made my PhD a productive, smooth and memorable period. Also, I am thankful to my committee members, Dr. Janet Hill, Dr. Yan Zhou, Dr. Darryl Falzarano and Dr. Trent Bollinger for all of their guidance and suggestions during the last four years.

My sincere thanks and gratitude must also go to Noreen, Linda and Lana who made my professional work environment feel like home. I would also like to acknowledge my lab mates (Ursula, Arinjay, Caleigh and Evelyn), my office mates (Salahuddin, Pashupati, Shakya, Nikki, and Carolyna), the staff at GMP. Special thanks to the team at National Microbiology lab, (Dave, Angela, Bryce, Derek, Rob, Allen, Shane, Robbin) for teaching me a lot of techniques during my externship there.

I really appreciate the support and sacrifice done by my family back in India, my father, my mother, my brother and sister in-law. I would also like to thank my friends here in Saskatoon, Poonam and Swarali. A special thanks to my wife, Rasika, for being there for me throughout this journey.

Table of Contents

List of Tables

List of Figures

List of abbreviations

ACE2	Angiotensin converting enzyme 2
AIDS	Acute immunodeficiency syndrome
ANOVA	Analysis of variance
APN	Aminopeptidase
ATF6	Activating transcriptional factor 6
Bax	Bcl2-associated X protein
Bcl2	B-cell lymphoma 2
BHK21	Baby Hamster Kidney 21
BLAST	Basic Local Alignment Search Tool
CAML	calcium-modulating cyclophilin ligand
CCP	Complement control protein
cDNA	Complementary DNA
CEACAM1	Carcinoembryonic antigen related cell adhesion molecule 1
cGAS	cyclic GMP-AMP synthase
cGMP	cyclic guanosine monophosphate
CRFK	Crandell Reese Feline Kidney
Ct	Cycle threshold
CWHC	Canadian Wildlife Health Cooperative
DAPI	4',6-diamino-2-phenylindole
DIC	Differential interference contrast
DMEM	Dulbecco Modified Eagle's Media
DNA	Deoxyribonucleic acid
dNTP	Deoxyribonucleotide triphosphate
dpol	DNA polymerase
DPP4	Dipeptidyl peptidase-4
dsDNA	double stranded DNA
Dsi-RNA	Dicer-ready small interference RNA
EBNA	Ebstein-Barr nuclear antigen
EBV	Ebstein-Barr Virus
*Ef*HV	*Eptesicus fuscus* Herpesvirus
*Ef*k	*Eptesicus fuscus* Kidney
ELISA	Enzyme linked immunosorbent assay
EM	Electron Microscopy
ERGIC	Endoplasmic reticulum golgi intermediate compartment
FBS	Feta Bovine Serum
FCoV	Feline enteric coronavirus
FDR	False Detection Rate
FFPE	Formalin Fixed Paraffin Embedded
FGAM	Formylglycinamidine
FIPV	Feline infectious peritonitis virus
GAPDH	Glyceraldehyde 3-phosphate Dehydrogenase
gB	Glycoprotein B
GHV	Gammaherpesvirus
GLMM	generalized linear mixed models
GO	Gene ontology
GST	Glutathione S-transferase
GTP	Guanosine triphosphate
H&E	Hematoxylin and Eosin
HCoV	Human CoV
HE	Hemagglutinin-esterase
HEK293	Human Embryonic Kidney 293
hpi	hours post infection
HRP	Horse Raddish Peroxide
HSV-1	Herpes Simplex Virus 1

IBV	Infectious bronchitis virus
IFA	Immunofluorescence assay
IFI16	Interferon-γ inducible gene 16
IFI6	Interferon-α inducible gene 6
IFN-β	Interferon Beta
IFN-γ	Interferon Gamma
IHC	Immunohistochemistry
IL-10	Interleukin 10
IL22RA1	Interleukin 22 receptor subunit alpha 1
IRE1	Inositol requiring protein 1
IRF1	Interferon regulatory factor 1
IRF3	Interferon regulatory factor 3
ISG	Interferon stimulated genes
ISH	in-situ hybridization
JAK-STAT	janus kinases – signal transducer and activator of transcription proteins
JNK	c-Jun N-terminal kinases
KCl	Potassium Chloride
kDa	Kilodalton
KSHV	Kaposi sarcoma associated herpesvirus
LANA	Latency Associated Nuclear Antigen
LMM	Linear mixed models
MAP3K11	mitogen-activated protein kinase 11
MAPK	Mitogen activated protein kinase
MBIC	Minimum biofilm inhibition concentration
MDA5	Melanoma differentiation-associated protein 5
MDBK	Madin-Darby Bovine Kidney
MDCK	Madin-Darby Canine Kidney
MERS-CoV	Middle eastern respiratory syndrome coronavirus
MHC	Major Histocompatibility Complex
MHV	Murine hepatitis virus
ML	Maximum likelihood
MOI	Multiplicity of Infection
MOMP	mitochondrial outer membrane permeability
mRNA	Messenger RNA
MS	Mass spectrometry
MyD88	Myeloid differentiation primary response 88
Myl-CoV	*Myotis lucifugus* CoV
N protein	Nucleocapsid protein
NaCl	Sodium Chloride
NCBI	National Center for Biotechnology Information
NF-κB	Nuclear factor kappa-light-chain-enhancer of activated B cells
NiV	Nipah Virus
ORF	Open Reading Frame
ORF5	Open Reading Frame 5
OsO4	Osmium Tetroxide
PBS	Phosphate Buffered Saline
PCR	Polymerase Chain Reaction
PED-CoV	Porcine Epidemic Diarrhea CoV
PELT	Pruned Exact Linear Time
PERK	protein kinase R (PKR) like endoplasmic reticulum kinase
PHEV	Porcine hemagglutinating encephalomyelitis virus
PHYIN	PHYRIN and HIN domain
PI3K	Phosphoinositide 3-kinase
PK15	Porcine Kidney 15
PML NB	Promyelocytic leukemia nuclear bodies
PO	Propylene oxide
PVDF	polyvinylidene difluoride
qPCR	Quantitative PCR
RdRp	RNA dependent RNA polymerase

RERG	RAS like estrogen regulated growth inhibitor
RFP	Red Fluorescent Protein
RIG-I	Retinoic Acid Inducible Gene-I
RK13	Rabbit Kidney 13
RNA	Ribonucleic acid
Rnase-L	Ribonuclease L
RNASeq	RNA Sequencing
RRAD	Ras related glycolysis inhibitor and calcium channel regulator
RSU1	Ras suppressor protein 1
RTA	Regulator of transcription activation
SADS	Swine acute diarrhea syndrome
SARS	Severe Acute Respiratory Syndrome
SDS-PAGE	Sodium Dodecyl sulfate Polyacrylamide gel electrophoresis
SILI	Susceptible Infectious Latent Infectious
SOCS6	Suppressor of cytokine signaling 6
STING	Stimulator of Interferon gene
STYK1	serine/threonine/tyrosine kinase 1
TBK1	TANK binding kinase 1
TCID50	Tissue Culture Infectious Dose 50
TEM	Transmission Electron Microscopy
TGEV	Transmissible Gastroenteritis virus
TLR	Toll-like receptors
TNE buffer	Tris NaCl EDTA buffer
TNFA	Tumor necrosis factor alpha
TPA	Tetradecanoyl-phorbol-13-acetate
TPCK	Tosyl phenylalanyl chloromethyl ketone
tRNA	Transfer RNA
UPR	Unfolded protein response
vFLIP	viral Fas-associated death domain-like interleukin-1β-converting enzyme-inhibitory protein
vMAP	viral mitochondrial antiapoptotic protein
WAG model	Whelan and Goldman model
WNS	White-nose syndrome

Chapter 1: Introduction

Bats are implicated as hosts for viruses which may have spilled over to other species including humans. My thesis focuses on the effect stressors might have on bat-virus relationships and if these effects alter viral shedding. My review initially focuses on literature on how bats and their viruses interact, specifically on the bat antiviral response, inflammation due to viral infection and the effect of stress on viral spillover. This follows an introduction to the bats in North America, which would aid in understanding the host species that we have studied. The literature review then describes current knowledge about viruses that are similar to the ones we have studied i.e., coronavirus and gammaherpesvirus. I have described the genome organization and life cycles of these viruses, their interaction with host pathways, their pathogenesis and the evidence for viral spillover to other species. For the gammaherpesvirus, I have reviewed factors that influence virus reactivation from latency.

Chapter 2: Literature review - Immune system modulation and viral persistence in bats: understanding the mechanisms behind spillover

2.1. Copyright

© 2019 by the authors. Licensee MDPI, Basel, Switzerland. This article is an open access article distributed under the terms and conditions of the Creative Commons Attribution (CC BY) license.

This manuscript has been reformatted from the original version for inclusion in this thesis.

2.2. Citation

Subudhi, S., N. Rapin, and V. Misra. "Immune System Modulation and Viral Persistence in Bats: Understanding Viral Spillover." Viruses 11, no. 2 (February 23, 2019): 192. https://doi.org/10.3390/v11020192.

2.3. Abstract

Bats harbor a myriad of viruses and some of these viruses may have spilled over to other species including humans. Spillover events are rare, and several factors must align to create the "perfect storm" that would ultimately lead to a spillover. One of these factors is the increased shedding of virus by bats. Several studies have indicated that bats have unique defense mechanisms that allow them to be persistently or latently infected with viruses. Factors leading to an increase in the viral load of persistently infected bats would facilitate shedding of virus. This article reviews the unique nature of bat immune defenses that regulate virus replication and the various molecular mechanisms that play a role in altering the balanced bat–virus relationship.

2.4. Introduction

Over the past few years, the interest in bat research has increased because of the range of viruses that they harbor and the potential of spillover to humans and other vertebrates [1]. In some instances, there is direct evidence that viruses have spilled over from bats to other vertebrates. For example, Nipah virus spilled over from bats to humans and pigs leading to outbreaks in South-east Asia and Hendra virus continues to spillover into horses and humans in Australia [2–6]. In other instances, the evidence of virus spillover from bats is circumstantial. For example, in case of ebolaviruses, serological evidence and the detection of viruses related to the ebolaviruses in bats [7,8] suggests that they are reservoirs of the virus. Recent discoveries of filoviruses in bats of China and Sierra Leone have further bolstered this claim [9,10]. However, viruses linked to specific Ebola virus disease (EVD) epidemics have not yet been detected in bats. Although bats harbor many diverse viruses, their spillover to other animals is extremely rare [11]. One of the reasons is that for a spillover event to take place several factors such as pathogen shedding, environmental conditions, pathogen persistence in environment and recipient host susceptibility, should all be conducive to transmission. This would result in the "perfect storm" required for spillover. A review by Plowright *et al.* describes the factors that could lead to such a perfect storm [12]. Here, we focus on one of the initial events affecting this spillover, i.e. an increase in pathogen shedding.

Pathogen shedding by bats is a complex phenomenon regulated by host antiviral defenses and viral factors. A host's defenses attempt to control virus infection but viruses have evolved mechanisms to counteract them [13]. When the host defenses are suppressed, or if the virus is able to circumvent the host immune system, virus replication is enhanced, leading to an increase in

virus shedding. The route of shedding is highly dependent on the tissue in which the virus replication occurs. For example, increased replication in the kidney would lead the bat to shed the virus in urine, whereas intestinal replication would result in dissemination through feces.

Therefore, it becomes important to study what factors might be responsible for decreasing the host defense or factors that allow the virus to circumvent host immune response. But before exploring factors affecting virus-host interactions, it is imperative to understand the viruses present in bats and the bat immune defenses. In 2013-14, bat immunology was at a nascent stage and Schountz and Baker *et al.* had summarized the preliminary knowledge about it in their reviews [14,15]. In 2017, Schountz *et al.* again reviewed bat immunology but the article also laid out gaps in our understanding of host pathogen interactions in bats [16]. Here, we include more recent advances in characterizing the bat immune system including a possible link between the evolution of flight in bats and viral persistence. Following that section, we discuss the factors identified so far that upset the balanced bat-virus relationship, potentially leading to the spillover of viruses.

One must be cautious when interpreting the literature on bat defenses. The order Chiroptera contains more than 1200 species [17]. Due to this diversity, the information obtained from one species may not apply to others. For instance, in the black flying fox (*Pteropus alecto*), the interferon gene locus is contracted whereas in Egyptian fruit bat (*Rousettus aegyptiacus*), this locus is expanded [18,19]. Other examples are discussed later in this review.

2.5. Bats have an efficient and varied antiviral response

It has been observed that viruses which severely affect other mammals, including humans, are apparently non-pathogenic for bats [20]. This adaptability of bats to harbor many viruses without showing overt pathology suggests that bats have evolved immune mechanisms that allow for benign virus-host relationships.

The immune response has two primary components, innate and adaptive. The host initially responds to infection by activating innate mechanisms. Genes such as those for sensing and repairing DNA damage and the inflammatory process are under positive selection in black flying foxes and David's myotis (*Myotis davidii*) [21]. For instance, there are mutations in the coding sequence of p53 functional domains that are unique to these bats. Interferons are the primary innate effector molecules that control viral replication. Several types of interferon have been identified in bats, especially Type I and Type III. Type I interferon is induced after virus infection in Egyptian fruit bats whereas type III interferon is induced similarly in pteropid bats [22,23]. It is interesting to note that interferon genes in black flying foxes have contracted in terms of diversity. The number of variants of interferon present in these bats is lower compared to those in the gene loci of ten other vertebrate species. Despite this decrease in interferon gene diversity, black flying foxes express these variants at higher basal levels than other mammalian species. This suggests that the interferon and interferon stimulated genes are constitutively expressed in these bats [18]. In contrast, a recent study of the genome of Egyptian fruit bats shows expanded diversity of Type I interferon genes. This, as well as expansion of various other immune genes, suggests novel modes of antiviral defense in bats of various species [24]. Novel modes of antiviral defenses could exists in other species of bats and future studies would help in revealing them.

Cruz-Rivera *et al.* showed that in cultured cells of black flying foxes, interferon-stimulated genes (ISGs) were expressed at higher levels than their human counterparts. They also demonstrated that an antiviral effector 2-5A-dependent endoribonuclease (RNase-L) is a unique downstream ISG gene, which is stimulated directly by interferon in bat cells [25]. The activated RNase-L can then cleave viral mRNA. In contrast, in human cells, RNase-L is not directly stimulated by interferon but via an intermediate molecule, 2',5'-oligoadenylate (2-5A) synthetase

[26]. Similarly, direct activation of RNase-L was also observed in *in-vivo* experiments with Jamaican fruit bats (*Artibeus jamaicensis*) [27]. Inactivation of the RNase -L gene renders bat cells more susceptible to virus infection and direct induction of RNase-L may provide bats with an additional layer of antiviral defense [25].

These studies suggest that in bats of several species, higher level of interferon and ISGs are always present in their cells, which makes them better prepared to control viruses. Overall, bats seem to possess either an "always ON" interferon strategy plus or a better antiviral ISG defense strategy.

2.6. Bats suppress the pathological effects of excessive virus-induced inflammation

While bats are well prepared to control viral infections, they also have mechanisms to avoid over-induction of inflammatory genes. Such excessive inflammation is detrimental in vertebrates of other species, such as humans, and is linked to pathology [28]. So, it is beneficial for the bats to have evolved mechanisms that would allow them to control excessive inflammation. Cell culture experiments have shown that cells of several species of bats have an inhibitor molecule (cRel) binding site in the promotor region of tumor necrosis factor alpha (TNFα), a key inflammatory cytokine. In cells of big brown bats (*Eptesicus fuscus*), stimulated with poly I:C, a surrogate for double-stranded viral RNA, cRel actively suppresses TNFα expression [29]. Genome analysis of black flying foxes and David's myotis have also demonstrated positive selection pressure on the cRel gene [21]. This suggests that many bats have a mechanism to suppress the expression of TNFα, thereby maintaining a balanced response to viral infection.

Several species of bats control inflammation by having a mutation at a highly conserved serine residue in one of the key adaptor molecules for sensing damaged DNA, i.e., stimulator of interferon genes (STING), which reduces its functionality. STING senses damaged DNA or

dsDNA from viruses and induces an interferon response. The replacement of serine at position 358 by other amino acids makes bat STING less effective in activating interferons [30]. In addition to possessing a less effective STING, the pyrin and HIN domain (PHYIN) genes, which are involved in microbial DNA sensing and formation of inflammasome, are absent in bats [21,31]. These findings demonstrate some of the reasons for reduced inflammation in bats during viral infection. Mechanisms to modulate inflammation may have evolved to mitigate the detrimental effects of flight. Excessive exposure to cytosolic DNA in bat cells during flight might have posed a strong natural selection pressure to reduce the activation of bat DNA sensors.

Unique immune features and relationship with the evolution of flight: The unique features of bats, whereby they tolerate viral infections without excessive inflammation while suppressing viral replication, leads to the obvious question - What is so special about bats? The answer to this has been linked to the evolution of the ability to fly. The increased rate of metabolism accompanying flight would lead to higher levels of oxygen-free radicals [32,33]. This makes bats more prone to generating damaged DNA [34]. As mounting an immune response is energetically expensive [35] and would be detrimental, bats probably evolved mechanisms to suppress activation of immune response due to damaged DNA generated via flight, thereby leading to reduced inflammation. This would also explain why bats of certain species live longer than expected given their high metabolism and small size [36]. In bats the evolutionary suppression of inflammation and consequent susceptibility to virus infection is counteracted by constitutive expression of innate immune genes or novel genes to target viruses as described earlier. This model has been depicted in in Figure 2.1.

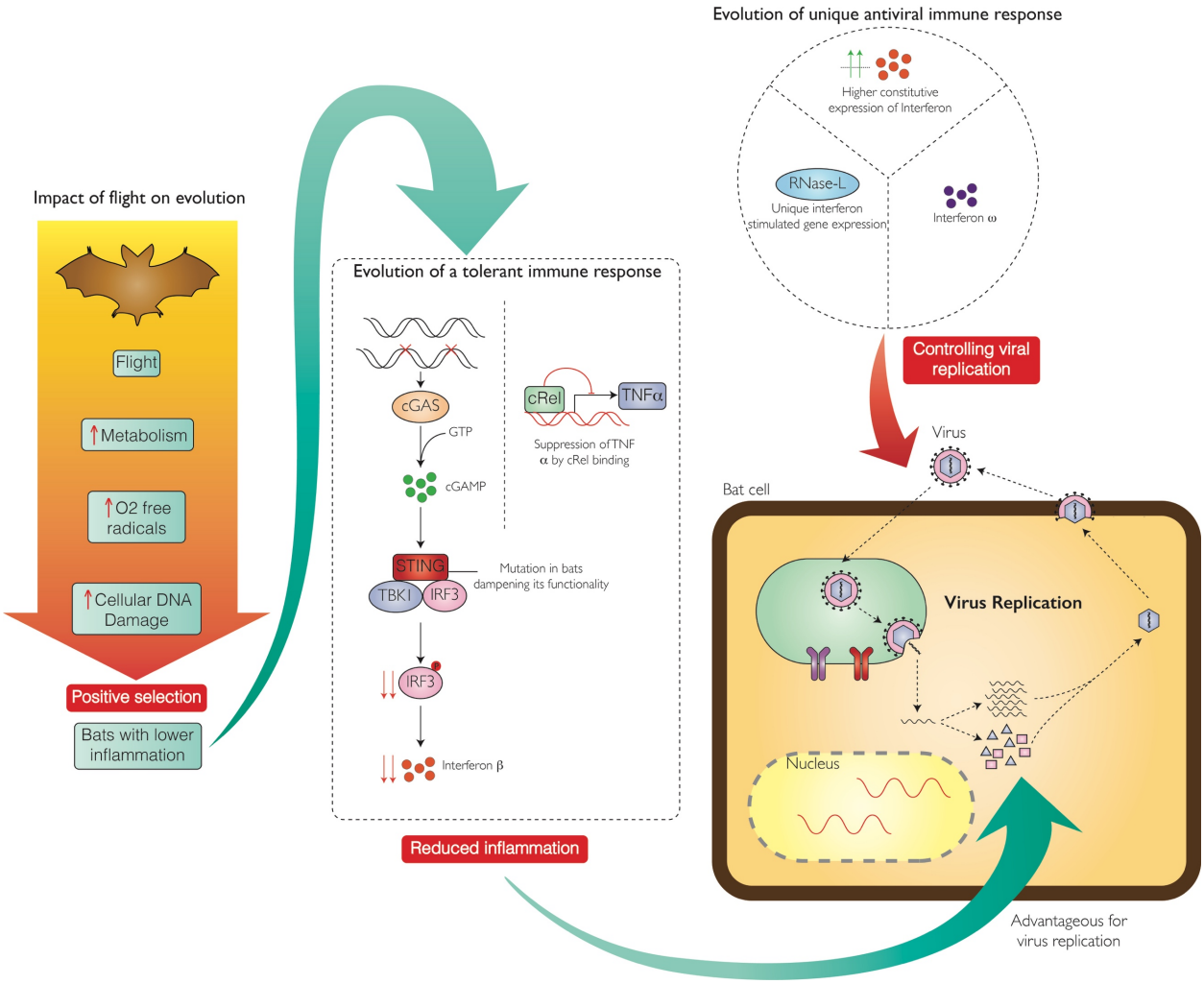

Figure 2.1. Evolution of tolerance to DNA damage and unique antiviral immune response in bats. Development of flight necessitated the evolution of bats with the ability to modulate the consequences of increased metabolic activity by suppressing inflammation (left). Inflammation was suppressed by dampening the activation of DNA sensors, such as STING, and reducing levels of inflammatory cytokines, such as TNFα (center). These traits were positively selected but a reduced inflammatory response made it advantageous for virus replication (lower right). Increased susceptibility of cells to virus replication was compensated by selection of more effective antiviral measures, such as higher constitutive expression of Interferons or unique ISG expressions (upper right). (Abbreviations used: cGAS - cyclic GMP-AMP Synthase, GTP – Guanosine triphosphate, cGMP – cyclic guanosine monophosphate, STING - Stimulator of interferon genes, TBK1 – TANK binding kinase 1, IRF3 – Interferon regulatory transcription factor 3, cRel, TNFα - Tumor necrosis factor α, RNase-L – Ribonuclease L).

2.7. Viral persistence in bats

Over the past few years, numerous viruses have been detected in bats and these viruses seldom cause any overt disease (with the exception of Tacaribe virus and rabies virus) [1,16,37]. Detection of virus and absence of disease has led researchers to suggest that bats are likely the reservoirs of these viruses. Asymptomatic infections have been observed in bats for human pathogens such as henipaviruses (Nipah and Hendra viruses), coronaviruses (Middle Eastern Respiratory Syndrome coronavirus (MERS-CoV)) and filoviruses (Marburg virus and ebolaviruses) [38–40]. For a species to be a viral reservoir, the virus needs to persist in the population. Two probable ways in which this can happen are: 1) virus infection and clearing from infected individuals is an ongoing process and introduction of naïve individuals maintains the virus in the population, 2) individuals infected with the virus are able to maintain the virus in the form of a persistent infection. Although either or both of these possibilities may influence the bat-virus relationship, there is considerable evidence for the maintenance of some viruses in bat populations by continued, low level persistence.

A study done by Sohayati *et al.* done on captive large flying foxes (also known as Malayan flying fox; *Pteropus vampyrus*) showed the possibility of recrudescence of Nipah virus (NiV) [41]. Regular sampling was done for over a period of one year to study the presence of virus and level of antibody against it. The authors discovered that one bat had a waning antibody titer with subsequent detection of virus in the urine. Following virus shedding, the antibody levels increased in this animal. As virus was undetectable in earlier samples of the same bat, the authors suggest that the virus may have persisted, probably in certain organs or cells, rendering it undetectable in blood, throat swab or urine. Within two weeks after NiV was isolated from the bat, two other male

bats seroconverted and demonstrated an increase in antibody titers, suggesting that recrudescence led to horizontal transmission.

Other studies on Marburg virus transmission among Egyptian rosette bats (*R. aegyptiacus*) showed that bats naturally infected by other experimentally inoculated bats, seem to have a prolonged incubation period [42,43]. Furthermore, the infected bats remained viremic and shed infectious virus for up to three weeks, after which there was no detectable virus in blood, oral swabs and urine samples. Despite the lack of detectable virus, even 4 months after initial infection, experimentally inoculated bats were able to transmit the virus to other contact bats [43]. One of the ways in which this can be explained is that Marburg virus persisted in the bats (probably in the spleen [42]), and a decrease in antibody levels led to increase in viral load which could then be shed to infect other bats/animals.

A bat coronavirus was also shown to persistently infect North American little brown bats (*Myotis lucifugus*) (Chapter 4) [44]. Little brown bats in captivity were able to harbor the coronavirus in their intestines and lungs during hibernation for a period of 4 months. In addition, there was no significant pathology seen in the bat tissues.

To further bolster the claim of viral persistence in wild bats, a population level study was performed to understand the circulation of zoonotic viruses in bat populations and the involved immune mechanisms (maternal antibody and acquired immune response) using mathematical modelling [45]. The study used sero-surveillance of an African henipavirus in straw-colored fruit bats (*Eidolon helvum*). While repeated introduction of virus and birthing of pups might drive viral dynamics in a large panmictic population of bats, prolonged infectious periods or latent infection of bats are required to explain henipavirus persistence in small populations (natural or colony of captive). They found that if repeated introduction of virus into small populations was the only

mechanism, then acute infections would have to be about 40 days in duration. This estimate is considerably longer than the current estimates of the detectable infectious period for henipaviruses in fruit bats, which is approximately 7 days [46]. Therefore, prolonged or latent infection has to occur in some bats for describing persistence of henipavirus in small populations.

2.8. Stress-induced spillover – a molecular perspective

Spillover events are complex and usually require successful alignment of several contributing factors [47]. One such critical factor is increased shedding of virus by bats. This factor is influenced by the host response and virus replication. Plowright *et al.* proposed a hypothesis which states that viruses infect naïve susceptible bats leading to acute infection. This subsequently progresses to a chronic or latent infection. The virus then reactivates from time to time in response to a variety of physiological and environmental triggers. This hypothesis is called as the SILI hypothesis: Susceptible-Infectious-Latent-Infectious [47]. As described above, the bat immune system is unique and virus infection probably persists in many bats.

Several factors may alter long-term, low level viral persistence in bats. Suppression of the immune response holding active virus replication in check would allow the virus to replicate to higher levels. This could happen in stressful conditions that affects the immune system. In other animals, a variety of stressors lead to reactivation of latent herpesviruses as reviewed by Grinde [48,49]. In neurons latently infected by herpes simplex virus -1 (HSV-1), viral replication is inhibited by the recruitment of $CD8^+$ T cells which secrete interferon-γ (IFN-γ) and suppress viral transcription factors via non-cytolytic granzyme mediated degradation [50]. During stress, there is a reduction of HSV-specific $CD8^+$ T cells capable of producing IFN-γ. This contributes to reactivation of the virus [51]. Studies on murine gammaherpesvirus-68 (MHV-68) in mice have shown that latent gammaherpesviruses are sequestered in cells in the spleen and can be reactivated

by stress [52,53]. Stressors, such as unfolded protein responses and hypoxia, can induce the expression of viral immediate early genes that help in initiating the lytic cycle of virus thereby reactivating it [54].

Arousal from hibernation is a stressful event for bats [55]. Many big brown bats are latently infected with a gammaherpesvirus [56]. Gerow *et al*. demonstrated that the virus reactivates from latency when big brown bats arouse from hibernation, leading to detection of the virus in blood (Chapter 8) [57]. This reactivation was also associated with a low level of antibodies against the virus. Following hibernation, the antibody levels increase, which subsequently drives the virus into latency.

In pteropid bats, immunological stress was suggested as a contributing factor in henipavirus shedding [41]. As described earlier, Sohayati *et al*. suspected that the recrudescence of NiV infection was triggered by waning antibody levels and an increased level of stress due to a combination of factors such as confinement in a cage, and physiological and behavioral changes during breeding season.

Secondary infections in humans are immunologically stressful [58]. Little brown bats are particularly susceptible to a frequently lethal fungal infection known as the white-nose syndrome, caused by *Pseudogymnoascus destructans* [59–61]. A study looking at the effects of white-nose syndrome fungus on a persistently infecting coronavirus showed that bats having the fungal infection in wings had 60 times more coronavirus in their intestines as compared to fungal uninfected bats (Chapter 5) [62]. The intestines of the fungus-infected bats exhibited a gene expression profile suggesting suppression of the innate antiviral response, which may have contributed to unrestrained viral replication. This suggests that secondary infections in bats persistently infected with viruses could increase the potential of viral shedding.

These studies indicate that waning antibody levels and suppression of innate immune response due to stress might be some of the factors leading to an increase in viral levels in persistently infected bats (Figure 2.2).

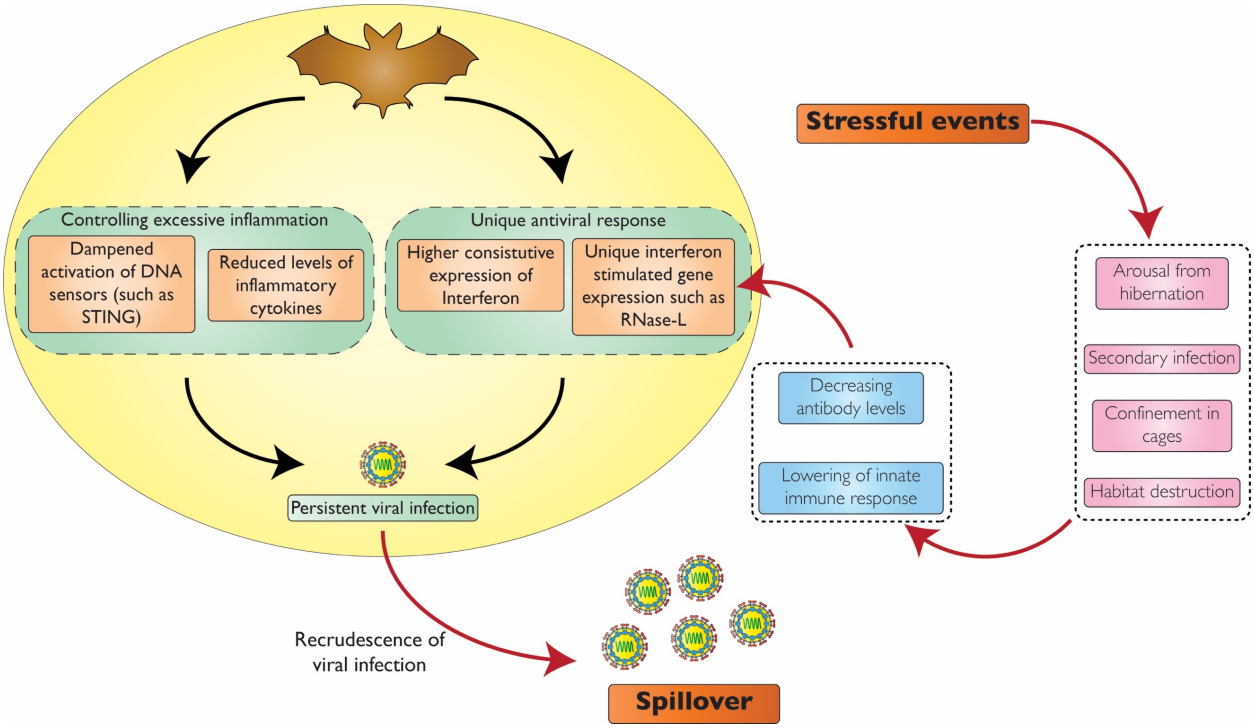

Figure 2.2. Model showing effect of stress on persistent viral infection. Viruses persistently infect bats due to their reduced inflammation (reduced DNA sensor activation and decreased inflammatory cytokine levels) and their effective antiviral immune response (Increased constitutive expression of interferons and unique ISG expressions), as depicted in Figure 2.1. Stressful events alter the balance between host and virus and lead to an increase in virus replication, thereby leading to viral shedding.

2.9. Future Directions for understanding bat-virus relationship

The unique features of bat immune responses that promote viral persistence may exert evolutionary pressures on the virus as well. Bats have superseded rodents in harboring greater number of viruses and also having greater proportion of zoonotic viruses [63]. It is, therefore, crucial to understand how evolutionary pressure may have a role in the emergence of new viral

strains. A recent study found that henipavirus genomes are best adapted to pteropid bats [64]. Adaptation of genomes refers to better capability of the virus to use host cellular machinery for its replication and protein synthesis, which is usually governed by natural selection, and diversity in codon usage bias may contribute to it. Codon usage is an interspecies bias where one codon is selected over other synonymous codons in a particular species [65]. Natural selection for viral variants works by selecting codons matching host tRNA abundance. It also selects for variants with the advantage of not activating innate response genes, such as those for toll-like receptor 9. Codon bias analysis suggested that henipaviruses have the highest level of adaptation to pteropid bats. It would be interesting to study whether other viruses also show such codon bias towards their reservoir hosts. We might be able to use such codon bias studies in the future to identify reservoir hosts of spilled over viruses. Due to coevolution with the reservoir host, the viruses would have a codon bias specific towards their reservoir host. Apart from codon bias, natural selection based on receptor utilization also has a role to play in the evolution of viruses. Variation in the efficiency of bat coronaviruses to recognize human receptors show that the viral spike protein evolved in a stepwise manner to infect human cells [66]. Despite several other receptor-binding studies [67,68], the mechanism of adaptation to new hosts is not definitively understood.

Although there is some evidence for the increase in virus replication and shedding in bats under stress, a direct link of this to spillover events has yet to be discovered. Future controlled experiments aimed at studying transmission dynamics in the presence and absence of stress in bats would lead to a more definitive answer. It is also important to look into various factors that might stress bats such as habitat destruction (deforestation), pregnancy, change in seasons and climate change. Additionally, the molecular mechanisms leading to the waning of antibodies and other aspects of adaptive immune response in bats is not known. A holistic picture of bat immune

systems and the factors leading to an increase in viral replication might help us further understand viral spillovers.

2.10. Bats of North America

Most species of bats in North America are insectivorous. They have only one pup per year during early summer and hibernate during the winter [69]. They roost in natural settings, such as trees, caves or rock crevices, and also in man made structures, such as mines, buildings and bridges. Some bat species are dependent on nectar and pollen for nutrition. Several species that spend the summer month in northern latitudes migrate south during winter to locations where food resources are available. The average life span of North American bats is 5-10 years, but some of them are known to live up to 40 years [70,71].

Bats in North American belong to four families, namely Vespertilionidae, Phyllostomidae, Mormoopidae and Molossidae. There are at least 32 species of bats belonging to the Vespertilionidae family, making it the most diverse family of North American bats. These bats are most likely to come in contact with humans. They have a small to mid-sized body, are dark brown in color, consume insects, and hibernate during winter. The two most commonly occurring species in this family are the big brown bat (*Eptesicus fuscus*) and the little brown bat (*Myotis lucifugus*). The genus *Myotis* is the most diverse genus and it comprises of bats that are adapted to capture insects in open spaces, in and around vegetation. Some of these bats like to forage over water bodies where they consume hatches of insects emerging from water. Other species of bats in the family Vespertilionidae include the Western and Eastern pipistrelles (*Pipistrellus hesperus* and *P. subflavus*), the migratory hoary and red bats (*Lasiurus* spp.), the long-eared bats belonging to the

genus *Plecotus, Euderma* and *Idionycteris*, the pallid bat (*Antrozous pallidus*) and the evening bat (*Nycticeius humaeralis*) [72].

There are five species of bats belonging to the family Phyllostomidae, also known as New World leaf-nosed bats, that are found in the Southern United States. Three of these bat species rely on nectar and pollen for food, namely Southern long-nosed bat (*Leptonycteris curasoae*), Mexican long-nosed bat (*L. nivalis*), and Mexican long-tongued bat (*Choeronycteris Mexicana*) [72]. The other two species are the California leaf-nosed bat (*Macrotus californicus*), which feeds on insects, and the hairy-legged vampire bat (*Diphylla ecaudata*), which primarily feeds on blood of wild birds [73–75].

The third family of bats found in North America is that of Molossidae, or free-tailed bats, which comprises of six species. These are the Brazilian free-tailed bat (*Tadarida brasiliensis*), the pocketed free-tailed bat (*Nyctinomops femorosaccus*), the big free-tailed bat (*N. macrotis*), and three species of mastiff bats (*Eumops*) [74,76]. The family Mormoopidae is represented by only a single species of bat, i.e., ghost-faced bat (*Mormoops megalophylla*) [73].

2.11. Coronavirus as a model for studying bat-virus relationship

2.11.1. Coronavirus detected in bats

After the SARS (Severe acute respiratory syndrome) epidemic, bats were identified as the hosts for coronaviruses and within the past 15 years, more than thirty complete coronavirus genomes and many more partial genomes have been recovered from various bat species. In most cases, these detected coronaviruses have not been isolated from bats, possibly due to lack of conducive cell culture. Coronavirus belongs to the order Nidovirales and family Coronaviridae. Coronaviridae comprises of two subfamilies, namely Coronavirinae and Torovirinae [77]. There

are four genera known for the subfamily Coronavirinae, namely, *Alphacoronavirus, Betacoronavirus, Gammacoronavirus* and *Deltacoronavirus* [78]. Among these four genera, only *Alphacoronavirus* and *Betacoronavirus* have been found in bats [79]. Bat coronaviruses have been detected in North and South America, Asia, Europe, Africa and Australia. The global distribution and detection rate in bats are high for both *Alphacoronaviruses* and *Betacoronaviruses* [80,81].

2.11.2. Genome organization and structure of the virion

Coronaviruses contain a non-segmented, positive-sense RNA genome of approximately 30kb in size. It is the largest known genome for any RNA virus [77,78]. The genome has a 5' cap and a 3' poly-A tail, which makes it act like a mRNA for translation of proteins. The replicase gene, which codes for RNA dependent RNA polymerase (RdRp) gene occupies 2/3rd of the genome (~20kb). The remaining ~10kb of the genome contains structural and accessory proteins. The organization of coronavirus genome is 5'-leader-UTR-RdRp-Spike(S)-Envelope(E)-Membrane(M)-Nucleocapsid(N)-3'UTR-poly-A tail (Figure 2.3). Accessory genes are usually interspersed in between the structural genes. Although these accessory genes are not imperative for virus replication in tissue culture, they play an important role in pathogenesis of the virus *in vivo* and variants that have a replicative advantage may be selected in particular species [82].

Coronaviruses virions are enveloped and approximately 125nm in size [83]. They are spherical in shape with club-like projections. These projections make the virion look like a crown, ergo "Corona" name was given. The virus particle contains four main structural proteins, namely spike, membrane, envelope and nucleocapsid. The spike protein is used by the virus for entry into the host cell. The S1 domain of the spike that interacts with host receptor is also known as the receptor binding domain, and is highly variable [84]. This variability determines the host species tropism for the coronavirus [85]. The membrane protein exists as a dimer in the virion and

promotes membrane curvature as well as binding to the internal nucleocapsid protein [86]. The envelope protein is found in small quantity in virion, but has a role as an ion channel and is required for pathogenesis of coronaviruses [87]. Nucleocapsid is present in the interior of the capsid and binds to the RNA aiding the packaging of the RNA into the virion [88]. Some *Betacoronaviruses* also contain a fifth structural protein, known as the hemagglutinin-esterase (HE) which binds to sialic acids on surface glycoproteins, which helps in enhancing the entry of the virion [89].

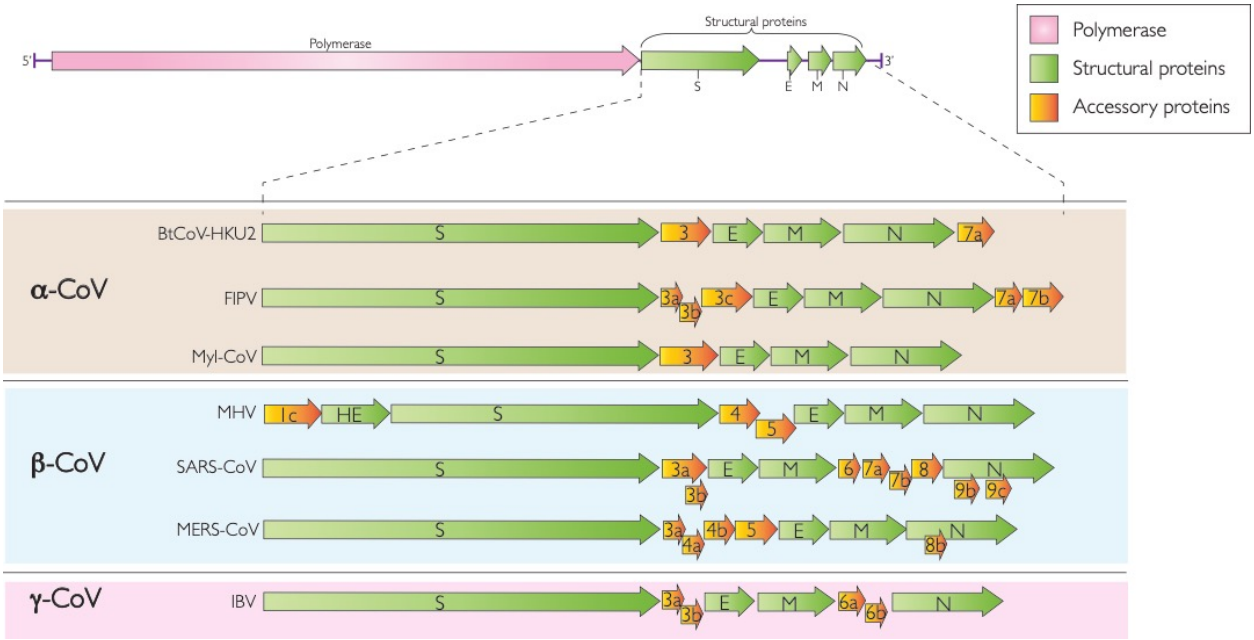

Figure 2.3. Genome organization and structure of coronaviruses

2.11.3. Life cycle of coronavirus

The attachment of the coronavirus is mediated largely via spike protein. The receptor binding domain in the S1 region of spike protein interacts with host receptors [78]. Most coronaviruses use peptidases for the attachment but the function of the peptidases in attachment is unclear, as entry of the virion occurs even in the absence of the enzymatic domain. *Alphacoronaviruses* usually utilize aminopeptidase N (APN) receptor [90], SARS-CoV and HCoV NL63 utilize the angiotensin-converting enzyme-2 (ACE2) as their receptor [91,92], murine

hepatitis virus (MHV) utilizes CEACAM1 as its receptor [93] and MERS-CoV uses dipeptidyl-peptidase-4 (DPP4) as their receptor [94].

Following attachment of spike with host receptor, entry of virus into host cell cytosol occurs via acid dependent proteolytic cleavage of spike protein by cathepsin, which occurs in the cytoplasm or endosome [95]. It cleaves the S1 domain of spike exposing the fusion domain in the S2 domain [84,95]. The fusion domain has heptad repeats which form a six-helix bundle that allows the virus and cell membranes to combine [84]. This is followed by the release of the virion into the cytoplasm.

Following release into the cytoplasm, the viral genome functions as an mRNA and is translated to produce the replicase protein. The replicase gene encodes 2 ORFs namely rep1a and rep1b which translates into pp1a and pp1ab protein [96]. The replicase gene has an RNA pseudoknot that causes a ribosomal frameshift resulting in the two proteins [97]. The viral RNA produces genomic and sub-genomic RNAs. These sub-genomic RNAs serve as mRNAs for the various structural and accessory genes. For the production of these genomic and sub-genomic RNAs, the RdRp protein has a unique mechanism. Every sub-genomic RNA also contains a leader sequence, which is shared by all subgenomic RNAs that possess coding sequences for viral proteins. The sub-genomic RNAs are produced by negative strand sub-genomic RNA which contains anti-leader sequence at 3'-end of it [98,99]. So, while synthesizing the negative strand, the RdRp jumps at the end of coding sequences to the leader sequence and joins the two non-contiguous sequences. It is still unclear, how RdRp bypasses all the other coding sequences to the 5'end of the genome to include the leader sequence. What determines the shift from making negative sense sub-genomic RNA to making full length negative sense genomic RNA, is also not known. In addition to these basic mechanisms, coronaviruses also have a mechanism of

recombining using homologous and non-homologous recombination [100]. This is crucial for viral evolution as it allows exchange of segments in between viruses.

From the negative sense full length genomic RNA, positive sense genomes are synthesized and from positive sense sub-genomic RNAs, spike, envelope and membrane proteins are made in the endoplasmic reticulum-Golgi intermediate compartment (ERGIC) [101,102]. Coronavirus genomes are first encapsidated using the nucleocapsid protein and then uses the ERGIC for viral envelopment. Membrane protein interacts with nucleocapsid protein to guide the assembly of virion [103]. The formed virions are then transported to the cell surface via vesicles and subsequently release by exocytosis [78].

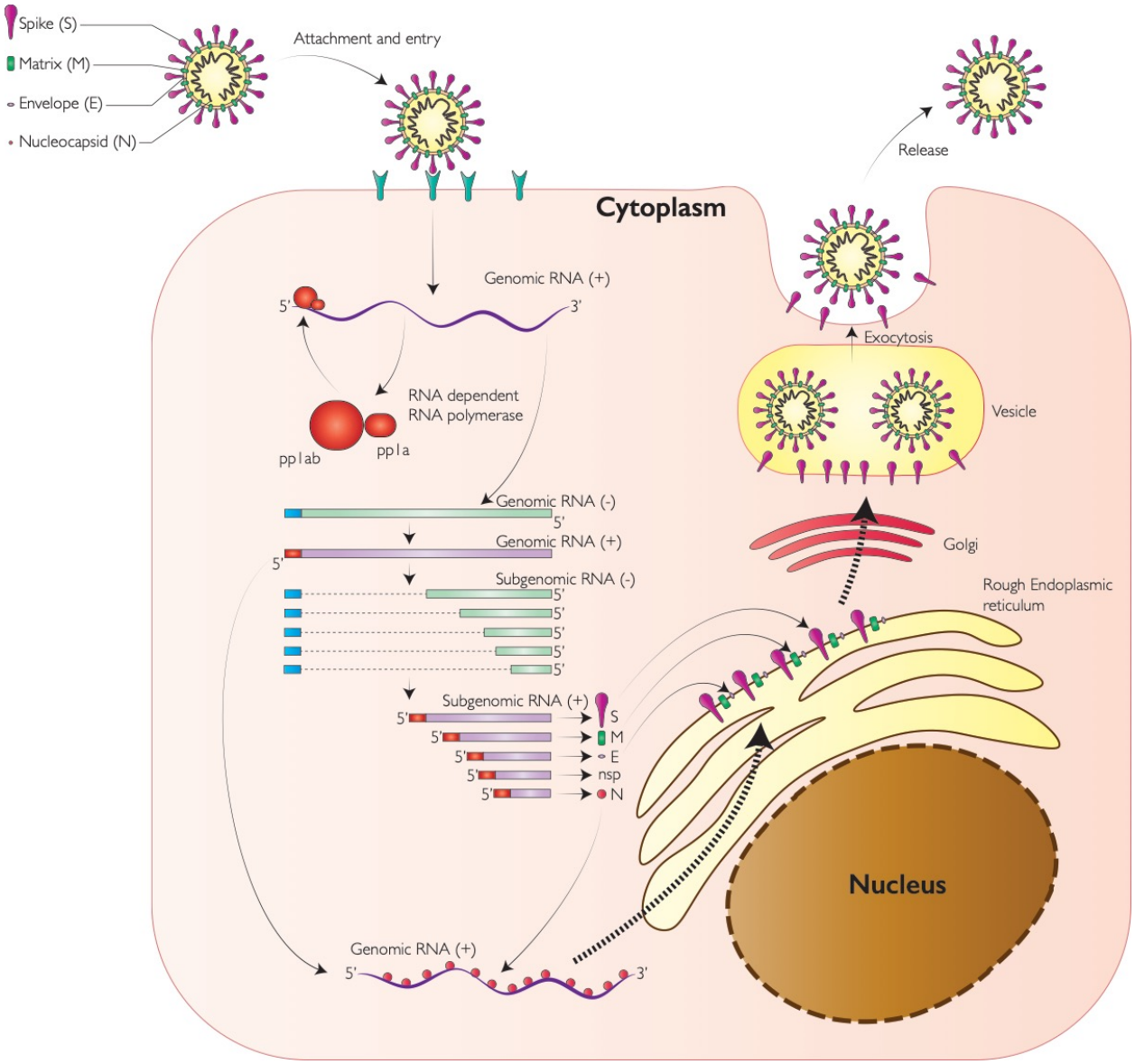

Figure 2.4. Schematic diagram depicting coronavirus replication. Coronavirus life cycle in the cell begins with the attachment of spike protein in the virion to cellular receptors. Following entry, the positive sense genomic RNA is released into the cytoplasm. Genomic RNA encodes for RNA dependent RNA polymerase protein (RdRp), structural proteins (S, M, E and N) and non-structural proteins. A non-coding segment upstream of E protein, known as UpE, is targeted by quantitative PCRs to detect the amount of MERS-CoV RNA in the cell. Following the release of positive sense genomic RNA into the cytoplasm, it is translated to produce RdRp, which then produces negative sense and more positive sense genomic RNA. This positive sense genomic RNA then aids in the production of subgenomic negative sense RNA, which subsequently helps in producing subgenomic positive sense RNA. Positive sense subgenomic RNA translates to produce structural and non-structural proteins. Protein translation takes place in the endoplasmic reticulum, and

subsequently, these proteins are processed in the Golgi bodies. Positive sense genomic RNA and structural proteins of the virus are then assembled and released via exocytosis.

2.11.4. Coronavirus interaction with host pathways

To control virus infections, host, in case of certain virus infections, induces apoptosis to control virus replication. But in case of coronaviruses, the virus engages in induction of apoptosis for efficient virus production [104]. The coronavirus exploits this mechanism to destroy immune cells which would otherwise limit virus production [105]. Apoptosis can be induced by either an extrinsic pathway, mediated via death ligands binding to death receptors, or an intrinsic pathway, regulated via pro-apoptotic or anti-apoptotic Bcl2 (B-cell lymphoma 2) family proteins which subsequently induces MOMP (mitochondrial outer membrane permeability) [106]. During coronavirus infection, viral proteins target both extrinsic and intrinsic apoptosis pathways. For example, SARS-CoV has evolved proteins that are pro-apoptotic like S, E, M, N, ORF-6, -7a and -9b [107–110].

During coronavirus infection, pattern recognition receptors, such as toll-like receptors (TLRs), retinoic acid inducible gene-I (RIG-I) and melanoma differentiation-associated protein 5 (MDA5), sense the viral infection and trigger signaling pathways, such as mitogen activated protein kinase (MAPK) and nuclear factor kappa-light-chain-enhancer of activated B cells (NF-κB), to produce interferons [107]. Secreted interferons can bind to interferon receptors, in an autocrine or paracrine manner, to stimulate janus kinases – signal transducer and activator of transcription proteins (JAK-STAT) signaling pathway which induces interferon stimulated gene production [111]. Coronavirus proteins, such as SARS-CoV N, E, ORF-3a and -7a and MERS-CoV PLPro, ORF-4a and -4b, are known to inhibit NF-κB pathway whereas [112,113]. MERS-CoV M, ORF-4a, -4b and -5 are known to inhibit IRF3 [114]. SARS-CoV ORF-3b and -6 inhibit

at a downstream signaling just prior to ISG production [107,115]. MAPKs are a serine or threonine kinases that are induced in response to stressors and ultimately results in the regulation of cellular processes like cell survival, cytokine production and apoptosis [116]. Coronaviruses have been shown to induce MAPK activation. Inhibition of p38 activation, one of the key adaptors in MAPK pathway, has suppressed the HCoV-229E-induced cytopathic effects and led to a decrease in viral titers [117]. The observation on c-Jun N-terminal kinases (JNK) activation, another key adaptor of MAPK, has shown that the pathway could have an anti-apoptotic (HCoV-229E and SARS-CoV) or pro-apoptotic role (IBV) depending on the strain of virus [118].

The primary organelle in the cell that handles protein synthesis, folding, processing and post-translational is the endoplasmic reticulum (ER) [119]. However, if the level of protein production exceeds the capacity of the ER, then misfolded or unfolded protein starts to accumulate. This eventually initiates a cascade of signaling pathways, known as the unfolded protein response (UPR) [120]. There are three primary ER transmembrane sensors that initiate UPR, namely protein kinase R (PKR) like endoplasmic reticulum kinase (PERK), inositol requiring protein 1 (IRE1) and activating transcriptional factor 6 (ATF6) [121]. UPR activation leads to restoration of ER homeostasis by enhancing protein folding, decreasing protein translation or producing more chaperones and other proteins aiding in folding. In case the UPR response is not able to restore homeostasis, then the cell triggers apoptosis mechanisms [120]. During viral infections, the virus hijacks the host protein translation machinery including ER and exploits it to produce viral proteins. This initiates the UPR response which works as an antiviral response. However, coronaviruses have evolved viruses that target the various signaling pathways of UPR such as SARS-CoV E, ORF-3a, -8ab [118].

2.11.5. Coronavirus pathogenesis

Coronaviruses usually have a predilection to cause disease in the respiratory system or in the gastrointestinal system [77]. Two of the deadly coronaviruses infecting human beings, namely SARS-CoV and MERS-CoV, primarily cause respiratory illness. The SARS-CoV infection leads to massive inflammation in the lungs and has a mortality rate of ~9% [122]. But since SARS-CoV transmission was poor, it led to the decline of incidence after 2003. MERS-CoV also leads to similar illness as SARS-CoV, but the mortality rate is much higher i.e. ~35% [123]. Other human coronaviruses like HCoV-229E, NL63 and OC43 causes common cold and more severe disease in neonates, elderly and people with underlying diseases [124].

One of the most well-studied coronavirus is the murine hepatitis virus (MHV) which causes respiratory, hepatic, enteric and neurologic manifestations in mice [125,126]. Other coronaviruses like Transmissible Gastroenteritis Virus (TGEV), Porcine epidemic diarrhea virus (PEDV) and the recently identified swine acute diarrhea syndrome (SADS) causes acute gastroenteritis in young piglets [127]. This leads to significant morbidity and mortality. Another coronavirus, Porcine hemagglutinating encephalomyelitis virus (PHEV) leads to enteric infection but is also able to infect nervous system leading to encephalitis. Feline enteric coronavirus (FCoV) leads to asymptomatic infection in cats but mutations in persistent infection leads to transformation of the virus generating a highly virulent strain known as Feline infectious peritonitis virus (FIPV) [128]. This leads to a lethal disease known as feline infectious peritonitis. In chickens, Infectious bronchitis virus (IBV) causes respiratory tract infection but some strains can also affect the uro-genital system leading to renal disease [129].

2.11.6. Animal origins of coronaviruses

Global screening of bats has led to the discovery of myriad of coronaviruses in bats. It has been thought that most of the coronaviruses have their origin among bats as depicted in figure 2.5. MERS-CoV likely spilled over to dromedary camels about 30 years ago and since then has circulated in camels [130]. Progenitor of HCoV-229E and NL63 have been detected in African bats and camelids probably are the intermediate hosts for HCoV-229E [131,132]. The SADS coronavirus is a novel strain of the *Rhinolophus* bat coronavirus-HKU2 [133].

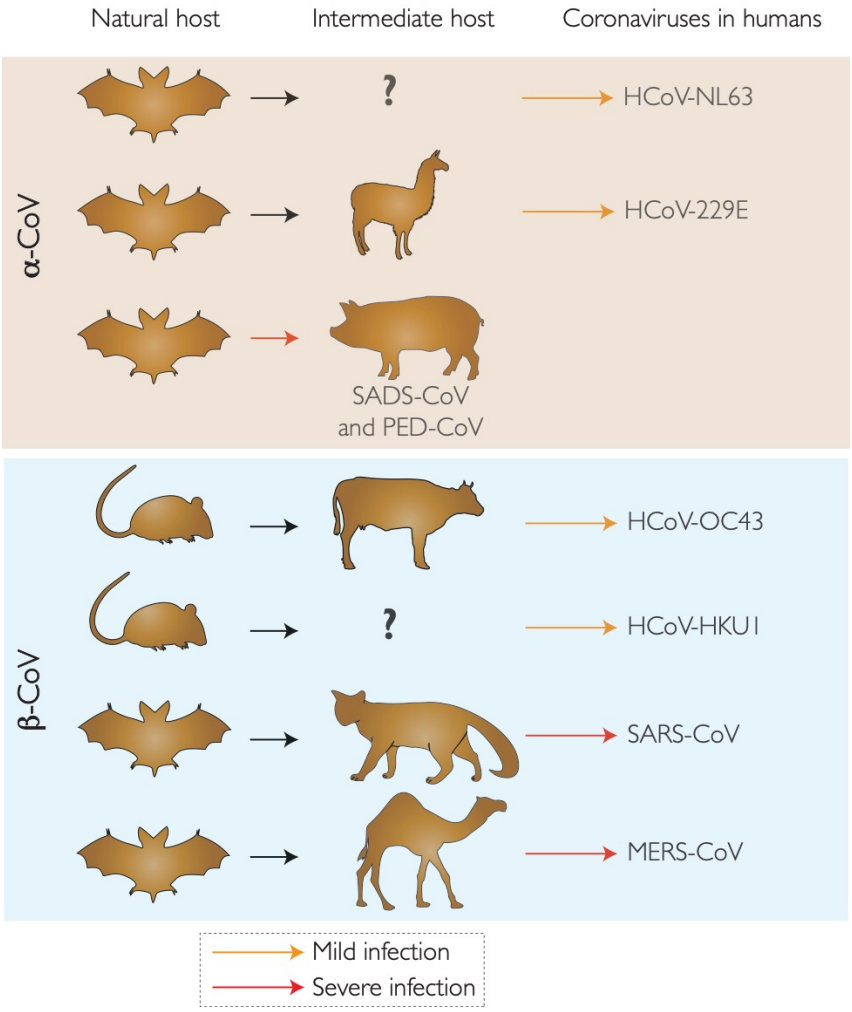

Figure 2.5. Animal origin of coronaviruses. Rodents and bats are the known natural hosts for coronaviruses. Infection in other species is a result of spillover. Some of the other species, such as civet cats and camels, act as intermediate host between natural host and humans.

2.11.7. Evidence of coronavirus peristence in hosts

For understanding spillovers, it is important to know about persistence of virus in hosts. Persistent infection would put a continuous evolutionary pressure on the virus which would have implications in pushing emergence of new variants. Such variants could facilitate spillovers to other species. Certain vertebrate hosts show persistence of coronavirus. In cats, feline coronavirus infections occur due to two pathotypes, namely feline enteric coronavirus (FECV – ubiquitous enteric biotype) and feline infectious peritonitis virus (FIPV – virulent biotype) [134]. Feline coronavirus infection occurs via feco-oral route and it can establish persistent infection (FECV) in enterocytes. This infection leads to mild, non-specific symptoms and the virus is intermittently shed in the feces. The FECV infection converts to FIPV in some hosts, the exact mechanism of which is not yet fully understood [135]. It is also interesting to note that coinfection of cats with other enteropathogens increases severity of feline coronavirus infection [136]. Another such host with persistent infection is in cows for bovine coronavirus. Oral inoculation of bovine coronavirus has shown that the virus can persist in the intestines of calfs. The virus is initially excreted at higher amounts but subsequently, sheds at low titers. The virus was shown to be present in peyer's patches, 3 weeks after inoculation [137].

Human coronavirus OC43 and 229E has also been shown to persistently infect human neuronal cells [138,139]. It has been hypothesized that SARS-CoV spillover from bats to humans occurred via an intermediary host, palm civet cats. Experimental inoculation of palm civet cats with two strains of SARS-CoV has shown that the virus can persist for several weeks but clinical signs of infection, such as lethargy and elevated temperature, were observed [140]. In case of MERS-CoV, spillover occurs from camels to humans [141]. In camels, MERS-CoV causes mild upper respiratory tract disease and viral RNA can persist upto 5 weeks [142]. During my thesis, I

have characterized persistence infection in bats (Chapter 4) and how this relationship alters in response to stress (Chapter 5).

2.12. Gammaherpesvirus as a model for studying bat-virus relationship

2.12.1. Gammaherpesviruses in bats

Herpesviruses have a double-stranded DNA genome and are enveloped. They belong to the family Herpesviridae [77]. There are three genera in this family namely, *Alphaherpesvirinae*, *Betaherpesvirinae* and *Gammaherpesvirinae*. *Gammaherpesvirinae* consists of oncogenic viruses like Ebstein-Barr virus (EBV) and Kaposi Sarcoma-associated herpesvirus (KSHV). Screening of bats worldwide has led to the detection of gammaherpesviruses in numerous bat species [143–146]. Two gammaherpesviruses isolated from bats are *Myotis* gammaherpesvirus 8 (isolated from a *Myotis velifer incautus* cell line) [147] and *Eptesicus fuscus* gammaherpesvirus (Chapter 7) [56].

2.12.2. Genome, virion structure and lifecycle of gammaherpesviruses

Gammaherpesviruses are enveloped, spherical or pleomorphic viruses of 150-200nm in size [77]. Genomes of gammaherpesvirus are linear and non-segmented dsDNA of about 180kb in length. Gammaherpesviruses bind to their surface receptors and enter the cell. KSHV uses Ephrin A2 and EBV uses CD21 as their receptors [148,149]. Such receptor binding can also initiate cell signals, such as phophoinositide 3-kinase (PI3K), that modify nuclear factors that are crucial for viral gene expression [150]. The viral capsids, with the viral genome inside are transported via microtubules such that the viral DNA does not activate DNA sensors in the cells [151,152]. The viral capsid then interacts with the nuclear pore which subsequently injects the viral genome into the nucleus [153]. IFNγ inducible protein 16 (IFI16) binds to the viral DNA and activates inflammasome pathway. Gammaherpesviruses are unable to inhibit activation of IFI16 and

therefore, it suggests that IFI16 probably has a crucial role to play in initiating latent infection [154].

Primary infection of gammaherpesviruses usually results in a slow and abortive lytic replication which is sometimes followed by a robust latent infection [54]. Epigenetic mechanisms play an important role in the switch from latent to lytic replication. Condensation of viral DNA ensures that it is protected from DNA damage. One of the ways the virus achieves this is by circularization. Histone modifications and chromatin assemble help in establishing latency. The host cell has promyelocytic leukemia nuclear bodies (PML NBs) that chromatin assembly and has a role in the intrinsic resistance against viral nuclear infection. However, the virus also codes for tegument proteins which destroys the PML NB [155].

Latent infection by Epstein-Barr virus could be established in four distinct ways [156,157]. Type 0 is the most restrictive type, where no viral gene expression occurs and primarily observed in resting memory B cells. In case of type 1 latency, expression of Epstein-Barr nuclear antigen 1 (EBNA1) is observed and this type of latency occurs in proliferating memory B cells or in Burkitt's lymphoma. Type 2 occurs in Hodgkin's lymphoma where along with EBNA1, other genes like LMP1, 2A and 2B are also expressed. Type 3 is the highly permissive latent infection which occurs in immortalized cell lines and expression of EBNA1, EBNA2, EBNA3A, EBNA3B, LMP1, 2A and 2B are observed. Kaposi sarcoma associated virus shows less variation than EBV. Its latent cycle is primarily regulated by latency associated nuclear antigen. It is the KSHV orthologue for EBNA1. LANA binds to the viral DNA and promotes DNA replication and episome maintenance during latency.

2.12.3. Reactivation of gammaherpesvirus

Reactivation of gammaherpesvirus is crucial for completing the virus life cycle resulting in new virus particle production. This reactivation could be stimulated by several stressors such as unfolded protein response and hypoxia, or by cellular differentiation signals [158]. For reactivation to start, disruption of repressive chromatin status of viral DNA is imperative. Viral Zta for EBV and RTA, for both EBV and KSHV, are required for transcription of immediate early genes which initiate the lytic replication (Figure 2.6) [54]. Reactivation of KSHV occurs due to chemicals, like sodium butyrate or tetradecanoyl-phorbol-13-acetate (TPA), viral coinfection, oxidative stress and hypoxia, all of which lead to activation of RTA promoter [159,160]. RTA is also capable of autoregulating itself by signaling repressor pathway or by self-ubiquitination [161,162]. LANA counteracts the RTA expression by interacting with its promoter. microRNAs from viruses also help in maintaining latency of gammaherpesvirus and knockdown of these microRNA also leads to reactivation of the virus [163].

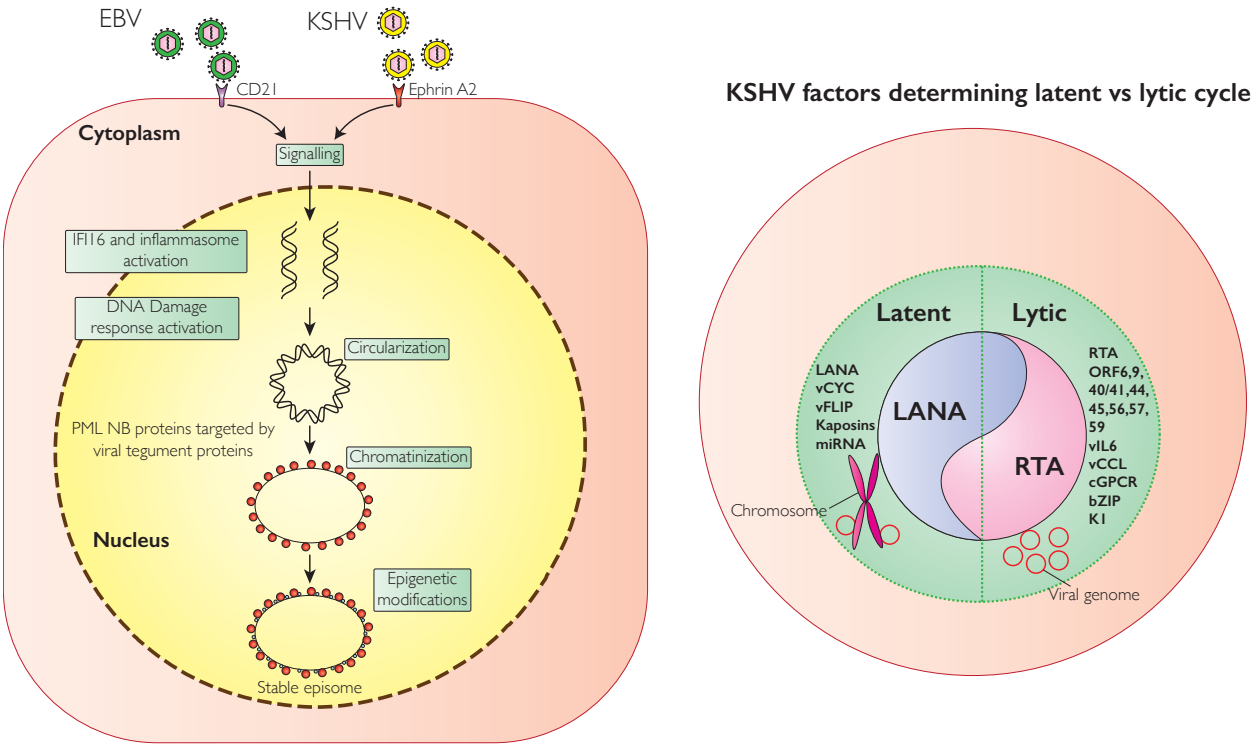

Figure 2.6. Life cycle of gammaherpesviruses (A) Early events that determine the establishment of latent infection in gammaherpesviruses (B) KSHV factors that determine latent vs lytic cycle. This figure is inspired from Purushothaman *et al* [164] and Lieberman [54].

2.12.4. Gammaherpesvirus interaction with host immune response and pathways

KSHV leads to Kaposi sarcoma in HIV patients who have a depleted CD4+ T cell population. This suggests that T cell response has an important role to play in the host-pathogen interaction in relation to gammaherpesviruses [165]. The virus has developed mechanisms to prevent detection by T cells but at the same time has to maintain either latency or lytic replication in the host [166]. While latent infection, gammaherpesviruses expresses atleast one latency protein. Evolutionarily gammaherpesviruses have selected this protein against MHC-I binding, which is advantageous for the virus, as MHC-I binding of viral peptide followed by presentation to CD8+ T cells is imperative for developing T cell response. Preventing this presentation allows the virus to go undetected in cells. Latency protein for EBV, EBNA-1, also controls its translation and degradation, thereby minimising the protein turnover rate [166]. Another strategy employed by latency protein is to prevent proteosomal degradation which in turn prevents the formation of peptides that can bing to MHC-I for presentation. The EBNA-1 latency protein achieves this with the help of central glycine-alanine repeats [167,168]. Similarly KSHV latency associated nuclear antigen (LANA) also has a similar central stable region preventing proteosomal degradation [169]. For gammaherpesviruses of other species, ORF73 protein aids in the escape of T cell mediated response [170,171]. During lytic cycle of gammaherpesvirus, the virus prevents MHC-I presentation at several levels such as inhibiting peptide transport across ER membrane, anchoring proteins to the ER membrane, or by endocytosing MHC-I from the cell surface by viral proteins [172–175]. KSHV vIRF3 protein is also known to inhibit class II transactivator which is necessary for inducing MHC-II proteins [176]. In addition to that endothelial cells infected with KSHV also

secreted a factor which prevented MHC-II expression in neighboring cells [177]. Overall, this prevents CD4+ activation.

Gammaherpesviruses have also evolved mechanisms and proteins to inhibit apoptosis and autophagy pathways. KSHV targets the extrinsic apoptotic pathway, i.e. pro-caspase 8 and activated caspase 3 with the help of vFLIP (viral Fas-associated death domain-like interleukin-1β-converting enzyme-inhibitory protein bcl2) and K7 proteins [165]. EBV vBcl2 inhibits the intrinsic apoptotic pathway, by preventing the oligomerization of Bax/Bak (Bcl2-associated X protein) and MHV-68 vMAP (viral mitochondrial antiapoptotic protein), which antagonizes VDAC that releases cytochrome c [178–180]. In addition to that KSHV K7 protein inhibits stress-induced apoptosis by interacting with calcium-modulating cyclophilin ligand (CAML) leading to an increase in cytosolic Ca^{+2} levels [181]. This mechanism protects cells from mitochondrial damage and thereby preventing apoptosis. Gammaherpesviruses have also evolved mechanisms to evade autophagy, a homeostatic process that engulfs and digests bulk cytoplam under nutrient-deprived conditions. vBcl2 targets Beclin 1, an autophagy regulator molecule, and vFLIP targets LC3 processing enzyme, a component of autophagosome, ultimately leading to inhibition of autophagy [182,183].

Like coronaviruses, gammaherpesviruses have also evolved mechanisms to antagonise interferon signalling. Gammaherpesviruses target several key interferon regulatory factors such as IRF-1, IRF-3, IRF-5 and IRF-7, by interfering with their activation using various viral proteins such as KSHV vIRF-1, -2, -3 and EBV PK and Zta [165,184]. KSHV also has mechanism to suppress RIG-1 and MyD88 (Myeloid differentiation primary response 88) mediated signalling [185,186]. These ultimately lead to inhibition of intereferon production.

2.12.5. Pathogenesis of gammaherpesvirus

KSHV and EBV are known to cause oncogenesis in humans. Mostly in AIDS (Acute immunodeficiency syndrome) patients, KSHV causes Kaposi sarcoma, primary effusion lymphoma, and Castleman's disease [77]. In normal individuals, KSHV infection usually remains latent. Ebstein-Barr virus causes Burkitt's lymphoma. But majority of the pathogenesis information comes from studies on MHV68. The acute lytic replication of MHV68 occurs in the epithelial and endothelial cells of the lungs [187]. This replication is typically cleared in 12 days following which the virus establishes latency in secondary lymphoid organs. The primary reservoirs of gammaherpesviruses are B cells, but other cells like macrophages, dendritic cells and endothelial cells can also be infected (Figure 2.7). Lymphoma is usually manifested in immunocompromised individual animals.

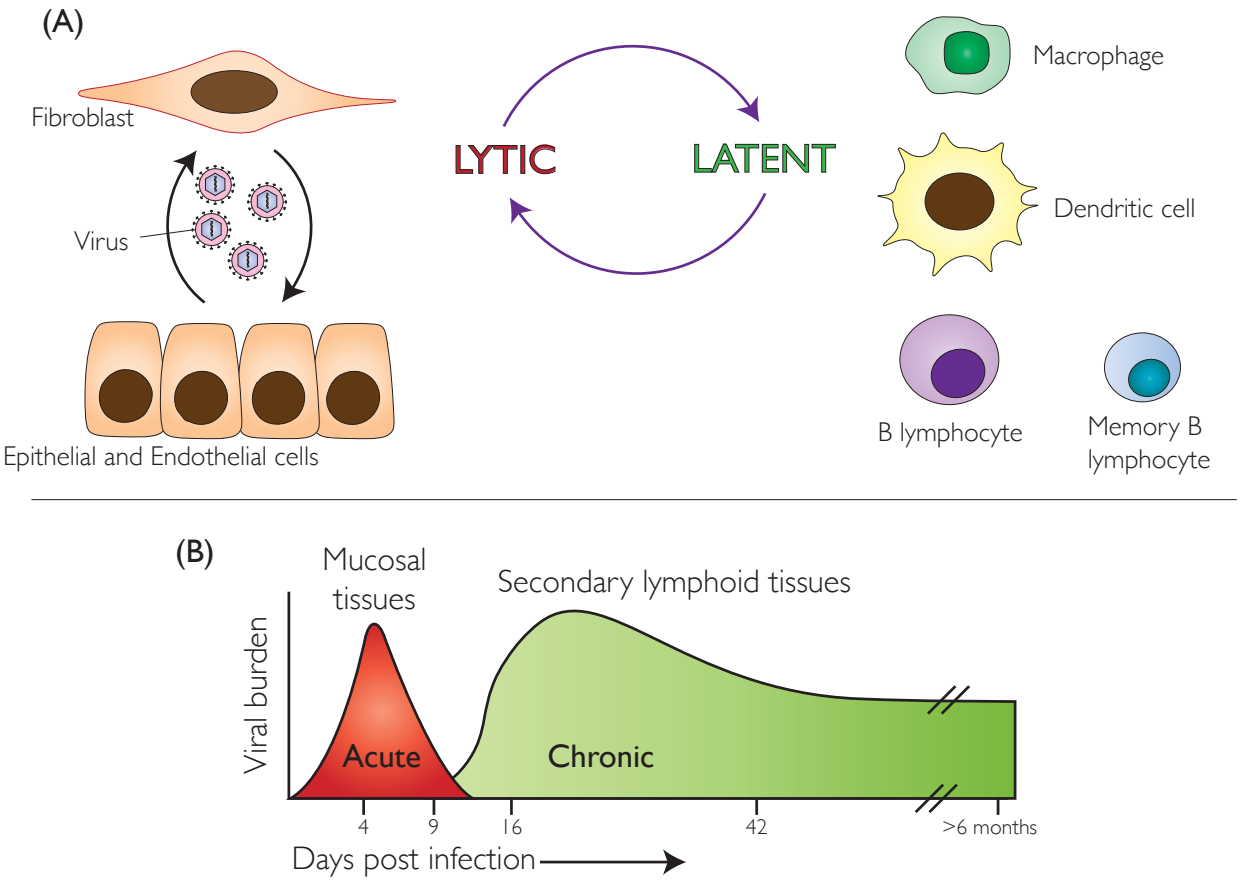

Figure 2.7. Pathogenesis of gammaherpesvirus. (A) Gammaherpesvirus lytic replication occurs in fibroblasts, epithelial and endothelial cells whereas latent life cycle has been observed in macrophages, dendritic and B lymphocytes. (B) The lytic replication happens during the acute stage of infection and latent replication takes place during the chronic stage. This figure is inspired from Cieniewicz *et al* [187].

Chapter 3: Rationale, hypothesis and objectives

3.1. Rationale to study factors altering bat-virus relationship

As mentioned in the Introduction and Literature review, bats are potential reservoirs of several emerging viral diseases in people and other animals. The circumstances under which these viruses spillover from bats to other species is not fully understood. However, several studies indicate that bats are likely to be persistently infected with viruses and increase in viral replication in response to stressors may increase the possibility of spillover. While there is considerable literature on the interactions of these viruses with their secondary hosts, their surrogate laboratory animals or cell-lines derived from them, little is known about the interactions of bat viruses in their natural hosts. A better understanding on how these viruses replicate in bats and how bats respond to them may uncover the reasons for spillovers and may also suggest strategies for mitigating the effects of disease caused in other species by bat viruses.

The objective of my thesis was to test the broad hypothesis that ***bats have long-term balanced and benign relationships with viruses, with whom they have co-evolved, and that a variety of stressors disrupt this balance allowing increased viral replication.*** Since viruses have co-evolved with their natural bat hosts over millennia, my objective was to study viruses that naturally infect two species of North American bats. I characterized a coronavirus that infects most little brown bats (Chapter 4) and a gammaherpesvirus that we isolated from big brown bats (Chapter 7).

For the little brown bat coronavirus, I had access to tissue samples archived from an earlier study of the pathophysiology of white-nose syndrome, a fungal disease that is lethal for most species of bats [188]. My objective was to test the hypothesis that the systemic stress of fungal infection would lead to changes in gene expression patterns in the intestine of bats, the site of

coronavirus persistence and that these changes would lead to increased virus replication (Chapter 5).

Since persistent viral infections in the animal, especially a wild-life species, are difficult to manipulate and examine in detail, my next objective was to establish a persistent coronavirus infection in cultured bat cells and to use this model to confirm my observations from bats and to study the molecular triggers that disrupt persistence (Chapter 6).

To determine if our observations on the effect of stress on the coronavirus-bat relationship would be borne out by other viruses as well, I studied the relationship of the big brown bat herpesvirus with its natural free-living host. My objective was to test the hypothesis that most bats would be latently-infected with the herpesvirus and that the physiological stress of arousal from hibernation would lead to reactivation of the latent virus (Chapter 8).

Chapter 4: A persistently infecting coronavirus in hibernating *Myotis lucifugus*, the North American little brown bat

4.1. Copyright

© 2017. Microbiology Society explicitly grants the authors permission to reuse their own content without seeking further permission, provided that the original source of the material is credited appropriately.

This manuscript has been reformatted from the original version for inclusion in this thesis.

4.2. Citation

Subudhi, S., N. Rapin, T. K. Bollinger, J. E. Hill, M. E. Donaldson, C. M. Davy, L. Warnecke, et al. "A Persistently Infecting coronavirus in Hibernating *Myotis Lucifugus*, the North American Little Brown Bat." *J Gen Virol* 98, no. 9 (September 2017): 2297–2309. https://doi.org/10.1099/jgv.0.000898.

4.3. Contribution

Several authors contributed significantly during this study. Bat samples were obtained from a previous experiment in our lab [189]. The initial polymerase chain reaction (PCR) for the detection of coronavirus and sequencing was done by NR. CMD and MED analyzed the RNASeq data and provided me with sequence reads that did not align with bat genome (non-bat RNASeq reads). The phylogenetic analysis of the coronavirus sequences was done by me. Janet Hill and I assembled the whole genome of the bat coronavirus using non-bat RNASeq reads obtained from bat intestines and also made the phylogenetic tree using complete genomes of 34 representative

coronaviruses. I developed antibodies against the bat coronavirus nucleocapsid protein and then developed immunohistochemistry assay for the detection of the virus which subsequently helped in the detecting the viral infection in the lungs. Trent Bollinger helped us with the pathological scoring of the lung tissues infected with virus. I wrote the initial draft of the manuscript and NR, MED, CMD, TKB and VM contributed to editing of the various drafts.

4.4. Abstract

Bats are important reservoir hosts for emerging viruses including coronaviruses that cause diseases in people. Although there have been several studies on the pathogenesis of coronaviruses in humans and surrogate animals, there is little information on interactions of these viruses with their natural bat hosts. We detected a coronavirus in intestines of 53/174 hibernating little brown bats (*Myotis lucifugus*), as well as in the lungs of some of these individuals. Interestingly, presence of the virus was not accompanied by overt inflammation. Viral RNA amplified from little brown bats in this study appeared to be from two distinct clades. The sequences in Clade 1 were very similar to the archived sequence derived from little brown bats and sequences from Clade 2 were more closely related to the archived sequence from big brown bats. This suggests that two closely related coronaviruses may circulate in little brown bats. Sequence variation among coronavirus detected from individual bats suggested that infection occurred prior to hibernation, and that the virus persisted up to four months of hibernation in the laboratory. Based on the sequence of its genome, the coronavirus was placed in the *Alphacoronavirus* genus along with some human coronaviruses, bat viruses and the porcine epidemic diarrhea virus. Detection and identification of an apparently persistent coronavirus in a local bat species creates opportunities to understand the dynamics of coronavirus circulation in bat populations.

4.5. Introduction

In recent years, three coronaviruses (CoV) have emerged to have a significant impact on global health and economy. Two of these, that cause Severe Acute Respiratory Syndrome (SARS, [190]) and Middle Eastern Respiratory Syndrome (MERS, [67,191–193]), are human pathogens. The SARS outbreak in 2002-2003 led to 8096 cases with 10% mortality in 27 countries [194]. Since September 2012, about 1900 cases of MERS have been reported with a mortality rate of about 35% [123]. The third coronavirus, porcine epidemic diarrhoea coronavirus (PED-CoV [195]), was introduced into North American commercial pig herds and led to an economic loss of almost 2 billion dollars in the United States [196]. These three coronaviruses are believed to have spilled over from bats because similar coronaviruses have been detected in bats [197,198]. Interestingly, while coronaviruses cause serious and often fatal disease in their secondary hosts, such coronaviruses do not cause any clinical disease in their putative reservoir hosts i.e. bats [39,199,200]. The reasons for this difference in outcomes of coronavirus infection, and factors that lead to virus spillover, are not clearly understood. There are numerous studies on the pathogenesis of SARS-CoV, MERS-CoV and PED-CoV in humans and pigs [201–204], but there are few reports examining coronavirus interactions with their primary bat hosts [39,200]. Our goal was, therefore, to identify coronaviruses in a common and widespread north American bat species and study virus-bat interactions within this species.

Access to a large number of archived samples from an unrelated experiment [188,189,205] gave us the opportunity to screen little brown bat tissues for the presence of coronaviruses, to determine the sequence of the genome of the virus and to identify specific tissues for which the virus had a predilection. Our results suggest that about a third of little brown bats are infected with

several distinct clades of an *Alphacoronavirus* and that the bats retain the virus for up to 4 months of hibernation. Since the bats we examined had been maintained as groups in isolated incubators or semi-isolated cages, we were able to test the hypothesis that little brown bats in the wild are infected with closely related variants of a coronavirus. We predicted that, since the bats were randomly assigned to different incubators/cages, 1) prevalence of infection should be similar across incubators and cages; and 2) any variation in viral genomes should be evenly distributed among cages and incubators.

4.6. Materials and methods

4.6.1. Bats

Bat tissues were obtained from two previous experiments [189,205], in the winters of 2010-2011 and 2011-2012 designed to study the pathogenesis of the fungus, *Pseudogymnoascus destructans*, the causal agent of WNS. Male little brown bats were collected from two different WNS-free caves in Manitoba, Canada under the Manitoba Wildlife Scientific Permits WB11145 and WB13148. Details of segregation of bats into incubators and cages in the 2010-11 and 2011-12 experiments are in Table 4.1. Bats were euthanized at the end of the experiment i.e. after 4 months (year 2010-11) and 3 months (year 2011-12). Bats which succumbed to the WNS-fungus infection were removed prior to the end of the experiment. Immediately following euthanasia, samples from brain, intestines, liver, kidney, and spleen were preserved in RNAlater (Qiagen, Cat #76106) or in formalin [189].

Table 4.1. Segregation of hibernating bats

Year	Incubator Name & Cage Name (if applicable)	Number of bats	Inoculation type	Incubator status
2010-11	A	18	Control	Relative humidity >97%; temperature 7^0C
	B	18	Fungus infected (European Strain)	Relative humidity >97%; temperature 7^0C
	C	18	Fungus infected (American Strain)	Relative humidity >97%; temperature 7^0C
2011-12	D (C)	21	Control	Relative humidity >97%; temperature 7^0C
	D (I)	23	Fungus infected	
	E (C)	10	Control	Relative humidity 99%; temperature 7^0C
	E (I)	10	Fungus infected	
	F (C)	10	Control	Relative humidity 95%; temperature 7^0C
	F (I)	11	Fungus infected	
	G (C)	10	Control	Relative humidity 90%; temperature 7^0C
	G (I)	11	Fungus infected	
	H (C)	11	Control	Relative humidity 85%; temperature 7^0C
	H (I)	10	Fungus infected	

4.6.2. RNA extraction and cDNA preparation

Bat tissues were homogenized and RNA extracted, using RNeasy® Plus mini kit (Qiagen, Cat #74136), as per manufacturer's protocol. cDNA was prepared using QuantiTect reverse transcriptase kit (Qiagen, Cat #205313) as per protocol mentioned in the kit.

4.6.3. Polymerase chain reactions (PCRs) and plasmid constructions

The sequence of all primers used in the PCRs are in Table 4.2. Semi-nested PCR primers amplified a portion of the RdRp region of the coronavirus genome [188] from cDNA prepared from bat tissues. For the primary and secondary reactions, the expected products were 441bp and 273bp respectively. All amplified products were sequenced using the amplification primers. These sequences have been submitted to GenBank, accession number KY820767 to KY820807.

The *Myotis lucifugus* coronavirus (*Myl*-CoV) nucleocapsid gene (1,278bp) was amplified from intestines and lungs using forward primer and reverse primer (Table 4.3). The veracity of the PCR products was confirmed by sequencing and the products cloned into pCR 2.1-TOPO vector

using TOPO® TA Cloning® Kit (Invitrogen, Cat #450641). The sequences were also cloned into pGEX-KG protein expression plasmid (a gift from Gerry Weinmaster (University of California, Los Angeles, CA)) using *Bam*HI and *Xba*I restriction sites at 5' and 3' ends, respectively.

Table 4.2. Primers used for PCR

Forward primer	Reverse primer	Purpose	Elongation Time	Product length
5'–CCATCATCAGATAGAATCATC–3'	5'–TGGTTGGGACTATCCTAAGTG–3'	Primary reaction for coronavirus detection	1 min	441 bp
5'–CGGTTCACATTAGCACTGACAG–3'	5'–TGGTTGGGACTATCCTAAGTG–3'	Secondary reaction for coronavirus detection	1 min	273 bp
5'–ATG GCC TCT GTT AAG TTC GCC AA–3'	5'–TTAAGCTGTGCTCTGAGAATT–3'	Coronavirus nucleocapsid amplification for TOPO-TA cloning	1 min 30 s	1,278 bp
5'–GCCGGATCCATGGCCTCTGTTAAGTTCGCCAA–3'	5'–GCCTCTAGATTAAGCTGTGCTCTGAGA–3'	Coronavirus nucleocapsid cloning into pGEX-KG vector	1min 30 s	1,296 bp
5'–GCCAAGCTTATGGCCTCTGTTAAGTTC–3'	5' –GCCTCTAGATTAAGCTGTGCTCTGAGA–3'	Coronavirus nucleocapsid cloning into P3X-Flag vector	1 min 30 s	1,296 bp

4.6.4. High-throughput Sequencing and assembling the *Myl*-CoV genome

Total RNA from 7 bats (4 from incubator-A and 3 from incubator-B) was sent to The Centre for Applied Genomics at The Hospital for Sick Children (Toronto, Canada), where RNA quality was assessed using a Bioanalyzer (Agilent Technologies), Poly(A) mRNA was enriched using oligo dT-beads, and cDNA libraries were prepared using the NEBNext Ultra Directional RNA Library Prep Kit (New England Biolabs). Barcoded libraries were pooled in equimolar quantities and sequenced on a HiSeq 2500 System (Illumina) to generate 126 bp paired-end reads.

Sequence data quality was assessed using FastQC v0.11.5 [206] and the reads were trimmed to remove adapter sequences and low-quality bases using Trimmomatic v0.36 [207] using the following settings: Illumina clip:2:30:10, leading:3, tailing:3, slidingwindow:4:15,

minlength:36. To identify host sequences, we used TopHat v2.1.1 [208] to align trimmed reads to the Ensembl *M. lucifugus* genome sequence assembly (Myoluc2.0) [209] in strand-specific mode (fr-firststrand) . We sorted the unmapped .bam files using samtools v1.2 [210],extracted the non-host sequences using bedtools v2.26.0 bamtofastq [211], and pooled the resulting sequences for transcript fragment (transfrag) assembly. We used Trinity v.2.2.0 to generate transfrags using the default parameters and *in silico* read normalization. We performed local BLASTn to search for sequence similarity between the Trinity-based transfrags and a coronavirus reference genome (KF430219). The sequence of the entire genome of the *Myl*-CoV was submitted to GenBank, accession number KY799179.

4.6.5. *Myl*-CoV nucleocapsid (N) protein purification

Myl-CoV N-pGEX-KG plasmid was transformed into Escherichia coli BL21 competent cells [212]. 500ml of cell culture at OD_{600} = 0.84 was induced to express *Myl*-CoV-N-GST with 1mM isopropylthio-b-D-galactoside (IPTG) at 28.5 0C for 7.5 hours. During protein extraction, temperature was maintained at +4 0C. BL21 cells were centrifuged down and resuspended using 1% Triton X-100 in TNE buffer. 10mg/ml of lysozyme was added for 15mins to accentuate the process of bacterial cell wall breakdown. 1ml of Halt™ Protease and Phosphate inhibitor cocktail (Thermo-scientific - Cat. #78440) and EDTA was added and the blob of bacteria was sonicated for 60 secs on ice. Supernatant was removed after centrifuging the bacteria at 15,000rpm for 20mins and pellet was treated with 1.5% N-lauroylsarcosine (Sigma L-9150) to further disrupt the cells and added onto the supernatant. From SDS-PAGE analysis later, we came to know that the N-lauroylsarcosine treatment of the pellet led to the release of fusion protein from the cell. Fusion protein was purified from the supernatant using Glutathione Sepharose 4B beads (GE Healthcare), followed by elution using 10mM glutathione for 16hours. Elution was done twice to obtain 6.1

mg/ml and 4.3 mg/ml protein concentration. Protein was verified using SDS-PAGE (Supplementary Figure S4.1.(A)).

4.6.6. Generation of polyclonal antibodies

Polyclonal *Myl*-CoV N anti-serum was generated in rabbits. This was carried out in strict compliance of Canadian Council on Animal Care guidelines (protocol 20090050). Two rabbits were procured by the Animal Care Unit at the Western College of Veterinary Medicine. On day 1, 28, 42 and 56, nucleocapsid protein mixed with Titermax was injected into rabbits. Rabbits were bled to obtain serum one day prior to each antigen injection. Binding of antibody was verified using immunoblot and immunofluorescence (Supplementary Figure S4.1.(B) and (C)), after which we proceeded with immunohistochemistry.

4.6.7. Immunohistochemistry (IHC)

Formalin-fixed-paraffin-embedded (FFPE) blocks of *M.lucifugus* tissues were obtained from our previous study [189] and sections (4-5 microns) were cut and mounted onto slides. Tissue sections were incubated twice in xylene for 15mins each and then rehydrated in graded alcohol. Tissue sections were then incubated overnight in 0.5mM PBS for better antigen retrieval. 0.5% hydrogen peroxide in methanol was added to tissue sections for 20mins at room temperature to block endogenous peroxidase. After distilled water wash, 500ul of Proteinase K (20ug in 1ml) treatment for 20mins at 37 ^{0}C was performed to enhance antigen retrieval. Slides were blocked using 1% bovine serum albumin for 30mins. The serum of the rabbits (56th day bleed) containing anti-*Myl*-CoV N were used as the primary antibodies for staining virus infected cells (1:100 dilution). For every slide processed, we also stained slides with the serum extracted prior to antigen injection (Pre-bleed) as a negative control. Formalin-fixed-*Myl*-CoV-N-transfected *Ef*k cells were used as a positive control. Tissue sections were incubated with the primary antibodies for 3 hours

at room temperature, followed by 3X 5mins washes with 0.5mM PBS. Anti-Rabbit-IgG conjugated with horse-raddish-peroxidase (HRP) (Zymed) was used as a secondary antibody (1:500 dilution) for 30mins at room temperature. After 3X 5mins washes with 0.5mM PBS, color was developed using 500ul of diaminobenzidine (30ul Diaminobenzidine; 9ul of 0.5% hydrogen peroxide and 3ml 0.5mM PBS) for 10mins at room temperature. Counterstaining was done using hematoxylin for 30seconds and then decolorized using acetic acid-acetone. Slides were dehydrated using graded alcohol and then treated with Xylene before applying coverslips. Formalin-fixed-*Myl*-CoV-N-transfected *Ef*k (*Eptesicus fuscus* kidney) cells [213] were used as a positive control. Counterstaining was done using hematoxylin.

4.6.8. Hematoxylin and Eosin (H&E) staining

Tissue sections for histopathology were stained with H&E by Prairie Diagnostic Services at the University of Saskatchewan. Each lung section was independently assessed for bronchiolar epithelial degeneration and inflammation by two veterinary pathologists, blinded to sample identity. Five categories of lesions were established: diffuse lung inflammation, inflammation of bronchus, bronchiolar epithelial vacuolation, bronchiolar epithelial hyperplasia, and bronchiolar epithelial erosion. All lung sections from all bats were examined to determine the range of changes and then changes were scored between 0 and 3, with 0 indicating normal and 3 indicating the most severe change within the 8 bats examined. The maximum score of 3 would still be considered mild within the typical pathology scoring system describing the severity of inflammatory response: mild, moderate or severe.

4.6.9. Electron Microscopy (EM)

Myl-CoV infected cells in the bronchial epithelium were marked in the corresponding IHC slides, so that the specific location could be sampled for electron microscopy (EM). The slide was

soaked in Xylene to remove the coverslip, soaked in Xylene:Propylene-oxide (PO) (2:1) and (1:1) for 30 mins and 15 mins respectively, followed by 1 hour soaking in PO. PO:Epon (1:1) was consistently dropped on the slides for 1 to 2 hours followed by pure Epon for 1 hour. Labelled capsules were filled and inverted on the tissues on the slide. Polymerization was done at 65^0C for 24 hours. The block was broken off the slide which lifted the section along with it and was then sectioned on to 200 mesh copper grids, which were viewed by transmission electron microscope.

4.6.10. Phylogenetic analysis and sequence alignments

For the whole genome phylogenetic tree, genome sequences of 33 representative coronaviruses and *Myl*-CoV were aligned using ClustalW (Version 1.83) [214]. Maximum likelihood (ML) trees were constructed with MEGA7 [215]. Divergence was estimated by Kimura's two parameter method. Bootstrapping with 1000 replicates was used to estimate the confidence of the tree nodes. The generated tree was then annotated using Adobe illustrator CC 2015.

For the phylogenetic tree of the RdRp gene segment, sequences obtained from Sanger sequencing were used along with corresponding segments from KF430219 and HQ336976. Only sequences that were completely unambiguous were used in the analysis. ML trees were constructed in a similar manner as that of the entire genome phylogenetic tree.

4.6.11. Accession numbers

41 sequences of RdRp gene using sanger sequencing were submitted to GenBank (accession number KY820767 to KY820807). *Myl*-CoV complete genome sequence was submitted to GenBank (Accession number KY799179). Nucleotide sequences for the phylogenetic tree were obtained from GenBank. Accession numbers of the sequences are AF353511 (PEDV.CV777), AF391541 (BCoV.ENT), AY585228 (HCoV.OC43.ATCC.VR.759), DQ001339

(Avian IBV.p65), DQ011855 (PHEV.VW572), DQ022305 (BtSARS.HKU3-1), DQ071615 (BtSARS.Rp3), DQ412042 (BtCoV.Rf1), DQ412043 (BtSARS.Rm1), DQ415904 (HCoV.HKU1.N6.GenotypeA), DQ445912 (HCoV.NL63.Amsterdam.496a), DQ648856 (BtCoV.273.2005), DQ648857 (BtCoV.279.2005) , DQ811789 (TGEV), DQ848678 (FCOV), EF065505 (BtCoV.HKU4.1), EF065509 (BtCoV.HKU5.1), EF065513 (BtCoV.HKU9.1), EF065514 (BtCoV.HKU9.2), EF065515 (BtCoV.HKU9.3), EF065516 (BtCoV.HKU9.4), EF203067 (BtCoV.HKU.HK.33.2006), EU420137 (BtCoV.1B.AFCD307), EU420138 (BtCoV.1A.AFCD62), EU420139 (BtCoV.HKU8.AFCD77), FJ647225 (MurineCoV.MHV.A59), KC164505 (MERS-CoV.England1), NC002645 (HCoV.229E), NC004718 (SARS-CoV), NC009019 (BtCoV.HKU4.1), NC009657 (Scotophilus BtCoV.512.2005), NC009988 (BtCoV.HKU2) and KF430219 (Myotis CoV - USA.2006)).

4.7. Results

4.7.1. Detection of a coronavirus in hibernating little brown bats.

To estimate the prevalence of coronavirus in little brown bats, and to determine the tropism of the virus, we performed PCR for coronavirus RdRp (RNA dependent RNA polymerase) gene on samples from brain, intestines, liver, kidney, and spleen of 157 little brown bats. We detected the coronavirus only in the intestines. On average, one third of the bats (Table 4.3) contained detectable coronavirus RNA. There was no difference in the prevalence of virus between experimental groups in the different cages/incubators (Chi-square test, n = 174, p value = 0.817). A lack of blood samples prevented us from confirming viral prevalence by serological methods.

Table 4.3. Prevalence of the *Myotis lucifugus*-Bat coronavirus (*Myl*-CoV) in little brown bats intestines based on detection of a portion the viral RdRp gene.

Year	Incubator name	Number of positive bats/Number of bats tested	Percentage Positive
2011	Incubator A	7/18	39
2011	Incubator B	3/13	23
2011	Incubator C	7/16	44
2012	Incubator DC	6/21	29
2012	Incubator DI	9/23	39
2012	Incubator EC	3/10	30
2012	Incubator EI	2/10	20
2012	Incubator FC	4/10	40
2012	Incubator FI	2/11	18
2012	Incubator GC	2/10	20
2012	Incubator GI	4/11	36
2012	Incubator HC	3/11	27
2012	Incubator HI	1/10	10
Total		**53/174**	**30**

We then compared the nucleotide sequences and the derived amino acid sequences of the PCR products. We included a corresponding segment from little brown bat coronavirus (KF430219) and from the Rocky Mountain coronavirus detected in a big brown bat (HQ336976) into the alignments. Sequences segregated into two distinct clades (Figure 4.1. (A)). Clade 1 sequences were most similar to KF430219 and Clade 2 sequences resembled sequences from HQ336976. Most of the sequence differences within each clade were synonymous (Figure 4.1. (B)), while there were seven amino acid differences between clades 1 and 2 (Figure 4.1. (C)). Except for some bats in incubator D, the nucleotide inter-clade and intra-clade polymorphisms were scattered among the hibernation incubators. This suggested that the bats were infected before being placed in the incubators rather than acquiring infection from incubator or cage mates.

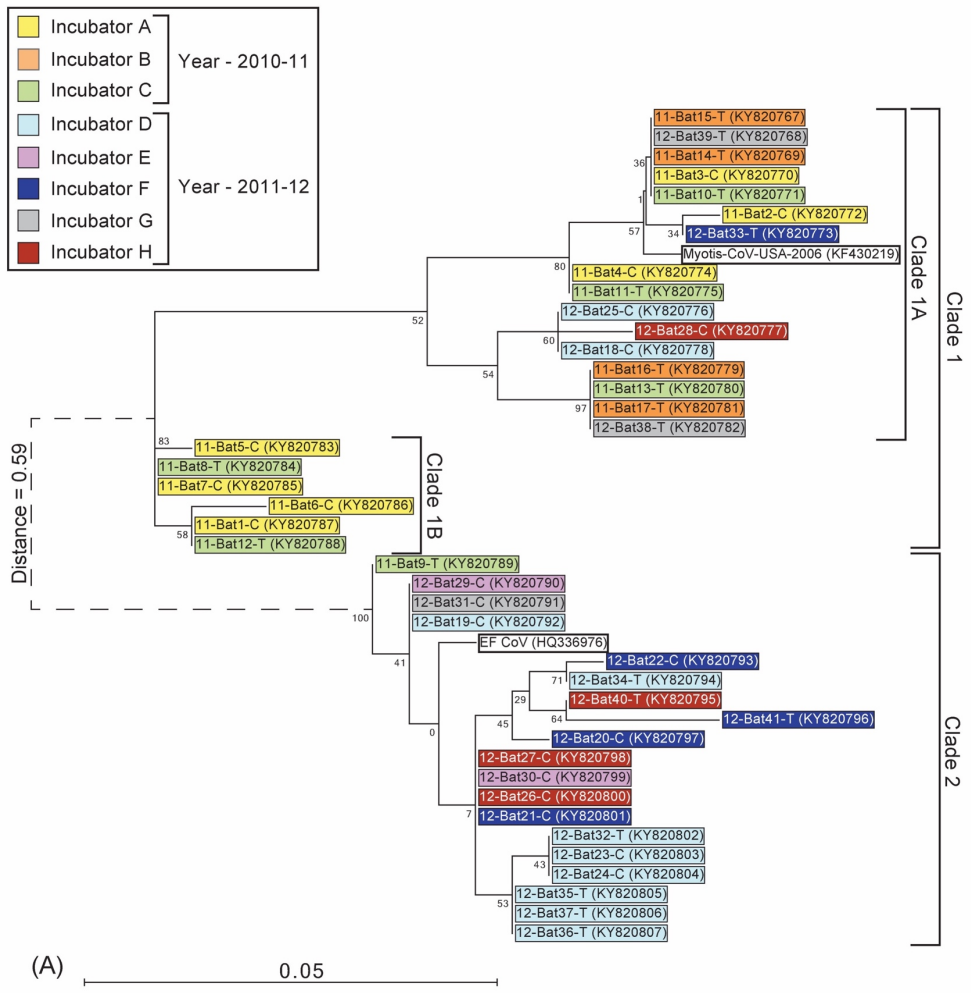

Figure 4.1. Comparison of nucleotide and amino acid sequence of PCR products from a 229 bp portion of the coronavirus polymerase gene amplified from the intestine of bats. Groups of bats were isolated in incubators with little likelihood of cross infection during hibernation. **(A)** Maximum likelihood tree of nucleotide sequences variation. The colour of the box indicates the bat's hibernation incubator. The first two digits indicate the year of the experiment (2010-2011 or 2011-2012) and the bat's identification number. For 2011-2012 each incubator contained two cages, designated either T or C. Corresponding sequences from a coronavirus from *Myotis lucifugus* (*Myotis*-CoV-USA-2006 - Genbank accession number KF430219) and from *Eptesicus fuscus* (HQ336976) were included in the analysis and are in white boxes. The numbers at the nodes are the bootstrap values (percent) obtained for 1,000 replicates. The inter-clade distance (distance between clade 1 and 2) was much larger than intra-clade distances (distance between individual coronavirus sequences within a clade) and therefore, it has been depicted with a dotted line and is not to scale.

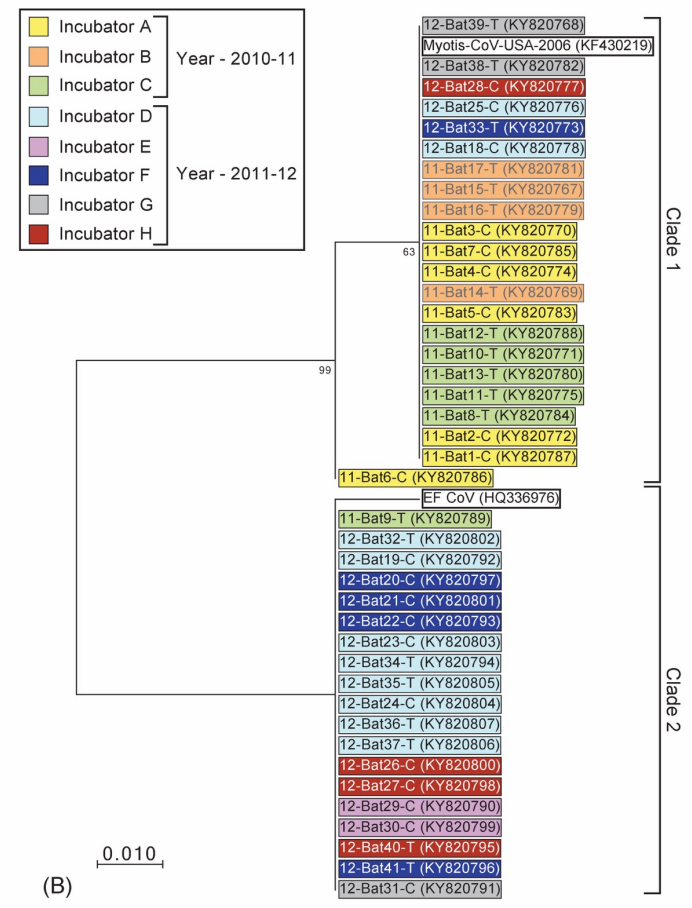

Figure 4.1. **(B)** Maximum likelihood tree for the amino acid sequence derived from the nucleotide sequences analyzed in Figure 4.1. (A).

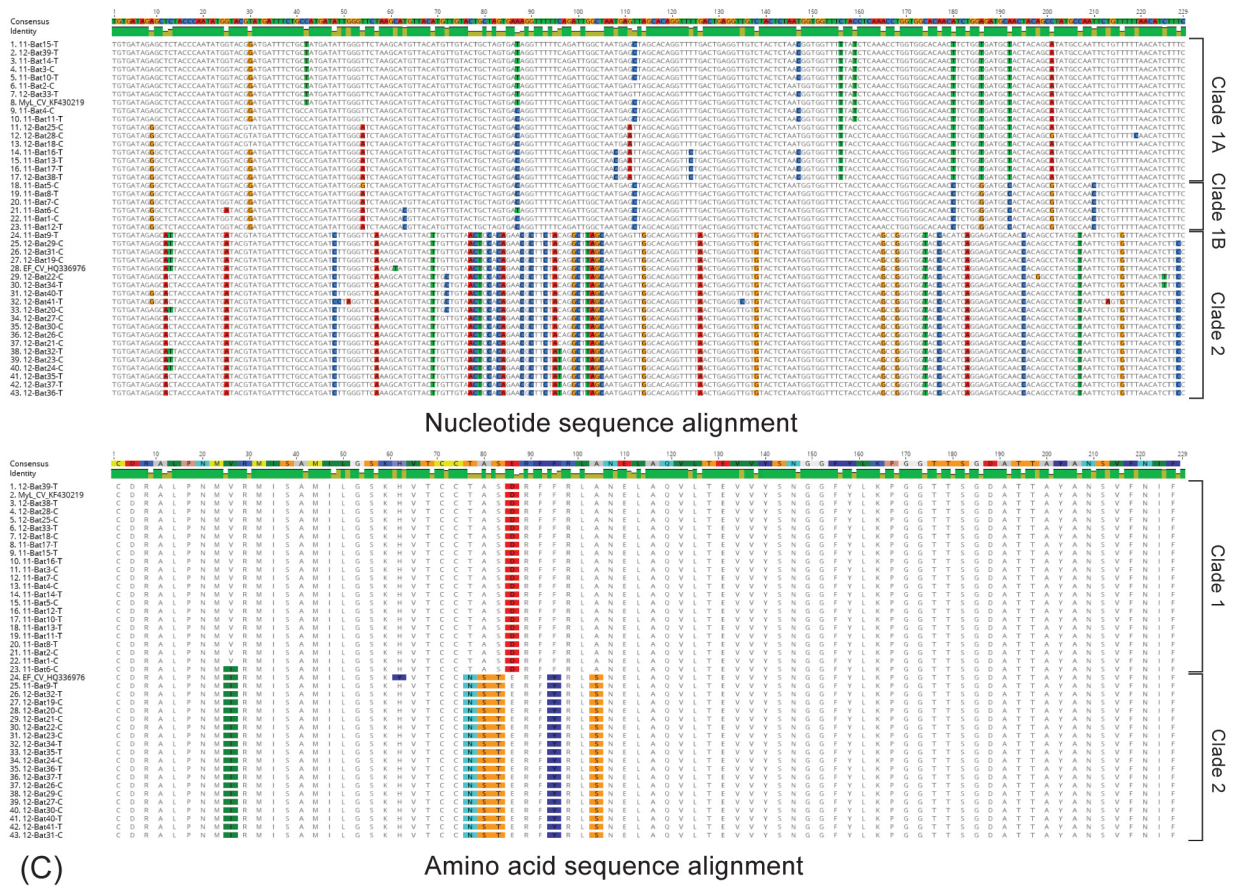

Figure 4.1. **(C)** showing the ClustalW alignments used to generate the trees for nucleotide and amino acid sequences. Residues that differ from the consensus are highlighted in colour.

4.7.2. Complete genome sequencing and phylogenetic analysis.

We assembled the entire genome of the coronavirus from RNASeq data from intestines of 7 bats (which contained clade 1 coronaviruses). The genome of the *Myotis lucifugus* bat coronavirus (*Myl*-CoV) is 28,173 bases. We assigned open reading frames based on the published KF430219 sequence. The assembled sequence includes a 3' poly-adenine tail, which is missing from the annotated KF430219 sequence.

Phylogenetic analysis of *Myl*-CoV and other representative coronaviruses places *Myl*-CoV within the genus *Alphacoronavirus*. *Myl*-CoV is more closely related to Scotophilus Bat coronavirus 512 and PEDV-CoV (CV777 strain). Other *Alphacoronaviruses* related to the *Myl*-

CoV are human CoV 229E, NL63 and coronaviruses detected in other bat species (BtCoV-HKU2, HKU8, HKU-HK33, 1B-AFCD307, and 1A-AFCD62) (Figure 4.2.).

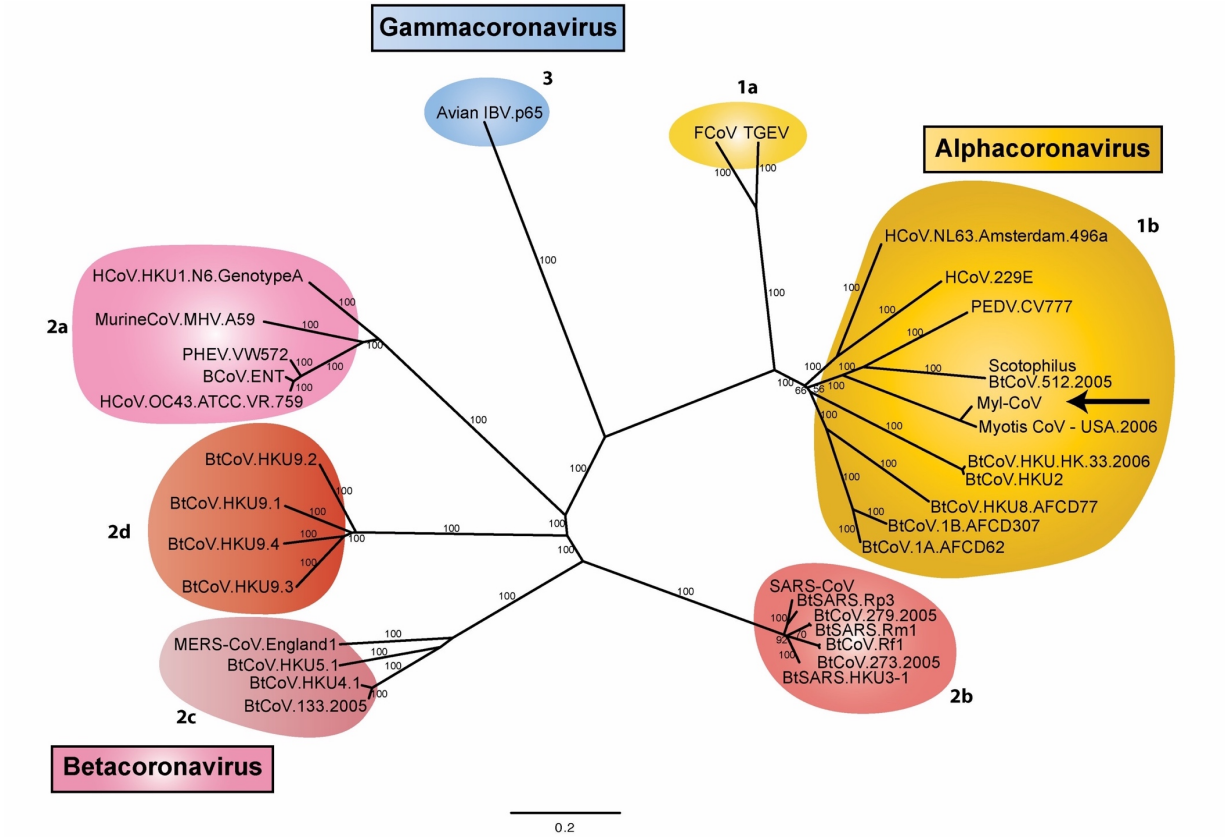

Figure 4.2. Whole-genome phylogeny comparing *Myl*-CoV with representative coronaviruses. The whole genome sequences of 34 coronaviruses, including *Myl*-CoV, were aligned. Three distinct phylogenetic genera are shown: *Alphacoronaviruses*, *Betacoronaviruses* and *Gammacoronaviruses.* The location of *Myl*-CoV within *Alphacoronaviruses* is indicated by an arrow. *Deltacoronaviruses* are newly characterized and are not shown. Recognised subgroup clusters are marked as 2a-2d for the *Betacoronaviruses* and 1a and 1b for the *Alphacoronaviruses*.

4.7.3. Detection of *Myl*-CoV in bronchial epithelium of bats.

Several coronaviruses have a predilection for respiratory as well as intestinal tissue. Although we had detected *Myl*-CoV RNA only in intestinal samples, we performed immunohistochemistry (IHC) to further explore the tropism of the virus. We were unable to detect coronavirus antigen in any of the tissues except for lungs. We detected the *Myl*-CoV antigen in the

lung of five bats, all of which were positive for viral RNA in intestines (Figure 4.3.(A)). In the lungs, the *Myl*-CoV antigen was present only in the bronchial epithelial cells. Cells containing nucleocapsid antigen showed degenerative changes in the form of vacuolation, and some cells appeared to have exfoliated.

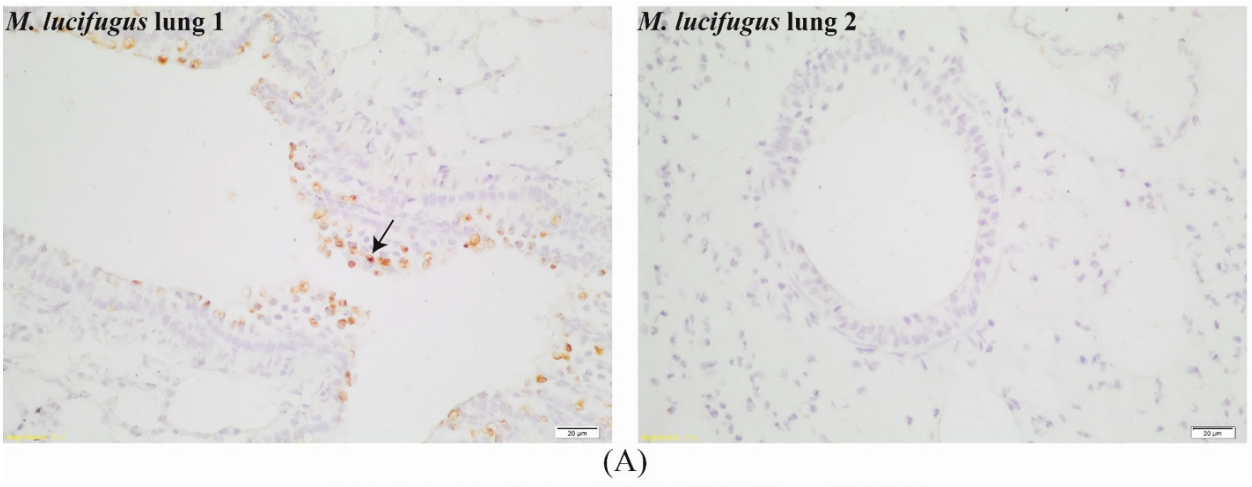

(A)

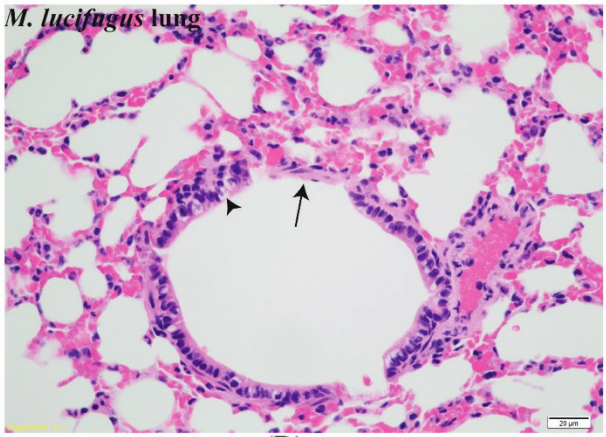

(B)

Figure 4.3. (A) Cells immuno-stained for *Myl*-CoV nucleocapsid in the bronchial epithelium of lungs. Immunohistochemistry performed using *Myl*-CoV N antiserum. Lungs 1 is from a bat with coronavirus detected in its intestine. Lung 2 is from an uninfected bat. Cells stained for *Myl*-CoV N protein (indicated by arrows) were vacuolated and in some cases sloughing into the bronchial lumen. Only bronchial epithelial cells had detectable viral antigen.

Figure 4.3. (B) Pathology of *Myl*-CoV infected lung. H&E staining of bat lung infected with coronavirus. Vacuolation of infected cells (shown by an arrowhead) were present along the bronchial epithelium. A portion of bronchial epithelium was sloughed off (shown by an arrow). Neutrophils were observed in the vicinity of the infected portion of the bronchus but the overall inflammation in the entire lung was low.

We also performed transmission electron microscopy on portions of the lung sections that contained viral antigen (Figure 4.4.). Although the quality was compromised due to formalin-fixation, we observed electron dense particles in the cells that were positive for *Myl*-CoV antigen. The size of these particles were as expected for coronaviruses (approximately 125 nm [216]). Cellular degenerative changes were evident in the cells containing the particles. In the same section, other cells were healthy and did not contain such particles. Furthermore, the presence of viral RNA was confirmed by performing PCR on lung cDNA (obtained from RNA) using the primers against *Myl*-CoV nucleocapsid gene. Sanger sequencing of the amplified PCR product showed a match with *Myl*-CoV nucleocapsid sequence.

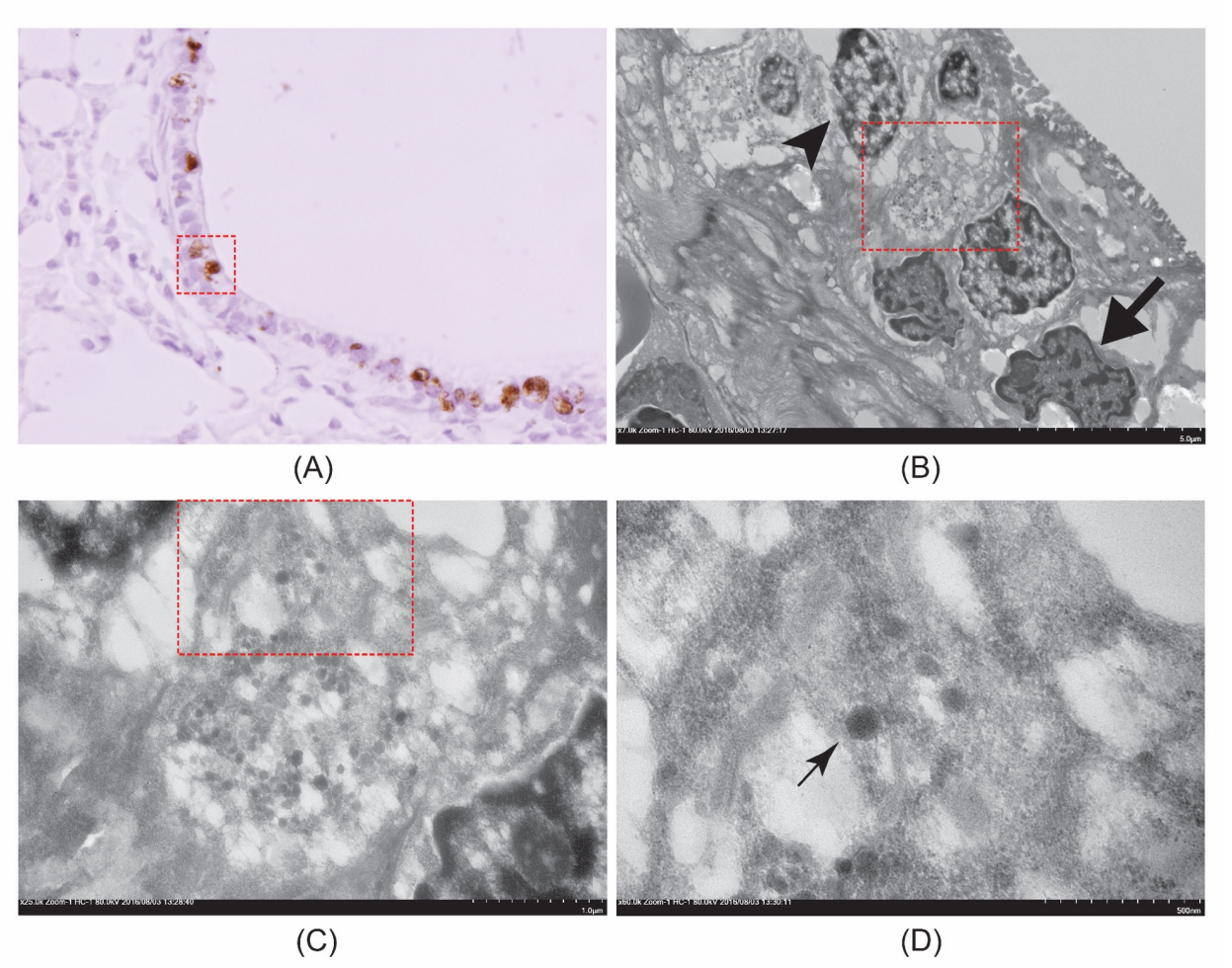

Figure 4.4. Transmission electron micrograph showing coronavirus-like particles in the bronchial epithelial cells. (A) A haematoxylin and immune-stained (*Myl*-CoV N protein) section of lung. The red square denotes the portion picked from a consecutive H&E section for electron microscopy. **(B)** Electron micrograph of cells selected in (A). Successive enlargement of portions of the section in a box with red dotted lines. **(C) (D)** Particles (around 125 nm in size) were observed in the bronchial epithelium (thin arrow). Those cells which contained the virus-like particles showed nuclear degradation (indicated by the arrow-head). Uninfected cell nucleus shows normal morphology (shown by thick arrow).

4.7.4. Pathology in bat lung due to *Myl*-CoV infection.

To assess pathology due to coronavirus infection, histologic sections of the *Myl*-CoV positive lungs of *M. lucifugus* were evaluated independently by two pathologists. Although lesions were very mild both pathologists had higher lesion scores for the categories of bronchiolar epithelial vacuolation and degeneration, bronchiolar epithelial hyperplasia and erosion of epithelium in virus-infected bats when compared to uninfected. There was no obvious consistent inflammation of the bronchus and, although there was mild diffuse inflammation of the interstitium and alveoli, there was no difference between virus-infected and uninfected bats (Figure 4.3. (B)).

4.8. Discussion

Although events of successful viral spillover to distantly related species are thought to be extremely rare, in recent years, coronaviruses including SARS-CoV [190], MERS-CoV [67,191–193] and PED-CoV [195] have spilled over from bats to other species. Circumstantial evidence suggests that most alpha and beta coronaviruses parasitizing other mammals may also have originated in bats [217]. Little is known at present about the dynamics of coronavirus infection in the reservoir bat hosts or how the viruses are spread from bat to bat, or from bats to other mammals. In this study, we examined a coronavirus in its natural host, the little brown bat. This study system provides a useful model for understanding factors that may promote spillovers. Our results suggest

the following: a) the *Myotis* coronavirus (*Myl*-CoV) is mainly present in the intestines and lungs, b) co-hibernating little and big brown bats may share closely related coronaviruses, c) *Myl*-CoV can persist in *M. lucifugus* for up to 4 months, the hibernation period of our experiment, and d) the presence of *Myl*-CoV in bronchial epithelium is associated with minimal pathology or inflammation. However, a larger sample size under controlled conditions of exposure, with more rapid fixation of tissues, is required to fully characterize the lesions in lung and intestines.

Dominguez [218] and others [188] previously detected a coronavirus in little and big brown bats suggesting that the virus may infect bats of both species, crossing between the bats at shared co-hibernation sites. The virus originally detected in a big brown bat was named the Rocky Mountain coronavirus [218] for the location of its initial detection. The RNA amplified from little brown bats in this study appeared to be from two distinct clades. The sequences in Clade 1 were very similar to the archived sequence derived from little brown bats and sequences from Clade 2 were more closely related to the archived sequence from big brown bats. This suggests that two closely related coronaviruses may circulate in little brown bats. Although the sequence traces did not suggest a mixture of PCR products, we cannot completely rule out the possibility that the individual bats were infected with viruses from both clades and that the PCR likely favoured the predominant viral component.

Complex strategies allow viruses to remain endemic in populations. These include: 1) a continuous source of susceptible hosts for viruses that cause short-term acute infections with long-lasting immunity (e.g., measles virus), 2) antigenic drift (e.g., influenza virus) of virus or waning immunity (e.g., respiratory syncytial virus) that allows reinfection, and 3) long-lasting latent (e.g., herpesviruses) or persistent infections (e.g., pestiviruses) with sustained or periodic shedding. How bat viruses are maintained in their natural host populations or how they avoid extinction as host

populations become immune and less susceptible, however, is not understood. It is possible to establish persistent infections in cultured cells with viruses that may have originated in bats, including Ebola virus [219] and SARS-CoV [220,221], but whether these viruses persist in their primary hosts is not known. The results of studies aimed at determining whether bat viruses persist in infected bats are controversial. There is no direct evidence for either persistence or transmission dynamics, and this is a knowledge gap in bat-virus ecology that needs to be addressed [12].

Based on the sequence of the amplified portion on the RdRp gene we observed considerable polymorphism among the *Myl*-CoV with sequences segregating into distinct clades. Based on the maximum mutation rate possible for the RdRp gene [222], we should have observed only 1.16 random mutations in the 229bp segment. Most of the intra and inter-clade polymorphisms exceeded this rate. Also, while viruses detected in 2011 were primarily clade 1 and 2012 viruses were primarily clade 2, both clades were detected in samples from either year. The differences between clades likely represent fixed nucleotide polymorphisms rather that random changes. Although recombination of coronavirus clades is possible, performing deep sequencing on the samples would enable us to negate this possibility. Ge and others also found co-existence of a variety of coronavirus in bat colonies [223].

Osborne and others [217] were unable to detect virus in the rectal swabs of individual bats sampled over time in an extensive survey of New World *Alphacoronaviruses*. They concluded that these coronaviruses do not persist in their hosts but are maintained in populations by the introduction of new susceptible individuals. Their results, however, do not rule out persistence in individual animals with low levels of virus replication and undetectable shedding, interspersed with short periods of increased replication and shedding. Our observations suggest that the *Myl*-CoV can persist in its hosts for at least the four-month hibernation period. Due to strict biosecurity,

spread of virus between incubators was unlikely and the distribution of variants among incubators (and cages) argues against spread within incubators (or cages). Our results therefore suggest that the bats were infected before they were collected.

Whole genome phylogenetic analysis revealed that the *Myl*-CoV belongs to the genus *Alphacoronavirus,* which includes three coronaviruses that infect human lungs and pig intestines (HCoV-229E, HCoV-NL63 and PED-CoV). We confirmed the presence of virus in intestine via PCR and in the lungs by immunohistochemistry, electron microscopy and PCR. But, we were unable to detect the *Myl*-CoV in the intestines using immunohistochemistry. The reason for this might be that the part of the intestine used for RNA extraction had the virus in it, whereas the part used for histology did not.

Our histological lung sections provide a novel insight into persistent infection of a coronavirus in its reservoir bat host. Firstly, we observed that the cells that were infected showed degenerative changes which resulted in rare multifocal areas of bronchiolar epithelial erosions with no obvious inflammation targeting these lesions. The absence of neutrophilic infiltration is contrary to what has been seen in non-bat species affected by similar coronaviruses. Previous studies in transgenic mice showed that HCoV-229E infection led to massive neutrophilic infiltrate [224]. Lung samples from piglets infected with PED-CoV showed presence of moderate neutrophilic infiltrate (even though PED-CoV has a predilection for intestines) [225]. Hibernating bats do appear to be capable of a local inflammatory response following fungal infection [226]. Low level of neutrophilic infiltration in coronavirus-infected lungs reinforces the fact that bats are unique in the way they respond to a coronavirus infection. Lower inflammation might be due to fewer chemotactic factors being produced as a result of infection, which might be an inherent feature of *M. lucifugus*. It might also be that bat neutrophils are more efficient in controlling virus

infection and obviating a massive neutrophilic infiltrate. An alternative explanation for the lack of inflammation in bats may be that cell necrosis occurs at the epithelial surface with dead cells sloughing into the lumen. Cytokines required to stimulate inflammation and immunity might not enter the interstitium and the systemic circulation. An infection that is localized to epithelial cells without breaching the basement membrane is a good strategy for a virus to allow persistence of infection. However, in our study the sample size was low and it is difficult to reach a firm conclusion about the host's response to coronavirus infection.

Although our results demonstrate viral persistence during hibernation and do not address it in normothermic bats, we propose a model for the maintenance of the coronavirus in little brown bat populations (Figure 4.5): Bats are infected with one of closely related coronaviruses distinguishable from each other by minor nucleotide polymorphisms. The virus then persists at low levels, probably undetectable in fecal material. Due to limited replication in bronchial epithelial cells there is little host-response against the virus favouring persistence. Naïve and susceptible young individuals acquire the virus in maternity roosts when viral replication and shedding increases, caused by hormonal changes or other stress factors [47,227].

Our study demonstrates for the first time that several bats in a population can maintain a coronavirus infection through the hibernation as apparently non-pathogenic infection. Our observations also support growing evidence that natural and experimental viral infections in bats are not accompanied by acute inflammation and pathology.

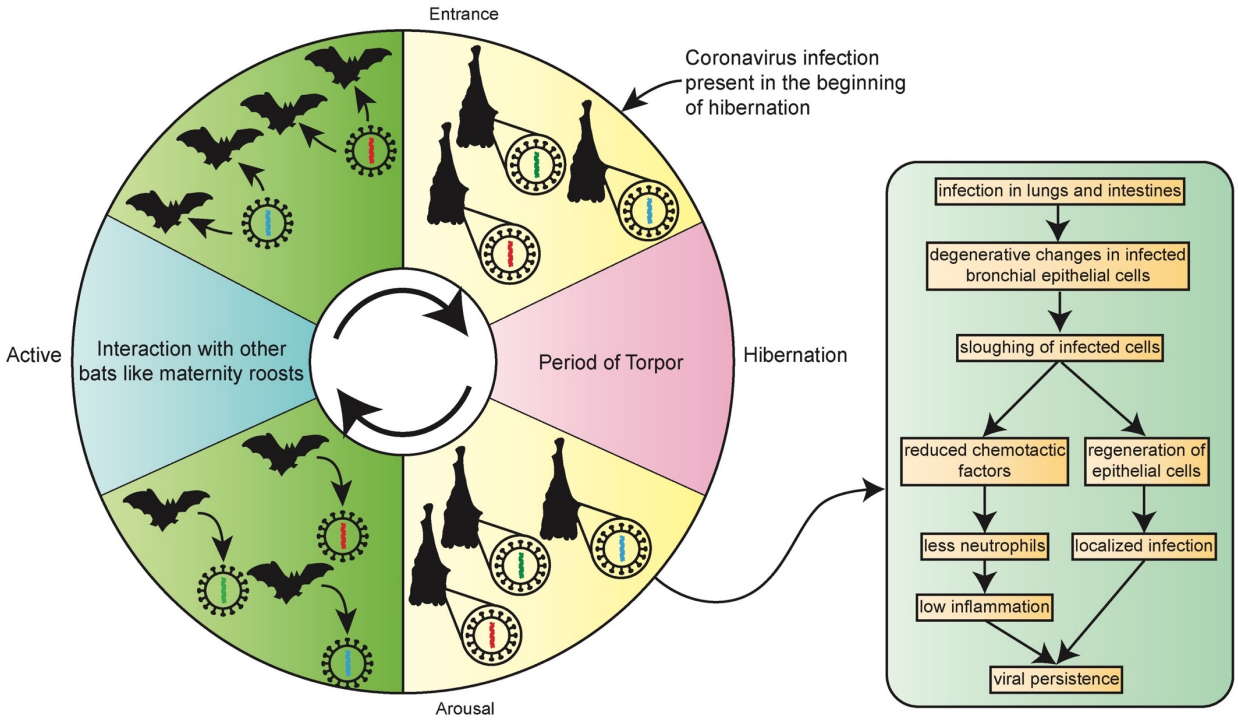

Figure 4.5. Proposed model of coronavirus maintenance in bat population. Bats are infected with one of closely related coronaviruses distinguishable from each other by minor nucleotide polymorphisms. The virus then persists at low levels during hibernation. Due to limited replication in bronchial epithelial cells there is little host-response against the virus favouring persistence. Naïve and susceptible young individuals acquire the virus in maternity roosts when viral replication and shedding increases, caused by hormonal changes or other stress factors Bats enter hibernation with the infection present in them. During hibernation, the virus persists due to low level of physiological and physical activity and low levels of inflammation.

4.9. Supplementary Information

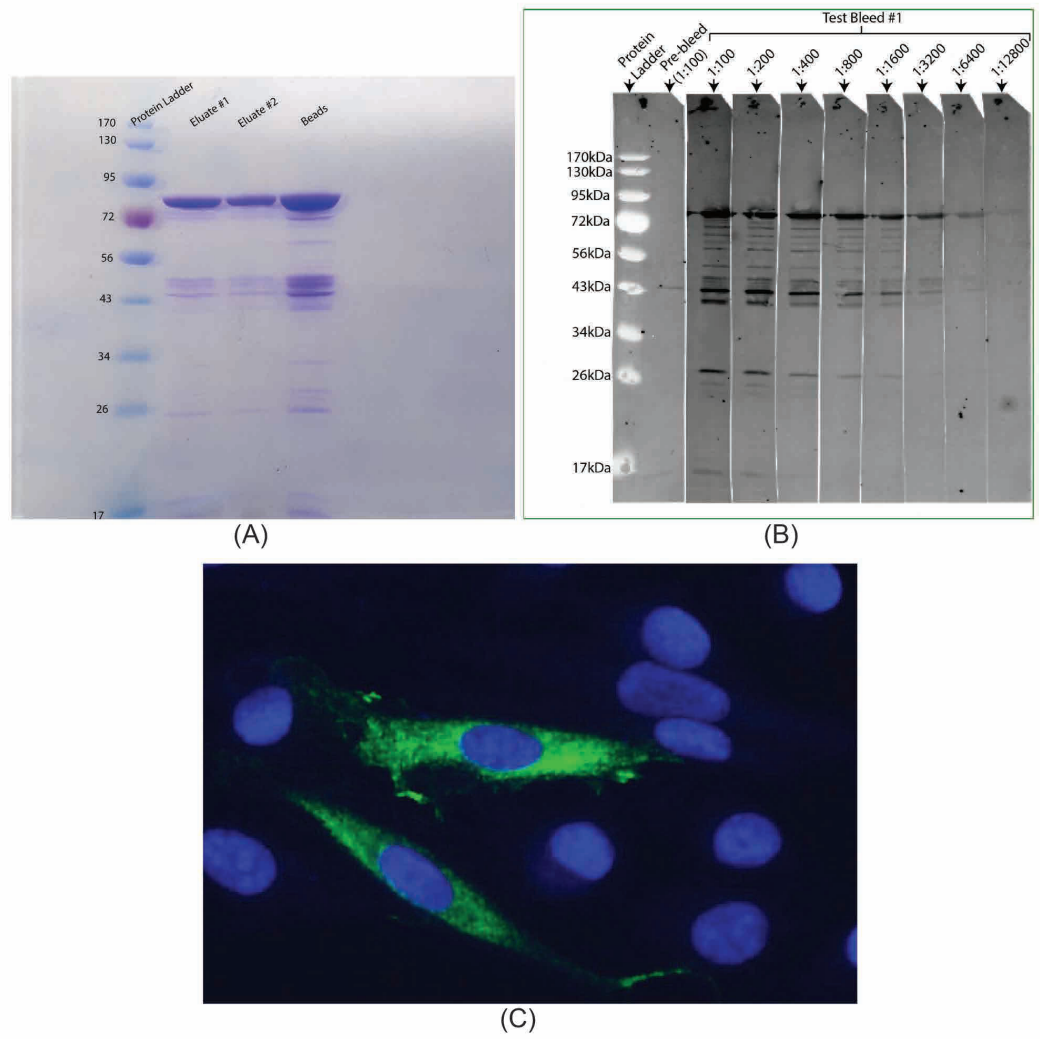

Figure S4.1. Figure showing the process of developing antibodies. (A) SDS-PAGE showing the fusion protein (*Myl*-CoV nucleocapsid protein-GST) purified using Glutathione Sepharose 4B beads. Lane 1 contains protein ladder; Lane 2 contains the Eluate#1 (blue band showing the fusion protein); Lane 3 contains the Eluate#2; Lane 4 contains the Beads. (B) Immunoblot done using 10ng of *Myl*-CoV N-GST protein to detect the titers of the antibody in rabbit serum. The first test bleed showed a titer of 6400. (C) Bat cells expressing *Myl*-CoV N with flag tag stained using rabbit serum (containing *Myl*-CoV N antibodies). Immunofluorescence assay showing the binding of the antibodies (N protein shown in green).

4.10. Transition Statement

In this chapter, I described our characterization of a coronavirus that infects many little brown bats. We obtained the nucleotide sequence of virus' entire genome allowing us to predict its component open reading frames and to demonstrate that the bats were infected prior to hibernation and that the viruses persisted in bat intestines at least while they were in hibernation. We also demonstrated the presence of the virus in the lungs and intestines of the bats were there was little evidence of virus replication-induced tissue damage and inflammation.

We had access to tissue samples archived from an earlier study of the pathophysiology of white-nose syndrome, a frequently lethal fungal disease of little brown bats. The data described in this chapter provided us with the information needed to test the hypothesis that the systemic effects fungal infection would cause changes in the gene expression patterns in bat intestines, the main site of viral persistence, perturbing the bat-virus relationship and leading to increased virus replication.

Chapter 5: Stress of secondary fungal infection increases coronavirus in little brown bats

5.1. Copyright

© This article is licensed under a Creative Commons Attribution 4.0 International License. Springer Nature allows the authors to retain non-exclusive rights to reproduce the contribution in whole or in part in any printed volume (book or thesis) of which they are the author(s).

This manuscript has been reformatted from the original version for inclusion in this thesis.

5.2. Citation

Davy, C. M.*, M. E. Donaldson*, **S. Subudhi***, N. Rapin*, L. Warnecke, J. M. Turner, T. K. Bollinger, et al. "White-Nose Syndrome Is Associated with Increased Replication of a Naturally Persisting coronaviruses in Bats." *Sci Rep* 8, no. 1 (October 2018): 15508. https://doi.org/10.1038/s41598-018-33975-x.

****Contributed equally to the study***

5.3. Contribution

Several authors contributed significantly during this study. **CMD, MED, NR and I contributed equally to the work described in the manuscript.** I prepared the initial draft of the manuscript and all authors were involved in editing and refining the manuscript. NR and I detected and quantitated viral and host transcripts, developed antisera against recombinant *Myl*-CoV N protein and optimized the ELISA assays for bat antibodies. CMD, MED and CK analyzed the RNASeq data and contributed to the writing of the manuscript. LW, JMT, CKRW and VM

conducted the WNS pathogenesis experiments in 2009 from which all tissue samples were obtained. ND, EK, KN, YD, CKRW conducted the WNS pathogenesis experiment in 2017 and provided samples for the serological analysis. TKB conducted all pathological analyses.

5.4. Abstract

Spillover of viruses from bats to other animals may be associated with increased contact between them, as well as increased shedding of viruses by bats. Here, we tested the prediction that little brown bats (*Myotis lucifugus*) co-infected with the *M. lucifugus* coronavirus (*Myl*-CoV) and with *Pseudogymnoascus destructans* (*Pd*), the fungus that causes bat white-nose syndrome (WNS), exhibit different disease severity, viral shedding and molecular responses than bats infected with only *Myl*-CoV or only *P. destructans*. We took advantage of the natural persistence of *Myl*-CoV in bats that were experimentally inoculated with *P. destructans* in a previous study. Here, we show that the intestines of virus-infected bats that were also infected with fungus contained on average 60-fold more viral RNA than bats with virus alone. Increased viral RNA in the intestines correlated with the severity of fungus-related pathology. Additionally, the intestines of bats infected with fungus exhibited different expression of mitogen-activated protein kinase pathway and cytokine related transcripts, irrespective of viral presence. Levels of coronavirus antibodies were also higher in fungal-infected bats. Our results suggest that the systemic effects of WNS may down-regulate antiviral responses in bats persistently infected with *M. lucifugus* coronavirus and increase the potential of virus shedding.

5.5. Introduction

Bats are hosts for many viruses and are thought to be the source of some viruses that have spilled over to humans and other mammals, causing fatal disease. These include coronaviruses causing severe acute respiratory syndrome (SARS [190]), Middle East respiratory syndrome (MERS [191,192,228,229]), porcine epidemic diarrhoea (PED [195]) and swine acute diarrhoea syndrome (SADS [133]); paramyxoviruses such as Hendra [230] and Nipah [231]; and filoviruses like Marburg [232] and Ebola [233]. Four families of viruses that are pathogenic for other mammalian species (Coronaviridae [234], Paramyxoviridae [235], Rhabdoviridae [236] and Filoviridae [237]) may also have originated in bats. These viruses often cause serious disease in their secondary hosts, but most do not appear to cause clinical signs or pathology in bats [38,46,238], suggesting that uniquely benign relationships have co-evolved between the viruses and their primary bat hosts [14,20]. While relatively little is known about the dynamics of viral infections in bats, these viruses may be maintained in bat populations as a result of either persistently infected individuals, reinfection after waning immunity, or spatial transmission dynamics [12,239].

The rare spill-over of bat viruses to other animals may require a “perfect storm” of conditions that include increased contact between bats or fomites and other mammals, possibly due to human impacts on habitat quality [240], and the ability of the virus to infect, replicate, and transmit in the secondary host. The rate of viral shedding and the amount of detectable virus associated with bat colonies fluctuates, with periodic increases often linked to parturition, waning maternal immunity, nutritional stress or increased energy consumption [46,241–246]. Increased shedding of virus by a colony of bats may reflect an increase in the proportion and number of susceptible individuals, or an increase in the replication of persistent or latent virus normally

suppressed by the host. For herpesviruses, reactivation from latency is linked to perturbations caused by a variety of physiological, immunological and psychological stressors [247]. The mechanisms that trigger the reactivation of latent or persistently infecting viruses are not clearly understood, but the increased shedding of viruses is correlated with some incidents of spill-over of bat viruses to other animals [248].

The Canadian prairies are home to three species of bats, including the little brown bat (*Myotis lucifugus*), big brown bat (*Eptesicus fuscus*), and northern long-eared bat *(Myotis septentrionalis*). All three species hibernate from October to May, sometimes in shared hibernacula. We recently demonstrated that ~30% of hibernating *M. lucifugus* sampled over two years from hibernacula in Manitoba were infected with a coronavirus (*Myl*-CoV), which persisted at low levels in the intestine [44]. A closely related coronavirus also infects *E. fuscus* [218].

Whereas bats appear to be relatively resistant to viral infections, a cold-adapted fungus that was recently introduced to North America has caused widespread mortality in some species of bats in eastern United States and Canada [189,249–251]. The fungus (*Pseudogymnoascus destructans)* causes white-nose syndrome (WNS) in hibernating bats, which is characterized by the growth of white fungal mycelia on the face and exposed skin of the wings and tail membranes. The visual and microscopic effects of *P. destructans* on the skin of the wings are associated with increased expression of several genes devoted to innate immunity and inflammation in wing tissue [226,252]. Profound systemic effects include dehydration, hypovolemia, metabolic acidosis, and fat depletion, which can lead to death [59–61]. Other systemic effects of bat WNS include an accumulation of neutrophils in the lungs, which is accompanied by an increase in the expression of several cytokine genes [253] suggesting that even the most severely afflicted hibernating bats are capable of at least some systemic immune response to fungal infection.

Previous studies on other species have demonstrated that a fungus and a virus could interact during co-infection and affect each other [254,255]. Similar interactive impacts of co-infection with *P. destructans* and viruses on bat immune responses are not known. We used *M. lucifugus* experimentally- infected with *P. destructans* and/or naturally infected with *Myl*-CoV as a model to understand how co-infections influence bat-virus interactions. This system allows us to avoid confounding factors of direct pathogen-pathogen interactions, because the fungus affects the skin, while the coronavirus infections occur internally, almost exclusively in the ileum and lungs [44]. We hypothesized that co-infection would alter the molecular response of bats to a persistent viral infection, and that viral shedding would change as a result of the increased or disrupted host immune response. To test this prediction, we examined tissues collected from *M. lucifugus* at the termination of an earlier study that quantified the effects and pathogenesis of *P. destructans* in hibernating bats experimentally infected with the fungus [189], some of which were naturally infected with *Myl*-CoV [44]. This combination of uninfected, virus-infected, fungus-infected and co-infected *M. lucifugus* allowed us to test our hypothesis that host responses to co-infection are synergistic and not simply additive.

5.6. Materials and methods

5.6.1. Sample acquisition

Fifty-four male *M. lucifugus* were collected from a WNS-free cave in Manitoba, Canada in November 2010. Details of the experimental design as well as protocols for collecting and transporting bats, infection with *P. destructans*, maintenance of bats in hibernation and sample collection have been described previously [189,253]. Briefly, bats in groups of 18 were either sham-inoculated or inoculated with North American or European isolates of *P. destructans*. Bats

were housed at 7°C and > 97% relative humidity with *ad libitum* water. All bats were equipped with data loggers to monitor skin temperatures. Bats were euthanized during the experiment when humanely required or at the termination of the experiment 120 days after inoculation. Immediately following euthanasia samples from segments of wing as well as various tissues were preserved in RNAlater (Qiagen, Cat #76016) or in formalin. Samples in RNAlater were kept at -20°C until they were processed. North American and European isolates of *P. destructans* caused similar disease outcomes [189], so we did not differentiate between the strains in subsequent analysis. The procedures for care, handling and euthanasia of bats were approved by the University Committee on Animal Care and Supply of the University of Saskatchewan (Protocol #20100120). Bats were collected under the province of Manitoba Wildlife Scientific Permit WB11145.

In 2017, a further 129 *M. lucifugus* were collected from a WNS-free cave in Manitoba, Canada in January under the Manitoba Sustainable Development Wildlife Scientific Permit No. SAR16009. Bats were euthanized during the experiment when humanely required or at the termination of the experiment 70 days after infection and a similar experiment was performed at the University of Winnipeg as described above (Protocol #AE08399).

5.6.2. Histological classification

During necropsy, we collected representative samples for histopathology from all major organ systems. In addition, representative samples were taken from all areas of the wing and rolled on dental wax before placing in 10% neutral buffered formalin. Tissues were processed routinely for histology. Five µm sections were cut and stained with periodic acid-Schiff stain to highlight fungal hyphae. Liver and other tissues were processed routinely and stained with hematoxylin and eosin. Wings were scored on a scale of 0 to 5 with 5 being very severe with > 50% of wing covered in fungal hyphae. We used a bacterial score from 0 to 5, with 5 indicating wide-spread and

abundant bacteria being present in many areas within the dermis and underlying connective tissues. Average scores from 5 sections of wing were used for analysis. Interstitial lung neutrophil assessment was similarly evaluated on a scale of 0 to 5, with 5 being very severe. Average scores from the 5 sections were used for analysis.

5.6.3. RNA Extraction

Tissues preserved in RNAlater were homogenized in 2ml sealed vials with a 5mm stainless steel bead, 0.1g of 0.1mm zirconia/silica beads and 350µl Buffer RLT Plus (with β-mercaptoethanol, RNeasy Plus Mini Kit, Qiagen, Cat #74136) using a Retsch MM400 Oscillating Mill at 30Hz for 4min. Total RNA was extracted following the manufacturers protocol. RNA integrity was assessed using RNA 6000 Nano Kit (Agilent, Cat #5067-1511) with the Agilent 2100 Bioanalyzer.

5.6.4. cDNA Synthesis

cDNA was synthesized from 1µg of RNA (or less if concentrations were too low) per reaction using QuantiTect Reverse Transcription Kit (Qiagen Cat #205313). cDNA samples were stored at -80°C until they were used for PCR.

5.6.5. Polymerase Chain Reaction (PCR)

Tissue samples were identified by their submission numbers with no reference to treatment class prior to analysis with PCR, so that evaluation of the results could not be inadvertently biased by knowledge of the treatment. We used semi-nested PCR to detect *Myl*-CoV. Primers were designed from the partial sequence of Rocky Mountain bat coronavirus replicase (accession number EF544563) (Table S9). The primary reaction used primers MyCVF1 and MyCVR1 to yield a 441 bp product. The secondary or nested reaction used primers MyCVF2 and MyCV R1 to give a 273 bp product. PCR were performed in a MJ Research PTC-200 thermal cycler using

TopTaq DNA Polymerase (Qiagen, Cat #200205). Each reaction (50 µl) contained 2 µl cDNA (or 1µl primary reaction), 200 nM of each primer, 200 µM of each dNTP (Invitrogen, Cat #10297018), TopTaq PCR buffer and 0.25 µl TopTaq. The thermal profile for the primary reaction was: 94°C for 3 min (denaturation), followed by 30 cycles of 94°C for 30 sec, 45°C for 30 sec (annealing), 72°C for 1 min and finally 72°C for 10 min. The thermal profile used for the secondary reaction was 94°C for 3min (denaturation), then 30 cycles of 94°C for 30 sec, 55°C for 30 sec (annealing), 72°C for 1 min and finally 72°C for 10min. PCR products were analyzed on ethidium bromide stained 1.0% agarose gels (Invitrogen, Cat #15510-027 in 0.5X TBE). PCR products were purified using MinElute PCR Purification Kit (Qiagen, Cat #28006) and verified by sequencing (Macrogen, Korea). If more than one DNA band was present, the appropriate size band was cut out and purified using QIAquick Gel Extraction Kit (Qiagen, Cat #28706) before sequencing.

5.6.6. Reverse-Transcription Quantitative PCR (RT-qPCR)

The Stratagene MX3005P qPCR System was used in conjunction with QuantiFast SYBR Green PCR Kit (Qiagen, Cat #204056). We quantified coronavirus with RNA primers MyCV F2 and MyCV R1 (Table S9). For initial experiments data were normalized to two transcripts – glyceraldehyde-3-phosphate dehydrogenase (GAPDH) and beta-actin [253]. As there were no differences in results, all subsequent experiments used only GAPDH as a normalizer using primers GAPDH US and GAPDH DS (designed for use in humans but also amplify *M. lucifugus* transcripts – Table S9). As well, a no-template (negative) control was included with every set of primers. Each 25 µl reaction contained: 1 µM of each primer set, 12.5 µl SYBR Green Master Mix and 8.5 µl of diluted cDNA.

To verify the RNASeq data, cDNA from ileum samples in which coronavirus RNA had been detected via RT-qPCR were analysed using the following primers, IL22RA1, IRF1, RERG

and SRC (for sequence of primers see Table S9). Primers were designed by aligning primers described for quantitating human cytokines (PrimerBank) with annotated transcripts of *M. lucifugus* genes: c-jun (Accession number: XM_006096110.1), cyclin D1 (XM_006098046.1), IL10 (XM_006094865.1) and TNF alpha (XM_006104644.1). The interferon beta primers were designed using the annotated transcript for the *E. fuscus* gene (XM_008145044.1), which also amplify transcripts from *M. lucifugus*. Primer efficiencies were determined from cycle threshold (Ct) values of purified PCR products serially diluted and re-amplified. Primers amplified targets with an efficiency of about 100% and in all cases the identities of the PCR products were confirmed by their specific dissociation temperature, specific sizes on agarose gels and by sequencing.

We observed primer-dimers in some reactions in addition to the PCR product. The dimers dissociated at 77°C, while the specific coronavirus polymerase product dissociated at 83°C. To avoid false positives due to primer-dimers, the thermocycler was programmed to read at 80°C (in the cycle after the primer-dimer had dissociated, and before dissociation of the target product). The thermal profile used was 95°C for 5 min followed by 40 cycles of 95°C for 10sec, 60°C for 30sec (readings taken at 80°C), and a final cycle of dissociation of product 95°C for 1 min, 55°C for 30 sec and 95°C for 30 sec (readings taken at every degree between 55°C and 95°C). Only results from reactions that yielded unambiguous results were used for analysis.

5.6.7. RNASeq Analysis

To explore the mechanisms driving high virus load in bats with WNS, we performed RNASeq analysis which could potentially screen all targets in the bat intestinal cells. We targeted the ileum transcriptome because this is the tissue in which *Myl*-CoV is present in detectable concentrations [44]. Extraction of RNA from ileum tissue, which includes the ileum and potential gut contents have been described in previous sections. Bats were screened for *Myl*-CoV using RT-

qPCR, and bats were assigned post hoc to treatment groups representing four infection histories (Figure 5.2.(A)): 1) Uninfected (bats were not infected with virus or fungus; n = 5), 2) Virus-infected (bats were naïve to the fungus but had a persistent *Myl*-CoV infection; n = 4), 3) Fungus-infected (bats were experimentally infected with *P. destructans* and no virus was detected*;* n = 3), or 4) Co-infected (bats with persistent *Myl*-CoV infections that were also experimentally infected with *P. destructans*; n = 4). All samples had adequate RNA quality for sequencing (i.e. RIN value >7).

5.6.8. RNA isolation

Tissues were homogenized in 2 ml sealed vials with a 5 mm steel bead, 0.1 g of 0.1 mm zirconium silica beads, 350 µL of RLT buffer (with β-mercaptoethanol) (RNeasy Plus Kit, Qiagen, Cat #74106) using a Retsch MM400 tissue homogenizer at 30 Hz twice for 2 minutes each. Total RNA from tissues was extracted using the procedure provided with the RNeasy Plus Kit.

5.6.9. cDNA library preparation and RNA Sequencing

Total RNA was sent to The Centre for Applied Genomics at The Hospital for Sick Children (Toronto, Canada). RNA quality was assessed using a Bioanalyzer (Agilent Technologies). We retained all samples with a DV200 (percentage of RNA fragments greater than 200 nt) greater than 85% (Table S1), discarding one Co-infected sample with a DV200 = 42%. Poly(A) mRNA was enriched using oligo dT-beads, and cDNA libraries were prepared using the NEBNext Ultra Directional RNA Library Prep Kit for Illumina (New England BioLabs). Barcoded libraries were pooled in equimolar quantities, and the sixteen libraries were sequenced on three lanes of a HiSeq 2500 System (Illumina Inc.), which generated 126 bp paired-end reads.

5.6.10. RNA Sequencing read alignment and analysis

We used FastQC v0.11.5 [206] to assess sequence quality and Trimmomatic v0.36 [207] to remove the adapter sequences and low-quality bases from reads with the following settings: Illumina clop:2:30:10, leading:3, tailing:3, slidingwindow:4:15, minlength:36. We used TopHat v2.1.1 [208] to align the trimmed paired-end reads from each library, separately, to the Ensembl *M. lucifugus* genome sequence (Myoluc2.0 [209]) in strand-specific mode (fr-firststrand) with mate-inner-dist values specific for the insert size of each library. We used featureCounts [256] to count reads mapped to the Myoluc2.0 genome annotation in strand-specific mode (reversely stranded), counting paired-end reads as fragments, counting only those fragments where both reads aligned successfully, counting multi-mapping fragments, and excluding chimeric fragments. We assessed the variability within and between the treatments using the R package SARTools v.1.3.0 [257]. The featureCount-estimated gene counts were transformed by a variance stabilizing method (VST) using SARTools.

We identified differentially expressed genes between each of the treatments using DESeq2 v.1.12.3, run in SARTools. Custom SARTools-based DESeq settings included: cooksCutoff=TRUE (perform outlier detection), independentFiltering=TRUE, alpha=0.05 (threshold of statistical significance), pAdjustMethod=BH (benjamini hochberg *p*-value adjustment method), and locfunc=median (estimate size factors). Differentially expressed genes were identified as having a fold-change > 2 and false discovery rate (FDR)-corrected *p*-values < 0.05 [258]. We produced volcano plots representing the differential expression comparisons by plotting the log of the adjusted *p* value as a function of the log ratio of differential expression. We used the Ensembl gene IDs identified by DESeq2 as input for the web-based g:Profiler [259] to test for gene ontology (GO) term enrichment among the differentially expressed genes, using a

FDR significance threshold <0.05. These GO-terms and their corresponding *p*-values were used in REViGO [260] to visualize significant enrichment of biological processes.

5.6.11. IgG capture ELISA against *Myl*-CoV N protein

Purified, glutathione-S-transferase (GST)-tagged *Myl*-CoV N protein expressed in infected *E. coli* BL21 cells was used as positive antigen, and GST-tagged protein expressed in uninfected BL21 cells was used as negative antigen. 96-well Costar high-binding round-bottom assay plates were coated with 0.05µg/well of either antigen diluted in 0.1M phosphate buffered saline (pH 7.4) in a total volume of 100µl. Plates were covered and incubated overnight at 4°C and washed three times with 300µl of PBS-Tween 20 (0.1%) immediately prior to use. Serum samples were diluted to 1:100 in PBS-Tween 20 (0.2%) supplemented with 5% fetal bovine serum (Gibco, Thermofisher, Cat #LS10082147). 100µl of each sample was added in parallel to a positive and negative antigen plate and incubated at 37°C for one hour and washed as above. A peroxidase-labelled goat anti-bat IgG secondary antibody (0.05µg in 100µl per well, Bethyl labs, Cat #A140-118P) was added, incubated for one hour at 37°C and washed as above. Peroxidase substrate (2,2'-azino-bis (3-ethylbenzthiazoline-6-sulfonic acid)) was added to each well and colour development was quantified 30 minutes later by measuring the optical density at 405nm using an ELISA microplate reader. The ELISA cut-off value (0.39) was calculated as the [(mean bat plasma O.D. values for bats that were PCR-negative for *Myl*-CoV in the ileum) + (3x standard deviations of those O.D values)].

5.6.12. Statistical analysis

Data from RT-qPCR and histopathological scores were analysed with SPSS Statistics version 23. The relative levels of a transcript for each bat were calculated as RT-qPCR Cycle threshold (Ct) normalized separately (ΔCt) to the "house-keeping" gene GAPDH. A ΔCt reduction

of one (1) indicates an approximately two-fold higher concentration of RNA. The significance of differences of mean values of ΔCt between co-infected bats and virus-infected bats were determined using an independent-samples Mann-Whitney U test. We calculated Pearson's coefficients to test the correlation between ΔCt levels for coronavirus polymerase cDNA for bats in each treatment class, and average scores for fungal hyphae, secondary bacteria, oedema, necrosis and inflammation in wing lesions, as well as bacteremia and levels of neutrophils in lung, spleen and liver interstitium.

5.6.13. Data Accessibility

All RNASeq fastq files have been submitted to the NCBI Sequence Read Archive database (accession number SRX3752319- SRX3752333).

5.6.14. Ethical Statement

Bat studies were carried out in strict compliance with Canadian Council on Animal Care guidelines and the procedure for care, handling, and euthanasia of bats were approved by the University Committee on Animal Care and Supply of the University of Saskatchewan (protocol s#20100120).

5.7. Results

Quantitation of *Myl*-CoV and *M. lucifugus* RNA through reverse transcription quantitative PCR (RT-qPCR) and dual-RNA Sequencing indicated that co-infected bats had significantly higher levels of *Myl*-CoV RNA than bats infected with virus alone. The amount of *Myl*-CoV RNA correlated with the severity of WNS pathology in co-infected bats. This phenomenon was associated with specific molecular responses to co-infection, even in the intestines of bats where only one of the two pathogens was directly interacting with the host tissue. The levels of antibodies

against *Myl*-CoV nucleocapsid (N) protein were also higher in co-infected bats. Each key result is discussed in detail below.

5.7.1. Bats co-infected with the fungus *P. destructans* and the virus *Myl*-CoV contained higher levels of *Myl*-CoV RNA

Myl-CoV genomic RNA was detected in bats infected only with *Myl*-CoV (virus-infected; 7/18), co-infected bats (European *P. destructans* (3/13), or with North American *P. destructans* (7/16) [189]). There was no difference in the frequency of *Myl*-CoV detected among these treatments (*chi-square* statistics; *p-value* = 0.49). We pooled bats infected with the two *P. destructans* isolates for all further analyses and tested whether co-infection with *P. destructans* and *Myl*-CoV correlated with an increase in viral replication. Our RT-qPCR data showed that the co-infected bats contained 60-fold more *Myl*-CoV RNA on average than the virus-infected bats (Mann Whitney test; *p-value = 0.014*; Figure 5.1).

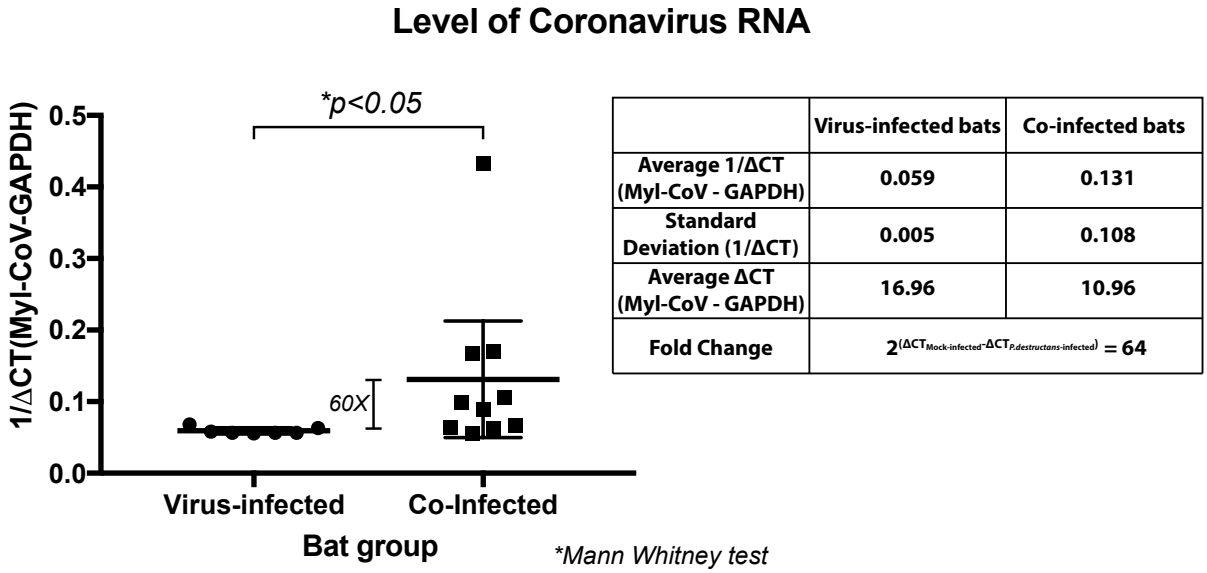

	Virus-infected bats	Co-infected bats
Average 1/ΔCT (Myl-CoV - GAPDH)	0.059	0.131
Standard Deviation (1/ΔCT)	0.005	0.108
Average ΔCT (Myl-CoV - GAPDH)	16.96	10.96
Fold Change	$2^{(\Delta CT_{Mock\text{-}infected} - \Delta CT_{P.destructans\text{-}infected})} = 64$	

Figure 5.1. Effect of white-nose syndrome on level of *Myotis lucifugus* coronavirus (*Myl*-CoV) RNA in hibernating little brown bats (*M. lucifugus*). Relative transcript levels for the coronavirus RNA polymerase gene for each bat are depicted as reciprocal of Cycle threshold (Ct)

normalized separately (ΔCt) for levels of glyceraldehyde 3-phosphate dehydrogenase (GAPDH) transcripts in each sample. The horizontal bar represents the mean while the vertical bar indicates standard deviation from the mean. Significance (*p* value) is as calculated with an independent Mann-Whitney test. Virus-infected bats had lower 1/ΔCt values for coronavirus RNA than co-infected bats. The average fold-differences between virus-infected and co-infected bats were calculated from the difference between the average ΔCt values.

Relative quantities of *Myl*-CoV RNA detected in the ileum of the virus-infected bats were low and showed low variation (Standard Deviation of 1/ΔCT=0.005), compared to the relative quantities of *Myl*-CoV RNA in the co-infected bats (Standard Deviation of 1/ΔCT=0.108; Figure 5.1). The severity of WNS fungal pathology varied in co-infected bats, and we therefore tested whether relative quantities of viral RNA in the ileum correlated with the severity of WNS symptoms. Levels of WNS severity were scored based on fungal hyphae on the wings, secondary bacteria in wing lesions, oedema, necrosis and inflammation in wing lesions, and levels of neutrophils in lung, spleen and liver interstitium. Severity scores for wing tissue, secondary bacteria in lesions, and neutrophils in the lung interstitium positively correlated with relative amounts of coronavirus RNA in hibernating bats (Table 5.1).

Table 5.1. Correlation between level of *Myotis lucifugus* coronavirus RNA and disease severity of white-nose syndrome (WNS) in co-infected *M. lucifugus*, based on three measures of WNS severity and pathology.

Correlate	Level of coronavirus RNA		
	Pearson Correlation[1]	Significance	N
Virus-infected/Co-infected	-0.610	0.009	17
Average hyphae score	-0.630	0.016	14
Average bacterial score	-0.680	0.007	14
Lung interstitial neutrophils	-0.618	0.043	11

[1]Pearson's coefficients were calculated for the ΔCt levels for cytokine transcripts for bats in each treatment class and lung interstitial neutrophil scores and mean bacterial and hyphae scores for 5 wing sections for each bat.

5.7.2. Bat responses to co-infection exceed the sum of responses to virus or fungal infection alone.

To determine the extent to which *Myl*-CoV and *P. destructans* infection interact to influence gene expression in bat intestines, we performed a transcriptomic analysis on bat intestines comparing gene expression among the uninfected, virus-infected, fungus-infected, and co-infected treatments (Figure 5.2. (A)). RNA sequencing resulted in ~ 700 million paired-end reads passing filters, 65% of which aligned to the *M. lucifugus* genome (Table S1). Pairwise differential gene expression varied widely among the four treatments with relatively low overlap in differentially expressed transcripts (Figure 5.2. (B); 5.2. (C), Supplementary figure S5.1). Similar transcript expression occurred between the uninfected and virus-infected bats, and between the fungus-infected and co-infected bats.

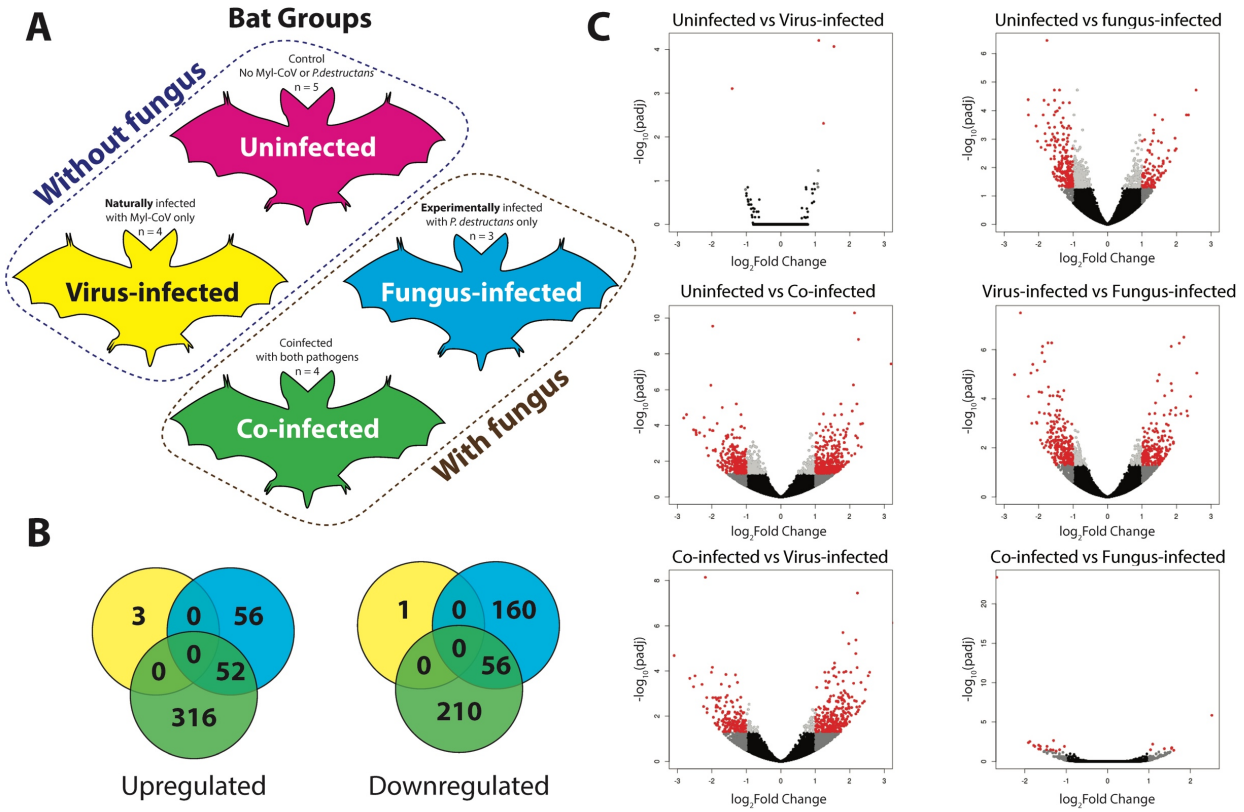

Figure 5.2. Co-infection of little brown bats (*Myotis lucifugus*) with *M. lucifugus* coronavirus (*Myl*-CoV) and *Pseudogymnoascus destructans* results in non-additive patterns of gene expression compared to sole infection with the virus or fungus. (A) Experimental design, showing the four treatments of little brown bat (*Myotis lucifugus*) established by experimental inoculation with *Pseudogymnoascus destructans* and by qPCR detection of persistent *Myl*-CoV infections: uninfected, virus-infected, fungus-infected and co-infected **(B)** Differential gene expression identified by DESeq2 among virus-infected, fungus-infected and Co-infected bats as compared to the change each exhibited relative to uninfected bats. **(C)** Differential gene expression among the four treatments, detected by DESeq2 and visualized in volcano plots. The log of the adjusted *p*-value is plotted as a function of the log ratio of differential expression. Colored data points represent different groups of genes based on fold change and false discovery rate (FDR) cutoff; red (>2 fold change, FDR<0.05), dark grey (>2 fold change, FDR>0.05), light grey (<2 fold change, FDR<0.05), black (<2 fold change, FDR>0.05).

The fungus-infected bats exhibited a much stronger response, differentially expressing 324 transcripts compared to the uninfected bats (Table S3). These transcripts were enriched for only two gene ontology (GO) terms (cell-cell junction and plasma membrane part; Table S8). The co-

infected bats differentially expressed 634 transcripts relative to the uninfected bats (Table S4). These transcripts showed significant enrichment for 16 GO terms (Table S8). The co-infected and fungus-infected bats shared 108 similar differentially expressed transcripts and overlapped in one enriched GO term relative to the uninfected bats (plasma membrane part; Table S8).

5.7.3. Effect of infection with the fungus *P. destructans* on the expression of genes linked to innate responses in the intestines of bats infected with the virus *Myl*-CoV.

When we directly compared responses of bats among the four treatments, response of the virus-infected bats differed strongly from the responses of fungus-infected or co-infected bats (virus-infected vs. fungus-infected: 461 differentially expressed transcripts and 9 significantly enriched GO terms; virus-infected vs. co-infected: 473 transcripts and 43 enriched GO terms; Tables S5, S6, S7; Supplementary figure S5.1). These differences in gene expression patterns included genes that clustered in two processes relevant to host-pathogen interactions – the mitogen-activated protein kinase (MAPK) pathways and cytokine and innate immune responses. Table 5.2 lists genes from the two processes that were significantly either up or down-regulated when virus-infected bats were compared to co-infected bats. For the MAPK pathway-related transcripts, genes such as RSU1 and RERG were up-regulated while those, such as STYK1, RRAD, MAP3K and SRC were down-regulated. For cytokine-related genes several transcripts were suppressed. When we compared the expression of the same genes for bats with WNS (combining fungus-infected and co-infected bats) and all bats without WNS (combining uninfected and virus-infected bats), we found similar differences (last two columns of Table 5.2). This suggested that superficial infection with fungus, *P. destructans*, was the driving factor for altered gene expression in the bat intestines.

Table 5.2. RNA Sequencing identified differential expression of transcripts related to the MAPK pathway and to cytokine-related processes, comparing gene expression in the ileum of little brown bats (*Myotis lucifugus*) infected only with the *M. lucifugus* coronavirus (*Myl*-CoV; virus-infected) or co-infected with *Myl*-CoV and *Pseudogymnoascus destructans*. The last 2 columns show the same comparisons made after grouping bats that were not exposed to the fungus, and bats that were exposed to the fungus and exhibiting symptoms of WNS (irrespective of their viral infection status).

		Virus-infected vs. Co-infected		All bats "without fungus" vs. all bats "with fungus"[1]	
Ensembl Gene Name	**Ensembl Description**	**$Log_2FoldChange$[2]**	**Padj**	**$Log_2FoldChange$[2]**	**Padj**
MAPK pathway-related transcripts					
STYK1	serine/threonine/tyrosine kinase 1	-1.268	0.025	-1.516	< 0.0001
RSU1	Ras suppressor protein 1	1.102	0.004		
RRAD	RRAD, Ras related glycolysis inhibitor and calcium channel regulator	-1.297	0.028	-1.3	0.025
RERG	RAS like estrogen regulated growth inhibitor	1.562	0.018	1.416	0.005
MAP3K11	mitogen-activated protein kinase 11	-1.14	0.040	-1.13	0.0002
SRC	SRC proto-oncogene, non-receptor tyrosine kinase	-1.539	0.013	-1.297	0.0037
Cytokine-related transcripts					
IRF1	Interferon regulatory factor 1	-1.551	0.001	-1.444	0.0001
IFI6	Interferon alpha inducible protein 6	-1.798	0.014	-1.352	0.039
IL22RA1	Interleukin 22 receptor subunit alpha 1	-1.411	0.015	-1.314	0.002
SOCS6	Suppressor of cytokine signaling 6	-1.278	0.008	-1.534	< 0.0001

[1](Uninfected + virus-infected) vs. (fungus-infected + co-infected)

[2]Positive log2 fold-change values indicate higher expression in the second listed treatments relative to the first.

To confirm the results of the RNASeq analysis, we selected 4 genes from Table 5.2, namely IRF1, RERG, SRC and IL22RA1, to be verified by RT-qPCR. We also included interleukin 10 (IL10) due to its biological relevance to immune regulation and because we had previously observed an increase in its expression related to fungal infection [253]. As we wanted to confirm whether WNS was driving gene expression in the intestines of bats, we performed a two-group

analysis for the RT-qPCR data. We combined all the bats without WNS into a single group (uninfected + virus-infected) and all the bats with WNS into the other group (fungus-infected + co-infected; Figure 5.3. (A)). Expression of Ras-like estrogen regulated growth inhibitor (RERG) increased while expression of Interleukin 22 receptor subunit alpha 1 (IL22 RA1) genes decreased in bats with WNS, irrespective of viral infection (Figure 5.3. (C) and (E)). Expression of the immune modulatory cytokine IL10 tended to be higher in bats with WNS than in bats without WNS, but the difference was not statistically significant (p-value = 0.07) (Figure 5.3. (F)).

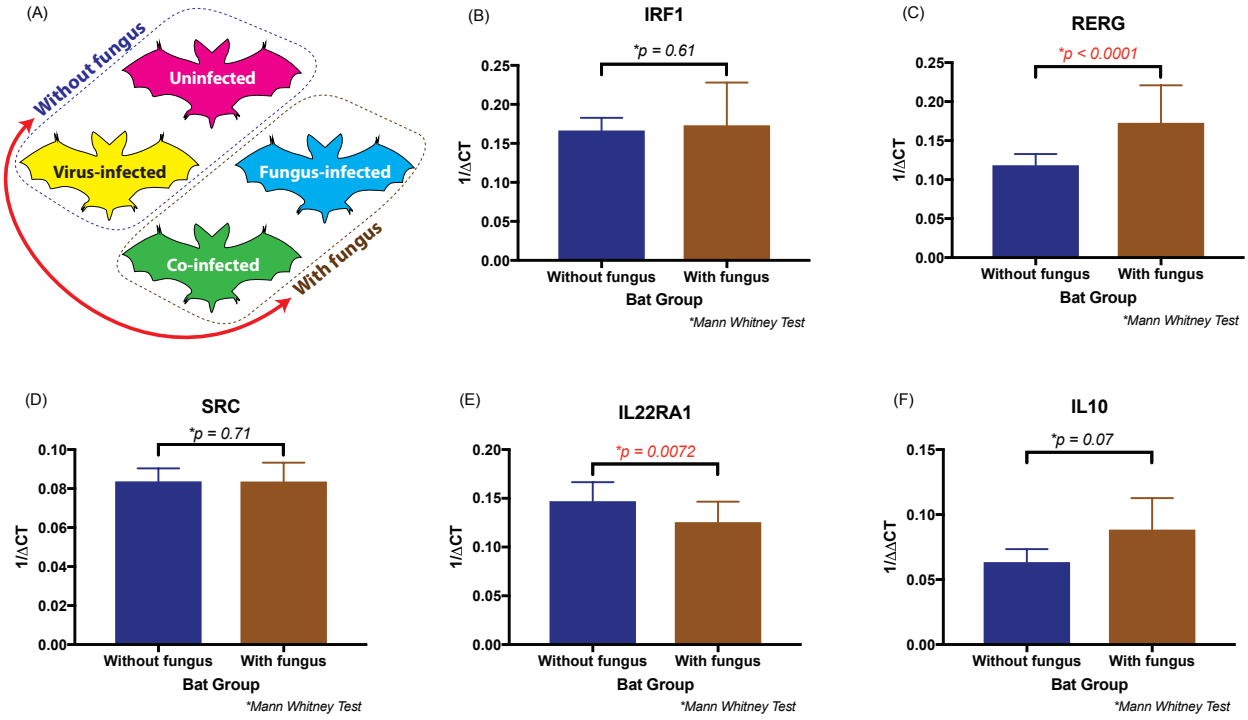

Figure 5.3. Effect of white-nose syndrome (WNS) on the levels of immune genes IRF1, RERG, SRC, IL22RA1 and IL10 expressed in the ileum of little brown bats (*Myotis lucifugus*). (A) Summary of the four treatments, with a red arrow indicating the two groups ("with fungus" and "without fungus") that were compared. (B-F) The relative transcript levels of each gene for bats with and without WNS, depicted as reciprocal of Cycle threshold (Ct) normalized separately (ΔCt) for levels of transcripts for GAPDH in each sample. Statistical significance was calculated based on the independent Mann Whitney test. The difference in the two groups was significant for RERG and IL22RA1 genes.

5.7.4. White-nose syndrome is associated with increased coronavirus antibody levels in the co-infected bats.

In 2017, we performed a similar study, experimentally exposing 63 *M. lucifugus* to *P. destructans* as described in Warnecke *et al* [189]. We performed IgG ELISA on blood plasma to detect *Myl*-CoV (coronavirus) N protein antibodies and found that 21/63 were positive for antibodies against the coronavirus. Of those 21 bats, 7 had detectable coronavirus RNA in their intestines suggesting an active infection, and 3 out of the 7 had been experimentally infected with *P. destructans* during the course of the study. We compared the ELISA optical density (O.D.) values of these virus-infected bats to co-infected bats (Figure 5.4. (A)) and found that the presence of *P. destructans* was associated with increased levels of coronavirus antibodies (Mann Whitney test, *p* value = 0.03; Figure 5.4. (B)).

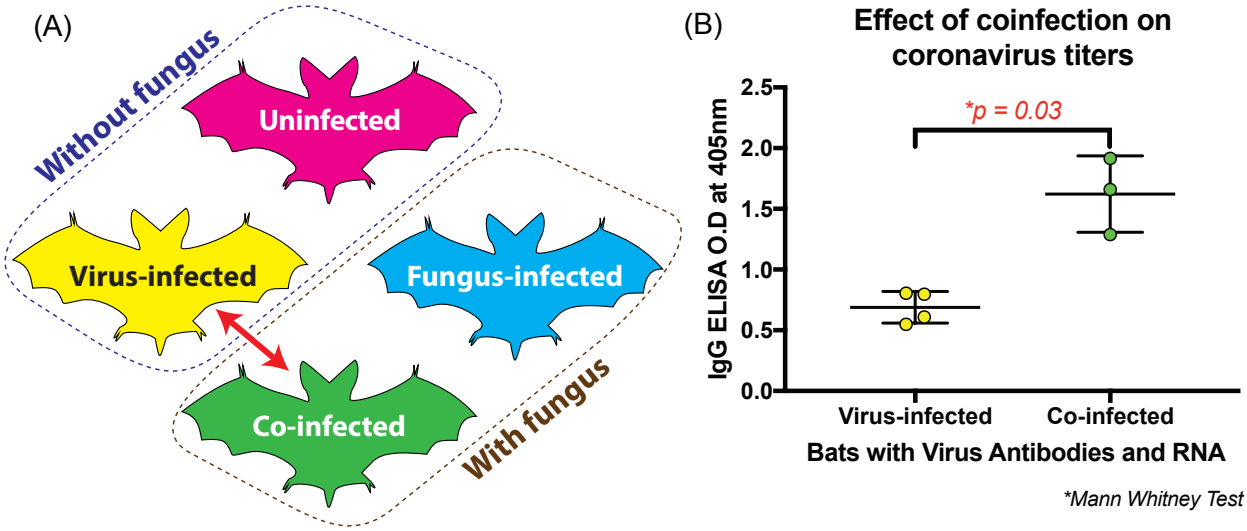

Figure 5.4. Little brown bats (*Myotis lucifugus*) coinfected with *M. lucifugus* coronavirus (*Myl*-CoV) and *Pseudogymnoascus destructans* produce more antibodies against *Myl*-CoV than bats infected only with *Myl*-CoV. (A) Diagram summarizes the four treatments; the red arrow shows the two groups between which antibody levels were compared. (B) Antibody levels against the *Myl*-CoV N protein detected by antibody capture ELISA expressed as optical density

(O.D.) values at 405nm. Co-infected bats had significantly higher antibody levels than bats infected only with *Myl*-CoV (independent Mann Whitney test; *p* value = 0.03).

5.8. Discussion

Our findings suggest that systemic responses of bats to WNS results in increased coronavirus replication and consequently, increased viral shedding, which may lead to subsequent infection of susceptible animals. Coronavirus infection may in turn increase the severity of WNS pathology. This is the first study to examine the systemic effects of co-infection on either bat coronavirus or WNS, and our results raise important questions in regard to zoonotic spillover events. Although events of successful viral spillover to distantly related species are thought to be extremely rare, in recent years several coronaviruses have spilled over, including SARS-CoV [190], MERS-CoV [191,192,228,229], PEDV-CoV [195] and SADS-CoV [133]. These viruses are thought to have originated in bats. In addition, circumstantial evidence suggests that most alpha and beta coronaviruses that parasitize other mammals may have originated in bats as well [217]. If so, then understanding host-pathogen interactions between bats and coronaviruses could inform our ability to predict or manage the risk of spillover. In this study, we showed that a coronavirus exhibits low activity in its natural host, *M. lucifugus,* but that co-infection with a fungus increases the quantity of viral RNA in the intestines. We have no reason to expect zoonotic transmission of the coronavirus i.e. *Myl*-CoV, but similar co-infection mechanisms may operate in tropical bat species harbouring potentially zoonotic viruses.

Our results suggest that secondary skin infection with the fungus, *P. destructans*, substantially increases the level of viral RNA in the intestine of hibernating bats. We showed that infection of the skin with *P. destructans* can cause profound changes in gene expression in the intestines, despite a lack of direct contact between intestinal tissue and the fungus. Infection with

P. destructans causes modulation of a number of immune responses, including down-regulation of interleukin and cell proliferation genes which may compromise bats' ability to suppress viral activity (Figure 5.5). Taken together, our results have implications for epidemiological studies of *P. destructans,* the WNS fungus and for research into viral spillovers, which should consider the potential implications of co-infections that increase viral shedding.

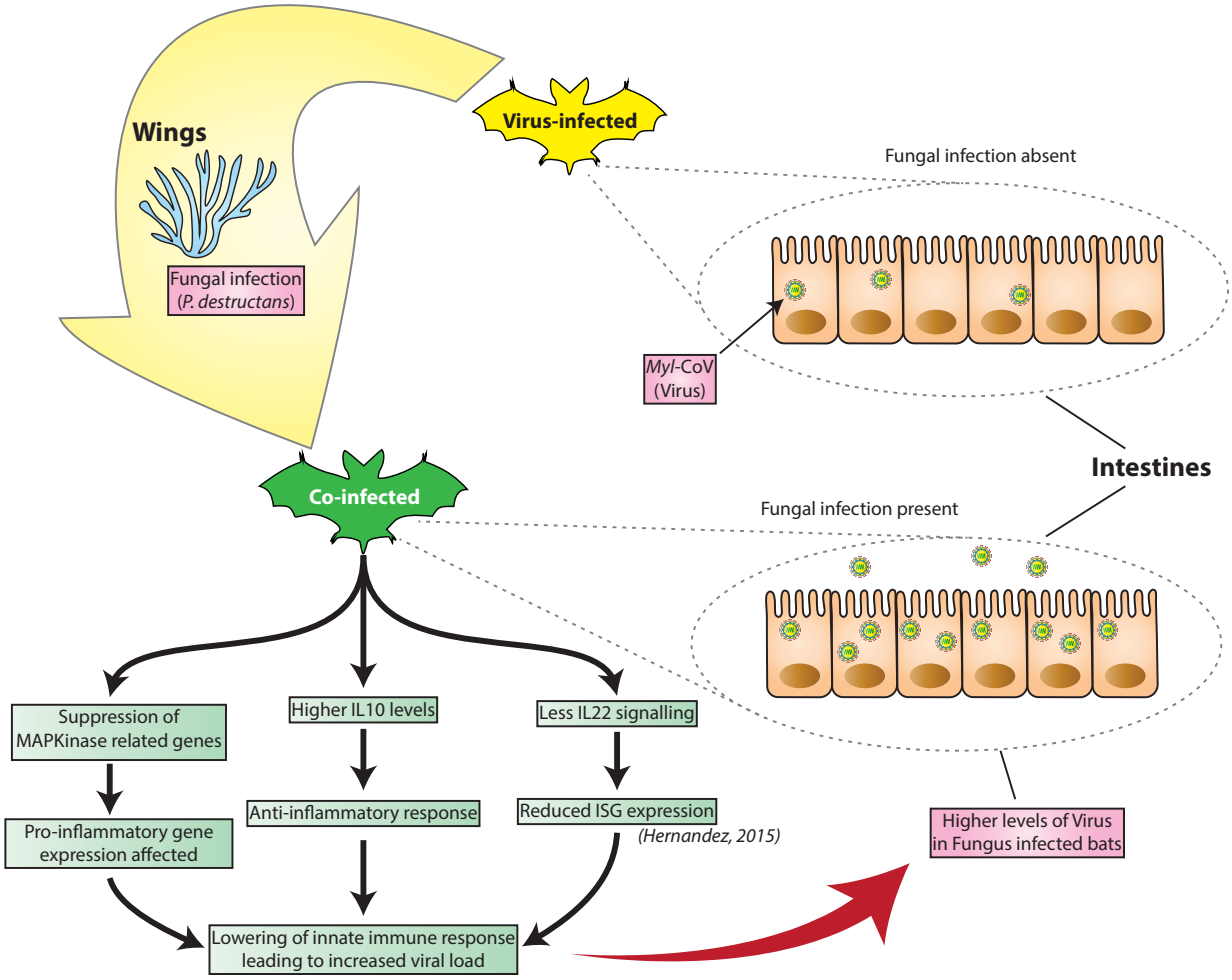

Figure 5.5. Hypothesized model of pathways involved in increased coronavirus shedding and white-nose syndrome (WNS) severity in little brown bats (*Myotis lucifugus*) co-infected with *M. lucifugus* coronavirus (*Myl*-CoV) and *Pseudogymnoascus destructans*. Diagram summarizes the changes observed by comparing co-infected bats with virus-infected bats. Bats with persistent *Myl*-CoV infection exhibit relatively low viral shedding. When bats are also infected with *P. destructans* (shown in yellow arrow) and develop WNS, the level of coronavirus increases. There is a change in the level of some immune genes, such as IL22, RERG and possibly

IL10, which may have an effect on immune response and cell proliferation. The increase in coronavirus levels in co-infected bats is possibly due to the bats' systemic response to WNS reducing innate antiviral responses.

Complex strategies allow viruses to remain endemic in populations. These include a continuously replenished source of susceptible hosts for viruses that cause short-term acute infections with long-lasting immunity (e.g. measles virus), antigenic drift of virus (e.g. influenza virus) or waning immunity (e.g. respiratory syncytial virus) that allows reinfection, and long-lasting latent (e.g. herpesviruses) or persistent infections (e.g. pestiviruses) with sustained or periodic shedding. It is not yet clear how bat viruses are maintained in their natural host populations, or how they avoid extinction as host populations become immune and less susceptible. Persistent infections can be established in cultured cells with viruses that may have originated in bats, including Ebola virus [219] and SARS-CoV [221,261,262], but whether these viruses persist in their primary hosts is not known. Studies of persistence of bat viruses in infected bats have produced equivocal results. The lack of direct evidence supporting specific models of persistence or transmission dynamics represents a major knowledge gap in bat-virus ecology [12].

We maintained *M. lucifugus* in controlled laboratory hibernation chambers for four months during these experiments, and we detected the coronavirus i.e. *Myl*-CoV, at the end of hibernation. These data imply that the coronavirus can persist in its host for at least the duration of hibernation, particularly as nucleotide variability among the detected coronavirus isolates showed that spread of coronavirus among bats within a chamber was unlikely [44]. In an extensive study of New World *Alphacoronaviruses*, no target viruses were detected in the rectal swabs of individual bats sampled over time [217], suggesting that persistence and intensity of shedding varies among species or viruses. The authors concluded that the targeted coronaviruses do not persist in their hosts but are maintained in populations by the introduction of new susceptible individuals.

However, their results could also reflect viral persistence in individual animals, with low baseline levels of virus replication and undetectable shedding interspersed with periods of increased replication and shedding that did not occur during the sampling period.

Periodic or seasonal increases in virus shedding associated with parturition, lactation, nutritional deprivation or environmental stress [12,246] suggest persistent or latent viruses may be activated by hormonal or other systemic cues. Direct evidence linking a specific trigger to increased shedding has not yet been found. However, viral replication in rodent and bat cells persistently infected with Ebola virus increased greatly following modulation of the Ras/MAPK pathway with lipopolysaccharides or phorbol esters, and with the resulting suppression of the cells' interferon response [219,261,262]. In experimental systems, the immune modulatory cytokine IL10 also influences viral persistence and replication [263–265], although more study is required to clarify the effects of circulating cytokines on the replication of persistently infecting viruses. Nevertheless, these results suggest that circumstances which induce anti-inflammatory cytokines or suppress antiviral innate responses, may provide a trigger for increased shedding of persistently infecting virus.

We discovered that bats with WNS (fungus-infected and co-infected) had significantly lower intestinal levels of transcripts for IL22RA1 and other interferon-related genes as compared to uninfected bats, and we observed the same trend in IL10 (although it was not significant; p value = 0.07). IL22RA1 is the receptor present on host cells, including intestinal cells, which help in initiating cellular signalling in response to IL22 produced by T-cells [266]. IL-22 leads to an increase in anti-microbial peptide production, cellular protection against damage and increases cellular proliferation [267]. Therefore, reduced IL-22 signalling in the intestines of bats with WNS, might suppress the bat defences that control the coronavirus infection. Additionally, previous

studies have shown that the anti-inflammatory gene, IL-10, is expressed more in the lungs of bats with WNS than in bats without it [253]. We saw a similar trend with the levels of IL-10 in the intestines which might play a role in suppressing the immune response against the coronavirus. Another altered cytokine gene which was of interest was the suppressor of cytokine signalling-6 (SOCS6) gene. Fungal-infected bats showed lower levels of SOCS6 transcripts, lack of which has been implicated in mild growth retardation in mice [268]. Overall, our results suggest that WNS triggers changes in gene expression in the ileum (Figure 5.5). These may influence expression of interferon-stimulated-genes (ISGs), thereby leading to increased viral replication at the site of viral persistence. Interferon-related transcripts were more highly expressed in the ileum of virus-infected bats that did not have WNS, suggesting that the bat's response to WNS causes down-regulation of interferon activity. Interferons may control coronavirus replication, as seen in cases of SARS-CoV [269] and MERS-CoV [270]. Therefore, a decrease in interferon activity might cause an increase in coronavirus (*Myl*-CoV) replication. In addition to interferon-related genes, we also found that RERG, which is related to growth inhibition, was upregulated in the fungus-infected bats when compared to virus-infected bats. Upregulation of RERG could affect the rate of cell proliferation in the intestines [271]. Finally, this cascade of responses is associated with increased severity of WNS symptoms.

Bats with WNS experience a range of systemic disturbances including dehydration, hypovolemia, metabolic acidosis and fat depletion [59,60], neutrophil infiltration of the lung interstitium, and increased expression of transcripts related to anti-microbial and pro- and anti-inflammatory cytokines [253]. Taken together, this evidence suggests that hibernating bats respond systemically to superficial fungal infection, and this hypothesis is further supported by our observations of altered gene expression in the ileum of fungus-infected bats.

Based on our results, we propose a model for how secondary infections may increase the replication and subsequent shedding of persistently infecting virus (Fig. 5). The establishment of WNS (or other secondary infection) impacts the tissue with which that pathogen interacts (in the case of *P. destructans*, the skin). Direct interactions between the host and the secondary pathogen are limited to the affected tissue, but the systemic response to the disease triggers a cascade of immune responses, including increased release of cytokines or neutrophils. Affected cells such as intra-alveolar macrophages in the lungs or cells lining the intestine, may produce pro- or anti-inflammatory molecules and influence cells that harbour viral genomes. This cascade of host responses disrupts the equilibrium between the persistently infecting virus and the cell's innate immune response, leading to a dramatic increase in the expression of coronavirus (*Myl*-CoV) replication.

Our assays were unfortunately limited to analysing viral and cytokine transcripts rather than protein, because reagents for detecting bat viral and host proteins are not yet available. We were not able to perform serial dilutions of the plasma to precisely quantify antiviral titre due to the limitation in the amount of plasma obtained from each bat. The sample size was also small for this assay, because only 7 of the sampled bats had detectable levels of coronavirus in their intestines and were positive for viral antibodies. Despite these limitations, we demonstrated higher antibodies against the coronavirus in the plasma of co-infected bats when compared with virus-infected bats. This increased antibody level in co-infected bats might reflect an adaptive immune response to increased coronavirus replication in the intestines.

Our proposed hypothesis for the mechanism driving increased viral replication following pathogenic co-infection was worth testing, but our results are also consistent with an alternative hypothesis. Increased viral replication or viral load may affect the severity and population-level

impacts of WNS. Bat mortality following the arrival of WNS varies widely from site to site, with populations decreasing from 30% to 99% [250]. Variation in the microclimate, and other ecological factors may drive some of this variation [272], but our data suggest that cryptic viral infections may also play a role in determining survival rates for bats hibernating in sites colonized by *P. destructans*. We recommend that future studies on population-wide impact of WNS incorporate viral sampling to help better understand the role of co-infections on bat populations in the wild.

5.9. Suplementary Information

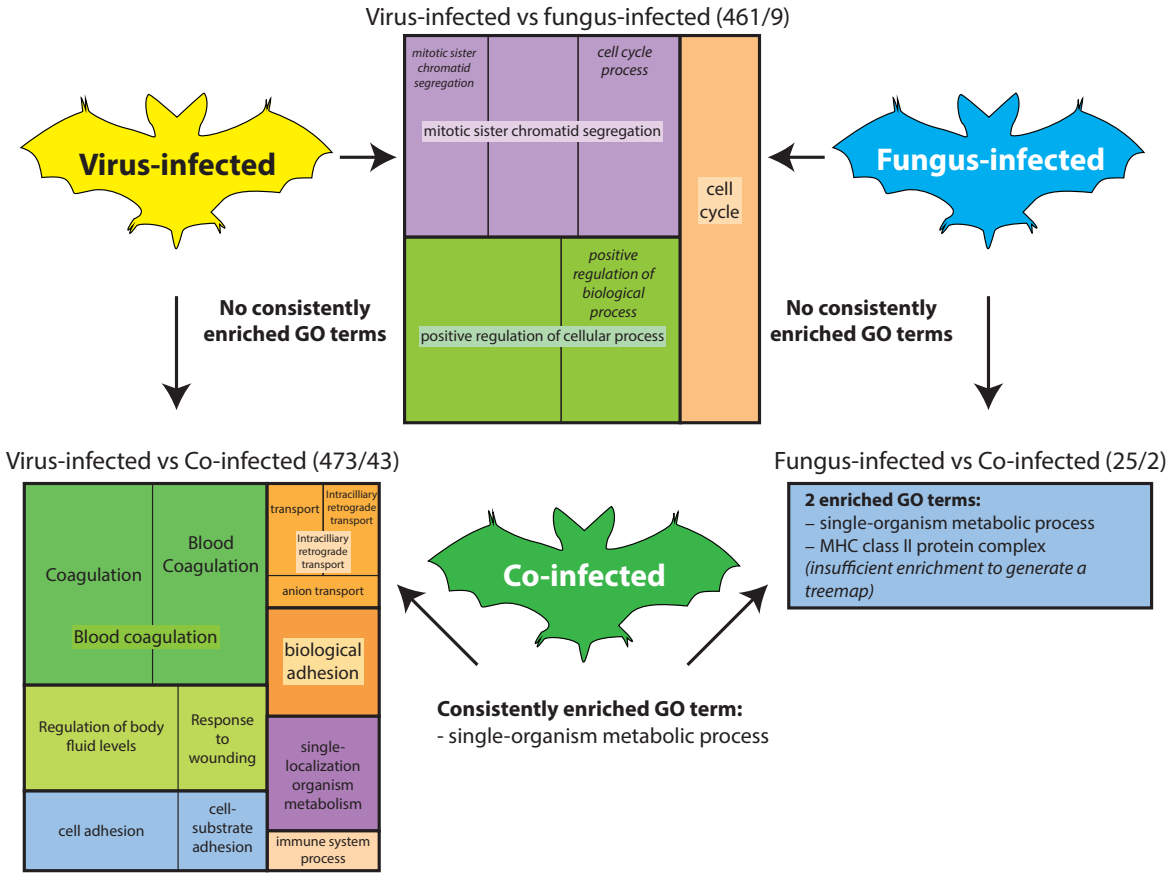

Supplementary figure S5.1. Pairwise differential gene expression enriched for various gene ontology (GO) terms.

Supplementary tables for chapter 6 in the Dataset file

Link - https://static-content.springer.com/esm/art%3A10.1038%2Fs41598-018-33975-x/MediaObjects/41598_2018_33975_MOESM2_ESM.xlsx

Table S1. Read statistics of RNASeq samples.
Table S2. Differentially expressed genes determined by DESeq2 for the Negative (mock-infected) vs. MylCoV comparison.
Table S3. Differentially expressed genes determined by DESeq2 for the Negative (mock-infected) vs. *P. destructans* comparison.
Table S4. Differentially expressed genes determined by DESeq2 for the Negative (mock-infected) vs. Coinfected comparison.
Table S5. Differentially expressed genes determined by DESeq2 for the MylCoV vs. *P. destructans* comparison.
Table S6. Differentially expressed genes determined by DESeq2 for the Coinfected vs. MylCoV comparison.
Table S7. Differentially expressed genes determined by DESeq2 for the Coinfected vs. *P. destructans* comparison.
Table S8. Gene Ontology Enrichment Analysis (g:GOSt) summary using DESeq2 determined differentially expressed genes (>2 fold change, FDR<0.05).
Table S9. Details of primers used for PCR

5.10. Transition statement

In this chapter, I described our studies showing that the extent of *P. destructans*-induced pathology in bat wings correlated with the amount of coronavirus in their intestines. Furthermore, the intestine of fungus-infected bats showed changes in gene expression suggesting suppressed innate anti-virus and increased apoptotic responses. To determine if these changes influenced the virus-host cell relationship in cells persistently-infected with the virus, we established a persistent coronavirus infection in cultured bat cells. Since we had not been able to isolate *Myl*-CoV, for these experiments we used the MERS-CoV, a virus thought to have originated in insectivorous bats. This cell culture model of coronavirus persistence allowed us to test the hypothesis that MERS-CoV would establish long-term persistent infections in bat cells because of the virus' inability to completely suppress the host anti-viral responses, and that forced suppression of these responses would allow increased virus replication.

Chapter 6: Host specific adaptations of Middle East Respiratory Coronavirus (MERS-CoV) for persistent infection of bat cells

6.1. Citation

Banerjee, A., **S. Subudhi**, N. Rapin, R. Jain, J. Lew, D. Falzarano and V. Misra. "Persistent infection of insectivorous bat cells with Middle East respiratory syndrome coronavirus." Manuscript under preparation. AB and I contributed equally to the study and are co-first authors.

6.2. Contribution

Several authors contributed significantly to this study. **AB and I contributed equally to the work described in this chapter**. AB and I prepared the initial draft of the manuscript and all authors were involved in editing and refining the manuscript. I designed experiments, performed *in-situ* hybridization, designed primers, quantitated RNA using real time PCR and analysed sequencing data. AB setup the initial persistent infection in bat cells and repeated the experiment. AB and NR performed cell culture related assays with MERS-CoV in level 3 lab. AB performed immunoblots, immunofluorescence imaging and siRNA knockdown. RJ, JL and DF performed sequencing of the mutated MERS-CoV.

6.3. Abstract

Many viruses that cause no apparent disease in their natural bat hosts are thought to have spilled over into people and other animals causing serious and often fatal illness. Coronaviruses such as those causing Severe Acute Respiratory Syndrome (SARS) and Middle East Respiratory Syndrome (MERS) may also have originated in bats as closely related viruses have been detected in insectivorous bat species. The mechanisms by which viruses are maintained in individuals or

populations of reservoir bat hosts is not known, but may involve long-term persistent infection with continuous low-levels of shedding and infection of susceptible individuals. The adaptations required for the viruses to infect and establish infections in spillover species are also not clearly understood. Here we describe the long-term persistent infection by MERS-coronavirus (MERS-CoV) in bat cells. Continued survival of the cells, accompanied by low levels of virus production, was depended on the inability of the virus to suppress cellular innate responses. Knocking down of interferon response factor 3 (IRF3), a critical mediator of the antiviral response, increased virus replication in the cells and resulted in their death. Persistence of virus replication in bat cells led to rapid selection of MERS-CoV variants with inactivating mutations in the viral open reading frame 5 (ORF5). Our results support the hypothesis that at a low multiplicity of infection, cells infected by rare ORF5 mutants survive because higher levels of expression of interferon and interferon stimulated genes suppress apoptosis. The ORF5 mutant-infected cells then resist infection by wild-type virus, quickly supplanting virus with functional ORF5. Our studies may provide a model for examining stressors that may unbalance the delicate virus-host relationship in reservoir bat species leading to increased chances of spillover to other animals.

6.4. Introduction

Viruses, on rare occasions, spillover from reservoir species to other animals. Establishment in these new hosts requires viruses to adapt to the use of viral receptors as well as circumvent innate antiviral defense mechanisms unique to each host species. The mechanisms underlying these changes that govern new virus-host dynamics are not clearly understood. Bats have been speculated to be reservoirs of several emerging viruses, including coronaviruses (CoVs) that cause severe acute respiratory syndrome (SARS) and Middle East respiratory syndrome (MERS) in

humans, and porcine epidemic diarrhea (PED) and swine acute diarrhoea syndrome (SADS) in pigs [1,20,133,273]. MERS-CoV is an on-going concern as it causes periodic outbreaks in the Middle East with a mortality rate of about thirty-five percent [123]. Human to human transmission of the virus occurs through aerosol or close contact. Camels are known to harbor MERS-CoV and play an important role in the transmission of the virus to humans [141,274]. Although camels are the direct source of MERS-CoV infection, bats are considered as the evolutionary source of such coronaviruses. MERS-CoV belongs to betacoronavirus lineage C (2c) and several 2c coronaviruses, such as HKU4, HKU5 and NeoCoV, have been detected in bats [192,275]. Coronaviruses, such as MERS-CoV, are able to rapidly adapt to the species which they infect. Such adaptations usually occur in the spike protein as its interaction with host receptor is necessary for infection [276,277]. Coronavirus adaptations in genes, apart from spike, that are driven by factors of their bat reservoir host, are less well known. Although bats harbor such coronaviruses, they do not cause obvious signs of disease in bats. In contrast, infection in spillover species such as humans and pigs, leads to disease with significant morbidity and mortality [39,122,199,278–281].

To understand the emergence of coronaviruses from bats, a more thorough understanding about the bat-virus relationship is needed. Currently, much of the information about these viruses derives from observations in the spillover species or from experimental animals; little is known about the molecular processes that govern the relationship of the viruses with their bat hosts. One of the studies conducted in our lab has shown that bat coronaviruses can persist in their natural host for at least four months of hibernation [44]. This persistent infection could be affected by stressful events such as secondary fungal infections [62]. Viral persistence in bats and its disruption

during stressful events has been observed for other viruses such as henipavirus [282]. Further studies would help elucidate the molecular pathogenesis behind this phenomenon.

Members of coronavirus family possess a high level of variability, specifically in their accessory proteins. These proteins are not required for replication but provide vital functions within the context of infection in a particular host. Primarily, these proteins are required for antagonizing the host response against the virus [283]. The MERS-CoV accessory proteins ORF4a and ORF4b are responsible for inhibiting the type I interferon response [283] and ORF5 has been shown to modulated the NF-κB pathway [284]. Despite these studies in cultured cells, interactions of these accessory proteins in their evolutionary ancestral bat hosts, is not fully understood.

As insectivorous bats are thought to be the ancestral hosts of coronaviruses, studying the mechanisms that lead to persistent infections in bats will provide clues about how bats can harbor different coronaviruses. In this study, we sought to identify unique coronavirus and host factors that enable a long-term persistent infection in cultured bat cells. We show for the first time that cells from an insectivorous bat can be persistently infected with MERS-CoV over a period of several months and disrupting the interferon response factor 3 (IRF3) signaling or MAP kinase pathways leads to an increase in virus replication in these cells. Although growth in bat cells led to point mutations in several genes, inactivating mutations in the ORF5 gene were observed repeatedly. Our results suggest a mechanism for the benign relationship of coronaviruses with their bat hosts that results in long-term, low levels of virus replication in these animals.

6.5. Materials and methods

6.5.1. Cell culture

Eptesicus fuscus kidney cells [213] (*Ef*k3 or bat cells) were grown in Dulbecco's Minimal Essential Medium with GlutaGro (DMEM; Corning. Cat #MT10017CV) containing 10% fetal bovine serum (FBS; Sigma, Cat #F0392), penicillin/streptomycin (Gibco, Cat #15140122) and 1% GlutaMax (Gibco, Cat #35050061). Vero E6 (green monkey kidney; ATCC, Cat #CRL-1586) cells were grown in DMEM supplemented with 10% FBS and penicillin/streptomycin. Cells were incubated in a humidified incubator at 37°C with 5% CO_2.

6.5.2. Virus infection

All work with MERS-CoV was performed under biosafety containment at Vido-intervac at University of Saskatchewan and was approved by the institutional biosafety committees. MERS-CoV (isolate hCoV-EMC/2012 [285]) was propagated in Vero E6 cells in DMEM (Sigma) supplemented with 10% fetal bovine serum, 50 U/ml penicillin and 50 µg/ml streptomycin (Gibco, Cat #15140122).

For establishing persistent infection, *Ef*k3 cells were seeded at a concentration of 3 x 10^5 cells/well in one well of a six well plate. The cells were infected with MERS-CoV (strain EMC/2012) at a multiplicity of infection (MOI) of 0.01. Growth medium on the cells was replaced regularly and surviving cells were split using 0.25% trypsin (Sigma, Cat #20233). Supernatant from each passage was saved at -80°C for virus titration. For acute infection, *Ef*k3 cells were seeded at a concentration of 3 x 10^5 cells/well in a six well plate. The cells were infected with MERS-CoV (strain EMC/2012) at a multiplicity of infection (MOI) of 10 $TCID_{50}$/ml. Virus infection and experiments with live MERS-CoV was carried out in a containment level 3 facility.

Following inactivation of the virus, other relevant studies were conducted in a containment level 2 laboratory.

6.5.3. Virus titration

Supernatant from persistently infected bat cells were titrated in triplicates on Vero cells using tissue culture infectious dose 50 ($TCID_{50}$) assay. Briefly, 10^4 cells were seeded in each well of a 96-well plate. The plates were incubated overnight to obtain a confluent layer of Vero cells. The virus sample (supernatant) was diluted ten-folds and 50µl of the diluted virus sample was added to each well of the 96-well plate. The plates were incubated at 37°C for 1hr. After incubation, the virus containing supernatant was discarded and 100µl of complete media with 5% FBS was added to the plates. The plates were incubated at 37°C for three days. The plates were incubated for 3 days and cytopathic effect was observed under a light microscope. Tissue culture infectious dose 50/ml ($TCID_{50}$/ml) was calculated using the Spearman and Karber algorithm [286,287].

6.5.4. Immunoblot

Persistently infected *Efk*3 cells were seeded at a concentration of 3x 10^5 cells/well in six well plates and incubated at 37°C overnight. Next day, cells were harvested in sample buffer for immunoblots. Immunoblots were carried out as previously mentioned [288]. Briefly, samples were denatured in a reducing sample buffer and electrophoresed on a reducing gel. Proteins were blotted from the gel onto polyvinylidene difluoride (PVDF, GE Healthcare, Cat #10600023) membranes and detected using primary and secondary antibodies. Primary antibodies used were: 1: 1,000 mouse anti-GAPDH (EMD Milipore, Cat #AB2302) and 1: 1,000 rabbit anti-MERS-CoV N protein (Sino Biological, Cat #40068-RP01). Secondary antibodies used were: 1:10,000 goat anti-mouse Alexa 488 (Molecular Probes, Cat #A-11001) and 1: 10,000 goat anti-rabbit Cy5 (GE

Healthcare, Cat #PA45012). Blots were observed and imaged using a Typhoon Scanner (Amersham Biosciences).

6.5.5. Electron microscopy

Persistently infected *Ef*k3 cells were scraped in phosphate buffered saline and pooled in a 15ml screw-cap centrifuge tube. The cells were recovered by centrifugation at 300xg for 5 mins and the supernatant was discarded. The cell pellet was resuspended in 10% neutral buffered formalin (10% NBF; Sigma, Cat #HT501128) for virus inactivation. The cells were later processed for electron microscopy. Briefly, cells were treated with osmium tetroxide (1% OsO_4, 0.1 M sodium cacodylate buffer) for one hour at room temperature. Samples were quickly rinsed with water, gradually dehydrated in ethanol and *en*-bloc stained with uranyl acetate. After rinsing three times (5 min each) in propylene oxide, samples were infiltrated with Epon/Araldite (electron Microscopy Sciences, Cat #50-980-381). samples were placed in molds and freshly prepared Epon/Araldite was added. The samples were then polymerized at 60°C for 24–48 h. Sections of 90 nm were cut and observed by transmission electron microscopy (TEM - Hitachi HT 7700, Tokyo, Japan).

6.5.6. Immunofluorescence

Persistently infected and mock/acute infected *Ef*k3 cells were seeded at a concentration of $3x10^4$ cells/chamber in chamber slides (Nunc, Thermo Scientific, Cat #154534). Each chamber was harvested at the respective time points by removing media, a quick rise with PBS and addition of 10% NBF. 10% NBF was added to inactivate and fix the cells over a period of 48h. After removing the cells from containment, cells in each chamber were washed twice with phosphate buffered saline (PBS). The slides were permeabilized using 0.2% TritonX-100 (VWR, 97062-208) diluted in PBS for 5 minutes. Cells were incubated in a blocking solution [PBS, 10% donor calf

serum (Sigma, Cat #C9676) and 0.1% Tween 20 (Fisher Bioreagents, Cat #BP337-500)]. Primary staining for MERS-CoV nucleoprotein (N) and GAPDH was performed using 1:100 dilution of rabbit anti-MERS-CoV N (Sino Biological, Cat #40068-RP01) and mouse anti-GAPDH (EMD Milipore, Cat #AB2302). Secondary staining was performed using 4µg/ml goat anti-mouse Alexa 488 (Molecular Probes, Cat #A-11001), 0.1µg/ml goat anti-rabbit Cy5 (GE Healthcare, Cat #PA45012) and 0.2µg/ml Hoechst 33342 (Molecular Probes, Cat #H3570) in blocking solution. Cells were observed under an Olympus IX83 fluorescence microscope.

6.5.7. In-situ hybridization

As for immunofluorescence, persistently infected and mock/acute infected *Ef*k3 cells were seeded at a concentration of $3x10^4$ cells/chamber in chamber slides (Nunc, Thermo Scientific). Each chamber was harvested at the respective time points by removing media, a quick rise with PBS and addition of 10% NBF. 10% NBF was added to inactivate and fix the cells over a period of 48h. MERS RNA was detected in the cells using ViewRNA ISH tissue 2-plex assay kit (Affymetrix, Thermofischer Scientific, Cat #QVT0012) and probes targeting MERS nucleocapsid sequence (Thermofischer Scientific, United States) as per manufacturer's instructions, with the exception of xylene treatment of slides, which was omitted. Counterstaining of cells was done using Gill's hematoxylin I (Sigma Aldrich, Cat #GHS-132). Coverslips were applied at the end of the assay and images were taken using brightfield microscope with 20X and 40X objectives.

6.5.8. RNA extraction, cDNA preparation and quantitative real-time PCR (qRT-PCR)

All RNA extractions were performed using the RNeasy Plus Mini kit (Qiagen, Cat #74136) as per manufacturer's instructions. cDNA was prepared using iScript gDNA clear kit (Bio-Rad) as per manufacturer's instructions. 500ng of RNA was used for cDNA preparation. cDNA was used as a template for the quantification of target genes.

Quantitative real-time polymerase chain reaction (qRT-PCR) assays amplifying targeted cellular genes and the normalizer gene (Glyceraldehyde-3-phosphate; GAPDH) were performed for both MRC5 and *Efk*3 cells. Primer sequences are listed in Suplementary table S6.1. Primers for quantifying GBP1, IL8, Mx1, IRF3, MDA5, IRF7, TNFα and IFI6 were used as mentioned in Banerjee *et al* [29]. Bio-Rad's CFX96 Touch PCR thermocycler was used in conjunction with Bio-Rad's Ssofast Evagreen supermix (Bio-Rad, Cat #1725204) and samples were prepared as previously mentioned [253]. For qRT-PCR, after the initial denaturation step of 95°C for 5 minutes, two step cycling for 40 cycles was performed at 95°C/10s, 56°C/30s. Absorbance readings were acquired after each cycle. The final three steps were carried out at 95°C/1min, 55°C/30s and 95°C/30s to generate the dissociation curve. Absorbance readings for the dissociation curve were acquired at every degree from 55-95°C. Relative fold change in gene expression was calculated after normalizing the Ct values using GAPDH. Difference of one Ct indicates a two-fold difference in gene expression. Graphs were plotted using GraphPad prism version 7.

6.5.9. IRF3 knockdown and MAP kinase inhibition

Dicer-ready siRNA (DsiRNA) specific to big brown bat and human IRF3 was designed and obtained through Integrated DNA Technologies (IDT). A 100nM final concentration of a 1:1 mixture of two DsiRNAs per cell line (Table S1) targeting separate regions on the big brown bat IRF3 transcript was transfected into persistently infected *Efk*3 cells using Lipofectamine 2000 (Invitrogen, Cat #11668019). Scrambled non-specific DsiRNA (NC DsiRNA; IDT) was used as a negative control.

For MAP kinase inhibition, URMC-099 drug (Cayman chemicals, Cat #1229582-33-5) was used at a concentration of 1μM [289]. DMSO (1μM) was used as a negative control. Cells

were harvested after 24 and 48 hours and virus replication was quantified using MERS-CoV UpE primers and qPCR.

6.5.10. Sequencing MERS-CoV

cDNA was prepared using random hexamers and SuperScript III reverse transcriptase (ThermoFisher Scientific, Cat #18080044) according to the manufacturer's protocol. The genome was amplified in ~600-2000 bp overlapping fragments using iProof High-Fidelity DNA polymerase (Bio-Rad, Cat #1725301). Each PCR reaction was purified using QIAquick PCR Purification (QIAGEN, Cat #28104) or GenepHlow kits (Geneaid, Cat #DFH100). DNA was quantified and subjected to Sanger sequencing using the previous PCR as well as internal primers.

6.5.11. Cloning MERS-CoV ORF5

Conventional PCR was carried out to amplify MERS-CoV ORF 5 with restriction sites KpnI and BamHI from *Ef*k3-MERS-CoV cDNA using ORF5 (full length) primers. Red fluorescent protein (RFP) with restriction sites BamHI and XhoI was amplified from pcDNA3-mRFP using mRFP primers. PCR was performed using the following thermal cycle profile: initial denaturation for 3 min at 94˚C, 35 PCR cycles at 94˚C/30s, 56˚C/30s and 72˚C/1min. The final extension was at 72˚C for 10 min. The two PCR products were ligated into a pcDNA3 backbone that was digested with KpnI and XhoI. Plasmid resulting from the double ligation was used to transform DH5α *E.coli* cells. The bacterial cells were plated on 2YT plates with ampicillin. Resistant bacterial colonies were scanned for plasmids carrying the ORF5-RFP insert. Positive clones were amplified in broth culture. Plasmids were later purified and concentrated using a MaxiPrep kit (QIAGEN, Cat #12163).

6.5.12. Statistics

Significance of the data was determined by two-tailed Mann Whitney *U* test for non-parametric independent samples using IBM SPSS (Version 21).

6.6. Results

6.6.1. MERS-CoV persistently infects insectivorous bat cells

To investigate if MERS-CoV could persistently infect cells from an insectivorous bat, we infected big brown bat (*Eptesicus fuscus*) kidney cells (*Ef*K) [213] with a low multiplicity of infection (MOI) of 0.01 $TCID_{50}$/cell (Figure 6.1. (A)). Twelve days after infection, most of the cells were dead (Figure 6.1. (C)). We passaged the surviving cells and titrated the amount of virus in the supernatant every week. During the first 35 days of infection, the amount of virus produced by cells was variable (Mean = 2.98×10^4; coefficient of variation = 105.4%) but after the 42^{nd} day, we detected a relatively low but stable amount of infectious virus produced in the growth supernatant (Mean = 1.5×10^4; coefficient of variation = 58.8%) (Figure 6.1. (B)). In comparison, human cells (MRC5) could not be persistently infected with MERS-CoV as all cells died several days after infection (data not shown). To determine if the persistently infected bat cells expressed viral proteins, we performed immune blots on cell lysates to detect MERS-CoV nucleoprotein (N). We detected N protein in cell lysates from every passage that was analysed (Figure 6.1. (E)). We also looked for virus particles in persistently infected bat cells by electron microscopy. We observed coronavirus-like particles in Golgi bodies and secretory vesicles of persistently infected bat cells (Figure 6.1. (D)).

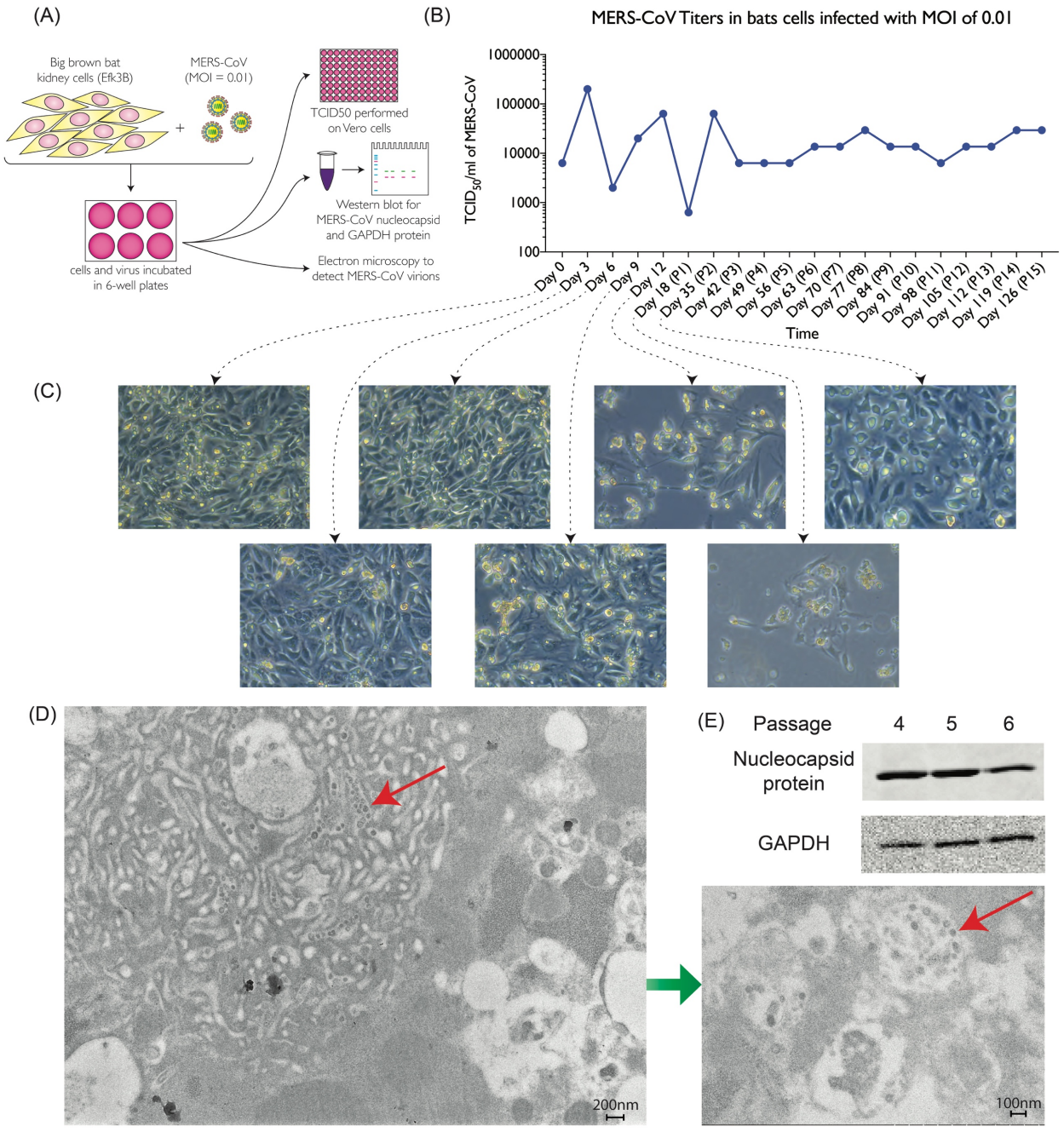

Figure 6.1. Bat cells can be persistently infected with MERS-CoV. (A) Big brown bat kidney cells (*Ef*k3B) were infected with MERS-CoV (MOI = 0.01 $TCID_{50}$/cell) for 12 days and then passaged weekly. Samples were obtained during passages to determine the presence of virus by $TCID_{50}$ assay, immunoblot and electron microscopy. **(B)** Levels of MERS-CoV at different time points following initial infection. **(C)** Phase contrast micrographs showing the cytopathic effect of MERS-CoV and subsequent recovery of the cells at various time points. **(D)** Electron micrograph showing the presence of particles similar to viral nucleocapsid (approximately 80 nm in size) in

persistently infected cells (red arrows). (**E)** Immuno blot showing the presence of MERS-CoV N-protein at passage 4, 5 and 6. The house-keeping protein, GAPDH is shown as a control.

6.6.2. MERS-CoV infects all bat cells in varying levels

To determine if all cells in our persistently infected cell population were infected, or if persistence was maintained by small numbers of lytically-infected cells producing virus to subsequently infect susceptible cells, we analyzed these cells for transcript and protein of the MERS-CoV N gene (Figure 6.2. (A)). Most of the persistently infected cells expressed very low levels of N protein compared to cells in an acutely infected culture (infected at a high MOI). A few cells expressed high levels of N protein (Figure 6.2. (B)). Consistent with our immunofluorescence data, we detected by *in-situ* hybridization varying levels of MERS-CoV N RNA in all cells in the persistently infected culture. We observed three types of cells in the population of cells persistently infected with virus based on the intensity of staining, we classified cells as having low, medium or high levels of coronavirus RNA (Figure 6.2. (C)).

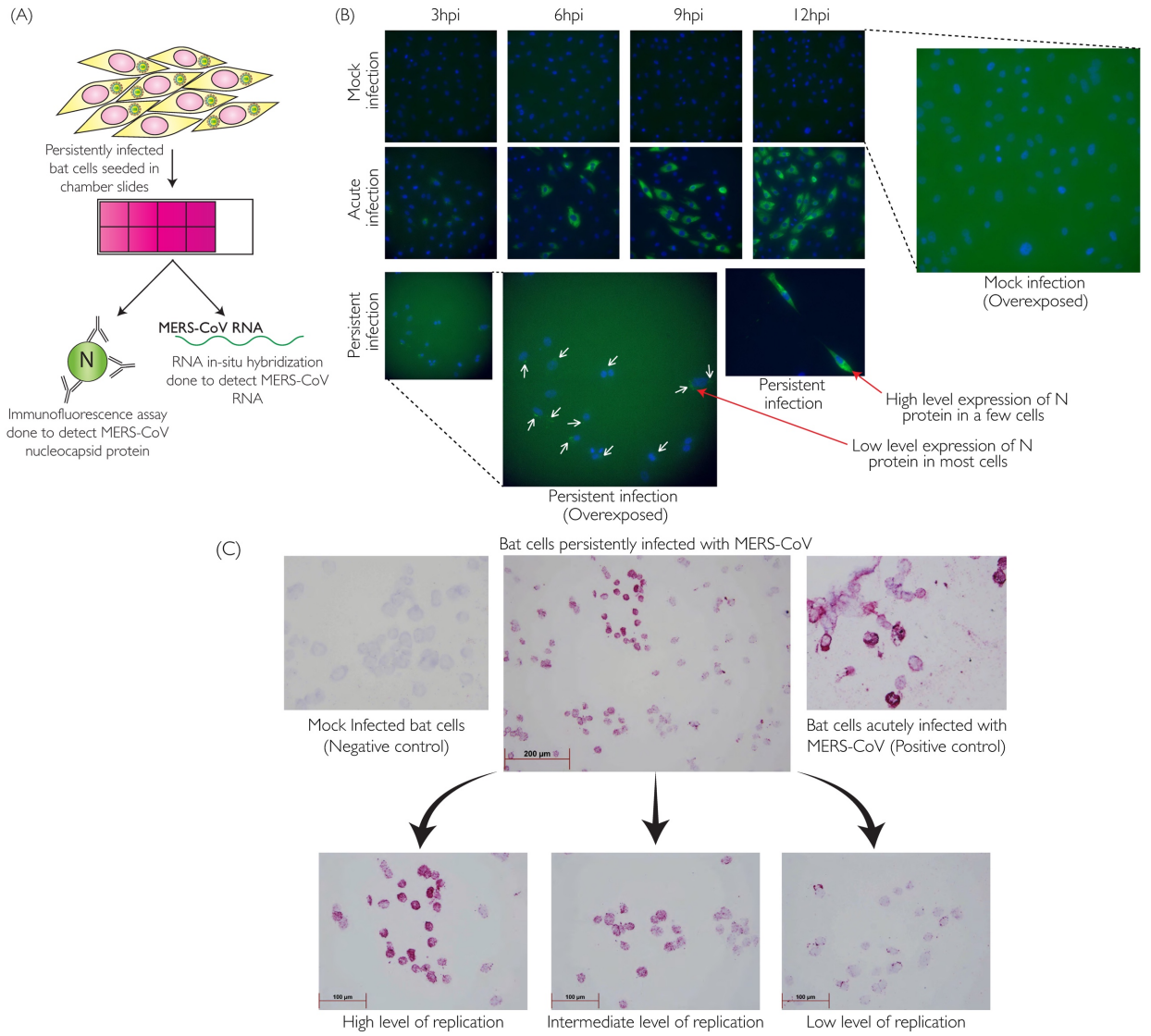

Figure 6.2. MERS-CoV RNA and protein can be detected in persistently infected cells. (A) Persistently infected bat cells with MERS-CoV were seeded in chamber slides for *in-situ* hybridization (ISH) and immunofluorescence assays (IFA). **(B)** IFA images to detect the presence of nucleocapsid protein in persistently infected bat cells (bottom row; red arrows). Acutely infected (middle row) and mock infected cells (top row) were considered as positive and negative controls respectively. **(C)** *In-situ* hybridization to detect the presence of MERS-CoV nucleoprotein RNA in persistently infected cells. High, intermediate and low levels of MERS-CoV nucleoprotein RNA have been highlighted. Acutely infected (right) and mock infected cells (left) were considered as positive and negative controls.

6.6.3. All MERS-CoV genes are expressed in bat cells except ORF5

Persistent infection is often accompanied by altered levels of gene expression as the pathogen and the host establish a delicate balance between cytolytic viral factors and host defense responses. To determine if there were differences in MERS-CoV gene expression between acute and persistently infected bat cells, we infected bat cells with MERS-CoV (MOI = 10 $TCID_{50}$/cell; acute infection) and compared virus gene expression with that of persistently infected cells at 0, 12, 24 and 48 hours post infection (hpi) (Figure 6.3. (A)). For persistently infected cells, the time points in the figure indicate when RNA from these cells was harvested after seeding them in six-well plates. MERS-CoV genes S, E, M, N, ORF3, 4a, 4b and 5 in acutely infected cells showed increasing levels of expression over time (Figure 6.3. (C-J)). This was concomitant with an increase in MERS-CoV genome quantities (UpE levels) (Figure 6.3. (B)) in acutely infected cells. In contrast, persistently infected bat cells maintained steady levels of genome (UpE) quantities and, with the exception of ORF5, of RNA from the various viral genes (Figure 6.3. (B-J)). We were unable to detect ORF5 mRNA in persistently infected bat cells.

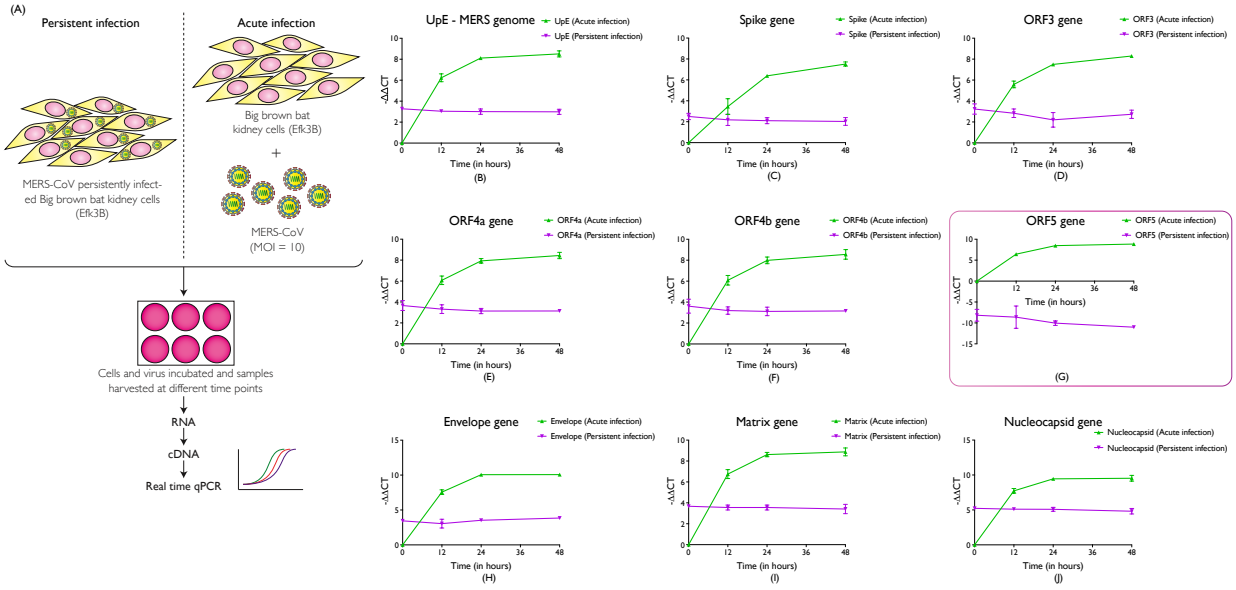

Figure 6.3. MERS-CoV gene expression varies between acute and persistently infected bat cells. (A) RNA from persistently infected cells and acutely infected cells were harvested at several time points and processed for cDNA synthesis and real time PCR. (**B-J)** Graphs showing the gene expression (- (ΔCT_{gene}-ΔCT_{GAPDH})) of MERS-CoV- UpE, S, ORF3, ORF4a, ORF4b, ORF5, E, M and N genes in acute (green) vs. persistent (purple) infections at 0, 12, 24 and 48 hours post-infection or seeding (n=4, Mean±SD). (n = number of biological replicates; SD = standard deviation)

6.6.5. Adaptation of MERS-CoV in bat cells

The MERS-CoV isolate used in our experiments was derived from a human infection and was subsequently propagated in primate cells. To determine if continuous growth in insectivorous bat cells leads to the selection of variants better adapted for replication in bats, we sequenced the genome of the virus from persistently infected bat cells that had been passaged 15 times over a period of 6 months. We observed point mutations in various genes of the bat-adapted virus (Figure 6.4. (A)), specifically in polymerase, spike and matrix genes. In addition, we observed a 347bp deletion in ORF5. The remaining ORF5 sequence in the bat-adapted MERS-CoV strain would only encode a putative 20 amino acid long protein. To identify when the ORF5 deletion mutant was selected during the establishment of persistently infected bat cells, we sequenced ORF5 from multiple early and late passage cells. We could detect the deletion in ORF5 as early as passage 2 in the persistently infected bat cells (supplementary figure S6.1). In the following portion of this article we refer to the original human-derived virus as the MERS-CoV wild-type (W+) virus and the ORF5 deleted variant as the ORF5 mutant virus.

To determine if the establishment of a persistent MERS-CoV infection, and the subsequent selection of viral variants was reproducible, we again infected bat cells with the W+ MERS-CoV at a low MOI. We also recovered ORF5 coding sequences from passages 2, 3 and 4. In sequences obtained as early as passage 2 we observed a point mutation which resulted in a stop codon that

would lead to the termination of the protein at amino acid 107 (out of 225, Supplementary data S6.1).

To determine if sequence variation led to changes in growth characteristics of the virus, we infected bat and human cells with W+ and mutant MERS-CoV, and we found that the mutant MERS-CoV grew better in bat cells whereas the W+ grew better in human cells (Figure 6.4 (B)).

(A)

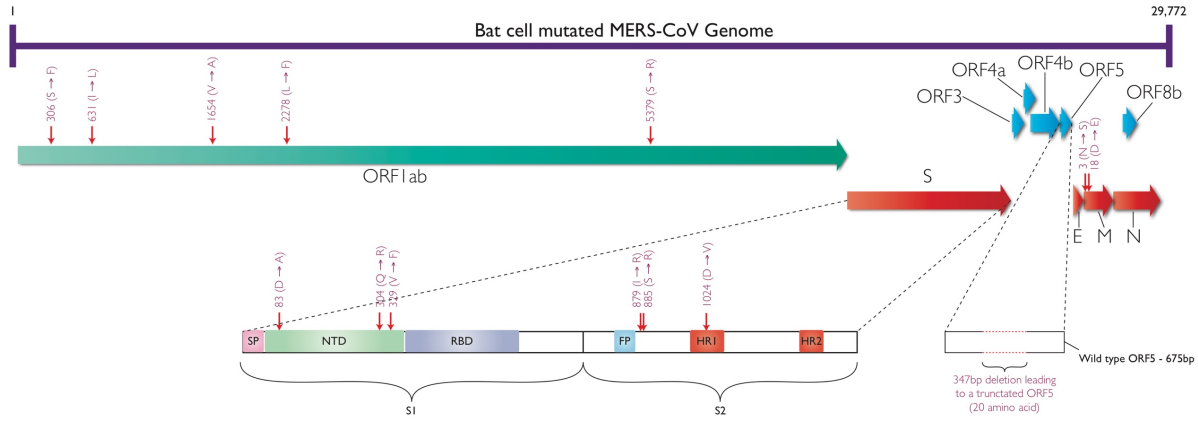

(B) Comparing Wild type and Mutant MERS-CoV growth in human and bat cells

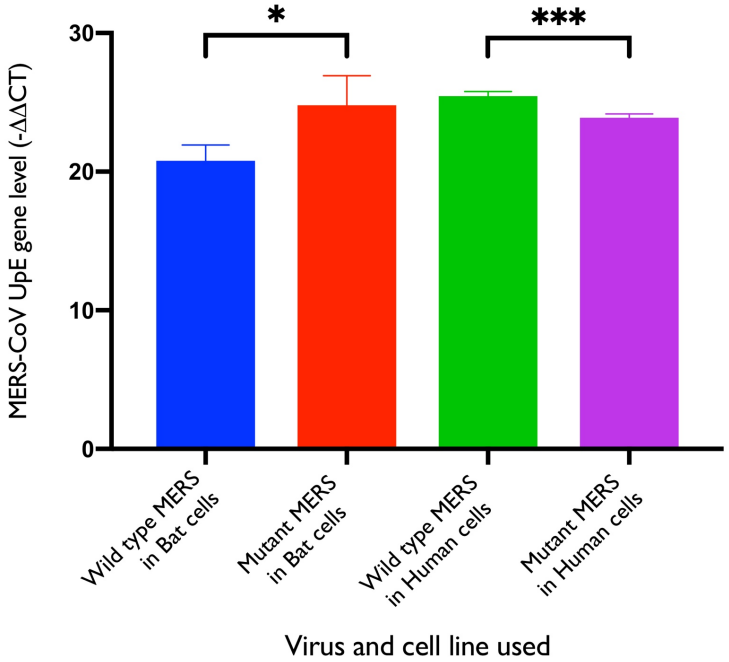

Figure 6.4. Sequence adaptation of MERS-CoV affecting growth characteristics. (A) Diagram showing the mutations (red arrows) in the MERS-CoV genome that were identified by sequencing the virus from persistently infected bat cells (Passage 15). (B) Comparing the growth of wild type and mutant MERS-CoV in bat and human cells. The 4 bars represent the level of MERS-UpE gene (- (ΔCT_{gene}-ΔCT_{GAPDH})) with respect to uninfected cells. The mutant MERS-CoV (red) grows better in bat cells whereas the wild type MERS-CoV (green) grows better in human cells. (n=4, Mean ± SD)

6.6.6. Differences in the fitness of mutant MERS-CoV in bat cells could be driven by interferon stimulated genes

We had previously reported [290] that in contrast to its ability to suppress innate antiviral responses in human cells, MERS-CoV in bat cells induces a robust interferon response. Since the ORF5 mutant grew better in bat cells than W+ MERS-CoV, we examined whether this may be related to differences in their ability to induce cellular innate responses. We compared the levels of transcripts for interferon beta (IFNβ) and IFN-induced genes: guanylate binding protein 1 (GBP1), interleukin 8 (IL8), myxovirus resistance 1 (Mx1), interferon regulatory factors 3 and 7 (IRF3 and 7), melanoma differentiation-associated protein 5 (MDA5) and interferon inducible protein 6 (IFI6) in human and bat cells infected with W+ or ORF5 mutant viruses.

Bat cells infected with the ORF5 mutant contained significantly ($p \leq 0.05$) higher levels of transcripts for IFI6 (Figure 6.5 (B)) and MDA5 (Figure 6.5 (E)). While differences in the levels of the other genes were not significant ($p = 0.08$ to 0.13), in all cases there was a trend towards higher levels in the ORF5 mutant - infected cells. There were no noticeable differences between human cells infected with the mutant and W+ viruses.

When comparing the effect of the viruses in human and bats cells – the W+ virus, consistent with our earlier reports [290], induced TNFα in human but not in bat cells (data not shown). The W+ virus induced IFI6 in bats cells but not in human cells (Figure 6.5 (B)). Similar to the W+

virus, the levels of most ISG transcripts in ORF5 mutant-infected cells were higher in bat cells than in human cells.

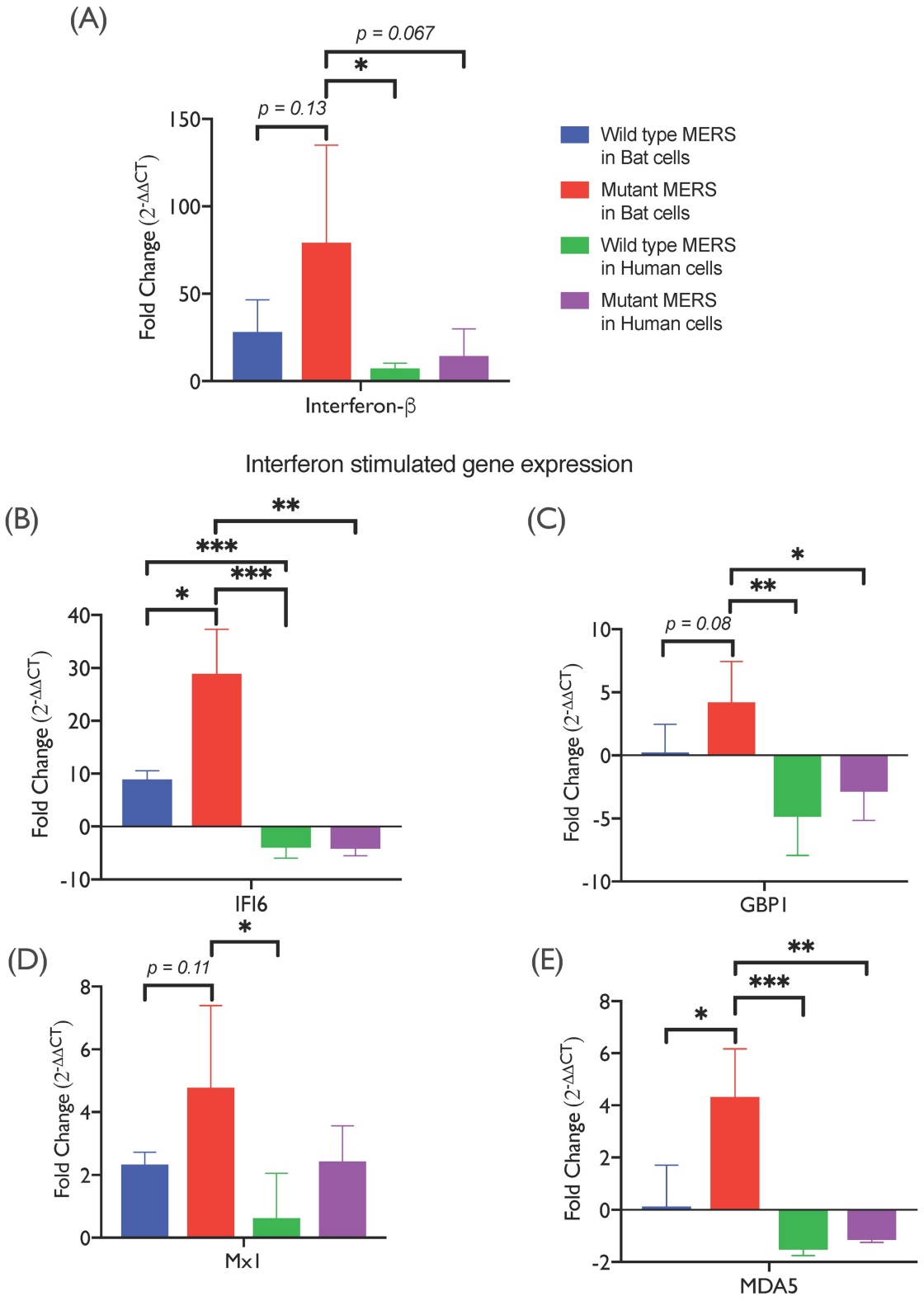

Figure 6.5. Comparing innate immune related gene expression in bat (*Efk*) and human (MRC5) cells in the presence of wild type vs mutant MERS-CoV. Variation in gene expression

observed for interferon-β (A) and interferon stimulated genes, IFI6, GBP1, Mx1 and MDA5 (B-E), between bat and human cells. Bars represent average fold changes ($2^{-\Delta\Delta CT}$) in transcript levels as compared with mock-infected cells, normalized to levels of GAPDH in each sample (n=4; Mean±SD).

6.6.7. Bat cells persistently infected with MERS-CoV are resistant to superinfection with wild type MERS-CoV

To explain the replacement of W+ MERS-CoV with the ORF5 mutant in the persistently-infected cultures, we determined if the cells were resistant to superinfection with the W+ virus. To differentiate between growth of W+ and mutant MERS-CoV in the same cell, we examined the expression levels of UpE RNA (Figure 6.3 (B)), present in both strains, and ORF5 transcripts, specified only by the W+ virus (Figure 6.3 (G)). We observed that when bat cells persistently infected with the ORF5 mutant MERS-CoV were infected again with W+ virus (MOI = 0.1 $TCID_{50}$/cell), the cells failed to show an increase in UpE expression, suggesting lack of replication at 24 and 48 hours post infection (Figure 6.6. (A)). As a control, we infected naïve bat cells with the same amount of W+ MERS-CoV and observed that the replication resulted in an increase in UpE transcripts at 24 and 48 hours post infection. At 0 hours post infection, the ORF5 transcripts in superinfected bat cells (persistent infection + W+ virus) were higher than bat cells persistently infected with MERS-CoV, suggesting that the difference was due to the input virus (Figure 6.6. (B)). We further observed that the level of interferon-β expression was higher in bat cells persistently infected with MERS-CoV than naïve bat cells ($p=0.08$) and these naïve bat cells, when infected with W+ MERS-CoV showed a significant increase in interferon-β transcripts (Figure 6.6. (C)).

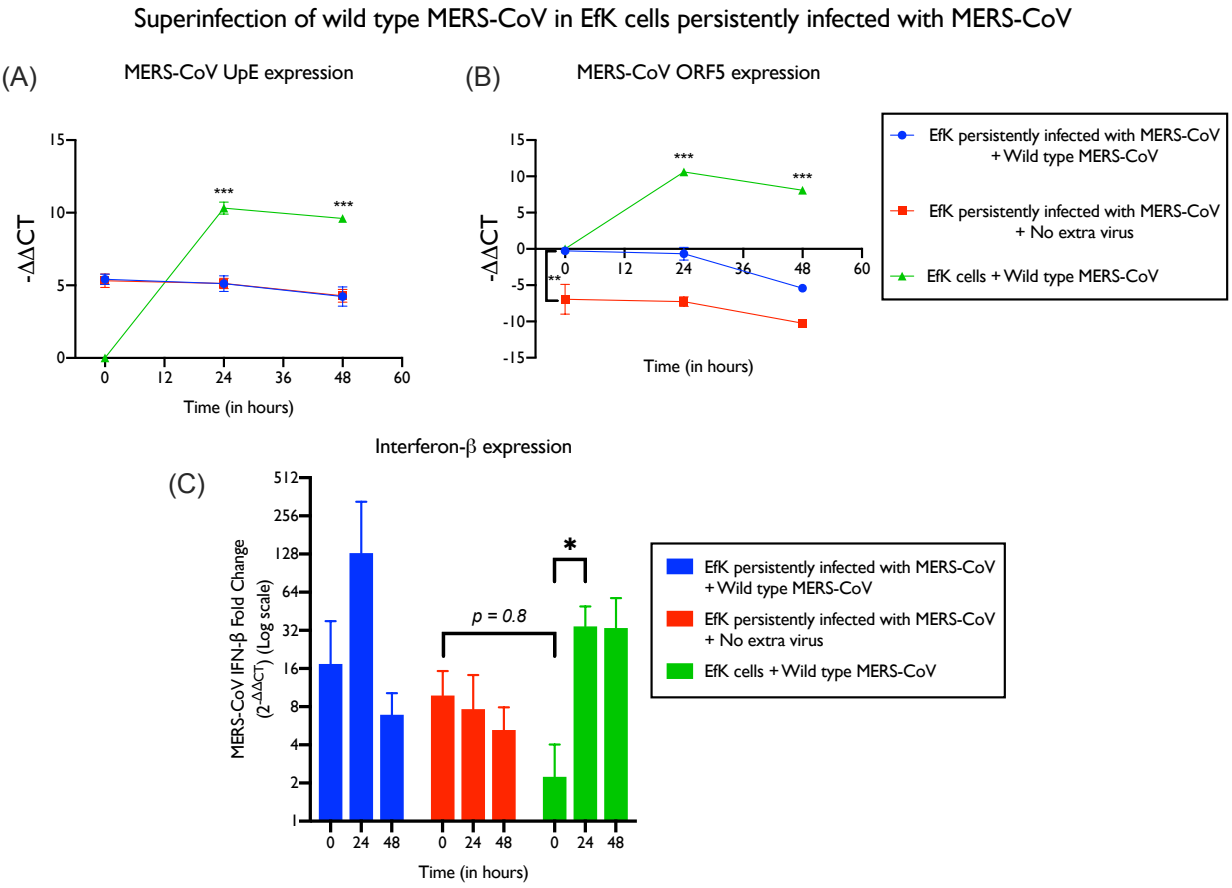

Figure 6.6. Bat cells persistently infected with MERS-CoV are resistant to superinfection with wild type MERS-CoV. Bat (*Ef*K) cells persistently infected with MERS-CoV were superinfected with wild type virus (blue) and transcripts for UpE (A) and ORF5 (B) were measured. The levels for UpE and ORF5 (-(ΔCT_{gene}-ΔCT_{GAPDH})) were also measured in bat cells persistently infected with MERS-CoV without additional virus (red) and naïve *Ef*K cells infected with wild type MERS-CoV (green) with respect to time 0 of input wild type virus. IFN-β levels were also measured in these samples (C). IFN β fold changes were reported with respect to naïve uninfected bat cells (n=3, Mean±SD).

6.6.8. Interferon response factor 3 (IRF3) and mitogen associated protein kinase (MAPK) signaling regulates persistent infection

To determine if the cellular antiviral innate response mediated by the IRF3 signaling pathway and IFNβ expression played a role in the maintenance of persistent infection in bat cells, we compared the IFNβ transcript levels in persistently infected cells with that of bat cells that were

acutely infected with MERS-CoV (MOI=10 $TCID_{50}$/cell). We also reduced IRF3 expression in persistently infected cells using small-interfering RNA (siRNA) and quantified the amount of virus in the supernatant of these cells and mock siRNA treated cells. MERS-CoV infected cells showed a significant increase in IFNβ transcript levels at 24 and 48 hpi relative to mock infected cells (Figure 6.7. (A)). Persistently infected bat cells expressed lower but consistent levels of IFNβ transcripts (Figure 6.7. (A)). Reducing IRF3 protein levels (Figure 6.7. (B) and 6.7. (D)) in persistently infected bat cells significantly increased virus replication in these cells (Figure 6.7. (C)). Reducing IRF3 protein levels in the persistently infected cells led to increased cell death within 48 hours of siRNA treatment compared to mock siRNA treated persistently infected cells (data not shown).

In previous experiments, we had observed that in little brown bats with a secondary infection with the white-nose syndrome-causing fungus, suppression of the MAPK pathway may have led to an increase in coronavirus replication [62]. To test if this pathway played a similar role in regulating viral load in persistently-infected cells, we inhibited the MAPK signaling pathway using the MAP kinase inhibitor URMC-99 [291]. We observed that the MERS-CoV levels increased upon inhibition of MAPK pathway (Figure 6.7. (E)). Expression of Ras superfamily protein, RERG, (a MAPK pathway related protein) was altered in the presence of URMC-99, confirming that the inhibitor was functional [292,293].

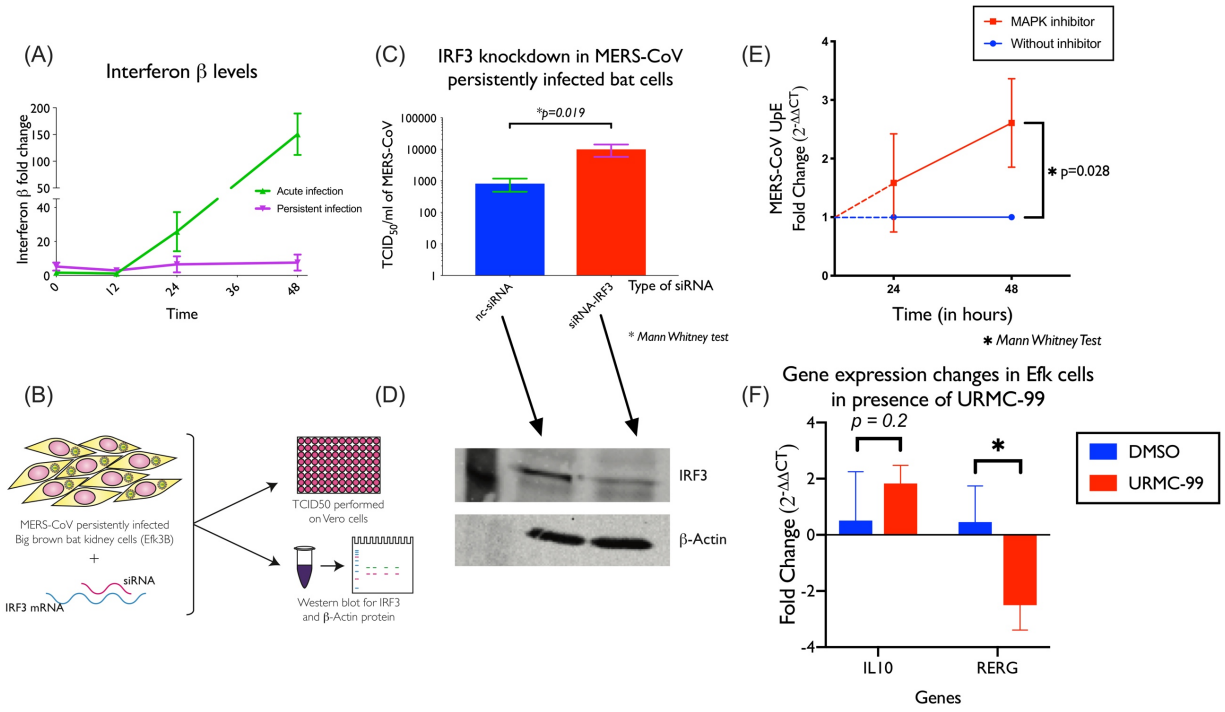

Figure 6.7. IRF3 and MAP kinase-mediated signaling regulates persistent infection in bat cells. (A) Interferon β levels (Fold change) in acute (green) and persistently (purple) infected bat cells at 0, 12, 24 and 48 hours post-infection or seeding. **(B)** Persistently infected cells were transfected with siRNA targeting IRF3 mRNA and the effect on virus replication was measured. **(C)** MERS-CoV titres in persistently infected bat cells 24 hours post treatment with siRNA (red bar; n=4, Mean±SD.). Scrambled siRNA (blue bar; nc-siRNA) was used as a negative control. **(D)** Immunoblot for IRF3 (and β-actin) in bat cells treated or mock treated with siRNA. **(E)** Effect of MAPK inhibitor on MERS-CoV transcript levels in bat cells. Quantification of MERS-CoV UpE RNA levels after 24 and 48 hours post seeding in cells with the MAPK inhibitor, URMC-99 (red), compared to the mock-treated cells (blue). **(F)** Quantification of IL10 and RERG transcripts after 48-hours of treatment with URMC-99 shows the effect of the drug. (n = 4; Mean±SD)

6.7. Discussion

There is growing direct and circumstantial evidence that bats are reservoirs for viruses that have spilled over to humans and other mammals. However, little is known about how these viruses are maintained in the reservoir individuals and populations, or the adaptations necessary for efficient infection, maintenance and spread in the spillover hosts.

Viruses may be maintained in reservoir populations by reinfection of partially immune or non-immune recovered individuals or by the infection of a continuously replenished sources of susceptible individuals. For viruses that engender long-term protective immunity following infection, transmission of the virus to susceptible hosts may require long-term persistence of the virus in infected individuals that act as a source of infection.

Successful spillover of a virus to a new host species requires viruses to adapt to the use of viral receptors as well as innate antiviral defense mechanisms unique to each host species. It is difficult to examine the process by which coronaviruses, such as those that cause SARS, MERS, PED and SAD, have adapted to infection and maintenance in bats or in the spillover species - humans, camels and pigs. While similar viruses have been detected in insectivorous bat species, the "culprit" viruses that initially spilled over have not been isolated or characterized.

We have attempted to answer questions about the dynamics of the interaction of coronavirus with their reservoir and spillover hosts by examining how MERS-CoV, isolated from a human infection, adapts to replication in cells from an insectivorous bat. We show the following: 1) At low multiplicities of infection, the virus established long-term persistent infections in bat cells (Figure 6.1) with viral RNA and proteins present in all cells (Figure 6.2). 2) Persistence depended on sustained innate antiviral responses (Figure 6.5) and the survival of infected cells that continuously produce low levels of progeny virus. Suppression of innate responses in the cells led to increased replication of the virus and death of the cells (Figure 6.7). 3) Viral persistence in bat cells led to the selection of MERS-CoV variants including the consistent selection of mutations in the accessory gene, ORF5 (Figure 6.5). 4) The ORF5 mutant grew more efficiently in bat cells than the W+ MERS-CoV (Figure 6.4). In contrast, the W+ virus grew more efficiently in human cells. 5) The ORF5 mutant induced a more robust innate response than the W+ virus (Figure 6.5).

This included significantly higher amounts of transcripts for IFI6, an anti-apoptotic protein (Figure 6.6 (B) and (E)) [294]. 6) Cells persistently infected with the ORF5 mutant were resistant to superinfection with the W+ virus (Figure 6.6).

Our results lead us to propose a model for the establishment of persistent MERS-CoV infection in bat cells and the rapid selection of variants with inactivated ORF5 (Figure 6.8).

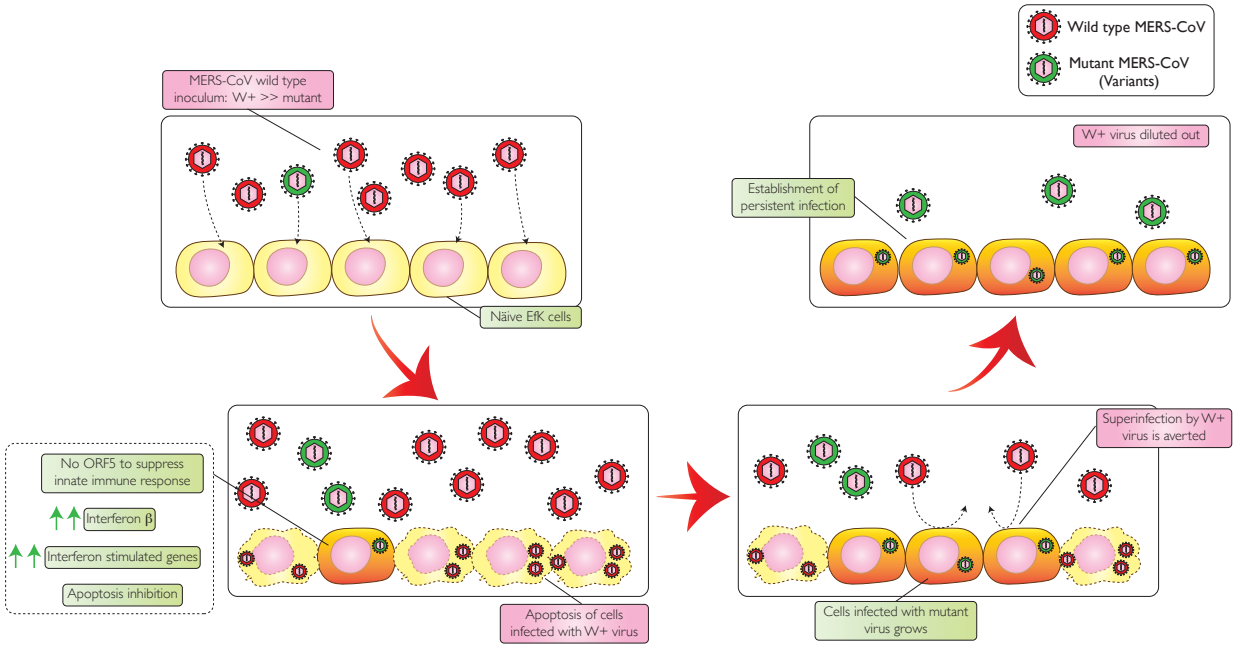

Figure 6.8. Proposed model for establishment of persistent MERS-CoV infection in bat cells. As with the stocks of most RNA viruses, the MERS-CoV inoculum is made up of the dominant wild-type virus as well as smaller numbers of variants, including variants with inactivating mutations in ORF5. The cells infected with the wild-type virus die while the small number of cells infected with the ORF5 mutant survive because of a more robust antiviral innate response. Apoptosis in these cells is suppressed by IFI6-mediated processes. The ORF5 mutant-infected cells are resistant to infection with the wild-type virus, which is soon diluted out. After a process of recovery, the ORF5 mutant infected cells survive and take over, leading to a culture of persistently infected cells that produce small amounts of virus over time.

Our study shows that MERS-CoV, a virus thought to have originated in bats, can establish persistent infections in bat cells. These results do not tell us much about the original bat virus that spilled over to camels and then to people. However, our results are consistent with our previous

studies [62] which demonstrated that little brown bats are persistently infected with an autochthonous coronavirus and that the stress of a fungal infection leads to a suppression of innate responses, including IFI6 in the bat intestines – the site of viral persistence and replication. That study also demonstrated a suppression in the expression of genes related to the MAP kinase pathway in fungus-infected bats. This is also consistent with our current observation that inhibition of the same pathway in cells persistently-infected with MERS-CoV, led to an increase in virus replication.

Our study also shows that infection of bat cells with MERS-CoV repeatedly led to the rapid selection of mutants with inactivated ORF5. In human cells, MERS-CoV structural proteins, such as M, and accessory proteins, such as ORF4a, 4b and 5, are known to effectively inhibit innate antiviral responses [283,295]. The virus also induces apoptotic cell death by upregulating Smad7 and fibroblast growth factor (FGF2) [296]. We have previously shown that in contrast to human cells, MERS-CoV is unable to suppress innate antiviral responses in bat cells and here we confirm those observations. In addition, one of the interferon induced genes, IFI6, which is expressed in bat cells infected with the W+ virus, and to a significantly greater extent in ORF5 mutant, inhibits apoptosis pathways [294]. While our study does not identify genetic changes needed for a coronavirus to adapt to growth in a different host species, it clearly demonstrates that abrogation of a protein, ORF5, provides the virus with growth advantages in bat cells, while the presence of the protein assists in growth in human cells. ORF5, along with the other accessory MERS-CoV genes ORF4a, 4b and structural proteins, such as M, are known to inhibit an antiviral IFNβ response in human cells [283,295]. Studies to determine the molecular mechanisms that allow ORF5 to fulfil these roles are underway.

6.8. Supplementary information

Supplementry table S6.1. Sequences of siRNA and primers used for qPCR/conventional PCR

Target gene	Forward primer (5'-3')	Reverse primer (5'-3')	Product length (in bp)
UpE	GCAACGCGCGATTCAGTT	GCCTCTACACGGGACCCATA	92
S	TGGTCTTTGCGATGCAGCTA	TTGGAAGTCAATCCCGGTGG	238
ORF3	TGAGAGTTCAAAGACCACCCAC	TGATTCTGCAGATGGGACGT	200
ORF4a	GCACTTCATTGCACCCTGTG	TGTAGCAACCAAGCGATTCG	127
ORF4b	TTCTGCGCCATGAAGACCTT	GGCCGCCATAAGGTTTAAGC	141
ORF5	TGTTTGACATGCGTTCCCAC	TTGCAGGCACGAAAACAGTG	249
E	ATGTTACCCTTTGTCCAAGAAC	TTAAACCCACTCGTCAGGTGG	249
M	TCGGTGCTTGTGACTACGAC	CCGTAATAGGCGGACTCCTG	165
N	ACCACGAGCTGCACCAAATA	ATGGACCCAAACGATGCCAT	277
Interferon beta	GCTCCGATTCCGACAGAGAAGCA	ATGCATGACCACCATGGCTTC	167
GAPDH	GGAGCGAGATCCCGCCAACAT	GGGAGTTGTCATACTTGTCATGG	198
ORF5 (Full length)	GCCGGTACCATGGCTTTCTCG	GCCGGATCCTTACGATAAGCG	693
mRFP	GCCGGATCCAAATGGCCTCCTCCGAG	GCCCTCGAGTTAGGCGCCGGTGGA	696
siRNA-IRF3 - 1 (duplex)	5' rCrArArGrArArGrCrUrArGrUrGrArUrGrGrUrCrArArGrGTT 3'		
	5' rArArCrCrUrUrGrArCrCrArUrCrArCrUrArGrCrUrUrCrUrUrGrGrU 3'		
siRNA-IRF3 - 2 (duplex)	5' rCrUrGrCrCrArArCrCrUrGrGrArArGrArGrGrArArUrUrUCA 3'		
	5' rUrGrArArArUrUrCrCrUrCrUrUrCrCrArGrGrUrUrGrGrCrArGrGrU 3'		

Supplementary figure S6.1. Mutations in ORF5 selected when bat cells were persistently infected with MERS-CoV.

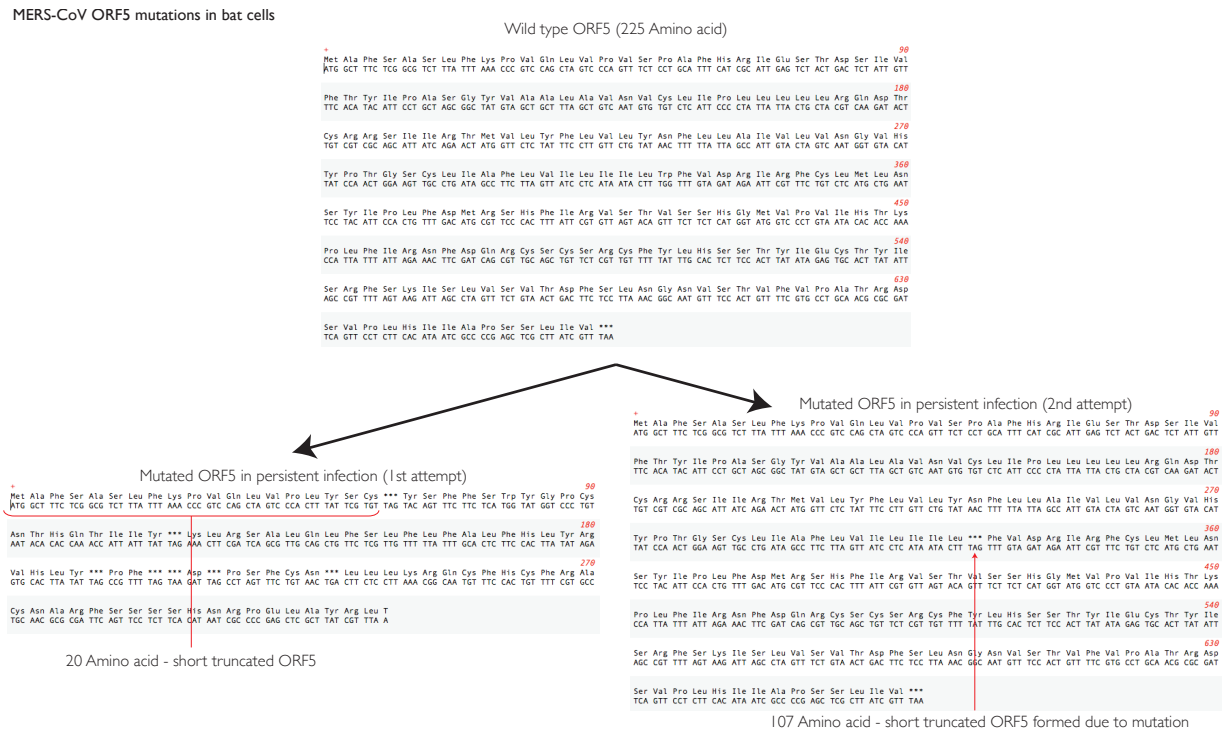

6.9. Transition statement

In chapter 4, I described the characterization of the little brown bat coronavirus and our observations demonstrated that the virus could persist in its host. In chapter 5, I described our observations that the stress of fungal infection leads to a resurgence of virus replication. The study suggested that the fungal infection suppressed innate anti-viral responses at the site of viral persistence allowing the virus to replicate without hindrance. In chapter 6, using a cell-culture model of coronavirus persistence in bat cells, I described our studies to show that viral persistence could be disrupted by artificially suppressing the host cell's innate antiviral response. These observations supported our contention that viruses establish long-term persistent infections in bats and that stress perturbs this relationship allowing the viruses to replicate more freely.

To establish that the effect of stress on the disruption of low-level viral persistence held for viruses other than coronaviruses, I studied a bat herpesvirus. Herpesviruses establish life-long

latent infections in their hosts and reactivate periodically from this quiescent state in response to stress. A brown bat herpesvirus would, therefore, allow us to examine the effects of natural internal and environmental stressors on bats and their relationship with their herpesvirus. In the next chapter, I describe our isolation and characterization of a big brown bat gammaherpesvirus.

Chapter 7: Characterization of a bat gammaherpesvirus isolated from big brown bats

7.1. Copyright

© 2018 Elsevier Inc. All rights reserved. Elsevier publishers allow authors to include their articles in full or in part in a thesis or dissertation for non-commercial purposes.

This manuscript has been reformatted from the original version for inclusion in this thesis.

7.2. Citation

Subudhi, S., N. Rapin, N. Dorville, J. E. Hill, J. Town, C. K. R. Willis, T. K. Bollinger, and V. Misra. "Isolation, Characterization and Prevalence of a Novel gammaherpesvirus in *Eptesicus Fuscus*, the North American Big Brown Bat." *Virology* 516 (3): 227–38. https://doi.org/10.1016/j.virol.2018.01.024.

7.3. Contribution

Several authors contributed significantly in this study. NR, VM and I isolated the virus and characterized its growth properties. JH and I sequenced the viral genome. I assembled of the whole genome, identified the open reading frames and analysed its phylogenetic relationships. I prepared samples for mass spectrometry. Characterization of growth of virus in cell lines of various species, serum neutralization assay and PCR were done by NR. I wrote the initial draft of the manuscript, while NR, VM and I edited and prepared its final version.

7.4. Abstract

Little is known about the relationship of gammaherpesviruses with their bat hosts. Gammaherpesviruses are of interest because of their long–term infection of lymphoid cells and their potential to cause cancer. Here, we report the characterization of a novel bat herpesvirus isolated from a big brown bat (*Eptesicus fuscus*) in Canada. The genome of the virus, tentatively named *Eptesicus fuscus* herpesvirus (*Ef*HV), is 166,748 base pairs. Phylogenetically *Ef*HV is a member of *Gammaherpesvirinae*, in which it belongs to the Genus *Rhadinovirus* and is closely related to other bat gammaherpesviruses. In contrast to other known gammaherpesviruses, the *Ef*HV genome contains coding sequences similar to those of class I and II host major histocompatibility antigens. The virus is capable of infecting and replicating in human, monkey, cat and pig cell lines. Although we detected *Ef*HV in 20 of 28 big brown bats tested, these bats lacked neutralizing antibodies against the virus.

7.5. Introduction

In recent years several bat viruses have been discovered, most appear to have little deleterious effect on their hosts [297,298]. These unique and benign virus-host relationships are likely a byproduct of evolutionary adaptations to flight and long-term associations between the bats and their viruses [15]. In addition to simply satisfying scientific curiosity, a better understanding of these unique relationships may provide clues to mitigating the much more serious pathologic virus-host interactions in other species.

Gammaherpesviruses are a sub-family of Herpesviridae with a primary tropism for cells of lymphoid lineage [77]. Gammaherpesviruses establish latent infections in long-lived lymphoid cells and in some cases cause neoplasias, such as Burkitt's lymphoma and Kaposi sarcoma in

humans [299]. One of the challenges in studying the reactivation and pathogenesis of these oncogenic viruses is the lack of a suitable animal model [300]. Murine gammaherpesvirus-68 in mice, the model used most extensively, is not ideal as the virus is not readily transmitted between laboratory mice [301]. Previous studies have shown that bats and primates harbor a large diversity of gammaherpesviruses that might have led to higher chances of cross-species transmission from these taxa to other mammals [143,302,303]. Therefore, a naturally occurring gammaherpesvirus in a readily accessible bat species may provide us with vital information on evolution of these viruses and serve as a model for studying pathogenesis.

Even though there are a few reports of detection of gammaherpesvirus genomes [304–306], and a single report of isolation of a gammaherpesvirus from bats [147], knowledge about bat gammaherpesviruses is limited. As bats do not appear to normally display viral pathology, studying a gammaherpesvirus in its natural bat host may provide information about novel co-evolutionary adaptations that lead to balanced and benign host-virus relationships.

Here, we report the discovery, isolation and characterization of a novel bat gammaherpesvirus from the lungs of a North American big brown bat (*Eptesicus fuscus)*. We provisionally name the virus, *E. fuscus* Herpesvirus (*Ef*HV). The morphology and protein composition of *Ef*HV are similar to those of other herpesviruses. Furthermore, we obtained the sequence of its genome, determined its ability to infect cells from several mammalian species and characterized its growth characteristics. A comparison of the sequence of *Ef*HV with those of other herpesviruses indicates that the virus is closely related to other bat gammaherpesviruses. In addition to transducing host cytokine genes like interleukin 10 (IL-10), the *Ef*HV genome is unique among gammaherpesviruses in that it contains the coding sequences for four putative host MHC-I antigens and one MHC-II antigen.

7.6. Materials and methods

7.6.1. Ethics Statement

All procedures related to the handling and euthanasia of bats were submitted to and approved by the Committee on Animal Care and Supply of the University of Saskatchewan Animal Research Ethics Board (protocol #20090036) and were in accordance with regulations approved by the Canadian Council on Animal Care.

7.6.2. Bats

A male bat was submitted to the Canadian Wildlife Health Cooperative (CWHC). Organs were harvested for virus isolation. Some tissue was also preserved in 10% neutral buffered formalin for histological analysis. The 28 bat samples to determine the prevalence of *Ef*HV were obtained from the University of Winnipeg.

7.6.3. Virus isolation

Tissues were screened for virus using a standard virus isolation protocol. Various tissues of the bat were placed in 250 µl Dulbecco's modified Eagle's medium (DMEM, Corning, Cat #MT10017CV) supplemented with 10% foetal bovine serum (Sigma-Aldrich, Cat #F0392) and penicillin, streptomycin and amphotericin B (Antibiotic-Antimycotic, Gibco, Cat #15290018) in tubes containing a stainless-steel ball and silica beads. The tubes were agitated at 30 Hz for 4 minutes (Retsch Mixer Mill, Fisher scientific, Cat #08-418-241) followed by centrifugation for 3 min at 16,000 ×g. The supernatants were added to *E. fuscus* kidney (*Ef*K) cells suspended in 2.5 ml DMEM supplemented with 50 µg/ml gentamicin (Gibco, Cat #15750060), 1 µg/ml TPCK trypsin (Invitrogen, Cat #20233) and 0.2% (w/v) bovine serum albumin (Sigma-Aldrich,Cat #A7284) (TPCK medium). The mixture was added to wells of 6 well plates (Greiner Cell Star, Cat #M0812). After 4 days, freshly dispersed *Ef*K cells were added to each well. One week later, the

cells and supernatant from each well were collected. Portions were saved for RNA extraction, and future inoculation and reinfection of *Ef*K cells. Four days later, discrete areas of rounded up cells were observed. When all cells had rounded up and detached from the monolayer, the cells were collected and a portion of cells were fixed with glutaraldehyde for electron microscopy.

Virus was further propagated in *Ef*K cells. To purify virus, culture supernatant was separated from the cells and debris by centrifuging twice, 850 × g for 5 mins each. Cells were washed and resuspended in PBS containing 0.5% (v/v) Tween 20 (Fisher Bioreagents, Cat #BP337-500) and kept on ice for 10 min. After vortexing for 30 secs, nuclei were removed by centrifugation and supernatant added to the previously collected culture supernatant. Cell debris was removed by centrifuging at 10,000 × g for 15 mins. The supernatant, containing the virus was then centrifuged at 80,000 × g for one hour. The pellet was then resuspended in TNE buffer (0.01M Tris (pH7.5) 0.001M EDTA and 0.15M NaCl) overnight at 4ºC. Concentrated virus was placed on electron microscope grids, fixed in glutaraldehyde and processed further for electron microscopy (negative staining).

7.6.4. Polymerase chain reaction

Pan-herpesvirus nested PCR was done using multiple primers as previously described [307]. Qiagen TopTaq DNA polymerase (Cat #200203) was used for setting up the reaction as described by the manufacturer. The denaturation, annealing and extension conditions for the first and second reaction were 94 ºC for 30 secs, 47 ºC for 30 secs and 72 ºC for 1 min (39 cycles). Initial denaturation was done at 94 ºC for 3 mins and final extension was 72 ºC for 10 mins.

Degenerate primers used for cytochrome B PCR (Table 7.1) and the denaturation, annealing and extension conditions were same as the previously described PCR, except the annealing temperature, which was 45 ºC. To screen for *Ef*HV infection in big brown bats we

amplified a portion of the BGLF4 (Protein kinase C-like superfamily) gene (Table 7.1). As a positive control, *Ef*HV genomic DNA was added and a control without template DNA was also included. The denaturation, annealing and extension conditions were same as for previously described PCRs, except the annealing temperature, which was 60 ºC.

Table 7.1. Details of Primers used for PCR

Target gene	Forward primer	Reverse primer	Product length
Cytochrome B	5' – TVG GHT AYG TVC TNC CVT GRG GMC AAA – 3'	5' – GGR TRT TCH ACD GGY TGK CCN CCR ATT – 3'	652 bp
BGLF4	5' – CAG CGT GAG CAG CCT ATG TA - 3'	5' - TAG AAT CCC GCA AGC GAC TC – 3'	238 bp
MHC-I (1) (873-1745)	5’ – ACG TCT AGG GTG CTG TTC ATC – 3’	5’ – ACT GTC TTC TGT CTT CCG TCC – 3’	253 bp
MHC-I (2) (3692-4018)	5’ – GGA GGC TTT AGC GTG TAC GG – 3’	5’ – TGG CTA AGA TGT TGG CAC AGT – 3’	178 bp
MHC-I (3) (4118-4414)	5’ – GAA AAG CTC ACC TCG AAC CG – 3’	5’ – GGG CCG TTG TGT ATG TCT CT – 3’	198 bp
MHC-I (4) (5477-6247)	5’ – AGG AGT CAA TGA GTG CCA CG – 3’	5’ – GGA GTC TTT CGG CAC CTT GA – 3’	332 bp
MHC-II (6437-6895)	5’ – TGG GTC ACC GGC TTT TAT CC – 3’	5’ – CAT CCC GCA GTC TCT GTC TG – 3’	328 bp
MHC-I (5) (7374-7772)	5’ – GTC AAG GGG TCG TGT CAA AC – 3’	5’ – CAG TTT TGT GGT GTG GCT CC – 3’	189 bp
Interleukin 10 homolog	5’ – TTT TCC ACT CTA GGC GAC CG – 3’	5’ – TCA CAC GGA GGT GAC GTA AG – 3’	204 bp
GAPDH	5’ – CAG GTT GTC TCC TGC GAC TT – 3’	5’ – GAC TGA TCT GGG GCA AGG AC – 3’	248 bp

7.6.5. Electron microscopy

Virus infected cells, which were fixed using glutaraldehyde, were processed for electron microscopy. Samples were then treated with osmium tetroxide (1% OsO_4, 0.1M sodium cacodylate buffer) for one hour at room temperature. Samples were quickly rinsed with water, gradually dehydrated in ethanol and en-bloc stained with uranyl acetate. After rinsing three times (5 minutes each) in propylene oxide, samples were infiltrated with Epon/Araldite (electron Microscopy Sciences, Fisher scientific, Cat #50-980-381). Samples were placed in molds and freshly prepared

Epon/Araldite was added. The samples were then polymerized at 60 ºC for 24-48 hours. Sections of 90 nm were cut and observed by transmission electron microscopy (TEM - Hitachi HT 7700). For the negative staining, a 300 mesh formvar/carbon grid was suspended on a drop of specimen for 1 min, after which the grid was passed through two drops of water to rinse it over a period of 40 secs. The grid was then suspended on 0.5% phosphotungstic acid for 1 min. The excess stain was blotted followed by drying of the grid. It was then viewed under TEM.

7.6.6. Restriction endonuclease site analysis and pulse-field gel electrophoresis

*Ef*HV DNA was digested using *Eco*RI, *Bgl*II, *Cla*I, *Swa*I, *Spe*I, *Pac*I or *Pme*I restriction endonucleases at 37 ºC for 1 hour. The digested DNA fragments were separated in a 1% agarose gel by electrophoresis in 0.5× TBE buffer at 14 °C for 20 hrs on a CHEF-DRIII electrophoresis system with an initial switch time of 2.16 secs, a final switch time of 54.17 secs, a 120° switch angle, and a gradient of 6.0 V/cm. *Salmonella enterica* serotype Branderup and 1 Kb Plus ladder (Invitrogen, Cat #10787018) was used as a reference ladder. Following electrophoresis, the gel was stained with 600 ml of distilled water containing ethidium bromide for 20 mins and de-stained with 600 ml of distilled water for 20 mins. DNA fragments were visualized with AlphaImager HP (Fisher Scientific, Cat #50-921-323) and photographed.

7.6.7. Sequencing and assembly of the *Ef*HV genome

To extract *Ef*HV DNA, purified virus in TNE buffer was incubated with SDS (0.5 % (w/v)) and Proteinase K (400 µg/ml) at 37 ^{0}C for 1 hr. After extraction with Tris saturated phenol:chloroform (Gibco, Cat #AM9730) DNA was recovered by spooling in ethanol. DNA was initially dissolved in TNE buffer and its integrity confirmed by electrophoresis on a 0.5% agarose gel. For paired-end sequencing on the MiSeq platform, the viral DNA was re-precipitated and suspended in 0.01M Tris (pH 7.5). The quantity and quality of DNA was assessed using Nanodrop

and Bioanalyzer (DNA 1000 chip, Agilent Technologies, Cat #5067). A genomic DNA library was prepared using the Nextera XT kit (Illumina, Cat #FC-121-1002) which was then sequenced on a MiSeq system (Nextera XT kit) (Illumina, Inc.) to generate 250 bp paired-end reads.

For Nanopore sequencing, 1-dimensional genomic DNA sequencing was performed on a MinION device (Oxford Nanopore technology, Cat #SQK-RAD004). Genomic DNA library was made based on the protocol provided by Oxford Nanopore Technologies.

De-novo assembly was first performed only using the MiSeq reads and the Geneious assembler [308]. Open reading frames (ORF) were predicted by MacVector software [309]. The translated amino acid sequences of the ORFs were compared to all existing amino acid sequences in the NCBI database using BLASTp [310] to determine whether they matched known proteins. Using these ORFs as a reference, we selected the longest forward and reverse long-read from the MinION reads which had several overlapping ORFs. By aligning the pair of reads, we were able to obtain the scaffold of the *Ef*HV genome. We re-mapped all the Mi-seq and Minion reads onto this scaffold to improve the quality of the sequence. After mapping, we selected the consensus of all the mapped reads onto the *Ef*HV scaffold.

The accuracy of the finally assembled genome was confirmed by matching restriction enzyme recognition sites with sizes of fragments observed in pulse-field gel electrophoresis.

7.6.8. Virus quantification

For testing susceptibility of cell lines for *Ef*HV, 3T3, *Ef*K, MDCK, MDBK, CRFK, BHK21, PK15, RK13, HEK293, Ederm and Vero cells (all, except for *Ef*K3 cells were originally obtained from the American Type Tissue Culture Collection) were cultured to test susceptibility of mouse, bat, canine, bovine, feline, hamster, porcine, rabbit, human, equine and monkey respectively. The species from which the cell lines originated was confirmed by sequencing

fragments of the cytochrome B gene obtained by PCR using the primers mentioned above. Cell monolayers on 12-well plates were infected with *Ef*HV with a MOI of 1 pfu/cell for one hour at 37 ^{0}C. After infection, the monolayer was rinsed with citrate buffer (40 mM citric acid, 10 mM KCl, 135 mM NaCl, pH 3) for 1 min. to inactivate extracellular virus and then rinsed again with PBS to remove the citrate buffer [311]. Cells were then incubated in complete medium at 30 ^{0}C. A set of plates representing all cell lines was frozen (-80 ^{0}C) as the time=0 samples. Forty-two hour later all other plates were frozen at -80 ^{0}. The plates were frozen and thawed three times, and cellular debris was removed by centrifugation (300 x g for 5 min). The supernatant was collected and assayed to determine $TCID_{50}$.

To assay for virus, samples were serially diluted (10-fold dilutions) in DMEM and 50 µl added onto a monolayer of *Ef*K cells in a 96-well plate. After 1 hour of infection, 100 µl of complete media was added and plates incubated at 37 ^{0}C. Plaques were counted on an inverted microscope after 4 days. $TCID_{50}$ was calculated using the Spearman and Kärber method [286,287] using the algorithm of Hierolzer and Killington [312]. The assays were done in triplicate.

7.6.9. *Ef*HV growth curve

Bat (*Ef*K) cells were seeded in a 6-well plate and infected with *Ef*HV for an hour followed by inactivation of extracellular virus by citrate buffer. Supernatant and cells were harvested by freeze-thawing thrice at 0, 1, 2, 4, 6, 8, 10, 12, 14, 16, 18, 20, 24, 36 and 48 hours after infection. Cellular debris was removed and virus titre ($TCID_{50}$) was determined on *Ef*K cells.

7.6.10. Mass spectrometry (MS)

Polypeptides from purified virus were separated by SDS-PAGE using 10 % acrylamide gel. The gel was stained with Coomassie blue (Thermofisher Scientific, Cat #20278) and all visible bands excised. The gel segments were sent to the University of Alberta Proteomics and Mass

Spectrometry facility for MS. The results were matched against a database created using the translated ORFs of *Ef*HV as determined from the assembled genome.

7.6.11. Serum Neutralization Assay

Bat plasma was heat inactivated at 56 ºC for 30 mins. 800 pfu/well (50 µl) of *Ef*HV was added to equal volume of 1/10, 1/20, 1/40, 1/80, 1/160 and 1/320 dilution of plasma from big brown bats and the mixture was incubated at 37 ºC for an hour. After the one hour incubation, 100 µl of the mixture was added to *Ef*K monolayer cells that were rinsed with PBS. Cytopathic changes were microscopically observed after 48 hours. As controls, "no virus and no serum" was used as a negative control and "only virus" was used a positive control.

7.6.12. *Ef*HV infection, RNA extraction, cDNA synthesis and quantitative real time PCR

For studying the Viral MHC gene and IL10 homolog expression, a monolayer of Bat cells (*Ef*k) in a 6-well plate were infected with *Ef*HV at a MOI of 5 pfu/cell. Uninfected bat cells were used as a negative control. RNA was extracted after 18 hours using QIAGEN RNAeasy kit (Qiagen, Cat #74136) as per manufacturers protocol. cDNA was prepared using iScript gDNA Clear cDNA synthesis kit (BioRad, Cat #172-5035) as per manufacturers protocol. A no reverse transcriptase control cDNA was prepared and used to rule out amplification of genomic DNA. Real time PCR was performed using 10 µl SsoFast Evagreen supermix (BioRad, Cat #172-5201) and 2.5 µl of 4 µM of forward and reverse primer for MHC-I (873-1745), MHC-I (3692-4018), MHC-I (4118-4414), MHC-I (5477-6247), MHC-II (6437-6895), MHC-I (7374-7772) and Interleukin 10 homolog (Table 3). Denaturation was at 95 ºC for 5 secs and, annealing and extension at 60 ºC for 5 secs for all primer pairs. The products were analysed on an agarose gel and were also sent for Sanger sequencing (Macrogen).

7.6.13. Phylogenetic analysis

Analyses were performed at the level of encoded amino acid sequences of glycoprotein B and DNA polymerase selected based on [303] (Supplementary table S7.1). Sequence were aligned using ClustalW [214] and the portion of amino acid sequence that corresponded to previously available bat gammaherpesvirus sequences were used for the phylogenetic analysis. We determined the most appropriate amino acid substitution model using ProtTest 3.4.2 [313]. Maximum likelihood (ML) trees were constructed using MEGA7 [215]. Using Le and Gascuel model and a gamma distribution (G) of variation with invariant sites (I), we constructed trees for the glycoprotein B gene whereas the same model with gamma distribution alone was used for DNA polymerase gene [314]. Bootstrapping with 500 replicates was used to estimate the confidence of the tree nodes. Phylogenetic trees for the MHC genes were also constructed in a similar manner. The model of evolution used for MHC-I (1) and MHC-II was WAG model [315] whereas for MHC-I (2), (4) and (5) was JTT model [316].

7.7. Results

7.7.1. Isolation of a novel herpesvirus from lungs of a big brown bat (*E. fuscus*)

As part of ongoing surveillance of viruses in local North American bats, we observed cytopathic effects in *Ef*K cells, a big brown bat kidney cell line [213], inoculated with a homogenate of lungs from a big brown bat submitted to the Canadian Wildlife Heath Cooperative (CWHC). Using pan-herpesvirus primers in a PCR [307] we established the presence of a herpesvirus. To further confirm this, we performed electron microscopy on the cells and observed virus particles having herpesvirus-like morphology (Figure 7.1. (A), (B) and (C)). In addition to

microscopy of the cells, we observed herpesvirus particles in negative stained preparations of purified virus (Figure 7.1. (D)).

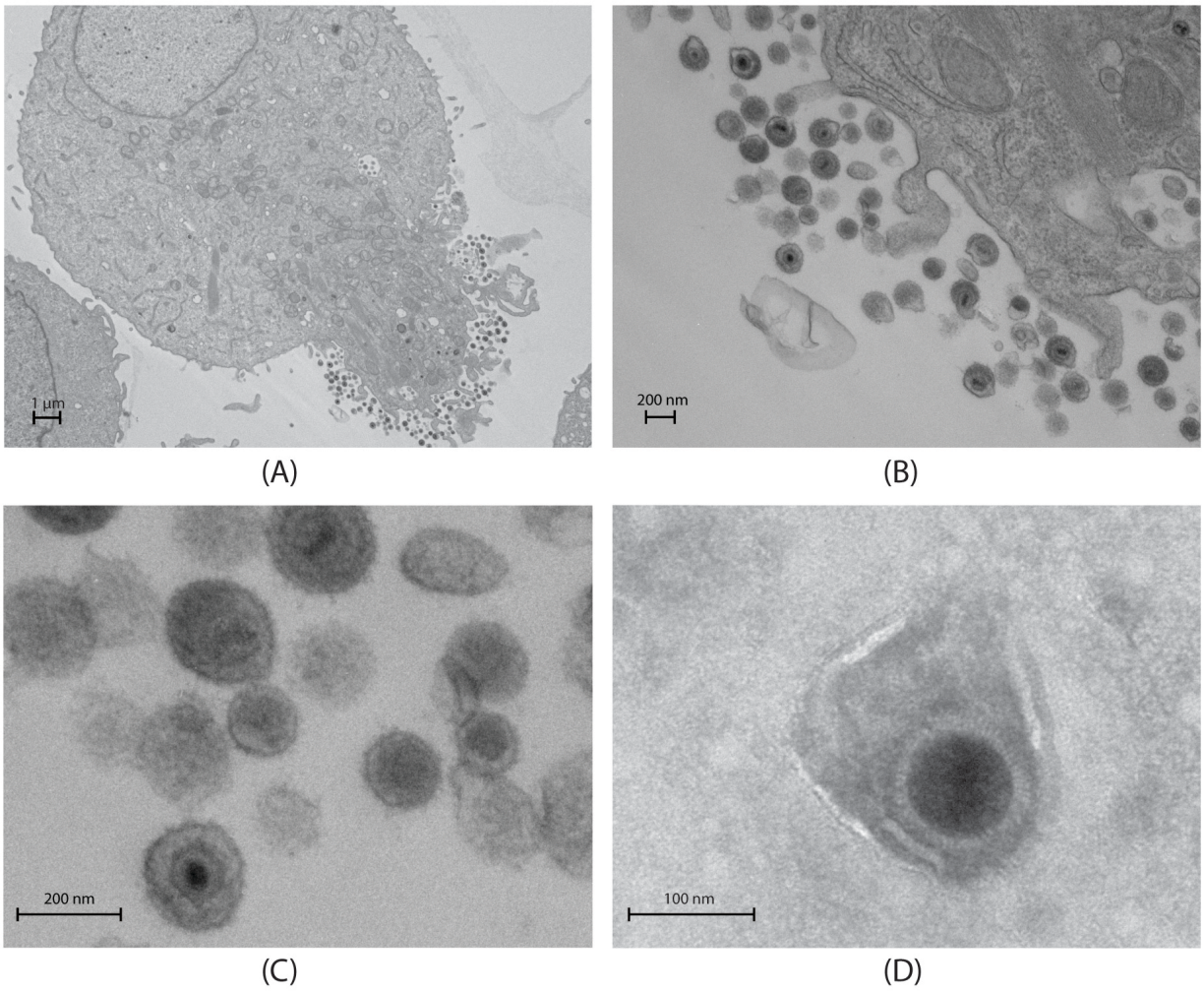

Figure 7.1. Electron micrographs of *Ef*HV. *Ef*k cells inoculated with homogenate of lungs from a big brown bat showing enveloped virions (approximately 200 nm in size) budding out from the cells (A), (B) and (C). Negative staining of purified virions showing a magnified image of the virus (D). The capsid is approximately 100 nm in size.

7.7.2. Genome sequencing of *Ef*HV

To determine the nucleotide sequence of the *Ef*HV genome, we used a combination of paired-end (Illumina MiSeq) and long read (Oxford Nanopore) sequencing. We obtained 1,458,704 paired-end reads from an Illunima Mi-seq run, and de-novo assembly on these reads

(using Geneious Assembler [308]) led to the assembly of contigs of a maximum of ~100kb. As we were unable to join all the contigs, we resorted to performing a long read sequencing i.e. Nanopore sequencing, from which 27,002 long reads were obtained. Finally, we used Geneious assembler to combine the long reads and the paired end reads in order to get the complete genome of the herpesvirus which is 166,748 bp with a GC content of 59.6% (NCBI Accession number MF385016) [308]. The arrangement of the sequence contigs was verified by restriction enzyme mapping (Supplementary figure S7.2). We annotated the genome based on results of BLASTp comparisons of predicted open codon reading frames (ORFs) [309] from the assembled sequence to all sequences in the NCBI database, which resulted in the successful identification of 75 genes (Table 7.2, Figure 7.2). Repeats in the genome were identified using Geneious R10 [308].

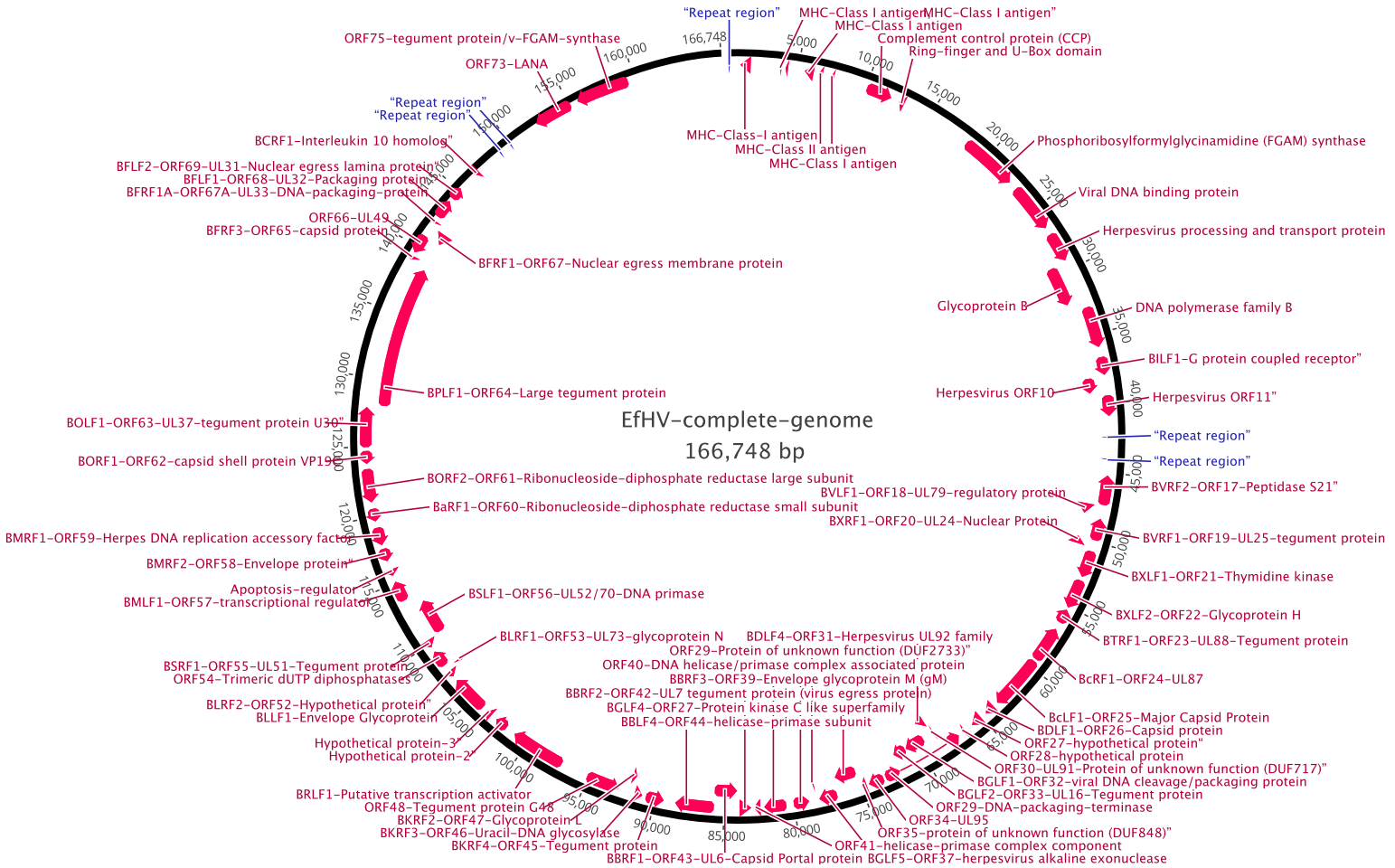

Figure 2. Map of the *Ef*HV genome. The 166 kb genome contains 75 open reading frames. The putative identity of the ORFs, based on similarity to those of other gammaherpesviruses, is indicated in red. Although depicted as a circle, the viral genome is linear. Repeated sequences are in blue.

Table 7.2. Genome annotation of *Ef*HV and its similarity with other herpesviruses. The first and second column shows the nucleotide range and the orientation of ORFs on the *Ef*HV DNA respectively. The third column indicates the superfamily to which the protein belongs, and the fourth column shows the closest match obtained after BLASTp search of the translated ORF against the NCBI database. The BLASTp similarity and percent coverage of the closest match is indictated in the fifth and sixth columns, respectively. The last three columns represent the coding of the ORF in three different formats used for viruses belonging to *Gammaherpesvirinae*.

Start and End location on genome	Coding strand (+/-)	Protein superfamily	Best Match from BLAST Search	Blastp % similarity	Percentage Coverage	ORF#	B#	UL#
873-1745	-	MHC Class I	MHC class I antigen [*Saimiri sciureus sciureus*]	49/90(54%)	16.90			
3692-4018	-	MHC Class I	major histocompatibility complex class I-related gene protein-like [*Labrus bergylta*]	40/77(51%)	37.04			
4118-4414	-	MHC Class I	HLA class I histocompatibility antigen, B-15 alpha chain-like [*Myotis lucifugus*]	34/69(49%)	34.69			
5477-6247	-	MHC Class I	MHC class I antigen [*Ornithorhynchus anatinus*]	57/108(52%)	22.27			
6437-6895	-	MHC Class II	DLA class II histocompatibility antigen, DR-1 beta chain-like [*Latimeria chalumnae*]	68/135(50%)	44.74			
7374-7772	-	MHC Class I	HLA class I histocompatibility antigen, B-67 alpha chain-like isoform X2 [*Myotis brandtii*]	48/102(47%)	36.36			
10060-12141	+	Complement control protein (CCP)	membrane cofactor protein-like isoform X2 [*Pteropus vampyrus*]	131/278(47%)	18.90			
12556-13143	-	Ring-finger and U-Box domain	Zinc finger, RING-CH-type domain and Zinc finger, RING/FYVE/PHD-type domain-containing protein [*Strongyloides ratti*]	52/104(50%)	26.67			
18219-22577	+	Phosphoribosylformylglycinamidine (FGAM) synthase	protein G3 [*Myotis* gammaherpesvirus 8]	552/1151(47%)	38.02			
23054-26713	+	Viral DNA binding protein	major DNA-binding protein [*Saimiriine* gammaherpesvirus 2]	790/1211(65%)	64.81	6		
27130-29439	+	Herpesvirus processing and transport protein	DNA packaging terminase subunit 2 [*Myotis* gammaherpesvirus 8]	479/750(63%)	62.29	7		
29336-32440	+	Glycoprotein B	glycoprotein B [*Myotis ricketti* herpesvirus 1]	558/866(64%)	53.97	8		

32956-36099	+	DNA polymerase family B	DNA polymerase [*Myotis ricketti* herpesvirus 1]	751/994(75%)	71.73	9	BALF5	
36647-38089	+	G protein coupled receptor	membrane protein BILF1 [*Equid* gammaherpesvirus 5]	116/290(40%)	24.17		BILF1	
38008-39336	+	Herpesvirus ORF10	unnamed protein product [*Saimiriine* gammaherpesvirus 2]	176/441(39%)	39.82	10	LF1	
39449-41116	+	Herpesvirus ORF11	orf 11 [*Ateline* gammaherpesvirus 3]	201/394(51%)	36.22	11	LF2	
45167-47434	-	Peptidase S21	ORF17 [Human gammaherpesvirus 8]	285/602(47%)	37.75	17	BVRF2	
47328-48302	+	Herpesvirus UL79	ORF18 [*Felis catus* gammaherpesvirus 1]	170/257(66%)	52.47	18	BVLF1	79
48335-50062	-	Herpesvirus UL25	DNA packaging tegument protein UL25 [*Myotis* gammaherpesvirus 8]	341/581(58%)	59.30	19	BVRF1	25
49851-50630	-	Herpesvirus UL24	nuclear protein UL24 family [*Myotis* gammaherpesvirus 8]	138/210(65%)	53.28	20	BXRF1	24
50660-52870	+	Herpesvirus Thymidine kinase	thymidine kinase [*Equid* gammaherpesvirus 5]	206/330(62%)	27.99	21	BXLF1	
52891-55245	+	Herpesvirus Glycoprotein H	ORF22 [*Felis catus* gammaherpesvirus 1]	374/715(52%)	47.70	22	BXLF2	75
55242-56411	-	Herpesvirus BTRF1 (Tegument Protein)	ORF23 [*Macaca nemestrina* rhadinovirus 2]	115/264(43%)	29.56	23	BTRF1	88
56802-59612	-	Herpesvirus UL87	hypothetical protein [*Bovine* gammaherpesvirus 4]	459/752(61%)	49.04	24	BcRF1	87
59611-63771	+	Herpesvirus Major Capsid Protein	major capsid protein [*Bovine* gammaherpesvirus 4]	1082/1379(78%)	78.07	25	BcLF1	
63963-64880	+	Herpesvirus VP23 like capsid protein	capsid protein [*Bovine* gammaherpesvirus 4]	238/301(79%)	78.03	26	BDLF1	
65092-66189	+	hypothetical protein; Provisional	ORF27 [*Bovine* gammaherpesvirus 6]	96/229(41%)	26.30	27		
66619-67026	+		ORF28 (Hypothetical protein-1)			28		
67187-68278 72050-73366	-	DNA packaging terminase subunit 1 (*2 exons*)	DNA packaging terminase subunit 1 [*Myotis* gammaherpesvirus 8]	516/660(78%)	64.42	29	BGRF1/BDRF1	89
68588-68857	+	Protein of unknown function (DUF717)	protein UL91 [*Myotis* gammaherpesvirus 8]	44/62(70%)	49.44	30		91
68755-69531	+	Herpesvirus UL92 family	orf 31 [*Ateline* gammaherpesvirus 3]	134/222(60%)	51.94	31	BDLF4	92
69474-71105	+	Herpesvirus UL17 protein	viral DNA cleavage/packaging protein [*Bovine* gammaherpesvirus 4]	240/545(44%)	44.20	32	BGLF1	17
71098-72153	+	Herpesvirus UL16/UL94 family (Tegument protein)	ORF33 [*Felis catus* gammaherpesvirus 1]	203/334(60%)	57.83	33	BGLF2	94
73365-74648	+	UL95 family	hypothetical protein [*Saimiriine* gammaherpesvirus 2]	205/419(48%)	48.01	34		95
74687-75256	+	Gammaherpesvirus protein of unknown function (DUF848)	hypothetical protein [Harp seal herpesvirus]	87/192(45%)	46.03	35		14
75087-76844	+	Protein kinase C like superfamily	tegument serine/threonine protein kinase [*Myotis* gammaherpesvirus 8]	228/424(53%)	38.97	36	BGLF4	
76890-78395	+	Herpesvirus alkaline exonuclease	deoxyribonuclease [*Myotis* gammaherpesvirus 8]	313/489(64%)	62.48	37	BGLF5	

78347-78619	+	Protein of unknown function (DUF2733)	ORF29 [*Callitrichine* gammaherpesvirus 3]	36/57(63%)	40.00	29		
78930-80219	-	Herpesvirus glycoprotein M	envelope glycoprotein M [*Equid* gammaherpesvirus 5]	265/419(63%)	61.77	39	BBRF3	
80570-82348	+	Herpesvirus DNA helicase/primase complex associated protein	hypothetical protein [*Bovine* gammaherpesvirus 4]	201/484(41%)	33.95	40		
82434-83117	+	Herpesvirus helicase-primase complex component	ORF41 [*Macaca nemestrina* rhadinovirus 2]	72/141(51%)	31.72	41		8
83103-84122	-	Herpesvirus UL7 tegument protein (virus egress protein)	tegument protein UL7 [*Delphinid* gammaherpesvirus 1]	162/283(57%)	47.79	42	BBRF2	7
84076-85974	-	Herpesvirus UL6 like	capsid portal protein [*Myotis* gammaherpesvirus 8]	449/592(75%)	71.04	43	BBRF1	6
85811-88720	+	helicase-primase subunit BBLF4	DNA helicase-primase complex component [Harp seal herpesvirus]	594/812(73%)	61.30	44	BBLF4	
89378-90847	-	Tegument Protein	tegument protein G45 [*Delphinid* gammaherpesvirus 1]	16/21(76%)	3.27	45	BKRF4	
90912-91724	-	Uracil DNA glycosylase superfamily	uracil-DNA glycosylase [*Delphinid* gammaherpesvirus 1]	200/272(73%)	74.07	46	BKRF3	
91660-92163	-	Viral glycoprotein L	envelope glycoprotein L [*Myotis* gammaherpesvirus 8]	56/106(52%)	33.53	47	BKRF2	
92716-95328	-	Herpesvirus protein of unknown function (DUF832)	tegument protein G48 [*Equid* gammaherpesvirus 5]	122/219(55%)	14.02	48		92
97184-101290	+	Herpesvirus transcription activation factor (transactivator)	protein Rta [*Equid* gammaherpesvirus 2]	149/283(52%)	10.89	50	BRLF1	
101879-102976	+		Hypothetical protein-2					
103225-103761	+		Hypothetical protein-3					
104121-106964	+	Envelope glycoprotein	envelope glycoprotein [*Myotis* gammaherpesvirus 8]	136/349(38%)	14.36		BLLF1	
107104-107808	-	Herpesvirus BLRF2 protein	hypothetical protein [*Bovine* gammaherpesvirus 4]	72/116(62%)	30.77	52	BLRF2	
107661-108050	-	UL73 viral envelope glycoprotein	ORF53 [*Felis catus* gammaherpesvirus 1]	43/49(87%)	33.33	53	BLRF1	73
108129-109538	+	Trimeric dUTP diphosphatases	orf 54 [*Ateline* gammaherpesvirus 3]	143/276(51%)	30.49	54		
109729-110454	-	Herpes virus U44 protein	tegument protein UL51 [*Equid* gammaherpesvirus 5]	154/237(64%)	63.90	55	BSRF1	51
110412-113177	+	Herpesviridae UL52/UL70 DNA primase	helicase-primase primase subunit [*Equid* gammaherpesvirus 5]	567/920(61%)	61.56	56	BSLF1	52
113585-115297	+	Herpesvirus transcriptional regulator family	putative post-transcriptional transactivator [*Bovine* gammaherpesvirus 4]	137/241(56%)	24.04	57		
115582-116214	-	Apoptosis regulator	apoptosis regulator BALF1 [*Delphinid* gammaherpesvirus 1]	35/69(50%)	16.67		BALF1	

116711-117817	-	Herpesvirus BMRF2 protein	envelope protein UL43 [*Delphinid* gammaherpesvirus 1]	181/344(52%)	49.18	58	BMRF2	43
117849-119357	-	Herpes DNA replication accessory factor	DNA polymerase processivity subunit [*Delphinid* gammaherpesvirus 1]	165/298(55%)	32.87	59	BMRF1	
119617-120726	-	ribonucleoside-diphosphate reductase small subunit	ribonucleotide reductase subunit 2 [*Equid* gammaherpesvirus 2]	238/302(78%)	64.50	60	BaRF1	
121014-123629	-	ribonucleoside--diphosphate reductase large subunit	ribonucleotide reductase subunit 1 [*Myotis* gammaherpesvirus 8]	531/736(72%)	60.96	61	BORF2	
123805-124917	-	Herpesvirus capsid shell protein VP19C	unnamed protein product [*Saimiriine* gammaherpesvirus 2]	218/333(65%)	58.92	62	BORF1	
124954-128085	+	Herpes virus tegument protein U30	tegument protein [*Bovine* gammaherpesvirus 4]	502/980(51%)	48.13	63	BOLF1	37
128015-138883	+	Large tegument protein	tegument protein [*Bovine* gammaherpesvirus 4]	870/1828(47%)	24.02	64	BPLF1	36
138932-139387	-	Gammaherpesvirus capsid protein	ORF65 [*Macaca nemestrina* rhadinovirus 2]	45/65(69%)	29.80	65	BFRF3	
139542-141089	-	UL49 family	protein UL49 [*Delphinid* gammaherpesvirus 1]	212/385(55%)	41.17	66	BFRF2	49
140900-141898	-	Herpesvirus virion protein U34	nuclear egress membrane protein [*Equid* gammaherpesvirus 5]	162/225(72%)	48.80	67	BFRF1	
142016-142351	-	DNA packaging protein UL33	hypothetical protein [*Bovine* gammaherpesvirus 4]	57/76(75%)	51.35	67A	BFRF1A	33
142561-144108	+	Herpesvirus putative major envelope glycoprotein	DNA packaging protein UL32 [*Myotis* gammaherpesvirus 8]	298/503(59%)	57.86	68	BFLF1	32
144249-145379	+	nuclear egress lamina protein UL31	hypothetical protein [Harp seal herpesvirus]	191/288(66%)	50.80	69	BFLF2	31
146542-147135	-	Interleukin-10 family	interleukin-10 [*Equid* gammaherpesvirus 2]	92/158(58%)	46.70		BCRF1	
152249-155281	-	Latency associated nuclear antigen	latency-associated nuclear antigen (lana) DNA binding domain [Harp seal herpesvirus]	46/87(52%)	4.55	73		
155602-159669	-	herpesvirus tegument protein/v-FGAM-synthase	tegument protein/v-FGAM-synthetase [*Bovine* gammaherpesvirus 4]	648/1334(48%)	47.82	75	BNRF1	

The genome length of *Ef*HV was well within the range of known herpesviruses, i.e. 124 kb to 295 kb [77]. Based on BLASTp percent similarity, most of the genes matched with orthologues in other gammaherpesviruses. Within the first 8 kb of the 5' end of the genome, we detected four putative major histocompatibility complex (MHC) class I genes and one MHC class II gene (Figure 7.2). In addition to MHC antigens, we detected an interleukin-10 homolog in the genome. We verified expression of all the MHC-I, MHC-II and IL-10 homolog genes in bat cells infected with *Ef*HV by analyzing transcripts from virus-infected cells - we used quantitative real time PCR (qRT-PCR) followed by analysis of the products by agarose gel electrophoresis (Supplementary figure S7.3) and determined their nucleotide sequence. *Ef*HV also encoded proteins similar to the latency associated nuclear antigen (LANA1) and replication and transcription activator (Rta), proteins that are key regulators of Kaposi sarcoma virus latency and lytic cycles [317,318].

7.7.3. *Ef*HV belongs to the Genus *Rhadinovirus* in *Gammaherpesvirinae*

We initially compared the amino acid sequence of the entire DNA polymerase protein of *Ef*HV with that of homologues in representative alpha, beta and gammaherpesviruses (Supplementary figure S7.4). *Ef*HV clustered with gammaherpesviruses, and most closely aligned with the *Rhadinoviruses* Kaposi's sarcoma herpesvirus and *Saimirine herpesvirus* 2. We next aligned the amino acid sequences of the DNA polymerase and glycoprotein B gene of representative viruses from *Gammaherpesvirinae* based on sequences reported by Escalera-Zamudio et al. [303] (Supplementary table S7.1). As complete sequences were not available for all viruses, we aligned sequences from portions of each protein that were common to all sequences. Maximum-likelihood trees were constructed using MEGA7 (Kumar *et al.*, 2016) using LG+G phylogenetic model for DNA polymerase (Figure 7.3. (A)) and LG+G+I for glycoprotein B (Figure 7.3. (B)) genes, as determined by ProtTest 3.4.2 [313] followed by 500 bootstrap replications. In

both the trees, *Ef*HV sequences were found to cluster with those of other bat *Rhadinoviruses*. *Ef*HV sequences most closely resembled those of bat *Rhadinoviruses* detected in *Myotis nattereri* (MYNARHV1, in Figure 7.3. (A)) and *Pipistrellus nathusii* (PIPNARHV1), both of which are European bats, and *Eptesicus serotinus* (EPSERHV1), a Eurasian bat.

Figure 7.3. Phylogenetic comparison of *Ef*HV with other gammaherpesviruses. To determine the phylogenetic relationship of *Ef*HV with other gammaherpesviruses, sequences of DNA Polymerase (A) and glycoprotein B (B) were compared. Only a portion of the amino acid sequences of *Ef*HV polymerase and gB proteins, that corresponded to the reported partial sequences for those of orthologues in other gammaherpesviruses, could be used in the comparison. Alignment lengths were 42 amino acids and 106 amino acids for DNA Polymerase and gB, respectively. Gammaherpesviruses derived from bats are indicated in green. *Ef*HV (arrows) was related to the *Myotis nattereri rhadinovirus, Pipistrellus nathusii rhadinovirus-1* and *Eptesicus serotinus rhadinovirus-1*. Bootstrap values (>50%) are shown at the branch points. Detail of the sequences [303] included in the phylogenetic tree are in Supplementary table S7.1.

7.7.4. Cell tropism of *Ef*HV

To understand the spectrum of species that *Ef*HV could infect, we infected different cell lines (bat kidney epithelial cell line), mouse (embryonic fibroblast cell line), canine (kidney epithelial cell line), bovine (kidney epithelial cell line), feline (kidney epithelial cell line), hamster (kidney fibroblast cell line), porcine (kidney epithelial cell line), rabbit (kidney epithelial cell line), human (kidney epithelial cell line), equine (skin fibroblast cell line) and monkey (kidney epithelial cell line) with *Ef*HV at a multiplicity of infection of 1 plaque forming unit (pfu) per cell, followed by inactivation of extracellular residual virus. We then measured virus yields 42 hours after infection. Virus yields were highest from bat cells (*Ef*K). Human, monkey, feline and porcine cell lines yielded moderate amounts of virus whereas mouse, hamster, canine, and bovine cells produced low levels of virus. Rabbit and equine cells did not yield virus (Figure 7.4).

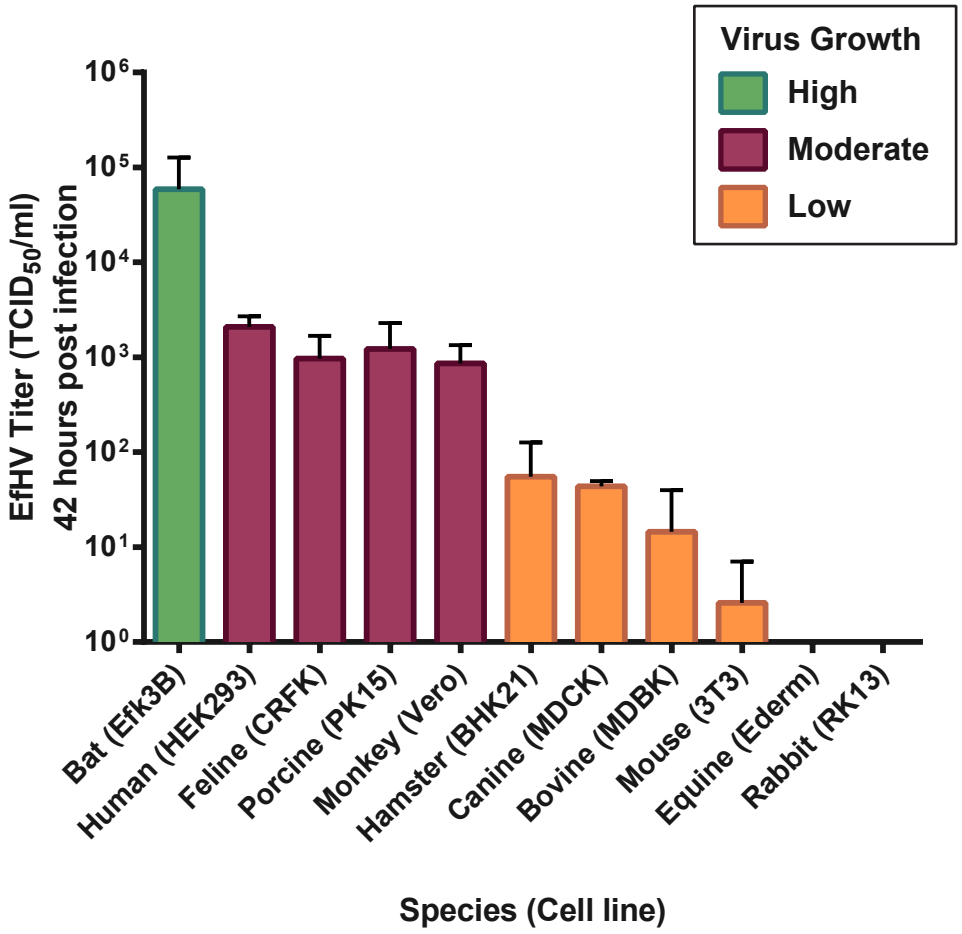

Figure 7.4. *Ef*HV infection of cell lines from various species. Bars represent virus yields (average of three experiments) expressed as $TCID_{50}$ per ml of growth supernatant recovered 42 hr after infection. Error bars represent standard deviations.

7.7.5. Growth kinetics of *Ef*HV

We infected bat cells with *Ef*HV followed by inactivation of extracellular residual virus. We quantified the virus at various time points following infection to plot a one-step growth curve. Virus yields increased 12 hours after infection and continued to increase up to 48 hours (Figure 7.5).

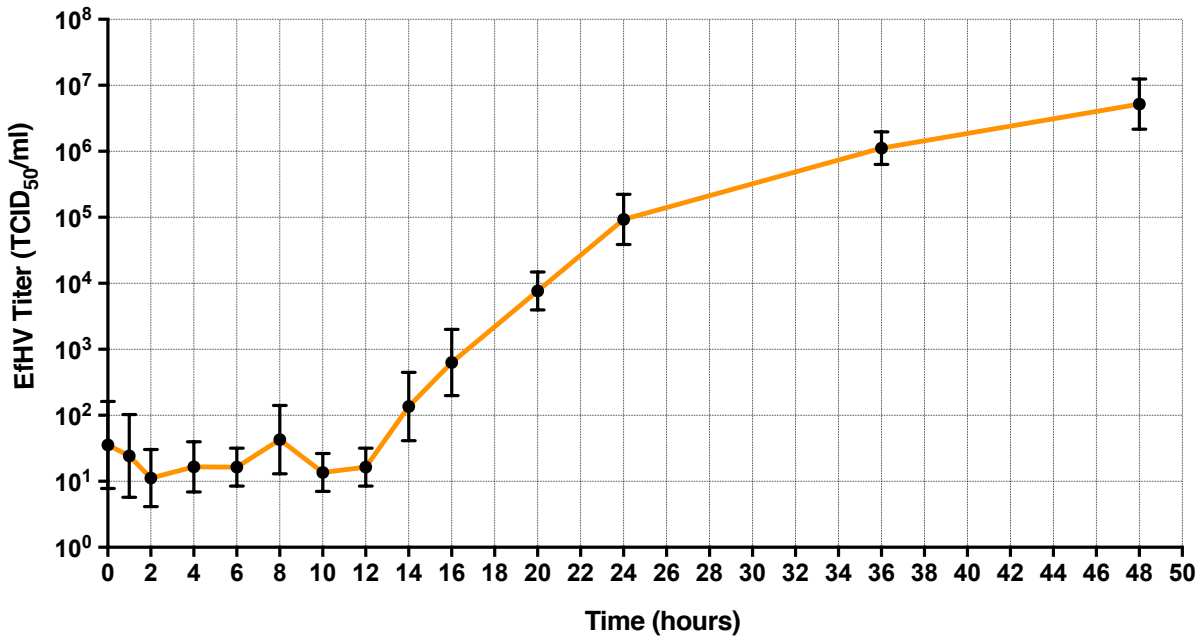

Figure 7.5. Growth curve of *Ef*HV. To understand the growth kinetics of *Ef*HV in bat cells, *Ef*K cells were infected at a MOI of 4 pfu/cell for 1 hour followed by the inactivation of residual virus. Dots represent virus yields (average of three experiments), expressed as $TCID_{50}$/ml of lysed cells and growth supernatant. Error bars represent standard deviation from means.

7.7.6. Protein composition of *Ef*HV

To identify *Ef*HV proteins present in the virion, we performed mass spectrometry on segments of a polyacrylamide gel used to separate virion proteins. A comparison of the masses of separated tryptic peptides with *Ef*HV ORFs confirmed the identity of the ORFs (Table 7.3). In addition, proteins present in *Ef*HV virions resembled those in other gammaherpesvirus virions [319].

Table 7.3. Proteins present in the *Ef*HV virion. The first column mentions the identity of the ORF (Table 7.2). The second and third column shows the molecular mass of the protein and coverage by the peptides obtained using mass spectrometry.

Protein Name with ORF codes	Molecular Mass (kDa)	Coverage
BcLF1; ORF25; major capsid protein	153.7	75.32
BNRF1; ORF75; herpesvirus tegument protein/v-FGAM-synthase	158.2	79.55
BPLF1; ORF64; Large Tegument Protein	397.5	51.13
BOLF1; ORF63; Herpes virus tegument protein U30	116.1	81.69
ORF48; Herpesvirus protein of unknown function (DUF832)	94.8	55.29
BALF4; ORF8; Envelope Glycoprotein B (gB)	108.8	43.9
BXLF2; ORF22; Glycoprotein H (gH)	85.6	47.19
BXLF1; ORF21; Thymidine Kinase	79	54.76
BKRF4; ORF45; Tegument Protein	52.9	48.26
BBRF1; ORF43; Capsid Portal Protein	71.4	37.5
BGLF4; ORF27; Probable Inactive Protein Kinase 38	65.3	39.32
LF2; ORF11	61.2	56.94
BVRF1; ORF19; DNA packaging tegument protein	63.6	39.13
BGLF1; ORF32; viral DNA cleavage/packaging protein	58.7	35.36
BTRF1; ORF23; Tegument Protein	41.9	24.94
BLLF1; Envelope Glycoprotein	100.88	9.5
BaRF1; ORF60; Ribonucleoside diphosphate reductase small subunit	41.7	19.24
BGLF2; ORF33; Herpesvirus UL16/UL94 family (Tegument protein)	38.7	42.74
BORF1; ORF62; capsid shell protein VP19C	41.4	41.89

7.7.7. Prevalence of *Ef*HV in Canadian big brown bats

Using PCR, we detected *Ef*HV DNA in blood cells from 20 of 28 bats (71%). The 250 bp PCR product detected was the same size as the PCR product obtained from *Ef*HV genomic DNA (positive control). The identity of the products was confirmed by determining their nucleotide

sequences. Although most bats appeared to be infected with *Ef*HV, we were unable to detect virus neutralizing antibodies in the plasma of any of the bats.

7.8. Discussion

Gammaherpesviruses have been studied in human and other animal hosts, but very little is known about these viruses in bats. Here, we report the characterization of a novel gammaherpesvirus isolated from *E. fuscus*, the North American big brown bat. Thus, we named the virus *E. fuscus* herpesvirus. We determined the complete sequence of the viral genome and its phylogenetic relationship to existing gammaherpesviruses. We discovered that *Ef*HV is structurally similar to other gammaherpesviruses. The protein composition of *Ef*HV is also similar to that of other gammaherpesviruses [319].

While gammaherpesviruses have been detected in other bat species, the *Myotis* gammaherpesvirus 8 is the only other bat gammaherpesvirus that has been isolated [147]. This virus belongs to the genus *Percavirus* within *Gammaherpesvirinae* along with *Equid herpesviruses 2* and *5*. A comparison of two *Ef*HV ORFs with the partial reported sequences from other bat gammaherpesviruses revealed that it is related to European and Eurasian bat gammaherpesviruses, which also belong to the genus *Rhadinovirus*. Since many of the sequences used in this analysis were incomplete and represented a conserved portion of the DNA polymerase and gB proteins, the boot strap values for several of the other nodes tended to be low.

Although databases contain complete genomes of gammaherpesviruses isolated from other mammals, existing sequences of bat gammaherpesviruses in the NCBI database are limited to short sequence segments or partial genomes. The *Ef*HV genome is the first bat gammaherpesvirus whose complete sequence has been determined, including repeated sequences. In addition to ORFs with

strong similarities to those of other gammaherpesviruses and an ORF resembling mammalian IL-10, which is also transduced by other gammaherpesviruses, we found four ORFs that resembled putative MHC-I and one that resembled putative MHC-II in the 5' end of the genome. These were not sequencing artefacts because of accidental sequencing of host DNA or because of assembling errors, since we confirmed the assembly of contigs by comparison with long stretches of contiguous sequences generated by Nanopore sequencing, and also by restriction endonuclease mapping. Protein BLAST of these MHC antigen sequences allowed us to select the MHC sequences of other species that resembled the *Ef*HV MHC sequences. Based on these sequences, we performed phylogenetic analysis and showed that one of the MHC I antigens, matched those of other bat species (Figure 7.6 (E)), implying that the virus might have acquired them during virus-host coevolution. Another MHC I antigen, closely resembled that of a rodent species (Figure 7.6 (A)). For the remaining MHC I and II antigens, the sequences did not cluster with any species (Figure 7.6 (B), (C) and (D)). Previously, MHC I antigens have been discovered in betaherpesviruses [320–323] and in one rodent gammaherpesvirus [324]. These MHC antigens might have a role to play in the immune evasion mechanisms of the virus. *In-vivo* studies using a betaherpesvirus (murine cytomegalovirus) has revealed that the absence of MHC I homologues led to restricted virus replication in the host [325]. Such MHC I homologues might serve as decoy ligands to allow virus to hide from natural killer cells, which are specialized to detect and target cells that have lost MHC class I [326]. Although MHC II homologues are present in a bat betaherpesvirus [320], this is first time that an MHC II homolog has been detected in a gammaherpesvirus. The MHC class II homologue may have a role to play in interfering with antigen presentation to CD4+ T cells. Further studies in this direction might reveal a novel immune evasion strategy.

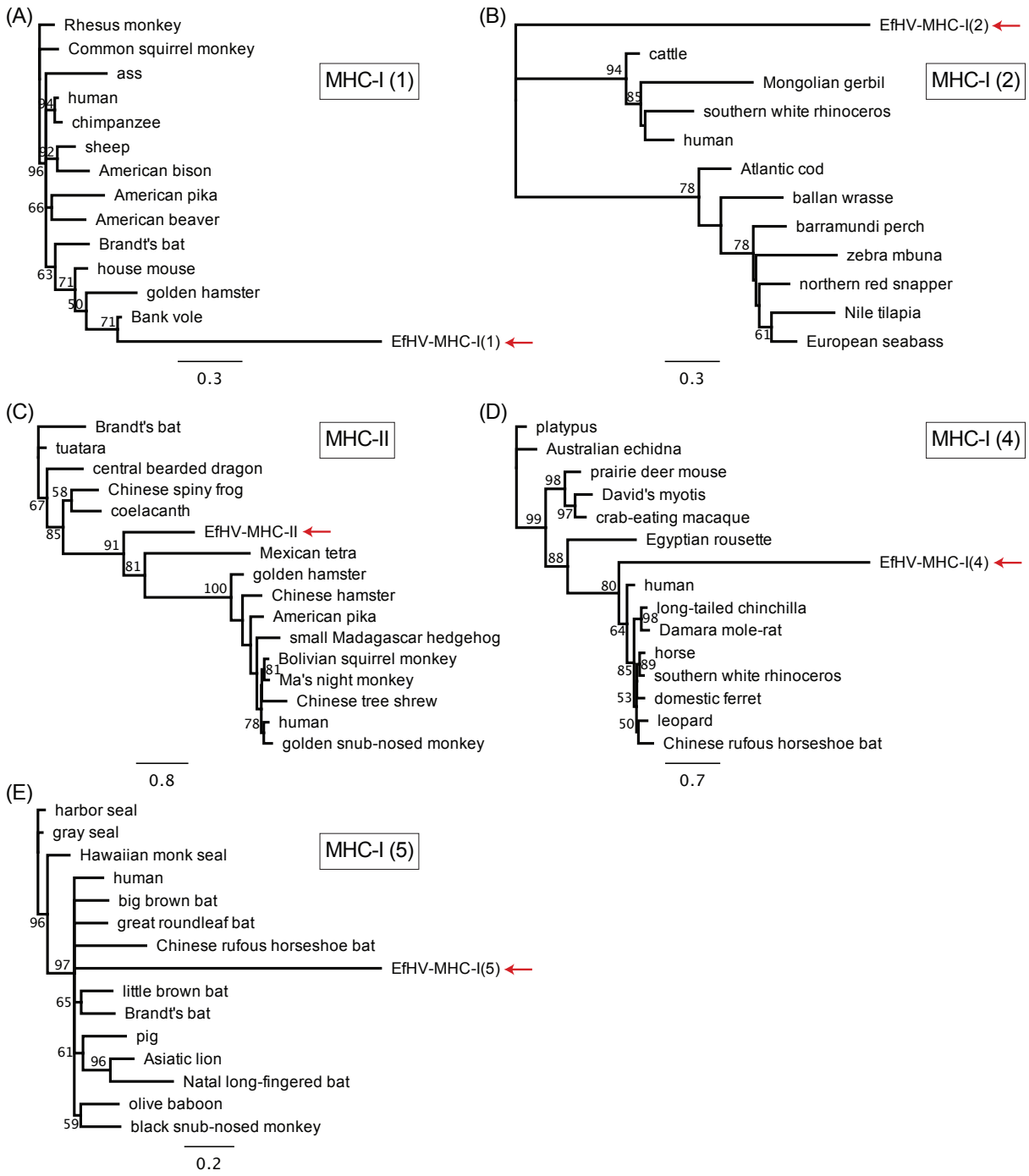

Figure 7.6. A comparison of *Ef*HV MHC antigens with those of other species (Maximum likelihood method). Comparison of *Ef*HV ORFs that resemble MHC antigens, with the most similar sequence from other species as determined by BLASTp search of the entire NCBI database. For MHC-I molecules (A and E), the *Ef*HV ORFs form a distinct branch closely related to bank vole and Chinese Rufous horseshoe bat, respectively. The remaining MHC I ((B), (D)) and MHC

II molecules (C), however, *Ef*HV sequences did not cluster with any specific species. Bootstrap values (>50%) are shown at the branch points.

---

*Ef*HV was shown to grow in cells from humans, monkeys, cats and pigs, and to a lesser extent in canine, bovine, and rodent cells. Although gammaherpesviruses show narrow species tropism *in-vivo* [327], they are able to produce non-permissive (or latent) infection in many cell lines apart from those of their primary host [328–330]. Our results indicate that *Ef*HV could productively infect cultured cells of mammalian species like human, monkey, feline and porcine, consistent with what had been previously described for bat gammaherpesviruses [143,302,303]. As the ability of a virus to grow in a cell line derived from an animal does not necessarily confirm its tropism for that species, further studies would be needed to understand the *in-vivo* susceptibility of these animals to *Ef*HV.

We detected *Ef*HV in the blood of over 70% of bats tested (20/28). However, our study involved populations of captured bats kept in two hibernating chambers, so we cannot rule out the possibility of transmission during hibernation. Further field studies would provide us with more robust evidence of *Ef*HV prevalence in big brown bat populations. Despite detecting *Ef*HV DNA in the blood of most big brown bats, we failed to observe any neutralizing antibodies against *Ef*HV in bat plasma. In the absence of a neutralizing plasma as a positive control, it is difficult to state with certainty the sensitivity of the assay. Nonetheless, this would serve as a preliminary data regarding antibodies against *Ef*HV in big brown bats. Waning IgG antibody in bats has also been noted in other viral infections like Nipah [38,41,46], Hendra [46], Japanese Encephalitis [331], and Marburg [332] suggesting transient antibody responses to viruses in several species of bats.

Our report provides the first complete sequence of a bat gammaherpesvirus, *Ef*HV, that appears to belong to the genus *Rhadinovirus* in *Gammaherpesvirinae.* It is unique among gammaherpesviruses in transducing MHC II genes.

7.9. Supplementary Information

Supplementary table S7.1. Accession numbers for the DNA polymerase (dpol) and glycoprotein B (gB) sequences from γHVs used in this study (based on Escalera et al. 2016 [303])

DPOL				gB		
Name	Accession number	Abbreviation	Common host name	Name	Accession number	Abbreviation
Alcelaphine herpesvirus 1	NC_002531.1	ALC_HV1	Wildebeest	Alcelaphine herpesvirus 1	NC_002531.1	ALC_HV1
Apodemus sylvaticus rhadinovirus 1	EF128051.2	APSY_RHV1	Wood mouse	Apodemus sylvaticus rhadinovirus 1	EF128051.2	APSY_RHV1
Ateline herpesvirus 3	NC_001987.1	ATE_HV3	Woolly monkey	Ateline herpesvirus 3	AF083424.1	ATE_HV3
Babyrousa babyrussa rhadinovirus 1	AY177146.2	BABA_RHV1	Golden babirusa hog	Babyrousa babyrussa rhadinovirus 1	AY177146.2	BABA_RHV1
Bandicota indica rhadinovirus 4	EF128043.1	BAIN_RHV4	Greater bandicoot rat	Bandicota indica rhadinovirus 4	EF128043.1	BAIN_RHV4
Bandicota savilei rhadinovirus 1	DQ821581.1	BASA_RHV1	Savile's bandicoot rat	Bandicota savilei rhadinovirus 1	DQ821581.1	BASA_RHV1
Bovine herpesvirus 4	AF318573.1	BOS_HV4	Cattle	Bovine herpesvirus 4	AF318573.1	BOS_HV4
Bovine herpesvirus 6	NC_024303.1	BOS_HV6	Cattle	Bovine herpesvirus 6	KJ705001.1	BOS_HV6
Bovine lymphotropic herpesvirus	AF327830.1	BOS_LHV	Cattle	Bovine lymphotropic herpesvirus	AF327832.1	BOS_LHV
Callitrichine herpesvirus 3	AF319782.2	CAL_HV3	Marmoset	Callitrichine herpesvirus 3	AF319782.2	CAL_HV3
Caprine herpesvirus 2	HQ116812.1	CAP_HV2	Goat	Caprine herpesvirus 2	AF283477.2	CAP_HV2
Crocuta crocuta gammaherpesvirus 1	DQ789371.2	CRO_GHV1	Spotted hyena	Crocuta crocuta gammaherpesvirus 1	DQ789371.2	CRO_GHV1
Cynopterus sphinx CS/12GZ1	KR261850	CYSP_M102	Greater short-nosed fruit bat	*Cynopterus sphinx 13HN70*	KR261906	CYSP_70
Cynopterus sphinx CS/14GZ24	KR261898	CYSP_M24	Greater short-nosed fruit bat			
Diceros bicornis gammaherpesvirus 1	AY197560.2	DIBI_GHV	Black rhinoceros	Diceros bicornis gammaherpesvirus	AY197560.2	DIEC_SD12
Elephas maximus gammaherpesvirus 1	EU085379.1	ELMA_GHV1	Asian elephant	Elephas maximus gammaherpesvirus 1	EU085379.1	ELMA_GHV1
Eptesicus fuscus herpesvirus	MF385016	EFHV	Big Brown bat	*Eptesicus fuscus herpesvirus*	MF385016	EFHV
Eptesicus serotinus rhadinovirus 1	DQ788623.2	EPSE_RHV1	Serotine bat	*Eptesicus serotinus rhadinovirus 1*	DQ788623.2	EPSE_RHV1
Equid herpesvirus 2	U20824.2	EQ_HV2	Horse	Equid herpesvirus 2	U20824.2	EQ_HV2
Equid herpesvirus 5	KM924295.1	EQ_HV5	Horse	Equid herpesvirus 5	KM924295.1	EQ_HV5
Equus zebra gammaherpesvirus 1	AY495965.2	EQZ_GHV1	Zebra	Equus zebra gammaherpesvirus 1	AY495965.2	EQZ_GHV1
Felis catus gammaherpesvirus 1	NC_028099.1	FECA_GHV1	Cat	Felis catus gammaherpesvirus 1	NC_028099.1	FECA_GHV1
Gorilla gorilla lymphocryptovirus 1	AF534225.3	GOGO_LCV	Gorilla	Gorilla gorilla lymphocryptovirus 1	AF534225.3	GOGO_LCV
Gorilla rhadinovirus 1	AY177144.2	GOGO_RHV1	Gorilla	Gorilla rhadinovirus 1	AY177144.2	GOGO_RHV1
Hexaprotodon liberiensis gammaherpesvirus 1	AY197559.2	HELI_GHV1	Pygmy hippopotamus	Hexaprotodon liberiensis gammaherpesvirus 1	AY197559.2	HELI_GHV1
Hipposideros diadema herpesvirus	AB490083.2	HIDI_HV	Diadem leaf-nosed bat	*Hipposideros diadema herpesvirus*	AB490083.2	HIDI_HV
Hipposideros larvatus HL/11HN1	KR261841	HL_HN1	Intermediate roundleaf bat			
Hipposideros pomona HP/11HN104	KR261843	HP_104	Pomona roundleaf bat	*Hipposideros pomona 211HN104*	KR261902	HP_104
Hipposideros pomona HP/11HN110	KR261845	HP_110	Pomona roundleaf bat			
Human herpesvirus 4	LN831023.1	HS_HV4	Human	Human herpesvirus 4	NC_007605.1	HS_HV4
Human herpesvirus 8	AF005477.2	HS_HV8	Human	Human herpesvirus 8	AF092928.1	HS_HV8
Lynx rufus gammaherpesvirus 1	KF840716.1	LYRU_GHV1	Bobcat	Lynx rufus gammaherpesvirus 1	KF840716.1	LYRU_GHV1
Macaca fascicularis lymphocryptovirus 1	AF534221.2	MAFA_LCV	Crab-eating macaque	Macaca fascicularis lymphocryptovirus 1	AF534221.2	MAFA_LCV
Macaca fascicularis rhadinovirus 2	EU085377.1	MAFA_RHV2	Crab-eating macaque	Macaca fascicularis rhadinovirus 2	EU085377.1	MAFA_RHV2
Macaca fuscata rhadinovirus	AY528864.1	MAFU_RHV	Japanese macaque	Macaca fuscata rhadinovirus	AY528864.1	MAFU_RHV
Miniopterus schreibersii MS/11HN95	KR261846	MSC_95	Common bent-wing bat	*Miniopterus schreibersii 11HN110*	KR261903	MSC_110
Miniopterus schreibersii MS/12HN28	KR261851	MSC_28	Common bent-wing bat	*Miniopterus schreibersii 211HN16*	KR261901	MSC_16
Murid herpesvirus 4	NC_001826.2	MUR_HV4	Mouse	Murid herpesvirus 4	NC_001826.2	MUR_HV4
Mus cervicolor rhadinovirus 1	DQ821582.1	MUCE_RHV1	Fawn-colored mouse	Mus cervicolor rhadinovirus 1	DQ821582.1	MUCE_RHV1
Mus musculus rhadinovirus 1	AY854167.1	MUMUS_RHV1	House mouse	Mus musculus rhadinovirus 1	AY854167.1	MUMUS_RHV1
Mustelid herpesvirus 1	AF376034.1	MUST_HV1	Ferret	Mustelid herpesvirus 1	AF376034.1	MUST_HV1
Myodes glareolus rhadinovirus 1	AY854169.2	MYGLA_RHV1	Bank vole	Myodes glareolus rhadinovirus 1	AY854169.2	MYGLA_RHV1
Myotis nattereri rhadinovirus 1	DQ788625.1	MYNA_RHV1	Natterer's bat			
Myotis ricketti herpesvirus 1	JN692429.1	MYRI_HV1	Rickett's big-footed bat	*Myotis ricketti herpesvirus 1*	JN692429.1	MYRI_HV1
Myotis ricketti herpesvirus 2	JN692430.1	MYRI_HV2	Rickett's big-footed bat	*Myotis ricketti herpesvirus 2*	JN692430.1	MYRI_HV2
Myotis velifer gammaherpesvirus 8	KU220026.1	MYVE_HV8	Cave myotis	*Myotis velifer gammaherpesvirus 8*	KU220026.1	MYVE_HV8
Nyctalus noctula rhadinovirus 1	DQ788626.1	NYNOC_RHV1	Common noctule bat			
Nyctalus noctula rhadinovirus 2	DQ788627.2	NYNOC_RHV2	Common noctule bat	*Nyctalus noctula rhadinovirus 2*	DQ788627.2	NYNOC_RHV2
Ovine herpesvirus 2	NC_007646.1	OVI_HV2	Sheep	Ovine herpesvirus 2	NC_007646.1	OVI_HV2
Pan troglodytes rhadinovirus 2	EU118145.1	PATR_RHV2	Common chimpanzee	Pan troglodytes rhadinovirus 2	EU085378.1	PATR_RHV2
Pan troglodytes rhadinovirus 3	GQ995451.1	PATR_RHV3	Common chimpanzee	Pan troglodytes rhadinovirus 3	GQ995451.1	PATR_RHV3
Panthera leo gammaherpesvirus 1	DQ789370.2	PALEO_GHV1	Lion	Panthera leo gammaherpesvirus 1	DQ789370.2	PALEO_GHV1
Papio hamadryas lymphocryptovirus 2	AF534229.3	PAHAM_LCV2	Hamadryas baboon	Papio hamadryas lymphocryptovirus 2	AF534229.3	PAHAM_LCV2
Pipistrellus nathusii rhadinovirus 1	DQ788629.2	PIPNA_RHV1	Nathusius's pipistrelle bat	*Pipistrellus nathusii rhadinovirus 1*	DQ788629.2	PIPNA_RHV1
Pipistrellus pipistrellus rhadinovirus 1	DQ788630.1	PIPI_RHV1	Common pipistrelle bat			

Supplementary table S7.1. Contd.

Plecotus auritus rhadinovirus 1	DQ788628.1	PLAUR_RHV1	Brown long-eared bat			
				Porcine lymphotropic herpesvirus 1	AF478169.1	SUS_LTV1
Porcine lymphotropic herpesvirus 2	AF191043.1	SUS_LTV2	Pig	Porcine lymphotropic herpesvirus 2	AY170317.1	SUS_LTV2
Porcine lymphotropic herpesvirus 3	AY170316.1	SUS_LTV3	Pig	Porcine lymphotropic herpesvirus 3	AY170316.1	SUS_LTV3
Procavia capensis gammaherpesvirus 2	JF705865.1	PROCA_GHV2	Rock hyrax	Procavia capensis gammaherpesvirus 2	JF705865.1	PROCA_GHV2
Ptenochirus jagori gammaherpesvirus	LC008326.1	PTEJA_GHV	Greater musky fruit bat			
Pteropus giganteus herpesvirus 1	KC692446.1	PTGIG_HV1	Indian flying fox			
Pteropus giganteus herpesvirus 2	KC692449.1	PTGIG_HV2	Indian flying fox			
Pteropus giganteus herpesvirus 3	KC692450.1	PTGIG_HV3	Indian flying fox			
Pteropus giganteus herpesvirus 5	KC692447.1	PTGIG_HV5	Indian flying fox			
Pteropus giganteus herpesvirus 6	KC692448.1	PTGIG_HV6	Indian flying fox			
Puma concolor gammaherpesvirus 1	KF840717.1	PUCON_GHV1	Cougar	Puma concolor gammaherpesvirus 1	KF840717.1	PUCON_GHV1
Rhinolophus blythi RB/13YF11	KR261856	RHIBLY_F11	Blyth's horsehoe bat	*Rhinolophus blythi 13HN56*	KR261905	RHIBLY_56
Rhinolophus blythi RB/13YF3	KR261882	RHIBLY_YF3	Blyth's horsehoe bat	*Rhinolophus blythi 13YF104*	KR261913	RHIBLY_104
Rhinolophus blythi RB/13YF6	KR261883	RHIBLY_YF6	Blyth's horsehoe bat	*Rhinolophus blythi 13YF79*	KR261908	RHIBLY_79
Rhinolophus blythi RB/13YF84	KR261887	RHIBLY_F84	Blyth's horsehoe bat	*Rhinolophus blythi 13YF82*	KR261910	RHIBLY_F82
Rhinolophus blythi RB/13YF87	KR261889	RHIBLY_F87	Blyth's horsehoe bat	*Rhinolophus blythi 13YF84*	KR261909	RHIBLY_F84
Rhinolophus blythi RB/13YF89	KR261891	RHIBLY_F89	Blyth's horsehoe bat	*Rhinolophus blythi 13YF87*	KR261911	RHIBLY_F87
Rhinolophus blythi RB/13YF96	KR261893	RHIBLY_F96	Blyth's horsehoe bat	*Rhinolophus blythi 13YF96*	KR261912	RHIBLY_F96
Rhinolophus blythi RB/13YF99	KR261895	RHIBLY_F99	Blyth's horsehoe bat			
Rupicapra rupicapra gammaherpesvirus 1	DQ789369.2	RURUP_GHV1	Chamois	Rupicapra rupicapra gammaherpesvirus 1	DQ789369.2	RURUP_GHV1
Saimiri sciureus gammaherpesvirus 2	AY138584.2	SAMCI_GHV2	Common squirrel monkey	Saimiri sciureus gammaherpesvirus 2	AY138584.2	SAMCI_GHV2
Saimiriine herpesvirus 2	NC_001350.1	SAM_HV2	Common squirrel monkey	*Scotophilus kuhlii 11HZ76*	KR261904	SCKUH_76
Scotophilus kuhlii SK/11HZ84	KR261848	SCKUH_84	Lesser Asiatic yellow bat	*Scotophilus kuhlii 13Y234*	KR261920	SCKUH_234
Scotophilus kuhlii SK/13YF121	KR261858	SCKUH_M121	Lesser Asiatic yellow bat	*Scotophilus kuhlii 13YF106*	KR261914	SCKUH_106
Scotophilus kuhlii SK/13YF14	KR261863	SCKUH_14	Lesser Asiatic yellow bat	*Scotophilus kuhlii 13YF114*	KR261915	SCKUH_114
Scotophilus kuhlii SK/13YF146	KR261865	SCKUH_146	Lesser Asiatic yellow bat	*Scotophilus kuhlii 13YF15*	KR261907	SCKUH_15
Scotophilus kuhlii SK/13YF15	KR261866	SCKUH_15	Lesser Asiatic yellow bat	*Scotophilus kuhlii 13YF155*	KR261916	SCKUH_155
Scotophilus kuhlii SK/13YF16	KR261872	SCKUH_16	Lesser Asiatic yellow bat	*Scotophilus kuhlii 13YF160*	KR261917	SCKUH_160
Scotophilus kuhlii SK/13YF185	KR261876	SCKUH_M185	Lesser Asiatic yellow bat	*Scotophilus kuhlii 13YF187*	KR261918	SCKUH_187
Scotophilus kuhlii SK/13YF239	KR261880	SCKUH_239	Lesser Asiatic yellow bat	*Scotophilus kuhlii 13YF206*	KR261919	SCKUH_206
				Scotophilus kuhlii 13YF244	KR261921	SCKUH_244
Sorex araneus gammaherpesvirus 1	EU085380.1	SORA_GHV1	Common shrew	Sorex araneus gammaherpesvirus 1	EU085380.1	SORA_GHV1
Sus barbatus rhadinovirus 1	AY177147.2	SUSBA_RHV1	Bornean bearded pig	Sus barbatus rhadinovirus 1	AY177147.2	SUSBA_RHV1
Symphalangus syndactylus lymphocryptovirus	GQ921924.1	SYMSY_LCV2	Siamang gibbon	Symphalangus syndactylus lymphocryptovirus 2	GQ921924.1	SYMSY_LCV2
Tapirus terrestris gammaherpesvirus 1	AF141887.3	TATER_GHV1	South American tapir	Tapirus terrestris gammaherpesvirus 1	AF141887.3	TATER_GHV1
Tupaia belangeri gammaherpesvirus 1	AY197561.2	TUBEL_GHV1	Northern treeshrew	Tupaia belangeri gammaherpesvirus 1	AY197561.2	TUBEL_GHV1
Type 2 ruminant rhadinovirus of mule deer	HM014314.1	T2MDRHV	Mule deer	Type 2 ruminant rhadinovirus of mule deer	HM014314.1	T2MDRHV
Suid alphaherpesvirus 1	JQ809330.1	SUS_AHV1	Pig	Suid alphaherpesvirus 1	NC_006151.1	SUS_AHV1
Human herpes simplex virus type 1	M10792.1	HS_AHV1	Human	Human herpes simplex virus type 1	JN555585.1	HS_AHV1
Pteropus dasymallus alphaherpesvirus 1	NC_024306.1	PTEDA_AHV1	Ryukyu flying fox	*Pteropus dasymallus alphaherpesvirus 1*	AB825953.1	PTEDA_AHV1
Cynopterus sphinx betaherpesvirus CS/14GZ1	KR261896	CYSP_A13	Greater short-nosed fruit bat			
Cynopterus sphinx betaherpesvirus CS/14GZ9	*KR261900*	CYSP_A9	Greater short-nosed fruit bat			

(A)

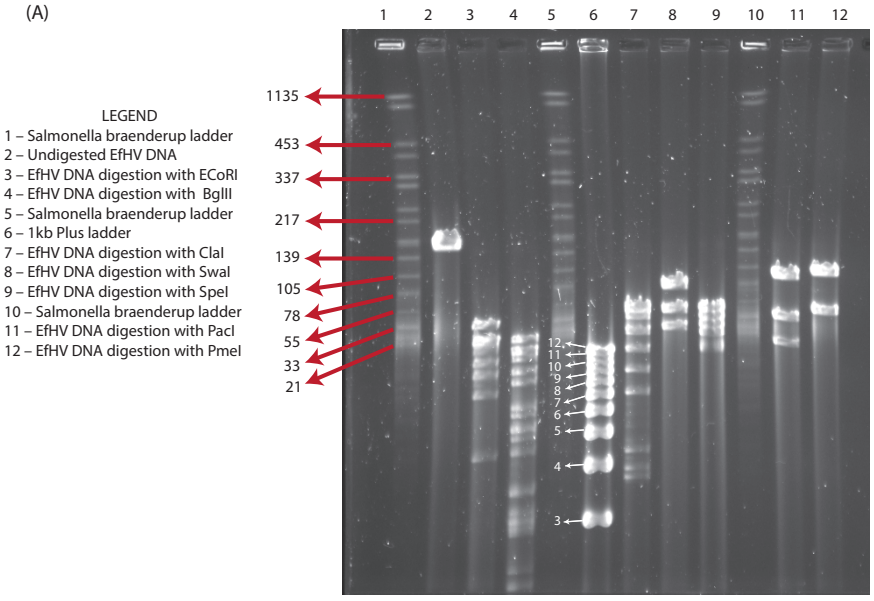

(B)

Digest with BglII:

Fragment Size	Left Overhang	Cut by Enzyme	Cut by From : To	Right Enzyme	Right Overhang
23286	[+ 4]	BglII	142752:166037	BglII	[+ 4]
14212	[+ 4]	BglII	95017:109228	BglII	[+ 4]
13478	[+ 4]	BglII	40966:54443	BglII	[+ 4]
13362	[+ 4]	BglII	59866:73227	BglII	[+ 4]
10777	[+ 4]	BglII	73228:84004	BglII	[+ 4]
9405	[+ 4]	BglII	110158:119562	BglII	[+ 4]
7017	[+ 4]	BglII	3774:10790	BglII	[+ 4]
6970	[+ 4]	BglII	33996:40965	BglII	[+ 4]
5928	[+ 4]	BglII	136211:142138	BglII	[+ 4]
5744	[+ 4]	BglII	84005:89748	BglII	[+ 4]
5268	[+ 4]	BglII	89749:95016	BglII	[+ 4]
4675	[+ 4]	BglII	15790:20464	BglII	[+ 4]
3788	[+ 4]	BglII	127419:131206	BglII	[+ 4]
3679	[+ 4]	BglII	10791:14469	BglII	[+ 4]
3374	[+ 4]	BglII	20465:23838	BglII	[+ 4]
3249	[+ 4]	BglII	26080:29328	BglII	[+ 4]
3200	[+ 4]	BglII	131207:134406	BglII	[+ 4]
3086	[+ 4]	BglII	122642:125727	BglII	[+ 4]
3079	[+ 4]	BglII	119563:122641	BglII	[+ 4]
3036	[+ 4]	BglII	54444:57479	BglII	[+ 4]
2559	[+ 4]	BglII	30025:32583	BglII	[+ 4]
2386	[+ 4]	BglII	57480:59865	BglII	[+ 4]
2241	[+ 4]	BglII	23839:26079	BglII	[+ 4]
1804	[+ 4]	BglII	134407:136210	BglII	[+ 4]
1691	[+ 4]	BglII	125728:127418	BglII	[+ 4]
1669	[+ 4]	BglII	2105:3773	BglII	[+ 4]
1412	[+ 4]	BglII	32584:33995	BglII	[+ 4]
1320	[+ 4]	BglII	14470:15789	BglII	[+ 4]
1003	[+ 4]	BglII	673:1675	BglII	[+ 4]
929	[+ 4]	BglII	109229:110157	BglII	[+ 4]
711	[+ 4]	BglII	166038:166748	3' end	
696	[+ 4]	BglII	29329:30024	BglII	[+ 4]
672	5' end		1:672	BglII	[+ 4]
613	[+ 4]	BglII	142139:142751	BglII	[+ 4]
429	[+ 4]	BglII	1676:2104	BglII	[+ 4]

Digest with ClaI:

Fragment Size	Left Overhang	Cut by Enzyme	Cut by From : To	Right Enzyme	Right Overhang
50870	[+ 2]	ClaI	3354:54223	ClaI	[+ 2]
43429	[+ 2]	ClaI	123320:166748	3' end	
22748	[+ 2]	ClaI	95847:118594	ClaI	[+ 2]
14045	[+ 2]	ClaI	64358:78402	ClaI	[+ 2]
9677	[+ 2]	ClaI	86170:95846	ClaI	[+ 2]
7767	[+ 2]	ClaI	78403:86169	ClaI	[+ 2]
4725	[+ 2]	ClaI	118595:123319	ClaI	[+ 2]
4211	[+ 2]	ClaI	60147:64357	ClaI	[+ 2]
4000	[+ 2]	ClaI	56147:60146	ClaI	[+ 2]
3353	5' end		1:3353	ClaI	[+ 2]
1923	[+ 2]	ClaI	54224:56146	ClaI	[+ 2]

Digest with EcoRI:

Fragment Size	Left Overhang	Cut by Enzyme	Cut by From : To	Right Enzyme	Right Overhang
39569	[+ 4]	EcoRI	84177:123745	EcoRI	[+ 4]
23619	[+ 4]	EcoRI	123746:147364	EcoRI	[+ 4]
20518	[+ 4]	EcoRI	63659:84176	EcoRI	[+ 4]
20441	[+ 4]	EcoRI	41308:61748	EcoRI	[+ 4]
14908	5' end		1:14908	EcoRI	[+ 4]
13229	[+ 4]	EcoRI	23154:36382	EcoRI	[+ 4]
10371	[+ 4]	EcoRI	147365:157735	EcoRI	[+ 4]
9013	[+ 4]	EcoRI	157736:166748	3' end	
8245	[+ 4]	EcoRI	14909:23153	EcoRI	[+ 4]
4925	[+ 4]	EcoRI	36383:41307	EcoRI	[+ 4]
1230	[+ 4]	EcoRI	61749:62978	EcoRI	[+ 4]
680	[+ 4]	EcoRI	62979:63658	EcoRI	[+ 4]

Digest with PacI:

Fragment Size	Left Overhang	Cut by Enzyme	Cut by From : To	Right Enzyme	Right Overhang
102984	5' end		1:102984	PacI	[- 2]
45999	[- 2]	PacI	120750:166748	3' end	
17765	[- 2]	PacI	102985:120749	PacI	[- 2]

Digest with PmeI:

Fragment Size	Left Overhang	Cut by Enzyme	Cut by From : To	Right Enzyme	Right Overhang
111343	5' end		1:111343	PmeI	[+ 0]
55405	[+ 0]	PmeI	111344:166748	3' end	

Digest with SpeI:

Fragment Size	Left Overhang	Cut by Enzyme	Cut by From : To	Right Enzyme	Right Overhang
54074	[+ 4]	SpeI	89378:143451	SpeI	[+ 4]
44211	[+ 4]	SpeI	45167:89377	SpeI	[+ 4]
30916	[+ 4]	SpeI	13512:44427	SpeI	[+ 4]
23297	[+ 4]	SpeI	143452:166748	3' end	
13511	5' end		1:13511	SpeI	[+ 4]
739	[+ 4]	SpeI	44428:45166	SpeI	[+ 4]

Digest with SwaI:

Fragment Size	Left Overhang	Cut by Enzyme	Cut by From : To	Right Enzyme	Right Overhang
86381	[+ 0]	SwaI	80368:166748	3' end	
50171	5' end		1:50171	SwaI	[+ 0]
30196	[+ 0]	SwaI	50172:80367	SwaI	[+ 0]

Supplementary figure S7.2. Restriction digestion analysis of *Ef*HV genomic DNA. (A) *Ef*HV DNA was digested using 7 restriction enzymes and ran on a Pulsed-field gel electrophoresis. (B) The bands obtained were matched with that of the predicted sizes based on complete *Ef*HV genome

obtained from mi-seq and nanopore sequencing. Two DNA ladders were used namely *Salmonella* Braenderup and 1kb plus DNA ladder.

Supplementary Figure S7.3. Expression of MHC-I and MHC-II antigen in bat cells. Agarose gel images showing bands obtained by real-time PCR. The contents of the lanes are mentioned above the gel images in orange boxes and the gene targeted is mentioned at the bottom. For every target, a 1kb DNA ladder, an *Ef*HV genomic DNA (positive control), an *Ef*HV infected bat cell cDNA without reverse transcriptase (genomic DNA contamination control), an *Ef*HV infected bat cell cDNA with reverse transcriptase, a bat cell cDNA and a no template control was used for PCR. All targets showed amplification in the *Ef*HV genomic DNA and *Ef*HV infected bat cell cDNA with reverse transcriptase (A-G). For GAPDH, the *Ef*HV infected bat cell cDNA and bat

cell cDNA showed a band but *Ef*HV genomic also showed a faint band (mostly due to residual bat cellular DNA in the viral DNA).

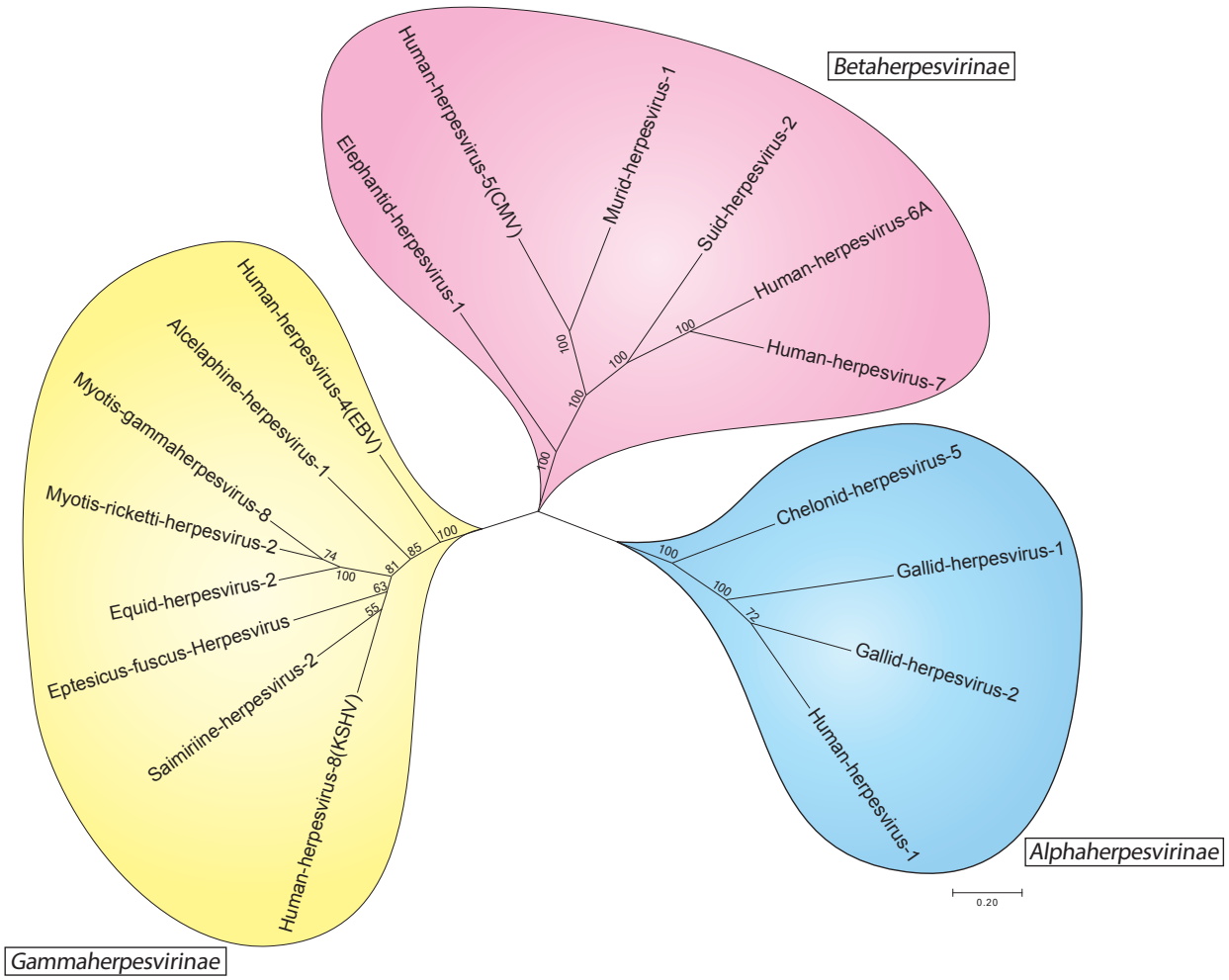

Supplementary figure S7.4. Alignment of entire amino acid sequences of DNA polymerase gene of representative alpha-, beta- and gammaherpesviruses. Phylogenetic tree was generated using Maximum likelihood method (JTT substitution model). Numbers at nodes indicate bootstrap values.

7.10. Transition statement

In this chapter, I described the first isolation and detailed characterization of a big brown bat gammaherpesvirus. Our studies allowed us to develop techniques for detecting the virus as well as for monitoring the adaptive antibody response against the virus. Since all herpesviruses

studied till date establish life-long latent infections and reactivate periodically from this quiescent state in response to a variety of stressors, we could use the tools we developed to test the hypothesis that most big brown bats are latently-infected with the gammaherpesvirus and that natural stressors, such as arousal from winter hibernation would lead to reactivation of the virus.

Chapter 8: Stress of arousal from hibernation reactivates gammaherpesvirus in big brown bats

8.1. Copyright

© 2019. John Wiley and Sons grants the authors permission to reuse the full article in dissertation/thesis in both print and electronic format.

This manuscript has been reformatted from the original version for inclusion in this thesis.

8.2. Citation

Gerow, C. M., N. Rapin, M. J. Voordouw, M. Elliot, V. Misra, and **S. Subudhi**. "Arousal from Hibernation and Reactivation of *Eptesicus Fuscus* gammaherpesvirus (*Ef*HV) in Big Brown Bats." *Transboundary and Emerging Diseases*, December 16, 2018. https://doi.org/10.1111/tbed.13102.

8.3. Contribution

CMG and VM and I were involved in the capture and sampling of the bats, development of ELISA, and PCR. I designed PCR primers, performed ELISA analysis and made the graphs. Hibernating bats were obtained from ME. MJV performed the statistical modelling. NR helped with DNA extraction and PCR. I supervised CMG while performing assays and was also the corresponding author for this manuscript. All authors were involved in editing the published version of the manuscript.

8.4. Abstract

Many viruses that cause serious and often fatal disease in humans have spilled over from bats. Recent evidence suggests that stress may enhance virus shedding by bats increasing the possibility of transmission to other species. To understand the reasons for spillover it is therefore important to determine the molecular pathways that link stress to virus reactivation and shedding in bats. We recently isolated and characterized a gammaherpesvirus (*Eptesicus fuscus* herpesvirus, *Ef*HV) autochthonous to North American big brown bats. Since herpesviruses are known to reactivate from latent infections in response to a wide variety of stressors, *Ef*HV presents us with an opportunity to study how physiological, behavioural or environmental changes may influence the big brown bats' relationship with *Ef*HV. To understand the biology of the virus and how the extended periods of torpor experienced by these bats during hibernation along with the stress of arousal might influence the virus-host relationship, we attempted to detect the virus in the blood of wild-caught non-hibernating bats as well as captive bats arising from hibernation. We compared the prevalence of *Ef*HV in the blood (using PCR) and *Ef*HV-specific antibodies (using ELISA) between captive hibernating bats and wild-caught non-hibernating bats. We detected *Ef*HV only in the blood of captive hibernating bats (27.8% = 10/36) and not in wild-caught non-hibernating bats (0.0% = 0/43). In contrast, the *Ef*HV-specific antibody titres were higher in the non-hibernating bats compared to the hibernating bats. Our study suggests that: (1) viral DNA in blood indicates reactivation from latency, (2) long periods of hibernation lead to suppression of immunity, (3) stress of arousal from hibernation reactivates the virus in bats with lower levels of antiviral immunity (indicated by humoral immune response), and (4) levels of antiviral immunity increase in non-hibernating bats following reactivation.

8.5. Introduction

Bats harbour many viruses and some of them have been implicated in epidemics like Nipah, Hendra and SARS (Severe Acute Respiratory Syndrome) [12]. Bat-borne viruses can either directly infect humans or spillover to humans via an intermediate host. There are over a thousand different bat species and they are the second most diverse group of mammals on the planet [14]. Unlike other mammalian species, bats do not appear to suffer from overt disease due to the viral infections (with the exception of rabies virus and Tacaribe virus) [16,37]. Bats are the only flying mammals and their tolerant immune system may have co-evolved with flight [21]. Flight elevates the body temperature and metabolism of bats, which might provide a selective advantage for controlling virus replication [20]. A recent large scale analysis found that the zoonotic potential of bats has surpassed that of rodents [333] and that bats harbour significantly more potentially zoonotic viruses than all other mammalian orders [334]. Studying bats and their viruses is therefore important for public health and safety around the world.

The causes of viral spillover are complex and rely to a large extent on interactions between the reservoir host and their viruses. Disruption of balanced host-virus relationships due to stressors, such as habitat loss or secondary infections, may increase virus shedding, and enhance the likelihood of spillovers [12,62,335]. Much is known about viruses in spillover hosts or in surrogate laboratory animals. However, there is little information on the relationship of viruses within their natural bat reservoir hosts. The purpose of the present study is to better understand the interaction between the North American big brown bat, *Eptesicus fuscus*, and its autochthonous gammaherpesvirus (*Ef*HV).

Gammaherpesviruses belong to the herpesvirus family, members of which have been detected in numerous vertebrate hosts, including humans [327]. The lifecycle of

gammaherpesviruses starts with a lytic infection of epithelial cells (primary infection) followed by a life-long latent infection in lymphoid cells (B cells) present in lungs and spleen [336,337]. The virus can reactivate from latency in response to a variety of stressors [338,339], leading to its detection in the blood by using relatively non-invasive procedures. This approach allows the study of virus-host cell dynamics without sacrificing the animal. Furthermore, we are able to examine the effects of stress-related changes in the virus-host relationships leading to increased virus shedding. This makes the "*Ef*HV – big brown bat" system an ideal model for our research.

Arousal from hibernation is a stressful event for bats [55]. In a previous study, we detected *Ef*HV in the blood cells of 80% of *E. fuscus* arousing from hibernation [56]. We therefore hypothesized that hibernation is a contributing factor to the reactivation of *Ef*HV within the big brown bat. To study the effects of hibernation on the bat-virus relationship, we compared the prevalence of *Ef*HV DNA and antibody titres against *Ef*HV between captive bats emerging from hibernation and wild-caught non-hibernating bats. Our results suggest that *Ef*HV is latent in a large proportion of the big brown bat population and that hibernation reduces immunity to *Ef*HV, contributing to its reactivation.

8.6. Materials and methods

8.6.1. Bat collection

From May to August 2018, hibernating and non-hibernating bats were collected in and around Saskatoon, Saskatchewan, Canada. The hibernating bats had originally been rescued from a house on Tobin Crescent, Saskatoon (Figure 8.2. (A)) by a rehabilitation Centre. These bats were allowed to overwinter at the rehabilitation Centre. In the beginning of May 2018, the bats were

transferred to the animal facility in the WCVM where they were sampled and subsequently released.

To find areas with foraging non-hibernating bats, an echo locator device was placed in areas in and around Saskatoon. Some of the other areas were chosen based on anecdotal evidence of bat captures from previous studies. Two mist nets for trapping bats, (10 – 12 m wide, 6 m high), were set in the evenings just before sunset. The mist nets were attached to two poles with shower curtain rings. The poles were secured using rebar stakes hammered into the ground. Captured bats were removed from the mist net, placed into a small cotton bag and put inside a plastic container. Bats were removed from the mist net as soon as possible to prevent excessive entanglement and damage to the bat or the net. We clipped the hair from the dorsal aspect of bats to facilitate identification so that resampling was avoided. The non-hibernating bats were released after sampling and the hibernating bats were returned to the care of the rehabilitator for subsequent release into the wild.

8.6.2. Sample Collection

For both hibernating and non-hibernating bats, leather and latex gloves were worn during handling of the bats, which were changed between bat sampling to prevent cross contamination. The weight of each bat was obtained using a 100 g scale and the radius/ulna length was measured using a 30 cm standard ruler.

Blood was collected by puncturing the saphenous vein of the left leg with a 27G x ½" monoject standard hypodermic needle and the blood droplet formed was collected into a heparinized capillary tube. Plasma and blood cells were separated using a fixed speed centrifuge (6,900xG) for 1 min. The capillary tube was cut at the junction of the plasma and blood cells and the two halves were stored separately at -20°C in Eppendorf tubes.

8.6.3. DNA extraction

Bat blood cells were removed from the cut capillary tube by centrifugation at 1500xG for 1.5 minutes. The blood cells were resuspended in 195 µL of sterile PBS and DNA was extracted using the Qiagen DNeasy Blood & Tissue Kit (Cat #69506) as per manufacturer's instructions. The final elution step was done using 100 µL of Buffer AE. The DNA concentration was determined using a Nanodrop 2000c (spectrophotometer).

8.6.4. Polymerase Chain Reaction

To detect *Ef*HV DNA in big brown bat blood cells, we amplified a 238 bp segment of the *BGLF4* gene (Protein kinase C-like superfamily) using 5' – CAG CGT GAG CAG CCT ATG TA – 3' (Forward) and 5' - TAG AAT CCC GCA AGC GAC TC – 3' (Reverse) primers. Qiagen TopTaq DNA polymerase (Cat #200203) was used to set up the PCR reaction as described by the manufacturer. Denaturation, annealing and extension cycles for the PCR reaction were 94°C for 30 secs, 60°C for 30 secs and 72°C for 1 min (40 cycles). An initial denaturation at 94°C for 3 mins and a final extension at 72°C for 10 mins were also included. To test each bat, 5 µL of blood cell DNA was used as a template. *Ef*HV genomic DNA was used as a positive control. PCR products were analysed on a 1% agarose gel. DNA from 238 bp bands was purified (QIAquick gel extraction kit; Cat #28704) and sent for Sanger sequencing (Macrogen, Rep. of Korea). BLAST search was performed using the sequencing file and we considered the first and closest match to the PCR product as the true sequence.

8.6.5. IgG capture Enzyme-Linked Immunosorbent Assay (ELISA) against *Ef*HV capsid protein

We used an ELISA to detect antibodies against *Ef*HV in the blood of the bats. Purified, glutathione-S-transferase (GST)-tagged *Ef*HV Capsid protein (GST-BFRF3) expressed in *E. coli*

BL21 cells was used as a positive antigen to capture antibodies. GST (without any protein attached) also expressed in BL21 cells was used as a negative antigen to determine non-specific antibody binding against GST. The difference in optical density (OD) between the capsid-GST and GST alone represent the levels of *Ef*HV antibodies for each plasma sample. The wells of ultra-high binding polystyrene flat-bottomed microtiter plates (96 well, Thermoscientific, Cat #3855) were coated with 0.05 µg of either antigen (GST-BFRF3 or GST) diluted in 0.1 M phosphate-buffered saline (pH 7.4) in a total volume of 100 µL. The coated plates were incubated overnight at 4°C and washed three times with 300 µL of PBS-Tween20 (0.1%) immediately prior to use. In a non-binding 96-well plate (Greiner Bio-One, Cat #655901), serum samples were diluted 1:200 in PBS-Tween 20 (0.2%) supplemented with 5% foetal bovine serum (Gibco, Thermofisher, Cat #16210-072). Serum from rabbits immunized with GST-BFRF3 was used as a positive serum control.

For each bat, 100 µL of diluted serum was added simultaneously to wells coated with either positive (GST-BFRF3) or negative (GST) antigen. Plates were incubated at 37°C for one hour then washed three times with 300 µL of PBS-Tween (0.1%). A peroxidase-labelled goat anti-bat IgG secondary antibody (0.05 µg in 100 µL per well, Bethyl labs, Cat #A140-118P) was added, incubated for one hour at 37°C and washed as above. Peroxidase substrate (2,2'-azino-bis (3-ethylbenzthiazoline-6-sulfonic acid) – TMB One component HRP microwell substrate, Bethyl labs, Cat #E102) was added to each well and colour was allowed to develop for 15 min. The colour reaction was stopped by adding 100 µl of 0.18M H_2SO_4. Optical density was measured at 450 nm using an ELISA microplate reader (Vmax, Molecular devices).

For each bat, we calculated the corrected OD value by subtracting the OD for the negative antigen from the OD for the positive antigen: $OD_{corrected} = OD_{positive} - OD_{negative}$. To determine the cut-off value for ELISA, we performed change-point analysis on the whole set of $OD_{corrected}$ values,

as this analysis does not need known positive or negative samples. Change-point analysis detects abrupt steps in the mean level of a series so that seropositive and seronegative $OD_{corrected}$ values would be separated by a step in the series. This approach is an efficient alternative to the usual cut-off formula of the form "mean + 3 standard deviations of the known negative controls" [340]. We used the R package "changepoint" [341] and selected the Pruned Exact Linear Time (PELT) algorithm to detect change-points [342,343].

8.6.6. Statistical Analysis and graphs

P values < 0.05 were considered statistically significant. We used R studio version 1.1.453 to analyze the data. Graphs were made using Graphpad prism 7.

A Student's two samples *t*-test was used to compare the mean *Ef*HV antibody titres between bats with positive versus negative *Ef*HV PCR status for the subsample of hibernating bats. A two samples proportion test was used to compare the percentage of seropositive bats between hibernating and non-hibernating bats. A one-way analysis of variance (ANOVA) was used to compare the *Ef*HV antibody titres between locations. The two samples *t*-test, two samples proportion test, and one-way ANOVA were run using the t.test(), prop.test(), and lm() functions, respectively, which are in the base package of R.

We used linear mixed models (LMMs) with normal errors to model body weight (g). The fixed effects were radius length (mm), sex (2 levels: female, male), and hibernation state (2 levels: hibernating, non-hibernating). Location (6 levels: Buckwold Park, Diefenbaker Park, Meewasin Park, Vikram's Acreage, Tobin Crescent and Wilson Park) was modeled as a random effect. We used generalized linear mixed models (GLMMs) with binomial errors to model bat infection status (negative, positive). The fixed effects were hibernation state, sex, radius length (mm), body weight (g), and antibody titre (OD). Location was modeled as a random effect. We used LMMs with

normal errors to model bat antibody titres. The fixed effects were hibernation state, sex, radius length (mm), body weight (g), and bat infection status (negative, positive). Location was modeled as a random effect. The data were analyzed for a subset of 79 bats because 3 bats did not have antibody titres.

8.7. Results

We obtained samples from 36 hibernating bats that were kept at a local rehabilitation center over the winter. We also sampled 43 non-hibernating bats captured at various locations around Saskatoon, Saskatchewan, Canada (Figure 8.2(A)).

8.7.1. Relationships between body weight, radius length, and sex

We used linear mixed models with normal errors to investigate the relationship between body weight and three fixed effects: radius length, sex, and hibernation status. We found a positive relationship between radius length and body weight (Figure 8.1; slope = 0.45 g/mm, S.E. = 0.120 g/mm, $t = 3.715$, $p < 0.001$). Males were 2.6 grams lighter than females, and this difference was significant (Figure 8.1; supplementary figure S8.1. (A); contrast male – female = -2.63, S.E. = 0.464, $t = -5.665$, $p < 0.001$). Non-hibernating bats had a higher body weight than hibernating bats, but this difference was not significant (contrast non-hibernating – hibernating = 1.03, S.E. = 0.681, $t = 1.517$, $p = 0.283$).

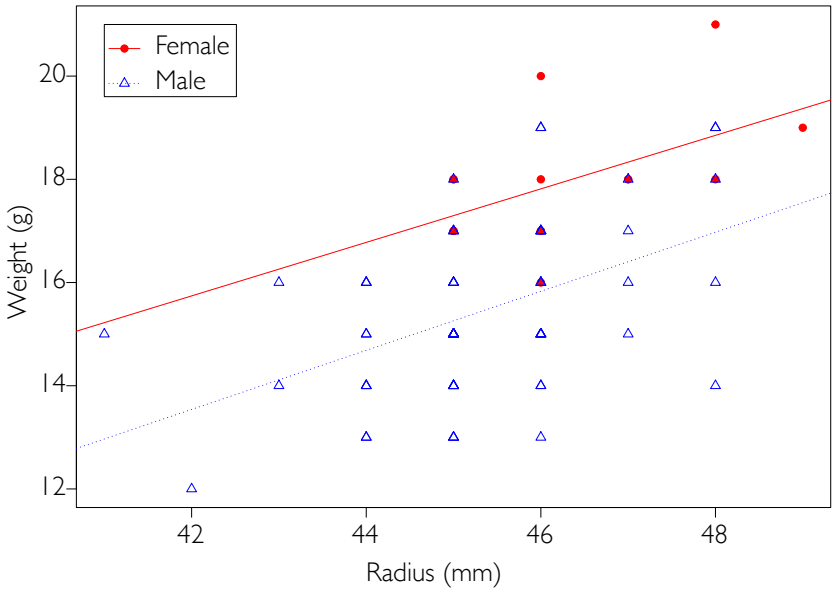

Figure 8.1. Relationship between body weight (grams) and radius length (mm) is shown for female and male bats. Bats with longer radius have a larger body weight and females are larger than males. Lines of best fit are shown for females (solid red) and males (stippled blue).

8.7.2. Hibernating big brown bats have detectable *Ef*HV DNA

To estimate the prevalence of *Ef*HV in big brown bats, we used PCR to amplify the herpesvirus *BGLF4* gene in DNA extracted from bat blood cells. We detected *Ef*HV DNA in 27.8% (10/36) of captive bats emerging from hibernation (6 positive males and 4 positive females), but in none of the non-hibernating bats (0/43) caught in the wild. The numbers of bats sampled at various locations are shown in Figure 8.2. (A). Infection with *Ef*HV was verified by sequencing; all the PCR products matched 100% with the *Ef*HV sequence (Accession number MF385016). To rule out the possibility that the non-hibernating bats were naïve to *Ef*HV, we screened all bats for the presence of antibodies against the *Ef*HV capsid protein.

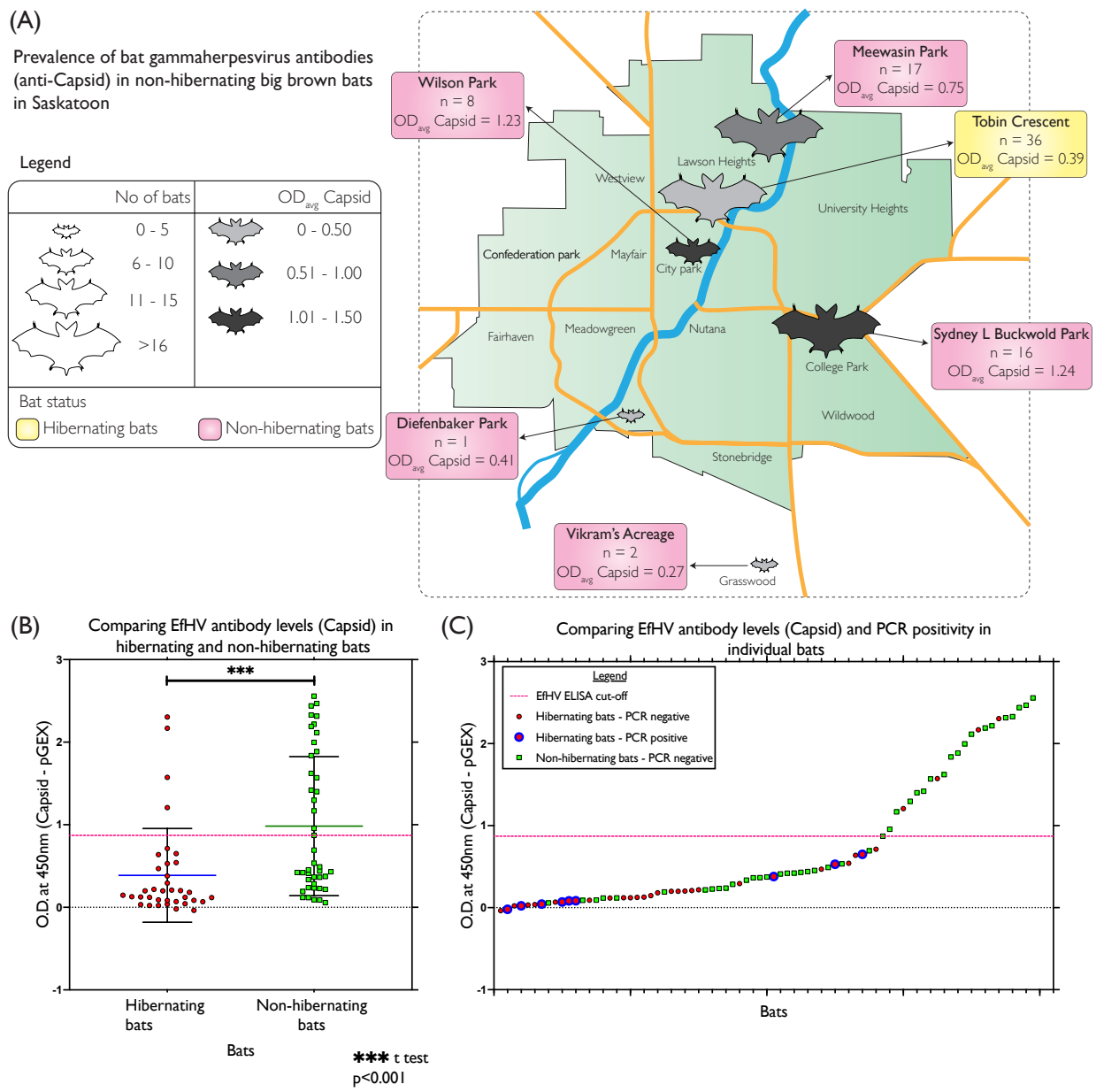

Figure 8.2. (A). Map representing areas in and around Saskatoon, Saskatchewan, Canada where North American big brown bats were captured and sampled. The map depicts the total number of bats caught in each area and the average optical density (OD) values at 450 nm of bat gammaherpesvirus antibodies (anti-Capsid). The size of the bat icon denotes the number of bats captured at each site and the density of the fill indicates the level of anti-*Ef*HV antibody. Pink boxes are captured non-hibernating bats while the yellow box represents hibernating bats.

Figure 8.2. (B). Comparison of levels of *Ef*HV antibody levels (Capsid) in the plasma of hibernating and non-hibernating big brown bats. Antibody levels against the *Ef*HV capsid protein are expressed as corrected OD values at 450 nm. These values were obtained by subtracting OD for the negative antigen (GST) from that of the positive antigen (GST-tagged *Ef*HV Capsid

protein). Non-hibernating bats had significantly higher antibody levels than hibernating bats (Welch two sample *t*-test: $p < 0.001$).

Figure 8.2. (C). Comparison of *Ef*HV antibody levels (Capsid) and viral DNA detected by PCR in individual big brown bats. Antibody levels against the *Ef*HV capsid protein are expressed as optical density (OD) values at 450 nm and arranged in an ascending order to show the change in mean based on which cut-off was determined (change-point analysis). Positive *Ef*HV DNA status and hibernation status is depicted as described in the legend. All bats that tested positive were hibernating and their levels was lower than the ELISA cut-off. More number of non-hibernating bats (18/43) were above the cut-off than hibernating bats (4/36) ($\chi^2 = 7.754$, df = 1, p-value = 0.005).

8.7.3. Seroprevalence of *Ef*HV antibodies in bats

We performed IgG capture ELISA on blood plasma obtained from 36 hibernating and 43 non-hibernating bats. Using change-point analysis, we determined the seropositive cut-off $OD_{corrected}$ as 0.871 (Change-point type: change in mean, PELT analysis, penalty: MBIC with value, 13.1). Bats having $OD_{corrected}$ values higher than the cut-off were considered seropositive for *Ef*HV. For the hibernating bats and non-hibernating bats, 11.1% (4/36) and 41.8% (18/43) were considered seropositive, respectively. This result shows that both groups were exposed to the virus, and that the percentage of seropositive bats was higher in the non-hibernating group (Two sample proportion test: $\chi^2 = 7.754$, df = 1, p-value = 0.005). Counter-intuitively, the $OD_{corrected}$ values of the 9 hibernating bats with reactivated virus were below the cut-off value (for the tenth bat that tested positive for *Ef*HV DNA, we did not obtain enough plasma to perform an ELISA) (Figure 8.2. (C)), which indicates that seronegativity does not rule out the possibility of *Ef*HV infection. Therefore, instead of assigning seropositive or seronegative status to bats, we decided to analyse the antibody titers to understand the immunological response of bats against *Ef*HV.

8.7.4. Lower *Ef*HV antibody levels in bats containing *Ef*HV DNA in their blood cells

For the sample of hibernating bats, the antibody levels of bats that were PCR-negative for *Ef*HV (n = 27 bats, 0.448 ± 0.109) were 2.2 times higher than the PCR-positive bats (n = 9 bats, 0.205 ± 0.189; two samples *t*-test: t = 1.652, df = 32.82, p = 0.108; Figure 8.2. (C)). This counter-intuitive result (although not significant) shows that bats with detectable levels of *Ef*HV DNA have lower antibody levels than bats with no detectable levels of *Ef*HV DNA.

8.7.5. Higher levels of *Ef*HV antibodies in non-hibernating bats

The mean level of capsid-specific antibodies was 2.5 times higher in the non-hibernating bats (mean = 0.983 ± 0.111) compared to hibernating bats (mean = 0.387 ± 0.122), and this difference was significant (*t*-test: t = 3.736, df = 73.89, p < 0.001; Figure 8.2. (B)). However, there were also significant differences in bat antibody titres based on the location where bats were captured (ANOVA: $F_{5, 73} = 4.184$, p = 0.002) (Figure 8.2. (A), supplementary figure S8.1. (B)). Specifically, non-hibernating bats from Buckwold Park (t = 3.983, p < 0.001) and Wilson Park (t = 2.850, p = 0.006) had significantly higher antibody titres than bats from all other locations. These results suggest that both location and hibernation state have an important effect on bat antibody titres. These analyses of antibody titres are limited because they only consider one explanatory variable at a time.

The independent samples *t*-test comparing the antibody levels between hibernating and non-hibernating bats did not consider other explanatory variables. We therefore used LME models to investigate the fixed effects (hibernation state, sex, radius length, body weight, and infection status) that influenced bat antibody levels against *Ef*HV. After including the other explanatory variables, the antibody titres were still higher in the non-hibernating bats compared to the hibernating bats, but this difference was no longer significant (Table 8.1: mean contrast of non-

hibernation – hibernation = 0.55, standard error of contrast = 0.368, t-value = 1.512, p = 0.266). None of the other explanatory variables had a significant effect on antibody titres (Table 8.1).

Table 8.1. Bat antibody titre was modeled as an LME with normal errors. Parameter estimates are shown from the model that contains an intercept and five fixed effects: hibernation state, sex, radius, body weight, and infection status. For each parameter, the estimate, standard error, z value, and p-value are shown.

Fixed effects	Estimate	Std. Error	df	t value	p
Intercept	0.50	3.170	72.19	0.157	0.875
Non-hibernation - hibernation	0.56	0.368	2.06	1.512	0.266
Male - female	-0.12	0.314	72.86	-0.371	0.712
Radius (mm)	0.01	0.074	72.89	0.198	0.843
Weight (g)	-0.04	0.067	72.92	-0.62	0.537
Positive - negative	-0.21	0.284	70.34	-0.756	0.452

8.7.6. Hibernation is the most important factor for *Ef*HV reactivation

We used GLME models to investigate the fixed effects (hibernation state, sex, radius length, body weight, and antibody titre) that influenced reactivation of *Ef*HV. Of the five fixed effects, only hibernation state had a significant effect on the prevalence of *Ef*HV infection. The prevalence of *Ef*HV infection was higher in the non-hibernating bats compared to the hibernating bats (Table 8.2: mean contrast on the logit scale of hibernating – non-hibernating = 2.84; standard error of contrast = 1.268, z-value = 2.240, p = 0.025).

Table 8.2. Bat infection status was modeled as a GLME with binomial errors. Parameter estimates are shown from the model that contains an intercept and five fixed effects: hibernation state, sex, radius, body weight, and antibody titre. For each parameter, the estimate, standard error, z value, and p-value are shown.

Fixed effects	Estimate	Std. Error	z value	p
Intercept	-4.44	15.275	-0.291	0.771
Non-hibernation - hibernation	-2.84	1.268	-2.24	0.025
Male - female	0.98	1.255	0.784	0.433
Radius (mm)	-0.05	0.353	-0.144	0.886
Weight (g)	0.33	0.288	1.153	0.249
Antibody titre	-0.74	0.806	-0.922	0.357

8.8. Discussion

Gammaherpesviruses are known to establish long-term latent infection in their hosts with periodic reactivation of the virus leading to lytic replication, virus shedding from the skin and mucosae, and transmission to new uninfected hosts. Previous studies in lab mice have shown that the latent gammaherpesvirus is sequestered in cells in the spleen and can be reactivated by stress [52,53]. Various stressors, such as unfolded protein responses and hypoxia, can induce the expression of viral immediate early genes that initiate the lytic cycle [54]. Although numerous studies have studied the switch from latent infection to reactivation, the exact mechanism is still not understood. This is also true for bat gammaherpesviruses.

Studies in bats and other hibernating mammalian species have shown that hibernation has a profound effect on innate and adaptive immune systems. Hibernation decreases leukocyte count, lymphocyte proliferation, cytokine levels and antibody production [344–346]. Arousal from hibernation is a stressful event. In arctic ground squirrels, for example, arousal from hibernation induces oxidative stress [347]. Studies in cell culture models have shown that oxidative stress induces reactivation of the Kaposi Sarcoma herpesvirus [339]. In the present study, we detected

*Ef*HV DNA in the blood cells of bats arousing from hibernation, but not in the non-hibernating bats caught in the wild. The high prevalence of *Ef*HV in hibernating bats was in agreement with our previous study on a research colony of bats that found *Ef*HV DNA in the blood of 20 of 28 hibernating individuals [56]. Our study suggests that the hibernation and/or the stress of arousal from hibernation caused the reactivation of the gammaherpesvirus in the big brown bats. An alternative explanation is that the stress of being housed at a rehabilitation centre contributed to the reactivation of *Ef*HV, but we view this explanation is unlikely.

To show that both hibernating and non-hibernating bats had been exposed to *Ef*HV, we screened the bats for *Ef*HV-specific antibodies. Importantly, the change point analysis showed that both hibernating and non-hibernating bats had been exposed to the virus and were possibly latently infected. Interestingly, the seroprevalence was lower in the hibernating bats than the non-hibernating bats, even though we detected virus only in the blood of hibernating bats. For hibernating bats, the antibody titres were higher for the *Ef*HV-negative bats than for the *Ef*HV-positive bats. This suggested that while the presence of high levels of anti-*Ef*HV antibody may indicate prior exposure to the virus, low levels of antibody did not indicate an absence of infection. Interestingly, we were only able to detect *Ef*HV in the blood of hibernating bats with low levels of antiviral antibody (below the seropositive cutoff of the change-point analysis). This result suggests that detection of virus in the blood indicates viremia due to reactivation rather than cells infected with latent virus, and this inference is in agreement with previous studies on murine herpesvirus-68 [52,337].

The immune response is crucial in controlling mammalian gammaherpesvirus infection. The virus-specific antibody response helps to contain persistent murine gammaherpesvirus-4 in mouse models [348,349]. We found that the antibody titres against *Ef*HV were higher in the non-

hibernating bats compared to the hibernating bats and this difference was highly significant when hibernation status was the only explanatory variable. (although when we included other explanatory variables in the analysis, the direction of the effect remained the same, but it was no longer significant). One explanation for the difference in antibody titres between the two groups is as follows. In hibernating bats, the antibody response waned over the duration of hibernation resulting in lower antibody titres in this group at arousal. In contrast, in the non-hibernating bats, recent exposure to the virus or recent re-activation of the virus triggered a strong antibody response, which subsequently cleared the virus from the blood and driven to latency in the spleen cells. An alternative explanation for the differences in antibody titres is that the bats were sampled from different locations in Saskatoon and these locations may differ in infection prevalence. Since the non-hibernating bats were captured while flying, we do not know the precise location of their roosts. As big brown bats can have a flight range of 4.4 km [350], these bats sampled (except 2 bats from Vikram's Acreage) might be considered as a random sampling of Saskatoon area bats. Therefore, it is crucial to note the higher antibody titres in the non-hibernating bats suggesting that while these individuals have been exposed to *Ef*HV they were successful in preventing the virus from reactivating.

How do stress and the host immune system interact to allow *Ef*HV to reactivate in the blood? The detection of *Ef*HV only in the blood of hibernating bats with low levels of antibody (below change-point analysis cut-off) suggests reactivation of virus from latency may require two conditions – low levels of antiviral immunity, as indicated by low levels of antibody, and arousal from hibernation. A combination of suppressed antiviral response during hibernation and the stress of arousal may allow the virus to reactivate and replicate in lymphoid cells. Antibody titres are not the only immunological mechanisms that control replication of gammaherpesviruses. T-cell

mediated responses are also important for controlling gammaherpesviruses [351]. We propose a preliminary model whereby decreased immunity and oxidative stress (due to arousal) explain reactivation of *Ef*HV in the big brown bat (Figure 8.3).

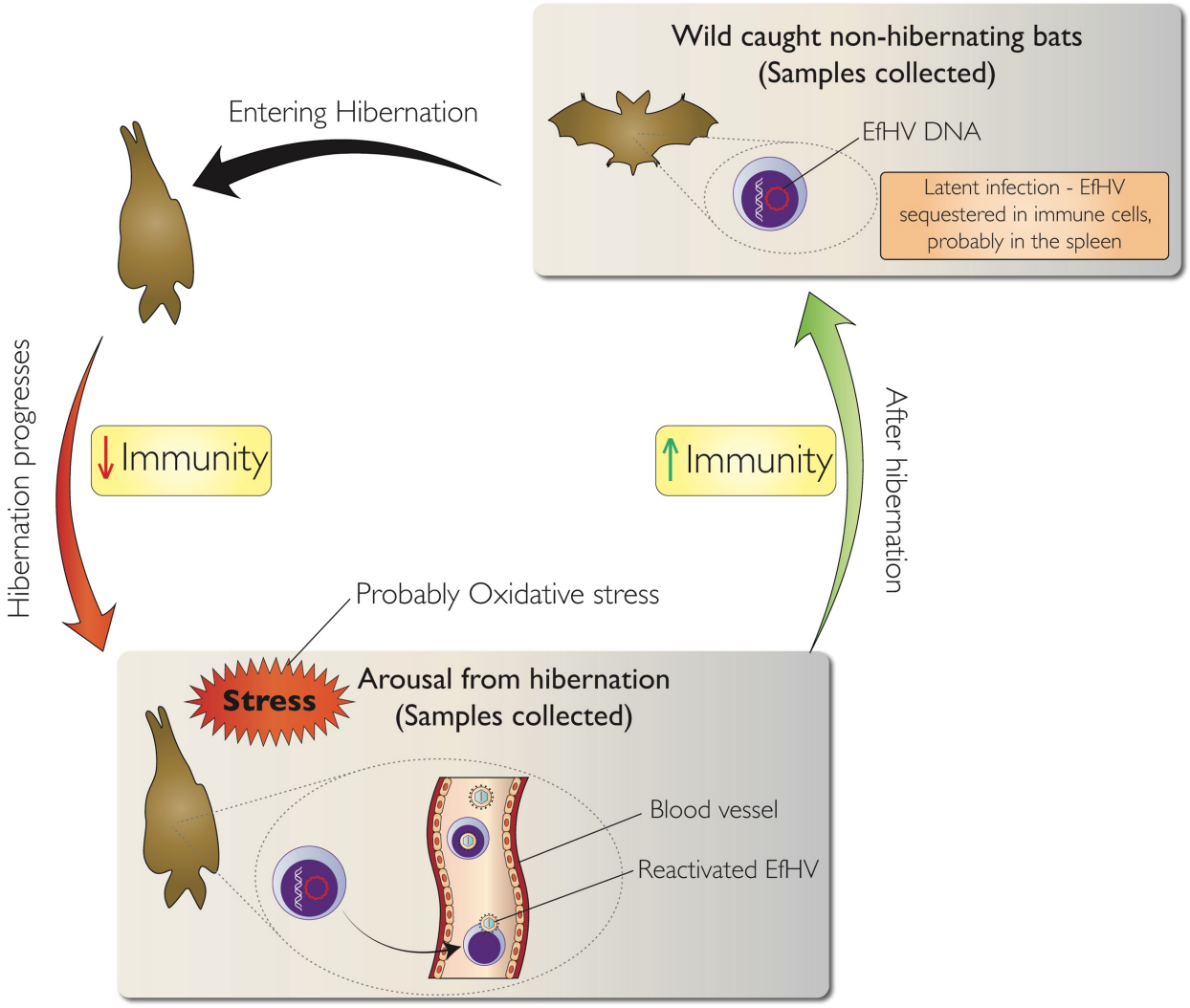

Figure 8.3. A model based on our results of hibernation related *Ef*HV reactivation. Long periods of hibernation leading to suppression of immunity, coupled with the stress of arousal from hibernation results in reactivation of latent *Ef*HV. Subsequently, antiviral immunity increases in non-hibernating bats reducing viral DNA in circulating blood cells. Latent *Ef*HV DNA is sequestered away from circulating blood, possibly in the spleen.

Ideally, to demonstrate that a decrease in antiviral antibodies correlated with viral reactivation upon arousal from hibernation, we could have assessed antibody levels and viremia

in the same bats before and after hibernation. However, we were unable to obtain paired samples from the bats in this study because we did not have access to the hibernating bats until just before their release in the spring. Controlled experiments with paired sampling of individual bats before and after hibernation are needed to confirm our observations. It would also be interesting to study if hibernation has an effect on other bat-virus interactions.

8.9. Supplementary information

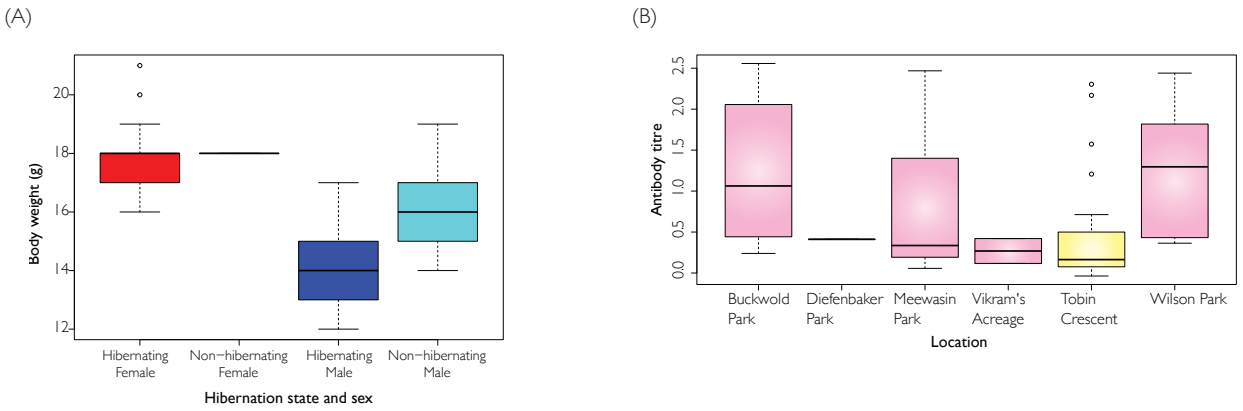

Supplementary figure S8.1. (A). Body weight (grams) of bats is shown as a function of hibernation status and sex. Females are heavier than males and non-hibernating bats are heavier than hibernating bats. Shown are the medians (black lines), 25th and 75th percentiles (edges of the box), minimum and maximum values (whiskers), and outliers (open circles). **(B)** Herpes virus-specific antibody titres of bats are shown as a function of location. One-way ANOVA found that location had a significant effect on the antibody titre ($F_{5, 73} = 4.184$, $p = 0.002$). Posthoc Tukey HSD tests found that the bats at the WCVM had antibody titres that were significantly lower than bats from Buckwold Park ($p < 0.001$) and Wilson Park ($p = 0.029$). Shown are the medians (black lines), 25th and 75th percentiles (edges of the box), minimum and maximum values (whiskers), and outliers (open circles).

Chapter 9: General discussion

9.1. Summary

Bats are considered as the reservoir and ancestral host of several viruses that are now established as pathogens in other animals [1]. Although numerous studies have been done to understand the bat-virus relationship using surrogate viruses, very few studies have looked at the native viruses and their relationship with their natural host. Understanding this bat-virus relationship is crucial to further comprehend the mechanism behind spillovers. Spillover events are dependent upon numerous factors such as pathogen shedding, environmental conditions, pathogen persistence in environment and recipient host susceptibility. These factors must align, in a "perfect storm" leading to a spillover [12]. Although several groups have studied the various factors responsible for such spillovers, the molecular mechanism of spillover is largely unknown.

In my thesis, I set out to prove the general hypothesis that bats have a long-term balanced and benign relationship with viruses and natural stressors disrupt this balance leading to an increase in virus replication. In this section, I have summarized my findings which help in proving the general hypothesis in a step by step manner using two virus-bat models.

9.1.1. Characterization of a coronavirus autochthonous to North American bat species

To study factors altering the bat-virus relationship, we required models which could be used to test hypotheses describing the relationship. The first model that I used was of a bat coronavirus, detected in North American little brown bats. We showed that coronaviruses were able to persist in intestines of hibernating bats, at least for a period of 4 months during which they were in hibernation. The tissues infected with bat coronavirus did not show any overt inflammation or pathology. Since we had access to tissue samples archived from an earlier study on the

pathophysiology of white-nose syndrome, we further studied the effect of this secondary fungal infection on the bat-coronavirus relationship.

9.1.2. Secondary infection increases coronavirus levels in little brown bats

Using the coronavirus-bat model, we showed that the presence of secondary infection by *P. destructans*, leads to increased severity of the fungal disease and viral shedding and molecular responses in the tissue harbouring the persisting coronavirus (Chapter 5). We identified MAP kinase and cytokine-related genes (like IFI6) altered in the intestines in the presence of fungal infection in wings of the bat. To summarize, my results suggested that the systemic effects of secondary fungal infection downregulates antiviral responses and upregulates apoptotic pathways in bats persistently infected with coronavirus in the intestines and increases the potential of virus shedding. Since manipulating persistent viral infection in bats is difficult, we established a persistent coronavirus infection in bat cell culture, which enabled me to study molecular pathways that disrupt viral persistence leading to an increase in viral replication.

9.1.3. Bat cells can be persistently infected with coronavirus and altering interferon and MAP kinase pathways leads to increased viral replication

After identifying innate immune pathways altering persistent coronavirus infection in *in-vivo* models, we exploited persistent infection of cultured bat cells by the MERS-CoV to explore the molecular mechanism that regulate coronavirus persistence in bat cells (*in-vitro* model). We discovered that infection of bat cells rapidly selected for variants in the accessory gene ORF5. Long-term infection of bat cells without significant cellular pathology was mediated through antiviral innate mechanisms and activated MAP kinase pathways. Suppressing these pathways, led to an increase in virus replication. We also showed that activation of the IFI6-mediated anti-apoptotic pathway, and resistance to superinfection with the more cytolytic wild-type MERS-CoV,

may prevent death of the cells and contributed to persistence of coronavirus (Chapter 6). The innate immune pathways that alter persistent virus infection in cell culture model, namely MAP kinase and IFI6, were comparable with pathways affected in little brown bats infected with white-nose syndrome fungus which increased the level of *Myotis lucifugus* coronavirus. Using the in-vivo and in-vitro bat-coronavirus system, we showed that bats have a long-term balanced and benign relationship with coronaviruses and stressful events affecting the innate antiviral pathways, could lead to increased coronavirus replication. To understand if stressors could disrupt low-level persistent infection of viruses other than coronavirus, I studied a bat herpesvirus relationship to big brown bats.

9.1.4. Characterization of a gammaherpesvirus autochthonous to North American bat species

The second bat-virus model that I tested was that of a gammaherpesvirus isolated from North American big brown bats. We established that the gammaherpesvirus was widely prevalent in big brown bats and could be detected in the blood. We were also able to monitor the adaptive antibody response of the bat against this virus. These observations allowed us to monitor infections in non-hibernating bats caught in the wild and bats emerging from hibernation. Since all herpesviruses examined to date establish long-term latent infections from which they reactivate in response to various stressors, the gammaherpesvirus-bat model, also enabled us to study the effects of stress on viral reactivation from latency.

9.1.5. Arousal from hibernation reactivates gammaherpesvirus in big brown bats

Using the gammaherpesvirus-bat model, we demonstrated that bat arousing from hibernation tend to have lower antibody levels and have detectable gammaherpesvirus in their blood. My findings suggest that long periods of hibernation lead to suppression of immunity and

stress from arousal reactivates the virus in bats with lower levels of antiviral immunity (Chapter 8). But after hibernation, antibody levels and, perhaps other components of the antiviral immune response, tend to increase and the gammaherpesvirus is no longer detectable. A controlled study on bats before and after hibernation would enable us to obtain paired samples, which would further confirm our findings. My findings show that big brown bats are latently infected with the gammaherpesvirus and a natural stressor, such as arousal from hibernation, would lead to its reactivation.

9.2. Conclusion

In my doctoral thesis, I tested the broad hypothesis that bats have long-term balanced and benign relationships with viruses, with whom they have co-evolved, and that a variety of stressors disrupt this balance allowing increased viral replication. My disseration provides evidence that viruses persistently infect bats and shows the characteristics of such infections. It also provides definitive clues about two factors that alter balanced bat-virus relationship, namely secondary fungal infection increasing coronavirus persistence and arousal from hibernation reactivating bat gammaherpesvirus. I also describe a mechanism of persistent coronavirus infection in bat cells and molecular pathways that alter the persistent infection. To summarize, my thesis outlines factors that alter balanced bat-virus relationships (using *in-vitro* and *in-vivo* models), which may increase the probability of spillover of these viruses to humans and other animals.

9.3. Challenges, limitations and future prospects

Although my thesis describes factors that affect bat-virus relationships, there were a few limitations to these studies. We studied the effect of secondary infection on bat coronavirus using

archived samples. We did not have access to fecal samples of these individual bats. Using fecal samples coronavirus shedding could have been monitored with and without the fungal infection. Also, since coronavirus was present in the intestines of these bats, it was not possible to know what bats were positive before harvesting the organs at the termination of the experiment.

Due to the white-nose syndrome, little brown bats are now considered endangered wildlife species [352]. This has made it challenging to perform *in-vivo* studies on this species. Recovery of little brown bat populations in the coming years, may allow further such studies on these bats.

Another challenge that we faced was during the study of arousal from hibernation on reactivation of gammaherpesvirus. We were unable to obtain paired samples from bats before and after hibernation because of the study design. We used statistically modelling tool to circumvent this challenge. But future studies using paired samples would confirm the findings obtained durng our study.

In the future, attempt to generate the bat coronavirus using reverse genetics could be attempted. If successful isolation of the bat coronavirus occurs, then appropriate controlled *in-vivo* studies could be conducted. Experimental inoculation of the bat coronavirus to a large sample size of bats followed by secondary infection by *P. destructans* would enable us to confirm our findings. Also, montoring fecal samples would allow us to test our hypothesis that stress of secondary infection leads to increase in viral shedding. By having a native bat coronavirus, future studies could also look at effect of other stressors such as pregnancy and climate change.

The ability of bats to promote viral persistence, may exert evolutionary pressure on the virus. The emergence of new viral strains due to such pressure is poorly understood. Future studies looking at the natural selection due to viral persistence may allow us to predict new virus emergence.

Studies on bats and their viruses is an emerging field. It is challenging to obtain species specific reagents, especially reagents (antibodies) that specifically detect bat viral proteins. As the field advances, we would be able to perform studies such as those examining the activation of enzyme-mediated pathways. Using cellular markers, we would also be able to examine the role of various bat immune cells and determine the cellular tropism of bat viruses. These studies would allow us to better understand the molecular mechanism behind factors affecting bat-virus balanced relationship.

References

1. Hayman, D.T.S. Bats as Viral Reservoirs. *Annual Review of Virology* **2016**, *3*, 77–99.
2. Al, M.I. et Nipah Virus Transmission from Bats to Humans Associated with Drinking Traditional Liquor Made from Date Palm Sap, Bangladesh, 2011–2014 - Volume 22, Number 4—April 2016 - Emerging Infectious Diseases journal - CDC.
3. Al, S.P.L. et Foodborne Transmission of Nipah Virus, Bangladesh - Volume 12, Number 12—December 2006 - Emerging Infectious Diseases journal - CDC.
4. Edson, D.; Field, H.; McMichael, L.; Vidgen, M.; Goldspink, L.; Broos, A.; Melville, D.; Kristoffersen, J.; de Jong, C.; McLaughlin, A.; et al. Routes of Hendra Virus Excretion in Naturally-Infected Flying-Foxes: Implications for Viral Transmission and Spillover Risk. *PLoS ONE* **2015**, *10*, e0140670.
5. Field, H.; Young, P.; Yob, J.M.; Mills, J.; Hall, L.; Mackenzie, J. The natural history of Hendra and Nipah viruses. *Microbes and Infection* **2001**, *3*, 307–314.
6. Kurup, A. From bats to pigs to man: the story of Nipah Virus. *Infectious Diseases in Clinical Practice* **2002**, *11*.
7. Vogel, G. Bat-filled tree source of Ebola epidemic? *Science* **2015**, *347*, 142–143.
8. Caron, A.; Bourgarel, M.; Cappelle, J.; Liégeois, F.; De Nys, H.M.; Roger, F. Ebola Virus Maintenance: If Not (Only) Bats, What Else? *Viruses* **2018**, *10*, 549.
9. Goldstein, T.; Anthony, S.J.; Gbakima, A.; Bird, B.H.; Bangura, J.; Tremeau-Bravard, A.; Belaganahalli, M.N.; Wells, H.L.; Dhanota, J.K.; Liang, E.; et al. The discovery of Bombali virus adds further support for bats as hosts of ebolaviruses. *Nature Microbiology* **2018**, *3*, 1084–1089.
10. Yang, X.-L.; Tan, C.W.; Anderson, D.E.; Jiang, R.-D.; Li, B.; Zhang, W.; Zhu, Y.; Lim, X.F.; Zhou, P.; Liu, X.-L.; et al. Characterization of a filovirus (Měnglà virus) from Rousettus bats in China. *Nature Microbiology* **2019**.
11. Streicker, D.G.; Turmelle, A.S.; Vonhof, M.J.; Kuzmin, I.V.; McCracken, G.F.; Rupprecht, C.E. Host Phylogeny Constrains Cross-Species Emergence and Establishment of Rabies Virus in Bats. *Science* **2010**, *329*, 676–679.
12. Plowright, R.K.; Eby, P.; Hudson, P.J.; Smith, I.L.; Westcott, D.; Bryden, W.L.; Middleton, D.; Reid, P.A.; McFarlane, R.A.; Martin, G.; et al. Ecological dynamics of emerging bat virus spillover. *Proceedings. Biological sciences / The Royal Society* **2015**, *282*, 20142124.
13. Duggal, N.K.; Emerman, M. Evolutionary conflicts between viruses and restriction factors shape immunity. *Nat Rev Immunol* **2012**, *12*, 687–695.
14. Baker, M.L.; Schountz, T.; Wang, L.F. Antiviral immune responses of bats: a review. *Zoonoses and public health* **2013**, *60*, 104–16.
15. Schountz, T. Immunology of Bats and Their Viruses: Challenges and Opportunities. *Viruses* **2014**, *6*, 4880–4901.
16. Schountz, T.; Baker, M.L.; Butler, J.; Munster, V. Immunological Control of Viral Infections in Bats and the Emergence of Viruses Highly Pathogenic to Humans. *Front Immunol* **2017**, *8*, 1098.
17. Peixoto, F.P.; Braga, P.H.P.; Mendes, P. A synthesis of ecological and evolutionary determinants of bat diversity across spatial scales. *BMC Ecology* **2018**, *18*, 18.
18. Zhou, P.; Tachedjian, M.; Wynne, J.W.; Boyd, V.; Cui, J.; Smith, I.; Cowled, C.; Ng, J.H.J.; Mok, L.; Michalski, W.P.; et al. Contraction of the type I IFN locus and unusual constitutive

expression of *IFN-α* in bats. *Proceedings of the National Academy of Sciences* **2016**, *113*, 2696–2701.
19. O'Connor, K.C. Bats are "blind" to the deadly effects of viruses. *Science Immunology* **2018**, *3*, eaau2559.
20. O'Shea, T.J.; Cryan, P.M.; Cunningham, A.A.; Fooks, A.R.; Hayman, D.T.; Luis, A.D.; Peel, A.J.; Plowright, R.K.; Wood, J.L. Bat flight and zoonotic viruses. *Emerging infectious diseases* **2014**, *20*, 741–5.
21. Zhang, G.; Cowled, C.; Shi, Z.; Huang, Z.; Bishop-Lilly, K.A.; Fang, X.; Wynne, J.W.; Xiong, Z.; Baker, M.L.; Zhao, W.; et al. Comparative analysis of bat genomes provides insight into the evolution of flight and immunity. *Science* **2013**, *339*, 456–60.
22. Omatsu, T.; Bak, E.-J.; Ishii, Y.; Kyuwa, S.; Tohya, Y.; Akashi, H.; Yoshikawa, Y. Induction and sequencing of Rousette bat interferon alpha and beta genes. *Vet. Immunol. Immunopathol.* **2008**, *124*, 169–176.
23. Zhou, P.; Cowled, C.; Todd, S.; Crameri, G.; Virtue, E.R.; Marsh, G.A.; Klein, R.; Shi, Z.; Wang, L.-F.; Baker, M.L. Type III IFNs in Pteropid Bats: Differential Expression Patterns Provide Evidence for Distinct Roles in Antiviral Immunity. *J Immunol* **2011**, *186*, 3138–3147.
24. Pavlovich, S.S.; Lovett, S.P.; Koroleva, G.; Guito, J.C.; Arnold, C.E.; Nagle, E.R.; Kulcsar, K.; Lee, A.; Thibaud-Nissen, F.; Hume, A.J.; et al. The Egyptian Rousette Genome Reveals Unexpected Features of Bat Antiviral Immunity. *Cell* **2018**, *173*, 1098–1110.
25. De La Cruz-Rivera, P.C.; Kanchwala, M.; Liang, H.; Kumar, A.; Wang, L.-F.; Xing, C.; Schoggins, J.W. The IFN Response in Bats Displays Distinctive IFN-Stimulated Gene Expression Kinetics with Atypical RNASEL Induction. *The Journal of Immunology* **2018**, *200*, 209–217.
26. Li, Y.; Banerjee, S.; Wang, Y.; Goldstein, S.A.; Dong, B.; Gaughan, C.; Silverman, R.H.; Weiss, S.R. Activation of RNase L is dependent on OAS3 expression during infection with diverse human viruses. *PNAS* **2016**, *113*, 2241–2246.
27. Gerrard, D.L.; Hawkinson, A.; Sherman, T.; Modahl, C.M.; Hume, G.; Campbell, C.L.; Schountz, T.; Frietze, S. Transcriptomic Signatures of Tacaribe Virus-Infected Jamaican Fruit Bats. *mSphere* **2017**, *2*, e00245-17.
28. Channappanavar, R.; Perlman, S. Pathogenic human coronavirus infections: causes and consequences of cytokine storm and immunopathology. *Semin Immunopathol* **2017**, *39*, 529–539.
29. Banerjee, A.; Rapin, N.; Bollinger, T.; Misra, V. Lack of inflammatory gene expression in bats: a unique role for a transcription repressor. *Sci Rep* **2017**, *7*, 2232.
30. Xie, J.; Li, Y.; Shen, X.; Goh, G.; Zhu, Y.; Cui, J.; Wang, L.-F.; Shi, Z.-L.; Zhou, P. Dampened STING-Dependent Interferon Activation in Bats. *Cell Host & Microbe* **2018**, *23*, 297–301.
31. Ahn, M.; Cui, J.; Irving, A.T.; Wang, L.-F. Unique Loss of the PYHIN Gene Family in Bats Amongst Mammals: Implications for Inflammasome Sensing. *Sci Rep* **2016**, *6*.
32. Maina, J.N. What it takes to fly: the structural and functional respiratory refinements in birds and bats. *J. Exp. Biol.* **2000**, *203*, 3045–3064.
33. Thomas, S.P.; Suthers, R.A. The Physiology and Energetics of Bat Flight. *Journal of Experimental Biology* **1972**, *57*, 317–335.
34. Cadet, J.; Wagner, J.R. DNA Base Damage by Reactive Oxygen Species, Oxidizing Agents, and UV Radiation. *Cold Spring Harb Perspect Biol* **2013**, *5*.

35. Sheldon, B.C.; Verhulst, S. Ecological immunology: costly parasite defences and trade-offs in evolutionary ecology. *Trends in Ecology & Evolution* **1996**, *11*, 317–321.
36. Jebb, D.; Foley, N.M.; Whelan, C.V.; Touzalin, F.; Puechmaille, S.J.; Teeling, E.C. Population level mitogenomics of long-lived bats reveals dynamic heteroplasmy and challenges the Free Radical Theory of Ageing. *Sci Rep* **2018**, *8*.
37. Cogswell-Hawkinson, A.; Bowen, R.; James, S.; Gardiner, D.; Calisher, C.H.; Adams, R.; Schountz, T. Tacaribe virus causes fatal infection of an ostensible reservoir host, the Jamaican fruit bat. *J Virol* **2012**, *86*, 5791–9.
38. Middleton, D.J.; Morrissy, C.J.; van der Heide, B.M.; Russell, G.M.; Braun, M.A.; Westbury, H.A.; Halpin, K.; Daniels, P.W. Experimental Nipah virus infection in pteropid bats (Pteropus poliocephalus). *Journal of comparative pathology* **2007**, *136*, 266–72.
39. Munster, V.J.; Adney, D.R.; van Doremalen, N.; Brown, V.R.; Miazgowicz, K.L.; Milne-Price, S.; Bushmaker, T.; Rosenke, R.; Scott, D.; Hawkinson, A.; et al. Replication and shedding of MERS-CoV in Jamaican fruit bats (Artibeus jamaicensis). *Sci Rep* **2016**, *6*.
40. Jones, M.E.B.; Schuh, A.J.; Amman, B.R.; Sealy, T.K.; Zaki, S.R.; Nichol, S.T.; Towner, J.S. Experimental Inoculation of Egyptian Rousette Bats (Rousettus aegyptiacus) with Viruses of the Ebolavirus and Marburgvirus Genera. *Viruses* **2015**, *7*, 3420–3442.
41. Sohayati, A.R.; Hassan, L.; Sharifah, S.H.; Lazarus, K.; Zaini, C.M.; Epstein, J.H.; Naim, N.S.; Field, H.E.; Arshad, S.S.; Aziz, J.A.; et al. Evidence for Nipah virus recrudescence and serological patterns of captive Pteropus vampyrus. *Epidemiology & Infection* **2011**, *139*, 1570–1579.
42. Amman, B.R.; Jones, M.E.; Sealy, T.K.; Uebelhoer, L.S.; Schuh, A.J.; Bird, B.H.; Coleman-McCray, J.D.; Martin, B.E.; Nichol, S.T.; Towner, J.S. Oral shedding of marburg virus in experimentally infected Egyptian fruit bats (Rousettus aegyptiacus). *Journal of wildlife diseases* **2015**, *51*, 113–24.
43. Schuh, A.J.; Amman, B.R.; Jones, M.E.B.; Sealy, T.K.; Uebelhoer, L.S.; Spengler, J.R.; Martin, B.E.; Coleman-McCray, J.A.D.; Nichol, S.T.; Towner, J.S. Modelling filovirus maintenance in nature by experimental transmission of Marburg virus between Egyptian rousette bats. *Nature Communications* **2017**, *8*, 14446.
44. Subudhi, S.; Rapin, N.; Bollinger, T.K.; Hill, J.E.; Donaldson, M.E.; Davy, C.M.; Warnecke, L.; Turner, J.M.; Kyle, C.J.; Willis, C.K.R.; et al. A persistently infecting coronavirus in hibernating Myotis lucifugus, the North American little brown bat. *J Gen Virol* **2017**, *98*, 2297–2309.
45. Peel, A.J.; Baker, K.S.; Hayman, D.T.S.; Broder, C.C.; Cunningham, A.A.; Fooks, A.R.; Garnier, R.; Wood, J.L.N.; Restif, O. Support for viral persistence in bats from age-specific serology and models of maternal immunity. *Scientific Reports* **2018**, *8*, 3859.
46. Halpin, K.; Hyatt, A.D.; Fogarty, R.; Middleton, D.; Bingham, J.; Epstein, J.H.; Rahman, S.A.; Hughes, T.; Smith, C.; Field, H.E.; et al. Pteropid bats are confirmed as the reservoir hosts of henipaviruses: a comprehensive experimental study of virus transmission. *The American journal of tropical medicine and hygiene* **2011**, *85*, 946–51.
47. Plowright, R.K.; Peel, A.J.; Streicker, D.G.; Gilbert, A.T.; McCallum, H.; Wood, J.; Baker, M.L.; Restif, O. Transmission or Within-Host Dynamics Driving Pulses of Zoonotic Viruses in Reservoir–Host Populations. *PLOS Neglected Tropical Diseases* **2016**, *10*, e0004796.
48. Prösch, S.; Wendt, C.E.C.; Reinke, P.; Priemer, C.; Oppert, M.; Krüger, D.H.; Volk, H.-D.; Döcke, W.-D. A Novel Link between Stress and Human Cytomegalovirus (HCMV)

Infection: Sympathetic Hyperactivity Stimulates HCMV Activation. *Virology* **2000**, *272*, 357–365.
49. Grinde, B. Herpesviruses: latency and reactivation – viral strategies and host response. *J Oral Microbiol* **2013**, *5*.
50. Knickelbein, J.E.; Khanna, K.M.; Yee, M.B.; Baty, C.J.; Kinchington, P.R.; Hendricks, R.L. Noncytotoxic lytic granule-mediated CD8+ T cell inhibition of HSV-1 reactivation from neuronal latency. *Science* **2008**, *322*, 268–71.
51. Freeman, M.L.; Sheridan, B.S.; Bonneau, R.H.; Hendricks, R.L. Psychological Stress Compromises CD8+ T Cell Control of Latent Herpes Simplex Virus Type 1 Infections. *J Immunol* **2007**, *179*, 322–328.
52. Flaño, E.; Kim, I.J.; Woodland, D.L.; Blackman, M.A. Gamma-herpesvirus latency is preferentially maintained in splenic germinal center and memory B cells. *J Exp Med* **2002**, *196*, 1363–72.
53. Weck, K.E.; Barkon, M.L.; Yoo, L.I.; Speck, S.H.; Virgin Hw, I.V. Mature B cells are required for acute splenic infection, but not for establishment of latency, by murine gammaherpesvirus 68. *Journal of Virology* **1996**, *70*, 6775–6780.
54. Lieberman, P.M. Keeping it quiet: chromatin control of gammaherpesvirus latency. *Nat Rev Microbiol* **2013**, *11*, 863–75.
55. Lee, M.; Choi, I.; Park, K. Activation of stress signaling molecules in bat brain during arousal from hibernation. *J Neurochem* **2002**, *82*, 867–73.
56. Subudhi, S.; Rapin, N.; Dorville, N.; Hill, J.E.; Town, J.; Willis, C.K.R.; Bollinger, T.K.; Misra, V. Isolation, characterization and prevalence of a novel Gammaherpesvirus in Eptesicus fuscus, the North American big brown bat. *Virology* **3**, *516*, 227–238.
57. Gerow, C.M.; Rapin, N.; Voordouw, M.J.; Elliot, M.; Misra, V.; Subudhi, S. Arousal from hibernation and reactivation of *Eptesicus fuscus* gammaherpesvirus (*Ef* HV) in big brown bats. *Transboundary and Emerging Diseases* **2018**.
58. Liberto, M.C.; Zicca, E.; Pavia, G.; Quirino, A.; Marascio, N.; Torti, C.; Focà, A. Virological Mechanisms in the Coinfection between HIV and HCV. *Mediators Inflamm* **2015**, *2015*.
59. Verant, M.L.; Meteyer, C.U.; Speakman, J.R.; Cryan, P.M.; Lorch, J.M.; Blehert, D.S. White-nose syndrome initiates a cascade of physiologic disturbances in the hibernating bat host. *BMC physiology* **2014**, *14*, 10.
60. Warnecke, L.; Turner, J.M.; Bollinger, T.K.; Misra, V.; Cryan, P.M.; Blehert, D.S.; Wibbelt, G.; Willis, C.K. Pathophysiology of white-nose syndrome in bats: a mechanistic model linking wing damage to mortality. *Biology letters* **2013**, *9*, 20130177.
61. McGuire, L.P.; Mayberry, H.W.; Willis, C.K.R. White-nose syndrome increases torpid metabolic rate and evaporative water loss in hibernating bats. *Am J Physiol Regul Integr Comp Physiol* **2017**, *313*, R680–R686.
62. Davy, C.M.; Donaldson, M.E.; Subudhi, S.; Rapin, N.; Warnecke, L.; Turner, J.M.; Bollinger, T.K.; Kyle, C.J.; Dorville, N.A.S.; Kunkel, E.L.; et al. White-nose syndrome is associated with increased replication of a naturally persisting coronaviruses in bats. *Sci Rep* **2018**, *8*, 15508.
63. Olival, K.J.; Hosseini, P.R.; Zambrana-Torrelio, C.; Ross, N.; Bogich, T.L.; Daszak, P. Host and viral traits predict zoonotic spillover from mammals. *Nature* **6**, *546*, 646–650.
64. Kumar, N.; Kulkarni, D.D.; Lee, B.; Kaushik, R.; Bhatia, S.; Sood, R.; Pateriya, A.K.; Bhat, S.; Singh, V.P. Evolution of Codon Usage Bias in Henipaviruses Is Governed by Natural Selection and Is Host-Specific. *Viruses* **2018**, *10*, 604.

65. Behura, S.K.; Severson, D.W. Codon usage bias: causative factors, quantification methods and genome-wide patterns: with emphasis on insect genomes. *Biol Rev Camb Philos Soc* **2013**, *88*, 49–61.
66. Lau, S.K.P.; Zhang, L.; Luk, H.K.H.; Xiong, L.; Peng, X.; Li, K.S.M.; He, X.; Zhao, P.S.-H.; Fan, R.Y.Y.; Wong, A.C.P.; et al. Receptor Usage of a Novel Bat Lineage C Betacoronavirus Reveals Evolution of Middle East Respiratory Syndrome-Related Coronavirus Spike Proteins for Human Dipeptidyl Peptidase 4 Binding. *J Infect Dis* **2018**, *218*, 197–207.
67. Yang, Y.; Du, L.; Liu, C.; Wang, L.; Ma, C.; Tang, J.; Baric, R.S.; Jiang, S.; Li, F. Receptor usage and cell entry of bat coronavirus HKU4 provide insight into bat-to-human transmission of MERS coronavirus. *Proc Natl Acad Sci U S A* **2014**, *111*, 12516–21.
68. Huang, C.; Qi, J.; Lu, G.; Wang, Q.; Yuan, Y.; Wu, Y.; Zhang, Y.; Yan, J.; Gao, G.F. Putative Receptor Binding Domain of Bat-Derived Coronavirus HKU9 Spike Protein: Evolution of Betacoronavirus Receptor Binding Motifs. *Biochemistry* **2016**, *55*, 5977–5988.
69. Barbour, R.W.; Davis, W.H. *Bats of America*; University Press of Kentucky: Lexington, 1969; ISBN 978-0-8131-1186-5.
70. Jones, J.K. Hill, J. E., and J. D. Smith. Bats: A Natural History. Univ. Texas Press, Austin, 243 pp., illustrated, 1984. Price (hardbound), $24.95. *J Mammal* **1985**, *66*, 424–425.
71. BATS Magazine Article: The Oldest Bat Available online: http://www.batcon.org/resources/media-education/bats-magazine/bat_article/152 (accessed on Mar 9, 2019).
72. Bats in North America Available online: http://www.umich.edu/~esupdate/library/96.04-05/bogan.html (accessed on Mar 9, 2019).
73. Jones, J.K. Hall, E. R. THE MAMMALS OF NORTH AMERICA. 2nd ed. John Wiley and Sons, New York, 1:xv + 1-600 + 90 and 2:vi + 601-1181 + 90, illustrated. 1981. $80.00. *Journal of Mammalogy* **1982**, *63*, 717–717.
74. Ammerman, L.K.; Hice, C.L.; Schmidly, D.J. *Bats of Texas*; W.L. Moody Jr. natural history series; 1st ed.; Texas A&M University Press: College Station, 2012; ISBN 978-1-60344-476-7.
75. Ross, A. Ecological aspects of the food habits of insectivorous bats.; Western Foundation of Vertebrate Zoology, 1967.
76. Tuttle, M.D. *America's neighborhood bats*; 2nd rev. ed.; University of Texas Press: Austin, 2005; ISBN 978-0-292-71280-5.
77. David M. Knipe, P.M.H. *Fields Virology - sixth edition*; Lippincott Williams & Wilkins: Philadelphia, PA, USA, 2013;
78. Fehr, A.R.; Perlman, S. Coronaviruses: An Overview of Their Replication and Pathogenesis. In *Coronaviruses*; Maier, H.J., Bickerton, E., Britton, P., Eds.; Springer New York: New York, NY, 2015; Vol. 1282, pp. 1–23 ISBN 978-1-4939-2437-0.
79. Woo, P.C.; Lau, S.K.; Lam, C.S.; Lau, C.C.; Tsang, A.K.; Lau, J.H.; Bai, R.; Teng, J.L.; Tsang, C.C.; Wang, M.; et al. Discovery of seven novel Mammalian and avian coronaviruses in the genus deltacoronavirus supports bat coronaviruses as the gene source of alphacoronavirus and betacoronavirus and avian coronaviruses as the gene source of gammacoronavirus and deltacoronavirus. *J Virol* **2012**, *86*, 3995–4008.
80. Ar Gouilh, M.; Puechmaille, S.J.; Diancourt, L.; Vandenbogaert, M.; Serra-Cobo, J.; Lopez Roïg, M.; Brown, P.; Moutou, F.; Caro, V.; Vabret, A.; et al. SARS-CoV related Betacoronavirus and diverse Alphacoronavirus members found in western old-world. *Virology* **2018**, *517*, 88–97.

81. Lin, X.-D.; Wang, W.; Hao, Z.-Y.; Wang, Z.-X.; Guo, W.-P.; Guan, X.-Q.; Wang, M.-R.; Wang, H.-W.; Zhou, R.-H.; Li, M.-H.; et al. Extensive diversity of coronaviruses in bats from China. *Virology* **2017**, *507*, 1–10.
82. Menachery, V.D.; Graham, R.L.; Baric, R.S. Jumping species-a mechanism for coronavirus persistence and survival. *Curr Opin Virol* **4**, *23*, 1–7.
83. Barcena, M.; Oostergetel, G.T.; Bartelink, W.; Faas, F.G.A.; Verkleij, A.; Rottier, P.J.M.; Koster, A.J.; Bosch, B.J. Cryo-electron tomography of mouse hepatitis virus: Insights into the structure of the coronavirion. *Proceedings of the National Academy of Sciences* **2009**, *106*, 582–587.
84. Bosch, B.J.; van der Zee, R.; de Haan, C.A.M.; Rottier, P.J.M. The Coronavirus Spike Protein Is a Class I Virus Fusion Protein: Structural and Functional Characterization of the Fusion Core Complex. *Journal of Virology* **2003**, *77*, 8801–8811.
85. Millet, J.K.; Whittaker, G.R. Host cell proteases: Critical determinants of coronavirus tropism and pathogenesis. *Virus Research* **2015**, *202*, 120–134.
86. Neuman, B.W.; Kiss, G.; Kunding, A.H.; Bhella, D.; Baksh, M.F.; Connelly, S.; Droese, B.; Klaus, J.P.; Makino, S.; Sawicki, S.G.; et al. A structural analysis of M protein in coronavirus assembly and morphology. *Journal of Structural Biology* **2011**, *174*, 11–22.
87. Nieto-Torres, J.L.; DeDiego, M.L.; Verdia-Baguena, C.; Jimenez-Guardeno, J.M.; Regla-Nava, J.A.; Fernandez-Delgado, R.; Castano-Rodriguez, C.; Alcaraz, A.; Torres, J.; Aguilella, V.M.; et al. Severe acute respiratory syndrome coronavirus envelope protein ion channel activity promotes virus fitness and pathogenesis. *PLoS Pathog* **2014**, *10*, e1004077.
88. Molenkamp, R.; Spaan, W.J. Identification of a specific interaction between the coronavirus mouse hepatitis virus A59 nucleocapsid protein and packaging signal. *Virology* **1997**, *239*, 78–86.
89. Kazi, L.; Lissenberg, A.; Watson, R.; de Groot, R.J.; Weiss, S.R. Expression of hemagglutinin esterase protein from recombinant mouse hepatitis virus enhances neurovirulence. *J. Virol.* **2005**, *79*, 15064–15073.
90. Yeager, C.L.; Ashmun, R.A.; Williams, R.K.; Cardellichio, C.B.; Shapiro, L.H.; Look, A.T.; Holmes, K.V. Human aminopeptidase N is a receptor for human coronavirus 229E. *Nature* **1992**, *357*, 420–2.
91. Li, W.; Moore, M.J.; Vasilieva, N.; Sui, J.; Wong, S.K.; Berne, M.A.; Somasundaran, M.; Sullivan, J.L.; Luzuriaga, K.; Greenough, T.C.; et al. Angiotensin-converting enzyme 2 is a functional receptor for the SARS coronavirus. *Nature* **2003**, *426*, 450–454.
92. Hofmann, H.; Pyrc, K.; van der Hoek, L.; Geier, M.; Berkhout, B.; Pöhlmann, S. Human coronavirus NL63 employs the severe acute respiratory syndrome coronavirus receptor for cellular entry. *Proc. Natl. Acad. Sci. U.S.A.* **2005**, *102*, 7988–7993.
93. Nédellec, P.; Dveksler, G.S.; Daniels, E.; Turbide, C.; Chow, B.; Basile, A.A.; Holmes, K.V.; Beauchemin, N. Bgp2, a new member of the carcinoembryonic antigen-related gene family, encodes an alternative receptor for mouse hepatitis viruses. *J. Virol.* **1994**, *68*, 4525–4537.
94. Raj, V.S.; Mou, H.; Smits, S.L.; Dekkers, D.H.W.; Müller, M.A.; Dijkman, R.; Muth, D.; Demmers, J.A.A.; Zaki, A.; Fouchier, R.A.M.; et al. Dipeptidyl peptidase 4 is a functional receptor for the emerging human coronavirus-EMC. *Nature* **2013**, *495*, 251–254.
95. Belouzard, S.; Chu, V.C.; Whittaker, G.R. Activation of the SARS coronavirus spike protein via sequential proteolytic cleavage at two distinct sites. *Proceedings of the National Academy of Sciences* **2009**, *106*, 5871–5876.

96. Baranov, P.V.; Henderson, C.M.; Anderson, C.B.; Gesteland, R.F.; Atkins, J.F.; Howard, M.T. Programmed ribosomal frameshifting in decoding the SARS-CoV genome. *Virology* **2005**, *332*, 498–510.
97. Brierley, I.; Digard, P.; Inglis, S.C. Characterization of an efficient coronavirus ribosomal frameshifting signal: requirement for an RNA pseudoknot. *Cell* **1989**, *57*, 537–547.
98. Sawicki, S.G.; Sawicki, D.L.; Siddell, S.G. A contemporary view of coronavirus transcription. *J Virol* **2007**, *81*, 20–9.
99. Sethna, P.B.; Hofmann, M.A.; Brian, D.A. Minus-strand copies of replicating coronavirus mRNAs contain antileaders. *J. Virol.* **1991**, *65*, 320–325.
100. Keck, J.G.; Makino, S.; Soe, L.H.; Fleming, J.O.; Stohlman, S.A.; Lai, M.M. RNA recombination of coronavirus. *Adv. Exp. Med. Biol.* **1987**, *218*, 99–107.
101. Krijnse-Locker, J.; Ericsson, M.; Rottier, P.J.; Griffiths, G. Characterization of the budding compartment of mouse hepatitis virus: evidence that transport from the RER to the Golgi complex requires only one vesicular transport step. *J. Cell Biol.* **1994**, *124*, 55–70.
102. Tooze, J.; Tooze, S.; Warren, G. Replication of coronavirus MHV-A59 in sac- cells: determination of the first site of budding of progeny virions. *Eur. J. Cell Biol.* **1984**, *33*, 281–293.
103. Hurst, K.R.; Kuo, L.; Koetzner, C.A.; Ye, R.; Hsue, B.; Masters, P.S. A major determinant for membrane protein interaction localizes to the carboxy-terminal domain of the mouse coronavirus nucleocapsid protein. *J. Virol.* **2005**, *79*, 13285–13297.
104. Collins, A.R. Induction of apoptosis in MRC-5, diploid human fetal lung cells after infection with human coronavirus OC43. *Adv. Exp. Med. Biol.* **2001**, *494*, 677–682.
105. Mesel-Lemoine, M.; Millet, J.; Vidalain, P.-O.; Law, H.; Vabret, A.; Lorin, V.; Escriou, N.; Albert, M.L.; Nal, B.; Tangy, F. A Human Coronavirus Responsible for the Common Cold Massively Kills Dendritic Cells but Not Monocytes. *Journal of Virology* **2012**, *86*, 7577–7587.
106. Benedict, C.A.; Norris, P.S.; Ware, C.F. To kill or be killed: viral evasion of apoptosis. *Nature Immunology* **2002**, *3*, 1013–1018.
107. Lim, Y.; Ng, Y.; Tam, J.; Liu, D. Human Coronaviruses: A Review of Virus–Host Interactions. *Diseases* **2016**, *4*, 26.
108. DeDiego, M.L.; Nieto-Torres, J.L.; Jiménez-Guardeño, J.M.; Regla-Nava, J.A.; Álvarez, E.; Oliveros, J.C.; Zhao, J.; Fett, C.; Perlman, S.; Enjuanes, L. Severe Acute Respiratory Syndrome Coronavirus Envelope Protein Regulates Cell Stress Response and Apoptosis. *PLoS Pathogens* **2011**, *7*, e1002315.
109. Ye, Z.; Wong, C.K.; Li, P.; Xie, Y. A SARS-CoV protein, ORF-6, induces caspase-3 mediated, ER stress and JNK-dependent apoptosis. *Biochimica et Biophysica Acta (BBA) - General Subjects* **2008**, *1780*, 1383–1387.
110. Surjit, M.; Liu, B.; Jameel, S.; Chow, V.T.K.; Lal, S.K. The SARS coronavirus nucleocapsid protein induces actin reorganization and apoptosis in COS-1 cells in the absence of growth factors. *Biochemical Journal* **2004**, *383*, 13–18.
111. Kanneganti, T.-D. Central roles of NLRs and inflammasomes in viral infection. *Nature Reviews Immunology* **2010**, *10*, 688–698.
112. Randall, R.E.; Goodbourn, S. Interferons and viruses: an interplay between induction, signalling, antiviral responses and virus countermeasures. *Journal of General Virology* **2008**, *89*, 1–47.

113. Clementz, M.A.; Chen, Z.; Banach, B.S.; Wang, Y.; Sun, L.; Ratia, K.; Baez-Santos, Y.M.; Wang, J.; Takayama, J.; Ghosh, A.K.; et al. Deubiquitinating and Interferon Antagonism Activities of Coronavirus Papain-Like Proteases. *Journal of Virology* **2010**, *84*, 4619–4629.
114. Lau, S.K.P.; Lau, C.C.Y.; Chan, K.-H.; Li, C.P.Y.; Chen, H.; Jin, D.-Y.; Chan, J.F.W.; Woo, P.C.Y.; Yuen, K.-Y. Delayed induction of proinflammatory cytokines and suppression of innate antiviral response by the novel Middle East respiratory syndrome coronavirus: implications for pathogenesis and treatment. *Journal of General Virology* **2013**, *94*, 2679–2690.
115. Frieman, M.; Heise, M.; Baric, R. SARS coronavirus and innate immunity. *Virus Research* **2008**, *133*, 101–112.
116. Cargnello, M.; Roux, P.P. Activation and Function of the MAPKs and Their Substrates, the MAPK-Activated Protein Kinases. *Microbiology and Molecular Biology Reviews* **2011**, *75*, 50–83.
117. Kono, M.; Tatsumi, K.; Imai, A.M.; Saito, K.; Kuriyama, T.; Shirasawa, H. Inhibition of human coronavirus 229E infection in human epithelial lung cells (L132) by chloroquine: Involvement of p38 MAPK and ERK. *Antiviral Research* **2008**, *77*, 150–152.
118. Fung, T.S.; Liu, D.X. Coronavirus infection, ER stress, apoptosis and innate immunity. *Frontiers in Microbiology* **2014**, *5*.
119. Stevens, F.J.; Argon, Y. Protein folding in the ER. *Seminars in Cell & Developmental Biology* **1999**, *10*, 443–454.
120. Ron, D.; Walter, P. Signal integration in the endoplasmic reticulum unfolded protein response. *Nat Rev Mol Cell Biol* **2007**, *8*, 519–29.
121. Chakrabarti, A.; Chen, A.W.; Varner, J.D. A review of the mammalian unfolded protein response. *Biotechnology and Bioengineering* **2011**, *108*, 2777–2793.
122. Perlman, S.; Netland, J. Coronaviruses post-SARS: update on replication and pathogenesis. *Nature Reviews Microbiology* **2009**, *7*, 439–450.
123. WHO updates on MERS Available online: http://www.who.int/emergencies/mers-cov/en/.
124. van der Hoek, L.; Pyrc, K.; Jebbink, M.F.; Vermeulen-Oost, W.; Berkhout, R.J.M.; Wolthers, K.C.; Wertheim-van Dillen, P.M.E.; Kaandorp, J.; Spaargaren, J.; Berkhout, B. Identification of a new human coronavirus. *Nat. Med.* **2004**, *10*, 368–373.
125. Wu, G.F.; Dandekar, A.A.; Pewe, L.; Perlman, S. CD4 and CD8 T cells have redundant but not identical roles in virus-induced demyelination. *J. Immunol.* **2000**, *165*, 2278–2286.
126. Weiner, L.P. Pathogenesis of demyelination induced by a mouse hepatitis. *Arch. Neurol.* **1973**, *28*, 298–303.
127. Wang, Q.; Vlasova, A.N.; Kenney, S.P.; Saif, L.J. Emerging and re-emerging coronaviruses in pigs. *Curr Opin Virol* **2019**, *34*, 39–49.
128. Tekes, G.; Thiel, H.-J. Feline Coronaviruses: Pathogenesis of Feline Infectious Peritonitis. *Adv. Virus Res.* **2016**, *96*, 193–218.
129. Bande, F.; Arshad, S.S.; Omar, A.R.; Bejo, M.H.; Abubakar, M.S.; Abba, Y. Pathogenesis and Diagnostic Approaches of Avian Infectious Bronchitis. *Adv Virol* **2016**, *2016*, 4621659.
130. Müller, M.A.; Corman, V.M.; Jores, J.; Meyer, B.; Younan, M.; Liljander, A.; Bosch, B.-J.; Lattwein, E.; Hilali, M.; Musa, B.E.; et al. MERS coronavirus neutralizing antibodies in camels, Eastern Africa, 1983-1997. *Emerging Infect. Dis.* **2014**, *20*, 2093–2095.
131. Huynh, J.; Li, S.; Yount, B.; Smith, A.; Sturges, L.; Olsen, J.C.; Nagel, J.; Johnson, J.B.; Agnihothram, S.; Gates, J.E.; et al. Evidence supporting a zoonotic origin of human coronavirus strain NL63. *J. Virol.* **2012**, *86*, 12816–12825.

132. Tao, Y.; Shi, M.; Chommanard, C.; Queen, K.; Zhang, J.; Markotter, W.; Kuzmin, I.V.; Holmes, E.C.; Tong, S. Surveillance of Bat Coronaviruses in Kenya Identifies Relatives of Human Coronaviruses NL63 and 229E and Their Recombination History. *J. Virol.* **2017**, *91*.
133. Zhou, P.; Fan, H.; Lan, T.; Yang, X.L.; Shi, W.F.; Zhang, W.; Zhu, Y.; Zhang, Y.W.; Xie, Q.M.; Mani, S.; et al. Fatal swine acute diarrhoea syndrome caused by an HKU2-related coronavirus of bat origin. *Nature* **2018**, *556*, 255–258.
134. Vogel, L.; Van der Lubben, M.; Te Lintelo, E.G.; Bekker, C.P.J.; Geerts, T.; Schuijff, L.S.; Grinwis, G.C.M.; Egberink, H.F.; Rottier, P.J.M. Pathogenic characteristics of persistent feline enteric coronavirus infection in cats. *Veterinary Research* **2010**, *41*, 71.
135. Ehmann, R.; Kristen-Burmann, C.; Bank-Wolf, B.; König, M.; Herden, C.; Hain, T.; Thiel, H.-J.; Ziebuhr, J.; Tekes, G. Reverse Genetics for Type I Feline Coronavirus Field Isolate To Study the Molecular Pathogenesis of Feline Infectious Peritonitis. *mBio* **2018**, *9*.
136. Marks, S.L. Rational Approach to Diagnosing and Managing Infectious Causes of Diarrhea in Kittens. In *August's Consultations in Feline Internal Medicine, Volume 7*; Elsevier, 2016; pp. 1–22 ISBN 978-0-323-22652-3.
137. Kapil, S.; Trent, A.M.; Goyal, S.M. Excretion and persistence of bovine coronavirus in neonatal calves. *Arch. Virol.* **1990**, *115*, 127–132.
138. Arbour, N.; Côté, G.; Lachance, C.; Tardieu, M.; Cashman, N.R.; Talbot, P.J. Acute and persistent infection of human neural cell lines by human coronavirus OC43. *J. Virol.* **1999**, *73*, 3338–3350.
139. Arbour, N.; Ekande, S.; Cote, G.; Lachance, C.; Chagnon, F.; Tardieu, M.; Cashman, N.R.; Talbot, P.J. Persistent infection of human oligodendrocytic and neuroglial cell lines by human coronavirus 229E. *Journal of virology* **1999**, *73*, 3326–37.
140. Wu, D.; Tu, C.; Xin, C.; Xuan, H.; Meng, Q.; Liu, Y.; Yu, Y.; Guan, Y.; Jiang, Y.; Yin, X.; et al. Civets Are Equally Susceptible to Experimental Infection by Two Different Severe Acute Respiratory Syndrome Coronavirus Isolates. *Journal of Virology* **2005**, *79*, 2620–2625.
141. Azhar, E.I.; El-Kafrawy, S.A.; Farraj, S.A.; Hassan, A.M.; Al-Saeed, M.S.; Hashem, A.M.; Madani, T.A. Evidence for camel-to-human transmission of MERS coronavirus. *N. Engl. J. Med.* **2014**, *370*, 2499–2505.
142. Adney, D.R.; van Doremalen, N.; Brown, V.R.; Bushmaker, T.; Scott, D.; de Wit, E.; Bowen, R.A.; Munster, V.J. Replication and shedding of MERS-CoV in upper respiratory tract of inoculated dromedary camels. *Emerging Infect. Dis.* **2014**, *20*, 1999–2005.
143. Zheng, X.Y.; Qiu, M.; Chen, S.W.; Xiao, J.P.; Ma, L.Z.; Liu, S.; Zhou, J.H.; Zhang, Q.H.; Li, X.; Chen, Z.; et al. High prevalence and diversity of viruses of the subfamily Gammaherpesvirinae, family Herpesviridae, in fecal specimens from bats of different species in southern China. *Arch Virol* **2016**, *161*, 135–40.
144. Mühldorfer, K.; Speck, S.; Kurth, A.; Lesnik, R.; Freuling, C.; Müller, T.; Kramer-Schadt, S.; Wibbelt, G. Diseases and causes of death in European bats: dynamics in disease susceptibility and infection rates. *PLoS ONE* **2011**, *6*, e29773.
145. Sano, K.; Okazaki, S.; Taniguchi, S.; Masangkay, J.S.; Puentespina, R.; Eres, E.; Cosico, E.; Quibod, N.; Kondo, T.; Shimoda, H.; et al. Detection of a novel herpesvirus from bats in the Philippines. *Virus Genes* **2015**, *51*, 136–139.
146. Jánoska, M.; Vidovszky, M.; Molnár, V.; Liptovszky, M.; Harrach, B.; Benko, M. Novel adenoviruses and herpesviruses detected in bats. *Vet. J.* **2011**, *189*, 118–121.

147. Shabman, R.S.; Shrivastava, S.; Tsibane, T.; Attie, O.; Jayaprakash, A.; Mire, C.E.; Dilley, K.E.; Puri, V.; Stockwell, T.B.; Geisbert, T.W.; et al. Isolation and Characterization of a Novel Gammaherpesvirus from a Microbat Cell Line. *mSphere* **2016**, *1*.
148. Chakraborty, S.; Veettil, M.V.; Bottero, V.; Chandran, B. Kaposi's sarcoma-associated herpesvirus interacts with EphrinA2 receptor to amplify signaling essential for productive infection. *Proc. Natl. Acad. Sci. U.S.A.* **2012**, *109*, E1163-1172.
149. D'Addario, M.; Libermann, T.A.; Xu, J.; Ahmad, A.; Menezes, J. Epstein-Barr Virus and its glycoprotein-350 upregulate IL-6 in human B-lymphocytes via CD21, involving activation of NF-kappaB and different signaling pathways. *J. Mol. Biol.* **2001**, *308*, 501–514.
150. Bhatt, A.P.; Damania, B. AKTivation of PI3K/AKT/mTOR signaling pathway by KSHV. *Front Immunol* **2012**, *3*, 401.
151. Loftus, M.S.; Verville, N.; Kedes, D.H. A Conserved Leucine Zipper Motif in Gammaherpesvirus ORF52 Is Critical for Distinct Microtubule Rearrangements. *J. Virol.* **2017**, *91*.
152. Sodeik, B.; Ebersold, M.W.; Helenius, A. Microtubule-mediated Transport of Incoming Herpes Simplex Virus 1 Capsids to the Nucleus. *J Cell Biol* **1997**, *136*, 1007–1021.
153. Fay, N.; Panté, N. Nuclear entry of DNA viruses. *Front Microbiol* **2015**, *6*.
154. Kerur, N.; Veettil, M.V.; Sharma-Walia, N.; Bottero, V.; Sadagopan, S.; Otageri, P.; Chandran, B. IFI16 acts as a nuclear pathogen sensor to induce the inflammasome in response to Kaposi Sarcoma-associated herpesvirus infection. *Cell Host Microbe* **2011**, *9*, 363–375.
155. Tsai, K.; Messick, T.E.; Lieberman, P.M. Disruption of Host Antiviral Resistances by Gammaherpesvirus Tegument Proteins with Homology to the FGARAT Purine Biosynthesis Enzyme. *Curr Opin Virol* **2015**, *14*, 30–40.
156. Rowe, M.; Rowe, D.T.; Gregory, C.D.; Young, L.S.; Farrell, P.J.; Rupani, H.; Rickinson, A.B. Differences in B cell growth phenotype reflect novel patterns of Epstein-Barr virus latent gene expression in Burkitt's lymphoma cells. *EMBO J.* **1987**, *6*, 2743–2751.
157. Babcock, G.J.; Hochberg, D.; Thorley-Lawson, A.D. The expression pattern of Epstein-Barr virus latent genes in vivo is dependent upon the differentiation stage of the infected B cell. *Immunity* **2000**, *13*, 497–506.
158. Aneja, K.K.; Yuan, Y. Reactivation and Lytic Replication of Kaposi's Sarcoma-Associated Herpesvirus: An Update. *Frontiers in Microbiology* **2017**, *8*.
159. Lukac, D.M.; Yuan, Y. Reactivation and lytic replication of KSHV. In *Human Herpesviruses: Biology, Therapy, and Immunoprophylaxis*; Arvin, A., Campadelli-Fiume, G., Mocarski, E., Moore, P.S., Roizman, B., Whitley, R., Yamanishi, K., Eds.; Cambridge University Press: Cambridge, 2007 ISBN 978-0-521-82714-0.
160. Cohen, A.; Brodie, C.; Sarid, R. An essential role of ERK signalling in TPA-induced reactivation of Kaposi's sarcoma-associated herpesvirus. *J. Gen. Virol.* **2006**, *87*, 795–802.
161. Gwack, Y.; Byun, H.; Hwang, S.; Lim, C.; Choe, J. CREB-binding protein and histone deacetylase regulate the transcriptional activity of Kaposi's sarcoma-associated herpesvirus open reading frame 50. *J. Virol.* **2001**, *75*, 1909–1917.
162. Liang, Y.; Chang, J.; Lynch, S.J.; Lukac, D.M.; Ganem, D. The lytic switch protein of KSHV activates gene expression via functional interaction with RBP-Jkappa (CSL), the target of the Notch signaling pathway. *Genes Dev.* **2002**, *16*, 1977–1989.
163. Grey, F. Role of microRNAs in herpesvirus latency and persistence. *J. Gen. Virol.* **2015**, *96*, 739–751.

164. Purushothaman, P.; Dabral, P.; Gupta, N.; Sarkar, R.; Verma, S.C. KSHV Genome Replication and Maintenance. *Frontiers in Microbiology* **2016**, *7*.
165. Feng, P.; Moses, A.; Früh, K. Evasion of adaptive and innate immune response mechanisms by γ-herpesviruses. *Current Opinion in Virology* **2013**, *3*, 285–295.
166. Blake, N. Immune evasion by gammaherpesvirus genome maintenance proteins. *Journal of General Virology* **2010**, *91*, 829–846.
167. Levitskaya, J.; Sharipo, A.; Leonchiks, A.; Ciechanover, A.; Masucci, M.G. Inhibition of ubiquitin/proteasome-dependent protein degradation by the Gly-Ala repeat domain of the Epstein-Barr virus nuclear antigen 1. *Proc. Natl. Acad. Sci. U.S.A.* **1997**, *94*, 12616–12621.
168. Daskalogianni, C.; Apcher, S.; Candeias, M.M.; Naski, N.; Calvo, F.; Fåhraeus, R. Gly-Ala Repeats Induce Position- and Substrate-specific Regulation of 26 S Proteasome-dependent Partial Processing. *Journal of Biological Chemistry* **2008**, *283*, 30090–30100.
169. Kwun, H.J.; da Silva, S.R.; Shah, I.M.; Blake, N.; Moore, P.S.; Chang, Y. Kaposi's sarcoma-associated herpesvirus latency-associated nuclear antigen 1 mimics Epstein-Barr virus EBNA1 immune evasion through central repeat domain effects on protein processing. *J. Virol.* **2007**, *81*, 8225–8235.
170. Gao, J.; Coulson, J.M.; Whitehouse, A.; Blake, N. Reduction in RNA Levels Rather than Retardation of Translation Is Responsible for the Inhibition of Major Histocompatibility Complex Class I Antigen Presentation by the Glutamic Acid-Rich Repeat of Herpesvirus Saimiri Open Reading Frame 73. *Journal of Virology* **2009**, *83*, 273–282.
171. Bennett, N.J.; May, J.S.; Stevenson, P.G. Gamma-herpesvirus latency requires T cell evasion during episome maintenance. *PLoS Biol.* **2005**, *3*, e120.
172. Ressing, M.E.; Horst, D.; Griffin, B.D.; Tellam, J.; Zuo, J.; Khanna, R.; Rowe, M.; Wiertz, E.J.H.J. Epstein-Barr virus evasion of CD8+ and CD4+ T cell immunity via concerted actions of multiple gene products. *Seminars in Cancer Biology* **2008**, *18*, 397–408.
173. Jochum, S.; Moosmann, A.; Lang, S.; Hammerschmidt, W.; Zeidler, R. The EBV Immunoevasins vIL-10 and BNLF2a Protect Newly Infected B Cells from Immune Recognition and Elimination. *PLoS Pathogens* **2012**, *8*, e1002704.
174. Wycisk, A.I.; Lin, J.; Loch, S.; Hobohm, K.; Funke, J.; Wieneke, R.; Koch, J.; Skach, W.R.; Mayerhofer, P.U.; Tampé, R. Epstein-Barr Viral BNLF2a Protein Hijacks the Tail-anchored Protein Insertion Machinery to Block Antigen Processing by the Transport Complex TAP. *Journal of Biological Chemistry* **2011**, *286*, 41402–41412.
175. Zuo, J.; Quinn, L.L.; Tamblyn, J.; Thomas, W.A.; Feederle, R.; Delecluse, H.-J.; Hislop, A.D.; Rowe, M. The Epstein-Barr Virus-Encoded BILF1 Protein Modulates Immune Recognition of Endogenously Processed Antigen by Targeting Major Histocompatibility Complex Class I Molecules Trafficking on both the Exocytic and Endocytic Pathways. *Journal of Virology* **2011**, *85*, 1604–1614.
176. Schmidt, K.; Wies, E.; Neipel, F. Kaposi's Sarcoma-Associated Herpesvirus Viral Interferon Regulatory Factor 3 Inhibits Gamma Interferon and Major Histocompatibility Complex Class II Expression. *Journal of Virology* **2011**, *85*, 4530–4537.
177. Butler, L.M.; Jeffery, H.C.; Wheat, R.L.; Long, H.M.; Rae, P.C.; Nash, G.B.; Blackbourn, D.J. Kaposi's Sarcoma-Associated Herpesvirus Inhibits Expression and Function of Endothelial Cell Major Histocompatibility Complex Class II via Suppressor of Cytokine Signaling 3. *Journal of Virology* **2012**, *86*, 7158–7166.

178. E, X.; Hwang, S.; Oh, S.; Lee, J.-S.; Jeong, J.H.; Gwack, Y.; Kowalik, T.F.; Sun, R.; Jung, J.U.; Liang, C. Viral Bcl-2-Mediated Evasion of Autophagy Aids Chronic Infection of γHerpesvirus 68. *PLoS Pathogens* **2009**, *5*, e1000609.
179. Altmann, M.; Hammerschmidt, W. Epstein-Barr virus provides a new paradigm: a requirement for the immediate inhibition of apoptosis. *PLoS Biol.* **2005**, *3*, e404.
180. Feng, P.; Liang, C.; Shin, Y.C.; E, X.; Zhang, W.; Gravel, R.; Wu, T.; Sun, R.; Usherwood, E.; Jung, J.U. A Novel Inhibitory Mechanism of Mitochondrion-Dependent Apoptosis by a Herpesviral Protein. *PLoS Pathogens* **2007**, *3*, e174.
181. Feng, P.; Park, J.; Lee, B.-S.; Lee, S.-H.; Bram, R.J.; Jung, J.U. Kaposi's Sarcoma-Associated Herpesvirus Mitochondrial K7 Protein Targets a Cellular Calcium-Modulating Cyclophilin Ligand To Modulate Intracellular Calcium Concentration and Inhibit Apoptosis. *Journal of Virology* **2002**, *76*, 11491–11504.
182. Pattingre, S.; Tassa, A.; Qu, X.; Garuti, R.; Liang, X.H.; Mizushima, N.; Packer, M.; Schneider, M.D.; Levine, B. Bcl-2 antiapoptotic proteins inhibit Beclin 1-dependent autophagy. *Cell* **2005**, *122*, 927–39.
183. Leidal, A.M.; Cyr, D.P.; Hill, R.J.; Lee, P.W.K.; McCormick, C. Subversion of Autophagy by Kaposi's Sarcoma-Associated Herpesvirus Impairs Oncogene-Induced Senescence. *Cell Host & Microbe* **2012**, *11*, 167–180.
184. de Weerd, N.A.; Nguyen, T. The interferons and their receptors-distribution and regulation. *Immunology and Cell Biology* **2012**, *90*, 483–491.
185. Kawai, T.; Akira, S. Innate immune recognition of viral infection. *Nature Immunology* **2006**, *7*, 131–137.
186. Inn, K.-S.; Lee, S.-H.; Rathbun, J.Y.; Wong, L.-Y.; Toth, Z.; Machida, K.; Ou, J.-H.J.; Jung, J.U. Inhibition of RIG-I-Mediated Signaling by Kaposi's Sarcoma-Associated Herpesvirus-Encoded Deubiquitinase ORF64. *Journal of Virology* **2011**, *85*, 10899–10904.
187. Cieniewicz, B.; Santana, A.L.; Minkah, N.; Krug, L.T. Interplay of Murine Gammaherpesvirus 68 with NF-kappaB Signaling of the Host. *Frontiers in Microbiology* **2016**, *7*.
188. Misra, V.; Dumonceaux, T.; Dubois, J.; Willis, C.; Nadin-Davis, S.; Severini, A.; Wandeler, A.; Lindsay, R.; Artsob, H. Detection of polyoma and corona viruses in bats of Canada. *The Journal of general virology* **2009**, *90*, 2015–22.
189. Warnecke, L.; Turner, J.M.; Bollinger, T.K.; Lorch, J.M.; Misra, V.; Cryan, P.M.; Wibbelt, G.; Blehert, D.S.; Willis, C.K. Inoculation of bats with European Geomyces destructans supports the novel pathogen hypothesis for the origin of white-nose syndrome. *Proceedings of the National Academy of Sciences of the United States of America* **2012**, *109*, 6999–7003.
190. Ge, X.Y.; Li, J.L.; Yang, X.L.; Chmura, A.A.; Zhu, G.; Epstein, J.H.; Mazet, J.K.; Hu, B.; Zhang, W.; Peng, C.; et al. Isolation and characterization of a bat SARS-like coronavirus that uses the ACE2 receptor. *Nature* **2013**, *503*, 535–8.
191. Corman, V.M.; Ithete, N.L.; Richards, L.R.; Schoeman, M.C.; Preiser, W.; Drosten, C.; Drexler, J.F. Rooting the phylogenetic tree of middle East respiratory syndrome coronavirus by characterization of a conspecific virus from an African bat. *J Virol* **2014**, *88*, 11297–303.
192. Ithete, N.L.; Stoffberg, S.; Corman, V.M.; Cottontail, V.M.; Richards, L.R.; Schoeman, M.C.; Drosten, C.; Drexler, J.F.; Preiser, W. Close relative of human Middle East respiratory syndrome coronavirus in bat, South Africa. *Emerg Infect Dis* **2013**, *19*, 1697–9.

193. Memish, Z.A.; Mishra, N.; Olival, K.J.; Fagbo, S.F.; Kapoor, V.; Epstein, J.H.; Alhakeem, R.; Durosinloun, A.; Al Asmari, M.; Islam, A.; et al. Middle East respiratory syndrome coronavirus in bats, Saudi Arabia. *Emerging infectious diseases* **2013**, *19*, 1819–23.
194. Summary of probable SARS cases with onset of illness from 1 November 2002 to 31 July 2003 Available online: http://www.who.int/csr/sars/country/table2004_04_21/en/.
195. Huang, Y.W.; Dickerman, A.W.; Pineyro, P.; Li, L.; Fang, L.; Kiehne, R.; Opriessnig, T.; Meng, X.J. Origin, evolution, and genotyping of emergent porcine epidemic diarrhea virus strains in the United States. *mBio* **2013**, *4*, e00737-13.
196. Paarlberg, P.L. UPDATED ESTIMATED ECONOMIC WELFARE IMPACTS OF PORCINE EPIDEMIC DIARRHEA VIRUS (PEDV). *Department of Agricultural Economics, Purdue University* **2014**.
197. Han, H.J.; Wen, H.L.; Zhou, C.M.; Chen, F.F.; Luo, L.M.; Liu, J.W.; Yu, X.J. Bats as reservoirs of severe emerging infectious diseases. *Virus Res* **2015**, *205*, 1–6.
198. Hu, B.; Ge, X.; Wang, L.F.; Shi, Z. Bat origin of human coronaviruses. *Virol J* **2015**, *12*, 221.
199. de Wit, E.; van Doremalen, N.; Falzarano, D.; Munster, V.J. SARS and MERS: recent insights into emerging coronaviruses. *Nat Rev Microbiol* **2016**, *14*, 523–34.
200. Watanabe, S.; Masangkay, J.S.; Nagata, N.; Morikawa, S.; Mizutani, T.; Fukushi, S.; Alviola, P.; Omatsu, T.; Ueda, N.; Iha, K.; et al. Bat coronaviruses and experimental infection of bats, the Philippines. *Emerg Infect Dis* **2010**, *16*, 1217–23.
201. Gu, J.; Korteweg, C. Pathology and pathogenesis of severe acute respiratory syndrome. *Am J Pathol* **2007**, *170*, 1136–47.
202. Singh, S.K. Middle East Respiratory Syndrome Virus Pathogenesis. *Semin Respir Crit Care Med* **2016**, *37*, 572–7.
203. Madson, D.M.; Magstadt, D.R.; Arruda, P.H.; Hoang, H.; Sun, D.; Bower, L.P.; Bhandari, M.; Burrough, E.R.; Gauger, P.C.; Pillatzki, A.E.; et al. Pathogenesis of porcine epidemic diarrhea virus isolate (US/Iowa/18984/2013) in 3-week-old weaned pigs. *Vet Microbiol* **2014**, *174*, 60–8.
204. Jung, K.; Saif, L.J. Porcine epidemic diarrhea virus infection: Etiology, epidemiology, pathogenesis and immunoprophylaxis. *Vet J* **2015**, *204*, 134–43.
205. McGuire, L.P.; Turner, J.M.; Warnecke, L.; McGregor, G.; Bollinger, T.K.; Misra, V.; Foster, J.T.; Frick, W.F.; Kilpatrick, A.M.; Willis, C.K. White-Nose Syndrome Disease Severity and a Comparison of Diagnostic Methods. *EcoHealth* **2016**, *13*, 60–71.
206. Andrews, S. FastQC: a quality control tool for high throughput sequence data. *Available online at: http://www.bioinformatics.babraham.ac.uk/projects/fastqc* **2010**.
207. Bolger, A.M.; Lohse, M.; Usadel, B. Trimmomatic: a flexible trimmer for Illumina sequence data. *Bioinformatics* **2014**, *30*, 2114–20.
208. Kim, D.; Pertea, G.; Trapnell, C.; Pimentel, H.; Kelley, R.; Salzberg, S.L. TopHat2: accurate alignment of transcriptomes in the presence of insertions, deletions and gene fusions. *Genome Biol* **2013**, *14*, R36.
209. Cunningham, F.; Amode, M.R.; Barrell, D.; Beal, K.; Billis, K.; Brent, S.; Carvalho-Silva, D.; Clapham, P.; Coates, G.; Fitzgerald, S.; et al. Ensembl 2015. *Nucleic Acids Res* **2015**, *43*, D662-9.
210. Li, H.; Handsaker, B.; Wysoker, A.; Fennell, T.; Ruan, J.; Homer, N.; Marth, G.; Abecasis, G.; Durbin, R.; Genome Project Data Processing, S. The Sequence Alignment/Map format and SAMtools. *Bioinformatics* **2009**, *25*, 2078–9.

211. Quinlan, A.R.; Hall, I.M. BEDTools: a flexible suite of utilities for comparing genomic features. *Bioinformatics* **2010**, *26*, 841–2.
212. Valderrama, X.; Misra, V. Novel Brn3a cis-acting sequences mediate transcription of human trkA in neurons. *J Neurochem* **2008**, *105*, 425–435.
213. Banerjee, A.; Rapin, N.; Miller, M.; Griebel, P.; Zhou, Y.; Munster, V.; Misra, V. Generation and Characterization of Eptesicus fuscus (Big brown bat) kidney cell lines immortalized using the Myotis polyomavirus large T-antigen. *J Virol Methods* **2016**, *237*, 166–173.
214. Li, K.-B. ClustalW-MPI: ClustalW analysis using distributed and parallel computing. *Bioinformatics* **2003**, *19*, 1585–1586.
215. Kumar, S.; Stecher, G.; Tamura, K. MEGA7: Molecular Evolutionary Genetics Analysis Version 7.0 for Bigger Datasets. *Mol Biol Evol* **2016**, *33*, 1870–4.
216. Wevers, B.A.; van der Hoek, L. Recently discovered human coronaviruses. *Clin Lab Med* **2009**, *29*, 715–24.
217. Osborne, C.; Cryan, P.M.; O'Shea, T.J.; Oko, L.M.; Ndaluka, C.; Calisher, C.H.; Berglund, A.D.; Klavetter, M.L.; Bowen, R.A.; Holmes, K.V.; et al. Alphacoronaviruses in New World bats: prevalence, persistence, phylogeny, and potential for interaction with humans. *PloS one* **2011**, *6*, e19156.
218. Dominguez, S.R.; O'Shea, T.J.; Oko, L.M.; Holmes, K.V. Detection of group 1 coronaviruses in bats in North America. *Emerging infectious diseases* **2007**, *13*, 1295–300.
219. Strong, J.E.; Wong, G.; Jones, S.E.; Grolla, A.; Theriault, S.; Kobinger, G.P.; Feldmann, H. Stimulation of Ebola virus production from persistent infection through activation of the Ras/MAPK pathway. *Proceedings of the National Academy of Sciences of the United States of America* **2008**, *105*, 17982–7.
220. Mizutani, T.; Fukushi, S.; Saijo, M.; Kurane, I.; Morikawa, S. Regulation of p90RSK phosphorylation by SARS-CoV infection in Vero E6 cells. *FEBS Lett* **2006**, *580*, 1417–24.
221. Palacios, G.; Jabado, O.; Renwick, N.; Briese, T.; Lipkin, W.I. Severe acute respiratory syndrome coronavirus persistence in Vero cells. *Chinese medical journal* **2005**, *118*, 451–9.
222. Zhao, Z.; Li, H.; Wu, X.; Zhong, Y.; Zhang, K.; Zhang, Y.-P.; Boerwinkle, E.; Fu, Y.-X. Moderate mutation rate in the SARS coronavirus genome and its implications. *BMC Evolutionary Biology* **2004**, *4*, 21.
223. Ge, X.-Y.; Wang, N.; Zhang, W.; Hu, B.; Li, B.; Zhang, Y.-Z.; Zhou, J.-H.; Luo, C.-M.; Yang, X.-L.; Wu, L.-J.; et al. Coexistence of multiple coronaviruses in several bat colonies in an abandoned mineshaft. *Virol Sin* **2016**, *31*, 31–40.
224. Lassnig, C.; Sanchez, C.M.; Egerbacher, M.; Walter, I.; Majer, S.; Kolbe, T.; Pallares, P.; Enjuanes, L.; Muller, M. Development of a transgenic mouse model susceptible to human coronavirus 229E. *Proc Natl Acad Sci U S A* **2005**, *102*, 8275–80.
225. Trujillo-Ortega, M.E.; Beltran-Figueroa, R.; Garcia-Hernandez, M.E.; Juarez-Ramirez, M.; Sotomayor-Gonzalez, A.; Hernandez-Villegas, E.N.; Becerra-Hernandez, J.F.; Sarmiento-Silva, R.E. Isolation and characterization of porcine epidemic diarrhea virus associated with the 2014 disease outbreak in Mexico: case report. *BMC Vet Res* **2016**, *12*, 132.
226. Field, K.A.; Johnson, J.S.; Lilley, T.M.; Reeder, S.M.; Rogers, E.J.; Behr, M.J.; Reeder, D.M. The White-Nose Syndrome Transcriptome: Activation of Anti-fungal Host Responses in Wing Tissue of Hibernating Little Brown Myotis. *PLoS Pathog* **2015**, *11*, e1005168.
227. Field, H.; Jordan, D.; Edson, D.; Morris, S.; Melville, D.; Parry-Jones, K.; Broos, A.; Divljan, A.; McMichael, L.; Davis, R.; et al. Spatiotemporal Aspects of Hendra Virus Infection in Pteropid Bats (Flying-Foxes) in Eastern Australia. *PLoS ONE* **2015**, *10*, e0144055.

228. Yang, L.; Wu, Z.; Ren, X.; Yang, F.; Zhang, J.; He, G.; Dong, J.; Sun, L.; Zhu, Y.; Zhang, S.; et al. MERS-related betacoronavirus in Vespertilio superans bats, China. *Emerg Infect Dis* **2014**, *20*, 1260–2.
229. Anthony, S.J.; Gilardi, K.; Menachery, V.D.; Goldstein, T.; Ssebide, B.; Mbabazi, R.; Navarrete-Macias, I.; Liang, E.; Wells, H.; Hicks, A.; et al. Further Evidence for Bats as the Evolutionary Source of Middle East Respiratory Syndrome Coronavirus. *MBio* **2017**, *8*.
230. Halpin, K.; Young, P.L.; Field, H.E.; Mackenzie, J.S. Isolation of Hendra virus from pteropid bats: a natural reservoir of Hendra virus. *The Journal of general virology* **2000**, *81*, 1927–32.
231. Yob, J.M.; Field, H.; Rashdi, A.M.; Morrissy, C.; van der Heide, B.; Rota, P.; bin Adzhar, A.; White, J.; Daniels, P.; Jamaluddin, A.; et al. Nipah virus infection in bats (order Chiroptera) in peninsular Malaysia. *Emerging infectious diseases* **2001**, *7*, 439–41.
232. Towner, J.S.; Amman, B.R.; Sealy, T.K.; Carroll, S.A.; Comer, J.A.; Kemp, A.; Swanepoel, R.; Paddock, C.D.; Balinandi, S.; Khristova, M.L.; et al. Isolation of genetically diverse Marburg viruses from Egyptian fruit bats. *PLoS pathogens* **2009**, *5*, e1000536.
233. Leroy, E.M.; Kumulungui, B.; Pourrut, X.; Rouquet, P.; Hassanin, A.; Yaba, P.; Delicat, A.; Paweska, J.T.; Gonzalez, J.P.; Swanepoel, R. Fruit bats as reservoirs of Ebola virus. *Nature* **2005**, *438*, 575–6.
234. Vijaykrishna, D.; Smith, G.J.; Zhang, J.X.; Peiris, J.S.; Chen, H.; Guan, Y. Evolutionary insights into the ecology of coronaviruses. *J Virol* **2007**, *81*, 4012–20.
235. Drexler, J.F.; Corman, V.M.; Muller, M.A.; Maganga, G.D.; Vallo, P.; Binger, T.; Gloza-Rausch, F.; Rasche, A.; Yordanov, S.; Seebens, A.; et al. Bats host major mammalian paramyxoviruses. *Nature communications* **2012**, *3*, 796.
236. Freuling, C.; Vos, A.; Johnson, N.; Fooks, A.R.; Muller, T. Bat rabies--a Gordian knot? *Berliner und Munchener tierarztliche Wochenschrift* **2009**, *122*, 425–33.
237. Gonzalez, J.P.; Pourrut, X.; Leroy, E. Ebolavirus and other filoviruses. *Current topics in microbiology and immunology* **2007**, *315*, 363–87.
238. Chu, D.K.; Poon, L.L.; Chan, K.H.; Chen, H.; Guan, Y.; Yuen, K.Y.; Peiris, J.S. Coronaviruses in bent-winged bats (Miniopterus spp.). *The Journal of general virology* **2006**, *87*, 2461–6.
239. Plowright, R.K.; Foley, P.; Field, H.E.; Dobson, A.P.; Foley, J.E.; Eby, P.; Daszak, P. Urban habituation, ecological connectivity and epidemic dampening: the emergence of Hendra virus from flying foxes (Pteropus spp.). *Proceedings. Biological sciences / The Royal Society* **2011**, *278*, 3703–12.
240. Webber, Q.M.R.; Brigham, R.M.; Park, A.D.; Gillam, E.H.; O'Shea, T.J.; Willis, C.K.R. Social network characteristics and predicted pathogen transmission in summer colonies of female big brown bats (Eptesicus fuscus). *Behavioral Ecology and Sociobiology* **2016**, *70*, 701–712.
241. Drexler, J.F.; Corman, V.M.; Wegner, T.; Tateno, A.F.; Zerbinati, R.M.; Gloza-Rausch, F.; Seebens, A.; Muller, M.A.; Drosten, C. Amplification of emerging viruses in a bat colony. *Emerging infectious diseases* **2011**, *17*, 449–56.
242. Field, H.; de Jong, C.; Melville, D.; Smith, C.; Smith, I.; Broos, A.; Kung, Y.H.; McLaughlin, A.; Zeddeman, A. Hendra virus infection dynamics in Australian fruit bats. *PloS one* **2011**, *6*, e28678.
243. Plowright, R.K.; Field, H.E.; Smith, C.; Divljan, A.; Palmer, C.; Tabor, G.; Daszak, P.; Foley, J.E. Reproduction and nutritional stress are risk factors for Hendra virus infection in little red

flying foxes (Pteropus scapulatus). *Proceedings. Biological sciences / The Royal Society* **2008**, *275*, 861–9.
244. Pourrut, X.; Delicat, A.; Rollin, P.E.; Ksiazek, T.G.; Gonzalez, J.P.; Leroy, E.M. Spatial and temporal patterns of Zaire ebolavirus antibody prevalence in the possible reservoir bat species. *The Journal of infectious diseases* **2007**, *196 Suppl 2*, S176-83.
245. Rahman, S.A.; Hassan, S.S.; Olival, K.J.; Mohamed, M.; Chang, L.Y.; Hassan, L.; Saad, N.M.; Shohaimi, S.A.; Mamat, Z.C.; Naim, M.S.; et al. Characterization of Nipah virus from naturally infected Pteropus vampyrus bats, Malaysia. *Emerging infectious diseases* **2010**, *16*, 1990–3.
246. McMichael, L.; Edson, D.; Smith, C.; Mayer, D.; Smith, I.; Kopp, S.; Meers, J.; Field, H. Physiological stress and Hendra virus in flying-foxes (Pteropus spp.), Australia. *PLoS One* **2017**, *12*, e0182171.
247. Roizman, B.; Sears, A.E. Herpesviruses and their replication. In *Fields Virology*; Fields, B.N., Knipe, D.M., Howley, P.M., Eds.; Lippincott-Raven: Philadelphia, New york, 1996; Vol. 2, pp. 2231–2295.
248. Amman, B.R.; Carroll, S.A.; Reed, Z.D.; Sealy, T.K.; Balinandi, S.; Swanepoel, R.; Kemp, A.; Erickson, B.R.; Comer, J.A.; Campbell, S.; et al. Seasonal pulses of Marburg virus circulation in juvenile Rousettus aegyptiacus bats coincide with periods of increased risk of human infection. *PLoS pathogens* **2012**, *8*, e1002877.
249. Blehert, D.S.; Hicks, A.C.; Behr, M.; Meteyer, C.U.; Berlowski-Zier, B.M.; Buckles, E.L.; Coleman, J.T.; Darling, S.R.; Gargas, A.; Niver, R.; et al. Bat white-nose syndrome: an emerging fungal pathogen? *Science* **2009**, *323*, 227.
250. Frick, W.F.; Pollock, J.F.; Hicks, A.C.; Langwig, K.E.; Reynolds, D.S.; Turner, G.G.; Butchkoski, C.M.; Kunz, T.H. An emerging disease causes regional population collapse of a common North American bat species. *Science* **2010**, *329*, 679–82.
251. Lorch, J.M.; Meteyer, C.U.; Behr, M.J.; Boyles, J.G.; Cryan, P.M.; Hicks, A.C.; Ballmann, A.E.; Coleman, J.T.; Redell, D.N.; Reeder, D.M.; et al. Experimental infection of bats with Geomyces destructans causes white-nose syndrome. *Nature* **2011**, *480*, 376–8.
252. Davy, C.M.; Donaldson, M.E.; Willis, C.K.R.; Saville, B.J.; McGuire, L.P.; Mayberry, H.; Wilcox, A.; Wibbelt, G.; Misra, V.; Bollinger, T.; et al. The other white-nose syndrome transcriptome: Tolerant and susceptible hosts respond differently to the pathogen. *Ecol Evol* **2017**, *7*, 7161–7170.
253. Rapin, N.; Johns, K.; Martin, L.; Warnecke, L.; Turner, J.M.; Bollinger, T.K.; Willis, C.K.; Voyles, J.; Misra, V. Activation of innate immune-response genes in little brown bats (Myotis lucifugus) infected with the fungus Pseudogymnoascus destructans. *PloS one* **2014**, *9*, e112285.
254. Pauli, G.; Moura Mascarin, G.; Eilenberg, J.; Delalibera Júnior, I. Within-Host Competition between Two Entomopathogenic Fungi and a Granulovirus in. *Insects* **2018**, *9*.
255. Whitfield, S.M.; Geerdes, E.; Chacon, I.; Ballestero Rodriguez, E.; Jimenez, R.R.; Donnelly, M.A.; Kerby, J.L. Infection and co-infection by the amphibian chytrid fungus and ranavirus in wild Costa Rican frogs. *Dis Aquat Organ* **2013**, *104*, 173–8.
256. Liao, Y.; Smyth, G.K.; Shi, W. featureCounts: an efficient general purpose program for assigning sequence reads to genomic features. *Bioinformatics* **2014**, *30*, 923–30.
257. Varet, H.; Brillet-Guéguen, L.; Coppée, J.Y.; Dillies, M.A. SARTools: A DESeq2- and EdgeR-Based R Pipeline for Comprehensive Differential Analysis of RNA-Seq Data. *PLoS One* **2016**, *11*, e0157022.

258. Benjamini, Y.; Hochberg, Y. Controlling the False Discovery Rate: A Practical and Powerful Approach to Multiple Testing. *Journal of the Royal Statistical Society. Series B (Methodological)* //, *57*, 289–300.
259. Reimand, J.; Arak, T.; Adler, P.; Kolberg, L.; Reisberg, S.; Peterson, H.; Vilo, J. g:Profiler-a web server for functional interpretation of gene lists (2016 update). *Nucleic Acids Res* **7**, *44*, W83-9.
260. Supek, F.; Bošnjak, M.; Škunca, N.; Šmuc, T. REVIGO summarizes and visualizes long lists of gene ontology terms. *PLoS One* **2011**, *6*, e21800.
261. Mizutani, T.; Fukushi, S.; Ishii, K.; Sasaki, Y.; Kenri, T.; Saijo, M.; Kanaji, Y.; Shirota, K.; Kurane, I.; Morikawa, S. Mechanisms of establishment of persistent SARS-CoV-infected cells. *Biochemical and biophysical research communications* **2006**, *347*, 261–5.
262. Mizutani, T.; Fukushi, S.; Saijo, M.; Kurane, I. Characterization of persistent SARS-CoV infection in Vero E6 cells. *Advances in experimental medicine and biology* **2006**, *581*, 323–6.
263. Ng, C.T.; Oldstone, M.B. IL-10: achieving balance during persistent viral infection. *Current topics in microbiology and immunology* **2014**, *380*, 129–44.
264. Puntambekar, S.S.; Bergmann, C.C.; Savarin, C.; Karp, C.L.; Phares, T.W.; Parra, G.I.; Hinton, D.R.; Stohlman, S.A. Shifting hierarchies of interleukin-10-producing T cell populations in the central nervous system during acute and persistent viral encephalomyelitis. *Journal of virology* **2011**, *85*, 6702–13.
265. Wilson, E.B.; Brooks, D.G. The role of IL-10 in regulating immunity to persistent viral infections. *Current topics in microbiology and immunology* **2011**, *350*, 39–65.
266. Hernández, P.P.; Mahlakoiv, T.; Yang, I.; Schwierzeck, V.; Nguyen, N.; Guendel, F.; Gronke, K.; Ryffel, B.; Hoelscher, C.; Dumoutier, L.; et al. Interferon-λ and interleukin 22 act synergistically for the induction of interferon-stimulated genes and control of rotavirus infection. *Nat Immunol* **2015**, *16*, 698–707.
267. Wolk, K.; Sabat, R. Interleukin-22: a novel T- and NK-cell derived cytokine that regulates the biology of tissue cells. *Cytokine Growth Factor Rev* **2006**, *17*, 367–80.
268. Krebs, D.L.; Uren, R.T.; Metcalf, D.; Rakar, S.; Zhang, J.G.; Starr, R.; De Souza, D.P.; Hanzinikolas, K.; Eyles, J.; Connolly, L.M.; et al. SOCS-6 binds to insulin receptor substrate 4, and mice lacking the SOCS-6 gene exhibit mild growth retardation. *Mol Cell Biol* **2002**, *22*, 4567–78.
269. Hensley, L.E.; Fritz, L.E.; Jahrling, P.B.; Karp, C.L.; Huggins, J.W.; Geisbert, T.W. Interferon-beta 1a and SARS coronavirus replication. *Emerg Infect Dis* **2004**, *10*, 317–9.
270. Falzarano, D.; de Wit, E.; Martellaro, C.; Callison, J.; Munster, V.J.; Feldmann, H. Inhibition of novel beta coronavirus replication by a combination of interferon-alpha2b and ribavirin. *Sci Rep* **2013**, *3*, 1686.
271. Finlin, B.S.; Gau, C.L.; Murphy, G.A.; Shao, H.; Kimel, T.; Seitz, R.S.; Chiu, Y.F.; Botstein, D.; Brown, P.O.; Der, C.J.; et al. RERG is a novel ras-related, estrogen-regulated and growth-inhibitory gene in breast cancer. *J Biol Chem* **2001**, *276*, 42259–67.
272. Langwig, K.E.; Frick, W.F.; Bried, J.T.; Hicks, A.C.; Kunz, T.H.; Kilpatrick, A.M. Sociality, density-dependence and microclimates determine the persistence of populations suffering from a novel fungal disease, white-nose syndrome. *Ecology letters* **2012**, *15*, 1050–7.
273. Moratelli, R.; Calisher, C.H.; Moratelli, R.; Calisher, C.H. Bats and zoonotic viruses: can we confidently link bats with emerging deadly viruses? *Memórias do Instituto Oswaldo Cruz* **2015**, *110*, 1–22.

274. Azhar, E.I.; Hashem, A.M.; El-Kafrawy, S.A.; Sohrab, S.S.; Aburizaiza, A.S.; Farraj, S.A.; Hassan, A.M.; Al-Saeed, M.S.; Jamjoom, G.A.; Madani, T.A. Detection of the Middle East Respiratory Syndrome Coronavirus Genome in an Air Sample Originating from a Camel Barn Owned by an Infected Patient. *mBio* **2014**, *5*, e01450-14.
275. Woo, P.C.Y.; Lau, S.K.P.; Li, K.S.M.; Poon, R.W.S.; Wong, B.H.L.; Tsoi, H.; Yip, B.C.K.; Huang, Y.; Chan, K.; Yuen, K. Molecular diversity of coronaviruses in bats. *Virology* **2006**, *351*, 180–187.
276. Wu, K.; Peng, G.; Wilken, M.; Geraghty, R.J.; Li, F. Mechanisms of Host Receptor Adaptation by Severe Acute Respiratory Syndrome Coronavirus. *Journal of Biological Chemistry* **2012**, *287*, 8904–8911.
277. Letko, M.; Miazgowicz, K.; McMinn, R.; Seifert, S.N.; Sola, I.; Enjuanes, L.; Carmody, A.; van Doremalen, N.; Munster, V. Adaptive Evolution of MERS-CoV to Species Variation in DPP4. *Cell Reports* **2018**, *24*, 1730–1737.
278. van den Brand, J.M.A.; Smits, S.L.; Haagmans, B.L. Pathogenesis of Middle East respiratory syndrome coronavirus. *J. Pathol.* **2015**, *235*, 175–184.
279. Weiss, S.R.; Navas-Martin, S. Coronavirus Pathogenesis and the Emerging Pathogen Severe Acute Respiratory Syndrome Coronavirus. *Microbiol. Mol. Biol. Rev.* **2005**, *69*, 635–664.
280. Coleman, C.M.; Frieman, M.B. Coronaviruses: important emerging human pathogens. *J. Virol.* **2014**, *88*, 5209–5212.
281. Lee, C. Porcine epidemic diarrhea virus: An emerging and re-emerging epizootic swine virus. *Virol J* **2015**, *12*.
282. Subudhi, S.; Rapin, N.; Misra, V. Immune System Modulation and Viral Persistence in Bats: Understanding Viral Spillover. *Viruses* **2019**, *11*, 192.
283. Yang, Y.; Zhang, L.; Geng, H.; Deng, Y.; Huang, B.; Guo, Y.; Zhao, Z.; Tan, W. The structural and accessory proteins M, ORF 4a, ORF 4b, and ORF 5 of Middle East respiratory syndrome coronavirus (MERS-CoV) are potent interferon antagonists. *Protein & Cell* **2013**, *4*, 951–961.
284. Menachery, V.D.; Mitchell, H.D.; Cockrell, A.S.; Gralinski, L.E.; Yount, B.L.; Graham, R.L.; McAnarney, E.T.; Douglas, M.G.; Scobey, T.; Beall, A.; et al. MERS-CoV Accessory ORFs Play Key Role for Infection and Pathogenesis. *mBio* **2017**, *8*.
285. Zaki, A.M.; van Boheemen, S.; Bestebroer, T.M.; Osterhaus, A.D.M.E.; Fouchier, R.A.M. Isolation of a Novel Coronavirus from a Man with Pneumonia in Saudi Arabia. *New England Journal of Medicine* **2012**, *367*, 1814–1820.
286. Kärber, G. Beitrag zur kollektiven Behandlung pharmakologischer Reihenversuche. *Naunyn-Schmiedebergs Archiv für experimentelle Pathologie und Pharmakologie* **1931**, *162*, 480–483.
287. Spearman, C. THE METHOD OF 'RIGHT AND WRONG CASES' ('CONSTANT STIMULI') WITHOUT GAUSS'S FORMULAE. *British Journal of Psychology, 1904-1920* **1908**, *2*, 227–242.
288. Bergeron, T.; Zhang, R.; Elliot, K.; Rapin, N.; MacDonald, V.; Linn, K.; Simko, E.; Misra, V. The effect of Zhangfei on the unfolded protein response and growth of cells derived from canine and human osteosarcomas. *Veterinary and comparative oncology* **2013**, *11*, 140–50.
289. Zhang, G.; Guo, D.; Dash, P.K.; Araínga, M.; Wiederin, J.L.; Haverland, N.A.; Knibbe-Hollinger, J.; Martinez-Skinner, A.; Ciborowski, P.; Goodfellow, V.S.; et al. The mixed lineage kinase-3 inhibitor URMC-099 improves therapeutic outcomes for long-acting

antiretroviral therapy. *Nanomedicine: Nanotechnology, Biology and Medicine* **2016**, *12*, 109–122.
290. Banerjee, A.; Falzarano, D.; Rapin, N.; Lew, J.; Misra, V. Interferon Regulatory Factor 3-Mediated Signaling Limits Middle-East Respiratory Syndrome (MERS) Coronavirus Propagation in Cells from an Insectivorous Bat. *Viruses* **2019**, *11*, 152.
291. Dong, W.; Embury, C.M.; Lu, Y.; Whitmire, S.M.; Dyavarshetty, B.; Gelbard, H.A.; Gendelman, H.E.; Kiyota, T. The mixed-lineage kinase 3 inhibitor URMC-099 facilitates microglial amyloid-β degradation. *Journal of Neuroinflammation* **2016**, *13*, 184.
292. Molina, J.R.; Adjei, A.A. The Ras/Raf/MAPK Pathway. *Journal of Thoracic Oncology* **2006**, *1*, 7–9.
293. Finlin, B.S.; Gau, C.-L.; Murphy, G.A.; Shao, H.; Kimel, T.; Seitz, R.S.; Chiu, Y.-F.; Botstein, D.; Brown, P.O.; Der, C.J.; et al. RERG Is a Novel ras-related, Estrogen-regulated and Growth-inhibitory Gene in Breast Cancer. *J. Biol. Chem.* **2001**, *276*, 42259–42267.
294. Qi, Y.; Li, Y.; Zhang, Y.; Zhang, L.; Wang, Z.; Zhang, X.; Gui, L.; Huang, J. IFI6 Inhibits Apoptosis via Mitochondrial-Dependent Pathway in Dengue Virus 2 Infected Vascular Endothelial Cells. *PLOS ONE* **2015**, *10*, e0132743.
295. Niemeyer, D.; Zillinger, T.; Muth, D.; Zielecki, F.; Horvath, G.; Suliman, T.; Barchet, W.; Weber, F.; Drosten, C.; Muller, M.A. Middle East Respiratory Syndrome Coronavirus Accessory Protein 4a Is a Type I Interferon Antagonist. *Journal of Virology* **2013**, *87*, 12489–12495.
296. Yeung, M.-L.; Yao, Y.; Jia, L.; Chan, J.F.W.; Chan, K.-H.; Cheung, K.-F.; Chen, H.; Poon, V.K.M.; Tsang, A.K.L.; To, K.K.W.; et al. MERS coronavirus induces apoptosis in kidney and lung by upregulating Smad7 and FGF2. *Nature Microbiology* **2016**, *1*, 16004.
297. Calisher, C.H.; Childs, J.E.; Field, H.E.; Holmes, K.V.; Schountz, T. Bats: important reservoir hosts of emerging viruses. *Clinical microbiology reviews* **2006**, *19*, 531–45.
298. Wynne, J.W.; Wang, L.F. Bats and viruses: friend or foe? *PLoS pathogens* **2013**, *9*, e1003651.
299. Jha, H.C.; Banerjee, S.; Robertson, E.S. The Role of Gammaherpesviruses in Cancer Pathogenesis. *Pathogens* **2016**, *5*.
300. Grinde, B. Herpesviruses: latency and reactivation - viral strategies and host response. *J Oral Microbiol* **2013**, *5*.
301. Aligo, J.; Walker, M.; Bugelski, P.; Weinstock, D. Is murine gammaherpesvirus-68 (MHV-68) a suitable immunotoxicological model for examining immunomodulatory drug-associated viral recrudescence? *J Immunotoxicol* **2015**, *12*, 1–15.
302. Ehlers, B.; Dural, G.; Yasmum, N.; Lembo, T.; de Thoisy, B.; Ryser-Degiorgis, M.P.; Ulrich, R.G.; McGeoch, D.J. Novel mammalian herpesviruses and lineages within the Gammaherpesvirinae: cospeciation and interspecies transfer. *J Virol* **2008**, *82*, 3509–16.
303. Escalera-Zamudio, M.; Rojas-Anaya, E.; Kolokotronis, S.O.; Taboada, B.; Loza-Rubio, E.; Mendez-Ojeda, M.L.; Arias, C.F.; Osterrieder, N.; Greenwood, A.D. Bats, Primates, and the Evolutionary Origins and Diversification of Mammalian Gammaherpesviruses. *MBio* **2016**, *7*.
304. Molnar, V.; Janoska, M.; Harrach, B.; Glavits, R.; Palmai, N.; Rigo, D.; Sos, E.; Liptovszky, M. Detection of a novel bat gammaherpesvirus in Hungary. *Acta Vet Hung* **2008**, *56*, 529–38.

305. Paige Brock, A.; Cortes-Hinojosa, G.; Plummer, C.E.; Conway, J.A.; Roff, S.R.; Childress, A.L.; Wellehan, J.F., Jr. A novel gammaherpesvirus in a large flying fox (Pteropus vampyrus) with blepharitis. *J Vet Diagn Invest* **2013**, *25*, 433–7.
306. Watanabe, S.; Ueda, N.; Iha, K.; Masangkay, J.S.; Fujii, H.; Alviola, P.; Mizutani, T.; Maeda, K.; Yamane, D.; Walid, A.; et al. Detection of a new bat gammaherpesvirus in the Philippines. *Virus Genes* **2009**, *39*, 90–3.
307. Ehlers, B.; Borchers, K.; Grund, C.; Frolich, K.; Ludwig, H.; Buhk, H.J. Detection of new DNA polymerase genes of known and potentially novel herpesviruses by PCR with degenerate and deoxyinosine-substituted primers. *Virus Genes* **1999**, *18*, 211–20.
308. Kearse, M.; Moir, R.; Wilson, A.; Stones-Havas, S.; Cheung, M.; Sturrock, S.; Buxton, S.; Cooper, A.; Markowitz, S.; Duran, C.; et al. Geneious Basic: an integrated and extendable desktop software platform for the organization and analysis of sequence data. *Bioinformatics* **2012**, *28*, 1647–9.
309. Rastogi, P.A. MacVector. Integrated sequence analysis for the Macintosh. *Methods Mol Biol* **2000**, *132*, 47–69.
310. Altschul, S.F.; Gish, W.; Miller, W.; Myers, E.W.; Lipman, D.J. Basic local alignment search tool. *J Mol Biol* **1990**, *215*, 403–10.
311. Highlander, S.L.; Sutherland, S.L.; Gage, P.J.; Johnson, D.C.; Levine, M.; Glorioso, J.C. Neutralizing monoclonal antibodies specific for herpes simplex virus glycoprotein D inhibit virus penetration. *J Virol* **1987**, *61*, 3356–64.
312. Hierholzer, J.C.; Killington, R.A. 2 - Virus isolation and quantitation A2 - Mahy, Brian WJ. In *Virology Methods Manual*; Kangro, H.O., Ed.; Academic Press: London, 1996; pp. 25–46 ISBN 978-0-12-465330-6.
313. Darriba, D.; Taboada, G.L.; Doallo, R.; Posada, D. ProtTest 3: fast selection of best-fit models of protein evolution. *Bioinformatics* **2011**, *27*, 1164–5.
314. Le, S.Q.; Gascuel, O. An improved general amino acid replacement matrix. *Mol Biol Evol* **2008**, *25*, 1307–20.
315. Whelan, S.; Goldman, N. A general empirical model of protein evolution derived from multiple protein families using a maximum-likelihood approach. *Mol Biol Evol* **2001**, *18*, 691–9.
316. Jones, D.T.; Taylor, W.R.; Thornton, J.M. The rapid generation of mutation data matrices from protein sequences. *Comput Appl Biosci* **1992**, *8*, 275–82.
317. Groves, A.K.; Cotter, M.A.; Subramanian, C.; Robertson, E.S. The latency-associated nuclear antigen encoded by Kaposi's sarcoma-associated herpesvirus activates two major essential Epstein-Barr virus latent promoters. *J Virol* **2001**, *75*, 9446–57.
318. Sun, R.; Lin, S.F.; Gradoville, L.; Yuan, Y.; Zhu, F.; Miller, G. A viral gene that activates lytic cycle expression of Kaposi's sarcoma-associated herpesvirus. *Proc Natl Acad Sci U S A* **1998**, *95*, 10866–71.
319. Bortz, E.; Whitelegge, J.P.; Jia, Q.; Zhou, Z.H.; Stewart, J.P.; Wu, T.T.; Sun, R. Identification of proteins associated with murine gammaherpesvirus 68 virions. *J Virol* **2003**, *77*, 13425–32.
320. Zhang, H.; Todd, S.; Tachedjian, M.; Barr, J.A.; Luo, M.; Yu, M.; Marsh, G.A.; Crameri, G.; Wang, L.F. A novel bat herpesvirus encodes homologues of major histocompatibility complex classes I and II, C-type lectin, and a unique family of immune-related genes. *J Virol* **2012**, *86*, 8014–30.

321. Vink, C.; Beuken, E.; Bruggeman, C.A. Complete DNA sequence of the rat cytomegalovirus genome. *J Virol* **2000**, *74*, 7656–65.
322. Schleiss, M.R.; McGregor, A.; Choi, K.Y.; Date, S.V.; Cui, X.; McVoy, M.A. Analysis of the nucleotide sequence of the guinea pig cytomegalovirus (GPCMV) genome. *Virol J* **2008**, *5*, 139.
323. Rawlinson, W.D.; Farrell, H.E.; Barrell, B.G. Analysis of the complete DNA sequence of murine cytomegalovirus. *J Virol* **1996**, *70*, 8833–49.
324. Loh, J.; Zhao, G.; Nelson, C.A.; Coder, P.; Droit, L.; Handley, S.A.; Johnson, L.S.; Vachharajani, P.; Guzman, H.; Tesh, R.B.; et al. Identification and sequencing of a novel rodent gammaherpesvirus that establishes acute and latent infection in laboratory mice. *J Virol* **2011**, *85*, 2642–56.
325. Farrell, H.E.; Vally, H.; Lynch, D.M.; Fleming, P.; Shellam, G.R.; Scalzo, A.A.; Davis-Poynter, N.J. Inhibition of natural killer cells by a cytomegalovirus MHC class I homologue in vivo. *Nature* **1997**, *386*, 510–4.
326. Sun, J.C.; Lanier, L.L. The Natural Selection of Herpesviruses and Virus-Specific NK Cell Receptors. *Viruses* **2009**, *1*, 362.
327. Barton, E.; Mandal, P.; Speck, S.H. Pathogenesis and host control of gammaherpesviruses: lessons from the mouse. *Annu Rev Immunol* **2011**, *29*, 351–97.
328. Ackermann, M. Pathogenesis of gammaherpesvirus infections. *Vet Microbiol* **2006**, *113*, 211–22.
329. Bechtel, J.T.; Liang, Y.; Hvidding, J.; Ganem, D. Host range of Kaposi's sarcoma-associated herpesvirus in cultured cells. *J Virol* **2003**, *77*, 6474–81.
330. Donofrio, G.; Cavirani, S.; Simone, T.; van Santen, V.L. Potential of bovine herpesvirus 4 as a gene delivery vector. *J Virol Methods* **2002**, *101*, 49–61.
331. van den Hurk, A.F.; Smith, C.S.; Field, H.E.; Smith, I.L.; Northill, J.A.; Taylor, C.T.; Jansen, C.C.; Smith, G.A.; Mackenzie, J.S. Transmission of Japanese Encephalitis virus from the black flying fox, Pteropus alecto, to Culex annulirostris mosquitoes, despite the absence of detectable viremia. *Am J Trop Med Hyg* **2009**, *81*, 457–62.
332. Schuh, A.J.; Amman, B.R.; Sealy, T.K.; Spengler, J.R.; Nichol, S.T.; Towner, J.S. Egyptian rousette bats maintain long-term protective immunity against Marburg virus infection despite diminished antibody levels. *Sci Rep* **2017**, *7*, 8763.
333. Luis, A.D.; Hayman, D.T.; O'Shea, T.J.; Cryan, P.M.; Gilbert, A.T.; Pulliam, J.R.; Mills, J.N.; Timonin, M.E.; Willis, C.K.; Cunningham, A.A.; et al. A comparison of bats and rodents as reservoirs of zoonotic viruses: are bats special? *Proceedings. Biological sciences / The Royal Society* **2013**, *280*, 20122753.
334. Olival, K.J.; Hosseini, P.R.; Zambrana-Torrelio, C.; Ross, N.; Bogich, T.L.; Daszak, P. Host and viral traits predict zoonotic spillover from mammals. *Nature* **2017**, *546*, 646.
335. Kessler, M.K.; Becker, D.J.; Peel, A.J.; Justice, N.V.; Lunn, T.; Crowley, D.E.; Jones, D.N.; Eby, P.; Sánchez, C.A.; Plowright, R.K. Changing resource landscapes and spillover of henipaviruses. *Ann N Y Acad Sci* **2018**, *1429*, 78–99.
336. Nash, A.A.; Dutia, B.M.; Stewart, J.P.; Davison, A.J. Natural history of murine gamma-herpesvirus infection. *Philos Trans R Soc Lond B Biol Sci* **2001**, *356*, 569–79.
337. Flaño, E.; Kim, I.J.; Moore, J.; Woodland, D.L.; Blackman, M.A. Differential gamma-herpesvirus distribution in distinct anatomical locations and cell subsets during persistent infection in mice. *J Immunol* **2003**, *170*, 3828–34.

338. Matar, C.G.; Rangaswamy, U.S.; Wakeman, B.S.; Iwakoshi, N.; Speck, S.H. Murine gammaherpesvirus 68 reactivation from B cells requires IRF4 but not XBP-1. *J Virol* **2014**, *88*, 11600–10.
339. Li, X.; Feng, J.; Sun, R. Oxidative stress induces reactivation of Kaposi's sarcoma-associated herpesvirus and death of primary effusion lymphoma cells. *J Virol* **2011**, *85*, 715–24.
340. Lardeux, F.; Torrico, G.; Aliaga, C. Calculation of the ELISA's cut-off based on the change-point analysis method for detection of Trypanosoma cruzi infection in Bolivian dogs in the absence of controls. *Mem Inst Oswaldo Cruz* **2016**, *111*, 501–4.
341. Killick, R.; Eckley, I.A. changepoint: An R Package for Changepoint Analysis. *2014* **2014**, *58*, 19.
342. Killick, R.; Fearnhead, P.; Eckley, I.A. Optimal Detection of Changepoints With a Linear Computational Cost. *Journal of the American Statistical Association* **2012**, *107*, 1590–1598.
343. Development Core Team, R. *R: A Language and Environment for Statistical Computing*; 2011; Vol. 1;.
344. Bouma, H.R.; Kroese, F.G.; Kok, J.W.; Talaei, F.; Boerema, A.S.; Herwig, A.; Draghiciu, O.; van Buiten, A.; Epema, A.H.; van Dam, A.; et al. Low body temperature governs the decline of circulating lymphocytes during hibernation through sphingosine-1-phosphate. *Proc Natl Acad Sci U S A* **2011**, *108*, 2052–7.
345. Logan, S.M.; Tessier, S.N.; Tye, J.; Storey, K.B. Response of the JAK-STAT pathway to mammalian hibernation in 13-lined ground squirrel striated muscle. *Mol Cell Biochem* **2016**, *414*, 115–27.
346. Chow, B.A.; Donahue, S.W.; Vaughan, M.R.; McConkey, B.; Vijayan, M.M. Serum immune-related proteins are differentially expressed during hibernation in the American black bear. *PLoS One* **2013**, *8*, e66119.
347. Orr, A.L.; Lohse, L.A.; Drew, K.L.; Hermes-Lima, M. Physiological oxidative stress after arousal from hibernation in Arctic ground squirrel. *Comp Biochem Physiol A Mol Integr Physiol* **2009**, *153*, 213–21.
348. Gangappa, S.; Kapadia, S.B.; Speck, S.H.; Virgin, H.W. Antibody to a lytic cycle viral protein decreases gammaherpesvirus latency in B-cell-deficient mice. *J Virol* **2002**, *76*, 11460–8.
349. Kim, I.J.; Flaño, E.; Woodland, D.L.; Blackman, M.A. Antibody-mediated control of persistent gamma-herpesvirus infection. *J Immunol* **2002**, *168*, 3958–64.
350. Brigham, R.M. Flexibility in foraging and roosting behaviour by the big brown bat (Eptesicus fuscus). *Can. J. Zool.* **1991**, *69*, 117–121.
351. Stevenson, P.G.; Simas, J.P.; Efstathiou, S. Immune control of mammalian gamma-herpesviruses: lessons from murid herpesvirus-4. *J Gen Virol* **2009**, *90*, 2317–30.
352. Hinterland Who's Who - Little Brown Bat Available online: http://www.hww.ca/en/wildlife/mammals/little-brown-bat.html (accessed on Feb 2, 2019).